Urban infrastructure inundation risk from permanent sea-level rise scenarios in London (UK), Bangkok (Thailand) and Mumbai (India): A comparative analysis

Shawn Pace

2021

Department of Physical Geography and Ecosystem Science

Centre for Geographical Information Systems

Lund University
Sölvegatan 12

S-223 62 Lund

Sweden

Shawn Pace (2021). Urban infrastructure inundation risk from permanent sea-level rise scenarios in London (UK), Bangkok (Thailand) and Mumbai (India): A comparative analysis.
Master degree thesis, 30 credits in Master in *Geographical Information Science*
Department of Physical Geography and Ecosystem Science, Lund University

Urban infrastructure inundation risk from permanent sea-level rise scenarios in London (UK), Bangkok (Thailand) and Mumbai (India): A comparative analysis

Shawn Pace

Master thesis, 30 credits, in Geographical Information Science

Supervisor

Andreas Persson

Department of Physical Geography and Ecosystem Science

Lund University

Abstract

This study aimed to fill knowledge gaps in understanding the exposure of urban infrastructure such as roads, railways, buildings and parks to SLR scenarios, and how this would affect local populations. Three economic hubs, namely London (United Kingdom), Bangkok (Thailand) and Mumbai (India) were chosen for comparison due to their coastal locations and regionally concentrated asset wealth with dense populations and economic influence regionally.

The data sources for this research study included three digital elevation models (DEMs); two traditionally used globally available datasets from the Japanese Aerospace Exploration Agency and United States Geological Survey (1 arc-second spatial resolution), and a recently released elevation model by ClimateCentral (3 arc-second spatial resolution). Vector data for the urban infrastructural layers was sourced from navigational supplier HERE, while population data in raster format was sourced from WorldPop (3 arc-second spatial resolution). A modified bathtub-fill modelling method approach was then used within GIS applications to model landward-creeping SLR (high-risk: 1 metre, medium-risk: 3 metres and low-risk: 5 metres) using the three DEMs, resulting in the extraction of the total lengths, areas and counts of the infrastructural layers and populations that intersected these flooded areas. Risk index maps were built for the cities' districts to understand where the greatest risks lie, while hypotheses for the inter-relationship between the cities and their infrastructure were tested using non-parametric Kruskal-Wallis independent tests.

From this method, the results showed that in a 1m (high-risk) scenario, Mumbai is consistently the most vulnerable city with between 6-10% of the city's area (particularly the central business district) showing flooding. Bangkok is at lower risk at 4-6% inundation of the city's area (in lower density suburbs), while approximately 2% of London's area (mainly in industrial riverside locations) is at risk. In the medium- and low-risk scenarios, Bangkok is the most vulnerable with 16-51% and 57-92% of its area showing flooding respectively. A 1m SLR shows greatest threat to Mumbai's functionality as a city as all infrastructural elements and up to 24% of the local population will be impacted on a day-to-day basis. On the other hand, a 3 and 5 metre SLR would impact up to 52% and 96% of Bangkok's population respectively.

Although this study gives a geographic indication of the SLR impact on these three cities, budgetary and network constraints precluded the sourcing of high-resolution elevation model data from ClimateCentral as well as locally sourced flood defence structure and hydrological input data. Accuracy within the findings in future studies would increase from inputs such as LiDAR elevation data, socio-economic asset values for the cities' urban infrastructure and multi-criteria hydrological information. In this way, researchers and municipalities would be better informed on the vulnerability to their cities, and use this to build resilience and mitigative efforts against SLR over the coming decades.

Keywords: Geography, GIS, Climate Change, Sea-Level Rise, DEM, Urban Infrastructure, London, Mumbai, Bangkok

Acknowledgenents

I would like to thank a number of people for helping me to undertake this research study and improve it over time.

Table of Contents

List of Abbreviations

ABBREVIATION	MEANING
SLR	Sea-level rise
GIS	Geographical Information Systems
IPCC	Intergovernmental Panel on Climate Change
JAXA	Japanese Aerospace eXploration Agency
SRTM	Shuttle Radar Topography Mission
CDEM	Coastal DEM
DEM	Digital Elevation Model
LiDAR	Light Detection and Ranging
USGS	United States Geological Survey
EPSG	European Petroleum Survey Group
ESRI	Environmental Systems Research Institute
QGIS	Quantum GIS
CE	Common Era
CFC	Chlorofluorocarbon
GBP	Great British Pound Sterling currency
USD	United States Dollar currency

List of Figures

List of Tables

1.   Introduction

1.1.   Sea-level rise literature

Due to anthropogenic activities and the increasing pressure on the Earth's natural resources with a growing population, the levels of greenhouse gas concentrations in the atmosphere (such as carbon dioxide and nitrous oxide) are creating a net radiation build-up of heat. This is not only affecting air temperatures but also bodies of water, where impacted stores of water in ice and snow within colder regions around the world are melting. Their continued and unchecked release into the world's oceans is resulting in a gradual sea-level rise around the planet, significantly affecting low-lying coastal areas particularly inhabited ones. This is particularly exacerbated by thermal expansion of the Earth's water, which will expand in volume as it warms up (Rahmstorf, 2007).

The amount by which the sea level would rise in effect depends on society's behaviour towards greenhouse gas emissions from industrial and commercial activities over time. Should these emissions peak in the first half of the 21st century and then reduce again, the sea level would rise significantly less than if emissions continued to match current levels or even increase further until the middle of the century (Solomon *et al.*, 2007; Wachsmuth *et al.*, 2018). Depending on four different scenarios, the IPCC (Intergovernmental Panel on Climate Change) has determined through its that a global warming amount of 1.5°C would amount to a sea-level rise of 0.26 to 0.77m by 2100, however higher global warming results would yield higher sea levels. It has been projected that with a global warming of 2°C the sea level would rise on average by 0.36 to 0.87m by the year 2100, while a sea-level rise of approximately 1 metre could be expected around the world. This sea level change would become the new baseline scenario, where storm surges and flood events would impact coastal urban regions in particular as they contain high concentrations of inhabitants who live near the water (Neumann *et al.*, 2015).

This threat to coastal regions around the world will require municipal authorities to act. Long-term strategic planning (such as the National Adaptation Programme and the Third Strategy for Climate Adaptation Reporting in the United Kingdom) identify unique threats to a country's infrastructure, economy and local populations while also setting the foundation for the coastal areas' adaptation to mitigate further damage (Department for Environment Food and Rural Affairs, 2018). Although governments and research bodies in developed countries around the world have already established their coasts' sensitivity to changes in sea level (as well as the sensitivity of coasts in developing countries), this has been done for the most part on a general environmental scale (such as the study done by Nistora). People have been made aware of how sensitive their coasts are through governmental geospatial websites such as the

coastal sensitivity to sea-level rise in Canada, however this gives a general picture of the coasts and does not look at their specific regions.

1.2. Definitions of key terms

The study will address the following key terms, which are defined in climate change terms as follows:

- **Vulnerability**, as defined by the IPCC: *"A function of the character, magnitude and rate of climate variation and change to which a system is exposed, together with sensitivity and adaptive capacity"* (IPCC, 2007)
- **Impact**, as defined by the IPCC: *"The effects of natural and human systems of extreme weather and climate change… on lives, livelihoods, health, economies, ecosystems, societies, cultures, services and infrastructure from exposure to hazardous climate events. Impacts are also referred to as consequences and outcomes"* (IPCC, 2007).
- **Risk**: a situation whereby a location or spatial asset is exposed to danger in the form of an extreme climatic event (Lexico.com, 2019)
- **Exposure**: *"The state of having no protection from something harmful"* (Lexico.com, 2019), which in climate change terms is an extreme weather event such as a storm, hurricane or flood
- **Resilience**, as defined by the IPCC: *"The ability of a social or ecological system to absorb disturbances while retaining the same basic structure and ways of functioning, the capacity of self-organization, and the capacity to adapt to stress and change."* (IPCC, 2007)

1.3. Challenges based on evolving surface elevation data

The increasing publication of scientific data predicting sea level changes over the 21st century with higher accuracy due to climate change pose additional challenges to regions and municipalities, in that information used as a basis for policy and adaptation strategy design is frequently updated (Carter, 2011; Solecki, Leichenko and O'Brien, 2011). This causes issues when policies and climate change mitigation strategies earmarked for certain local areas show changes in exposure and risk as data get updated (Adler and Hirsch Hadorn, 2014; Oppenheimer *et al.*, 2019). For example, global sea-level rise projections published by the IPCC assuming equal carbon emissions scenarios have increased from 65cm by 2100 when published in 1990, to 98cm by 2100 in the most recent assessment report (Church *et al.*, 2013). Research by Barnett (1984), Church *et al.* (2004), and Suzuki and Ishii (2011) however shows that sea level realistically is expected to rise at different rates on a regional scale due to factors such as post-glacial isostatic adjustment (GIA), potential Antarctic ice-sheet melting instability and local tidal and storm surge ranges. The Antarctic ice-sheet stability may cause a difference

between global sea levels remaining at approximately 1 metre higher than the baseline (2000) level, or reaching and exceeding 2 metres in sea-level rise (Kopp *et al*., 2017).

With technological advancements and access to funding, elevation data is being updated frequently. Previously, satellite imagery data captured in the year 2000 from the Shuttle Radar Topography Mission (SRTM) have been published with a near-global coverage by NASA. These digital surface model raster tiles have a spatial resolution of up to 1 arc-second (30 metres), and are used for vulnerability assessments worldwide (Aina and Aleem, 2014; Hasan, Khan and Hong, 2015; Rasmussen *et al.*, 2018). The vertical errors and striping artefacts within SRTM images have however reduced their reliability; an element which was addressed by the Japanese Aerospace Exploration Agency (JAXA) when it supplied its own global coverage of surface elevation data in 2015. These data originated from the Advanced Land Observing Satellite with the same spatial resolution as SRTM (1 arc-second/30 metres) (Alganci, Besol and Sertel, 2018). Using machine learning algorithms, artificial neural networks and Gaussian process models, the research team at ClimateCentral have tweaked these datasets due to the lack of highly accurate global elevation data (Kulp and Strauss, 2019). From the authors' findings in 2016, Kulp and Strauss have identified that SRTM and JAXA data generally underestimate the impact of sea-level rise and flooding on a global scale. The benefit of using the data from this research (published in 2019) is that they provide a more accurate digital elevation framework for regions at higher risk such as East Asia, the Middle East and North Africa (Dasgupta *et al*., 2007), where LiDAR based elevation data (of up to 50cm spatial resolution and therefore the benchmark of elevation data accuracy) is not yet available and further analysis of sea-level rise is needed (Johnston *et al*., 2014; Boyd & Ghosh, 2015; Ahsan *et al*., 2016).

1.4. Motivation

Assessing a city's vulnerability through the examination of detailed urban infrastructural elements (roads, buildings, railways etc.) can be beneficial when considering future impacts to economic activity, local populations and the city's functioning through urban planning (Nicholls *et al*., 2010; Demirel *et al*., 2015; Eidho *et al*., 2018). Navigational data (organised into links and nodes) highlights the resilience of the local road network as well as the impact of sea-level rise on accessibility and function, particularly when exposed to temporary flood events (Nicholls *et al*., 2010; Arnesten, 2019). As the backbone of a city's navigability, the road and rail networks of a city outline its ability to move people and goods around effectively and successfully.

London's location on the south east of the United Kingdom is vulnerable to eastward flowing weather events such as hurricanes and storms from the Atlantic Ocean, which are

funnelled through the North Sea before reaching the river Thames (Shih and Nicholls, 2007). As a result, London is sheltered from the full effects of a greater ocean, unlike the other two cities in this study. Bangkok is found in the Chao Phraya River catchment area on the coast of the Gulf of Thailand. It is located in a tropical savanna climate, and thus faces annual periods of high rainfall (known as monsoon seasons) between April to October. Not only is it sinking by up to 2cm per year because of its location on a shifting river delta, but its location in the Gulf of Thailand means that the local sea level is rising at a rate higher than the global average, at 4mm per year (Thanvisitthpon *et al.,* 2018; Gluckman, 2019; Natakun *et al*., 2019). It has a tidal range between 0.1m and 3.9m. Mumbai, found on the eastern coast of India, also has a tropical savanna climate according to the Köppen Climate Classification model. It is subject to increasing numbers of extreme rainfall days, and is located on a low-lying series of reclaimed islands on the Arabian Sea (Koppikar, 2018). Mumbai's tidal range varies between a minimum of -0.2m and a maximum of 4.1m.

Through the TE2100 impact study and assessment, it has been defined that up to 1.3 million people, £275billion in residential property value, 550,000 properties and 40,500 commercial properties are at stake within the tidal flood risk area defined by the Environmental Agency (2012). The London Assembly has however noted that urban infrastructural exposure risk has not yet been assessed using this new CoastalDEM elevation data, where further research has not yet taken place and would add additional value to their research.

Considering that Asian countries are at a high risk of sea-level rise impacts due to their coastal development on low-lying land and exposure to frequent and extreme hydrometeorological climate events, the analysis of their surface urban infrastructure would benefit policy makers and the public to identify high risk prone areas and provide a catalyst for the designation of adaptation strategy projects (Saroar and Routray, 2012; Nguyen and Tran, 2016; Jayaram, 2019).

Through this study, a knowledge gap regarding the urban infrastructural exposure and risk in a developed city (London) using new elevation data would be addressed. The urban infrastructure (such as roads, railways, buildings etc.) that is at higher risk of inundation due to tidal flooding from permanent sea rise could be compared against the findings from the Environment Agency in their 2012 adaptation strategy for the Thames Estuary. This could then be compared against the exposure risk to urban infrastructure in high-risk coastal Asian cities with similar parameters such as age, urban planning style and population numbers. From the report publishing this dataset together with studies undertaken by (Dasgupta et al., 2007; ONEP, 2008; Boyd & Ghosh, 2015; Nguyen & Tran, 2016; Zhang et al., 2019), Asia is among the global regions expected to face the largest percentage of sea-level rise impacts, although globally the level of exposed coastal land is exacerbated by a factor of three or higher than SRTM based elevation data (Kulp & Strauss, 2019). The cities of Bangkok in Thailand and Mumbai in India have been chosen for this study's purpose as they also reflect a similar

regional economic influence. This study would therefore apply this new globally available CoastalDEM data as the basis for understanding how functional structures of these cities would be affected comparatively. This would be done using GIS and statistical analysis tools, which have been found to be suitable for the quantification and visualising of geospatial data in terms of spatial analysis for numerous studies (Demirel *et al.*, 2015; Malik & Abdalla, 2016; Fitton *et al.*, 2018; Nistora, 2018).

1.5.   Objectives

The general objective of this study would be to use GIS software and statistical analysis tools to assess the potential exposure to surface urban infrastructure towards projected sea-level rises using spatially projected urban infrastructure and new elevation model data published by ClimateCentral (Kulp & Strauss, 2019). The cities to be examined comparatively are as follows:

- London, United Kingdom
- Bangkok, Thailand
- Mumbai, India

This analysis would then be used to compare the level of the potential infrastructural exposure between the cities for permanent sea-level rise together with their populations. Although temporary flood protection structures and strategies for the 21st century exist for London (Environment Agency, 2012), amendments to existing local structures such as the Thames Barrier have not yet been made. Such investment and implementation is significantly lacking in Bangkok and Mumbai despite available municipal funds (Boyd & Ghosh, 2015; Jayaram, 2019). The study therefore aims to quantify the loss to potential surface infrastructural assets and number of people potentially affected should no adaptation be applied in the coming decades. The objective will also examine whether climate change from a sea-level rise perspective will affect these three cities to the same extent using the newest available data.

1.5.1. Specific Study Objectives

The specific objectives within this study are to answer the following research questions using geospatial data, GIS analytical tools and statistical calculations:

1. How much of each city's land area is at risk from simulated SLR of 1, 3 and 5 metres respectively?
2. Will SLR simulations using a newer elevation dataset show differences in flooding next to older datasets?
3. Within the three cities, where is the urban infrastructure at risk concentrated? Will this affect the cities' future functionality?
4. Do the measurements of infrastructural layers at risk match across the three cities?
5. How many local residents will be impacted by SLR in each city? Do these numbers match across the three cities?
6. Is a bathtub-fill modelling approach effective in simulating local SLR?

2. Background

2.1. Climate Change and Sea-level rise Literature

Through the assessed studies published by the Intergovernmental Panel on Climate Change (IPCC) as well as scientists monitoring environmental variables over the last 7 decades, it has been found that anthropogenic activity for economic, commercial and industrial purposes have been contributing significantly to the rise in harmful greenhouse gas emissions to the atmosphere such as carbon dioxide, methane and chlorofluorocarbons (CFCs), particularly since the beginning of the 19th century (Solomon *et al*., 2007; IPCC, 2014). The release of these gases increases concentrations in the atmosphere and results in an increase of trapped net incoming solar radiation from the sun, ultimately warming up the atmosphere around the planet and influencing its atmospheric climate. The impacts of this are several and long-lasting, depending on how much the concentrations of greenhouse gases in the atmosphere increase. The main effects of a rising atmospheric temperature have been the melting of ice bodies and glaciers stored particularly near the planet's Poles, together with changes to the movement of air and ocean currents.

Naturally, the global thermohaline circulation model exchanges heat between the Equator (which receives the most incoming solar radiation) and the Poles (which receive the least) across the hydrosphere, atmosphere and cryosphere (Blumberg and Mellor, 1987). Warm water found at the ocean's surface is less dense than cold water found at the sea-bed (Figure 1.1 below). The influence of wind currents also allows the warm surface water to travel faster than the colder sea-bed water.

With direct increasing meltwater volumes from key glaciers and ice stores around the planet (in particular, Greenland in the north Atlantic, the Antarctic continent at the south Pole, and sea ice at the North Pole), denser freshwater inputs disrupt the thermal circulation in the Earth's oceans by slowing them down. This takes place in contrast to the heat increasing at the Equatorial regions, the oceans of which are experiencing higher temperatures than before and building up more water vapour in the atmosphere. This reduced thermal circulation has been modelled to show increases in the frequency and intensity of extreme climatic events such as hurricanes and tropical cyclones, as we have seen in recent decades (Bender and Ginis, 2000; Anthes *et al*., 2006).

Thermohaline Circulation

Red = Surface flow
Blue = Deep flow
Purple = Deepest flow
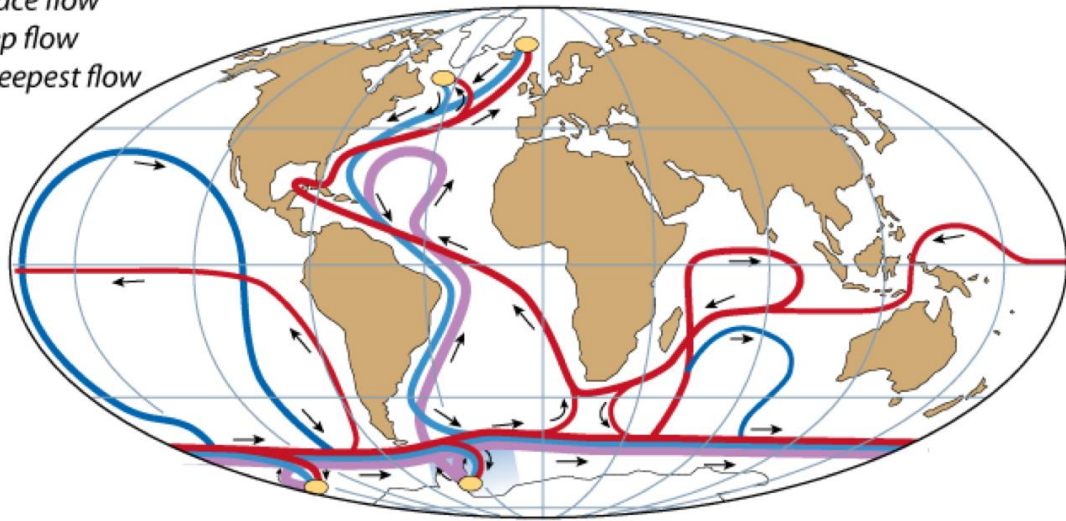
Rahmstorf, 2002

about 1 kyr to make a loop

Figure 1.1: A simplified image of the ocean's thermohaline circulation model
Source: (Ramstorf, 2002)

Storm events releasing a large amount of energy also cause bulges of ocean water at the surface due to a prolonged and sustained exposure to low atmospheric pressure (known as storm surges), which raise localised volumes of water and thus cause more damage when these storm surges meet the land. Furthermore, the phenomenon of thermal expansion to liquids means that the increased inputs of meltwater from ice bodies increases the volume of water present in the Earth's oceans at a higher rate than the volume of ice being melted away (Blumberg and Mellor, 1987; Church *et al*., 1991). The impacts of this occurring are two-fold. Firstly, the expanding volume of the Earth's oceans and increased inputs lead to steady sea-level rise on coastlines around the world. Secondly, the reduction of high-reflectance frozen surface areas lead to the presence of darker surfaces of bare rock, deep ocean or land supporting vegetation in their stead. This darkening of patches of the Earth's surface reduces their albedo (or reflection) effect of incoming solar radiation where some radiation gets dispersed back out to space from the atmosphere. Together with the increasing concentration of greenhouse gases, the land now absorbs more solar radiation than it did before, leading to a positive feedback loop for more ice water in the area melting faster (Church *et al*., 1991; Church *et al*., 2013).

Due to this positive feedback loop trend, future global sea levels are therefore expected to rise faster than they did over the 20th century and extreme climate events are set to increase in frequency and intensity, particularly if the planet's nations do not change their present contributions to greenhouse gas concentrations in the atmosphere. The IPCC predicts in its fifth synthesis report that the global mean sea level will rise by 0.3 – 1.0 metres in 2100 CE relative to the period 1986-2005 CE, depending on various emissions scenarios (IPCC 2014, p.11). Coastlines will be significantly affected, in particular their inhabitants, infrastructural network and indigenous coastline ecosystems (Nicholls and Cazenave, 2010).

2.2. Climate Change Adaptation Strategies to Transport Infrastructure

The world's nations are increasingly responding to these threats of sea-level rise and exposure to intense climatic events through national and regional climate change adaptation strategies. The surface urban infrastructure for three heavily populated coastal cities, namely London (United Kingdom), Bangkok (Thailand) and Mumbai (India), embodies the key study focus for this research study.

2.2.1. Strategies for Climate Change Adaptation to London's urban infrastructure

In the United Kingdom, the National Adaptation Programme aims to raise the availability and accessibility of information to its inhabitants, while enhancing the community spirit of its people to pool their resources together and tackle climate change effectively (Department for Environment Food and Rural Affairs, 2018). For this to happen, flooding risk needs to be taken into account for land use decisions and infrastructural adaptation, while the long-term resilience of the country's coasts, resources and infrastructure needs to be increased (Department for Environment Food and Rural Affairs, 2018; Golding *et al.*, 2019). Where possible, the country also aims to reduce further risk of flooding and coastal erosion through an investment of GBP £2.6 billion between 2018 and 2023, intending to benefit the economy by up to GBP £30 billion. Connectivity infrastructure (such as road networks and railways) are expected to be handled by the organisation operating them, in this case Highways England, city/county councils and Network Rail.

Highways England have released a Progress Report in 2016 highlighting their recognition of the risks to the infrastructure of its key arteries (main roads and high ways) and their next steps to take action (Highways England, 2016). Despite the research into the field, the Adaptation Sub-Committee Progress Report recognises that detailed action plans are limited to internal reference and are not available to the public, while resilience spending plan information on GBP £300 million is also withheld (Highways England 2016, p.22). It is currently working on a Flooding Action Plan under the Environmental Strategy, which is due to be released in 2020. Information on the vulnerability of and adaptation strategies to London's local road network is also lacking within the London Adaptation Strategy and council website, while Network Rail are working to protect eight core routes across the country, one of which contains Greater London (the Anglia route). This is currently in review for the publishing of the Weather Resilience and Climate Change Adaptation Plan for the period 2019-2024, though flood vulnerability maps of the local rail network have not been published at a large scale within the report (Network Rail, 2017).

2.2.2. The Thames Estuary 2100 Plan

Research into the British transport network expresses that effects of climate change are likely to be exacerbated in London since it is the country's capital and economic powerhouse (Clarke *et al*., 2002). The UK is now seen as a leading European country which has developed a framework of action based off the Climate Change Act 2008, assigning policies on climate change impacts to the Department for Business, Energy and Industrial Strategy, and Department for Environment and rural Affairs (DEFRA) (Committee on Climate Change; 2008; Lucas and Pangbourne, 2012). At this time, it was also recognised that existing protection infrastructure against floods within the Thames estuary requires further maintenance and stronger reinforcements. The key structure protecting the urban area of London from encroaching high tides and storm surges is the Thames Barrier, opened in 1982 following a flooding catastrophe event in 1953 to prevent high tides/storm surges higher than 4.87 metres from travelling upstream and damaging property, infrastructure and risking people's safety. The structure is expected to remain operational against storm surges entering the Thames estuary from the North Sea up until 2070 CE, by which time it must be replaced.

In response to this need, the Thames Estuary 2100 Plan has been devised by the Environment Agency (published 2012) in consultation with stakeholders and technical economic and climate experts to study flood risk to the Thames Estuary and its response to global sea-level rise projections. From 2010 until 2034 (overlapping the present date), the active maintenance and upkeep of the existing tidal flood barrier system shall take place at a national cost of £1.2 billion. This is to be followed by a £1.8 billion expenditure until 2050 in the renewal and replacement for relevant defence structures, providing floodplain management activities and intertidal habitat replacement for long-term spatial planning. Following 2050, reviews will be made to the TE Plan where two adaptation options may be selected: either working with existing flood defences and management strategies or constructing a new tidal barrier at Long Reach; the latter of which is suggested to cost in the order of £6-7 billion. This plan is crucial in the future management for the Thames Estuary as it is currently considering changes taking place within the Thames Estuary, including indicators such as sea level, peak surge level, peak river flows, asset condition, barrier operation, development, erosion and deposition, habitat, land use planning and development activities; as well as public/institutional attitudes to flood risk. Of particular value in this instance is the development indicator, as it has found that within the last 5 years, the tidal flood area assessed has seen a total increase from 1.25 to 1.3 million residents, 500,000 to 551,000 residential dwellings, £200 billion to £275 billion in total property value, and 40,500 additional commercial properties. This provides a sound basis for future economic asset and population projections as sea levels rise over the rest of the 21st century (Environmental Agency, 2012).

2.2.3. Bangkok's climate change strategy to urban infrastructure

Recognition of the city's vulnerability to sea-level rise has taken place within the authoritative bodies responsible for Bangkok, in Thailand. The Office of Natural Resources and Environmental Policy and Planning (ONEP) within the Thai national government has published a National Strategy on Climate Change Management in 2008 with a focus on vulnerability, risk and recommended action plans. Vulnerability of the region is dependent on the city's main economic activities, whereby threats to agricultural land, agri-processing functions and tourism are focused on. Upon recognising that more action would be needed to safeguard these assets and economic activities, the metropolitan area teamed up financially with the World Bank to publish a Climate Change and Adaptation Study for Bangkok Metropolitan Region (ONEP, 2008).

Within this report, experts across a range of disciplines provided consultancy advice on the physical and socio-economic actions required to address climate change in Bangkok, particularly focusing on issues relating to changes in inundation patterns, the impacts on the population and socio-economic realm, and coping strategies to handle ongoing climate change in the area. While it is expected that the city will subside between 0.05 and 0.3 metres by the year 2030, storm surge events on the urban infrastructural setting have been simulated to project impacts with 1/10 year, 1/30 year and 1/100 year flooding occurrences with and without land subsidence and storm surge influences. The results of these simulations have found a 30% increase in the flood-prone areas up to the year 2050 with some provinces facing inundation for several weeks at a time. The west of the city will have focused impacts of flooding which are expected to overwhelm existing flood protection structures such as dikes and pumps. This will happen in tandem with an increase in expected discharge volumes from the Chao Phraya River while storm surges are expected to have less of an effect on flooding than the remaining parameters (Webster, McElwee and Worldbank, 2009).

As a result of the above findings, it is expected that in the year 2050 approximately 1 million people will inhabit frequently inundated areas by flooding, facing local water levels of about 0.5 metres above ground. The economic damage is predicted to reach USD $1 billion in 2050 at the current conditions, rising to USD $4.22 billion in the A1F1 climate change scenario as predicted by the IPCC. 70% of this cost will be due to land subsidence, exacerbated by incoming high volumes of rain and seawater. 300,000 buildings are expected to be mostly impacted by flooding in 2050, exceeding USD $3.14 billion in damages to existing and new structures. Industrial and commercial enterprises are also expected to face a loss of income of USD $0.29 to 0.63 billion respectively (Babel, 2009).

The findings stress that action needs to be taken to raise awareness of the issues from climate change, a shift in policies to favour climate change adaptable strategies in the local area and studies outlining potential strategy solutions for the city in future, with an emphasis on the urgency required. Since the publishing of this report ten years ago, studies on impacts from

climate change and flood vulnerability in the city have focused on qualitative interviews with local residents and assisting policy instruments to devise suitable strategies for climate change management, rather than quantifying the expected impacts on local urban infrastructure (Thanvisitthpon, Shreshta and Pal, 2018; Natakun *et al*., 2019).

2.2.4. Mumbai's climate change adaptation strategy situation

The efforts in Mumbai are significantly different to the strategies and economic implications of climate change impacts to London and Bangkok. Although the Municipal Corporation of Greater Mumbai, also known as the Brihanmumbai Municipal Corporation (BMC), is responsible for the city's infrastructure, administration, water and health sanitation within the city whilst also acting as the city's main governing body, it invests little in the way of research efforts and funding into recognising the current impacts faced by climate change and adapting the local urban infrastructure accordingly. Shaped by legal, financial, socio-cultural and technological instruments, adaptation within the area would require the cooperation and conjoined effort of multiple municipal departments, experts and stakeholders (Tol, 2007; Boyd & Ghosh, 2015; Adam, Parthasarathy & Narayan, 2018).

In 2005 (14 years ago), a 1 in 200 year-event flood hit the city, resulting in 100 km^2 of inundated land, over 1000 deaths, the damage of property reaching up to USD \$407.9 million (USD \$145.6 million of which was damage to urban infrastructure alone, such as railway lines, road networks, air services, the local port and key economic buildings). Up to 100,000 people are estimated to have been displaced in the flood event, where 945 millimetres of rain fell in 24 hours (Boyd and Ghosh, 2015; Adam, Parthasarathy & Narayaran, 2018; Singh, 2018). The results of such a flood event were made worse by the lack of urban planning in the region and lack of adaptable structures installed to safeguard the local population from such events. Since this event, floods still impact the region on an almost yearly basis due several factors, including the warming Arabian Sea, the low-lying geomorphological composition from having been settled on reclaimed land, and the increased urban development on the peninsula, steadily eroding the city's available vegetation to absorb and retain excess moisture in the ground (Ranger *et al*., 2011; Butsch *et al*., 2016). Three types of flooding, namely isolated localised flooding, flooding due to the overflowing of existing shallow watercourses such as the Mithi River, and the combination of high river flows with high tide cycles, preclude the efficient drainage of excess water from the urban setting and allow it to accumulate rapidly. This is further exacerbated by the deposition of silt and mud from nearby agricultural land and eroded land cleared for urban development.

In response to these floods, the BMC sought to develop the Brihanmumbai Stormwater Disposal System to increase the capacity of drainage of excess water from the city's urban area and set up pumping stations to clear out water that has been blocked from drainage. This is however still in Phase 1 of the greater plan after 14 years, due to bureaucratic struggles, administrative processes and land acquisition laws together with political lack of will. The project was initially expected to cost USD $364.2 million, but this has increased to USD $655.74 million by the year 2017 and is still far from complete. According to the BMC, the city was ready to handle its annual rainfall amounts and successfully drain the water around the Mithi river in 2015, when it spent USD $29.15 million to build 6 pumping stations since 2011. The statement has however not comforted local residents, who still face inundation due to flooding year in year out. Climate Change Adaptation Strategies have not been yet implemented into the city's local policy decisions, while the city's peninsula shape and extensive exposure to the Arabian Sea continue to act as challenges in the way of setting up offshore flood protection infrastructural projects (Ranger *et al*., 2011; Boyd and Ghosh, 2015; Butsch *et al*., 2016; Adam, Parthasarathy & Narayaran, 2018; Singh, 2018).

2.3. Urban Infrastructural Exposure to Inundation Scenarios

Calculating potential exposure levels of urban infrastructure can be done through several methods such as multi-criteria analyses, classification trees, geographic data overlays and risk classification. The data inputs utilised for such purposes in similar studies by Abuodha and Woodroffe (2010), Arnesten (2019), Demirel *et al.* (2015), Johnston *et al.* (2014), Malik and Abdalla (2016) and Nistora (2018) have been similar, focusing on the following information:

- Raster data: **Digital Elevation Model** (DEM) data or its derivatives (surface or terrain models)
  - o This is point data storing information regarding a location's elevation above mean sea level, typically in a text file format or a geo-referenced raster grid format. The size of the grid cells depends on the resolution of the data (for example 30m resolution means that points are spaced out equally 30m from each other in the latitudinally and longitudinally)
- Raster data: **Storm surge/tidal data** (where available)
  - o This contains information containing locations of where storm surge/tidal information was captured, together with its value. Raster 8-bit unsigned GeoTIFF format datasets may also be available containing inundation bins at predefined measurements (such as 0.3 m in vertical height above mean sea level).
- Vector data: **Layers of urban infrastructure**, often including line features (roads, railways), polygons (key economic facility footprints) and points (locations of local services, industries and assets)
  - o These may be downloadable from multiple authority or open data sources and contain individual files with geometric vector data capturing points (such as points of interest), lines (such as road links) and polygons (such as protected areas). They are generally compatible with a wide range of GIS software tools such as ESRI, MapInfo and QuantumGIS (QGIS).
- Vector data: **Hurricane evacuation zone layers** from past events (where applicable)
  - o Information captured as polygons attributing municipalities with zone numbers or risk values to use within GIS applications, or data isolating regions which have previously been evacuated. These areas come projected to a referenced coordinate system to match the areas they serve and contain information about the historic event's date, severity, wind speed and potentially also wave height.

The above layers have been analysed against each other in the aforementioned studies to understand the following:

- Risk and vulnerability assessment levels for the local infrastructure
- Consequence mapping via multi-criteria analyses
- Adaptation cost scheme opportunities at specific, systemic and regional levels

- Relationships between predictors for evaluating evacuation efficacy (using classification trees and random forest methods)
- Accessibility and connectivity measures (using indices for elements such as network density, graph density, detours, geodesic distances and clustering of road network node points)

The data used has however been focused on higher value infrastructure where lower value information has been either omitted or discussed at a surface level. For example, when looking at road networks at risk of inundation by sea-level rises in the South-East of Spain and Scania in Sweden, the authors only extracted the functional classes of the roads with key arterial properties, which are state-owned (Demirel *et al.*, 2015; Arnesten, 2019). While these roads are key to the communication capacity of local communities and spread of people and goods, they do not address service roads or links that join residential areas to the main arterial network. When looking at the likely impacts involved by extreme weather conditions, vulnerable areas can be adapted and made more resilient through assets information within those areas.

The accuracy of data analyses depends on the level of inputs provided and translatable information from them, however more data also leads to longer processing times, the requirement of data filters to maximise computing processing memory, and additionally increased disk storage occupation. Within these studies, DEM data with varying resolutions were used. The highest resolution (approximately 30 metres or 1-arcsecond per grid cell side) was deemed optimal for evacuation model purposes, whereas other vulnerability studies used low resolutions (90 metres per grid cell side) (Johnston *et al*., 2014; Demirel *et al*., 2015; Malik & Abdalla, 2016; Nistora, 2018; Arnesten, 2019). The latter leads to larger generalised areas of infrastructural vulnerability in flood events, assuming that all elements within a vulnerable grid cell will be inundated and therefore unusable (Demirel *et al*. 2015, p.68). Often, this is not strictly the case, as infrastructure may be only partially submerged and still available for use.

Generalised data sources could thus be applied across the world with successful results for understanding sea-level rise impacts to a region. The methodologies mentioned above all provide specific and quantified information regarding coastal urban infrastructure vulnerability, economic impacts and potential adaptation strategies for future planning. Their similarity depends ultimately on the purpose of the research and the audiences they're intended for (whether the academic communities, the general public or local authorities/decision-makers). As such, equal methods for different locations will yield varying accuracy results depending on the locations' environmental and topographic parameters. With this study, the same sources of data and methods will be used across three locations within the Pacific and Atlantic Oceans, in order for vulnerability comparisons to be made and analysis on the feasibility of applying the same procedures to be examined

3. Data & Methodology

3.1. Study Area

This research project will focus on three greater metropolitan areas found in different locations around the Earth. Due to the nature of the project, only the coastal and drainage catchment areas for major river networks within these boundaries are expected to be analysed in the project results. The cities are as follows:

London (51.09°N, 00.11°W), as the capital city of the United Kingdom, covers a greater metropolitan area of 1,569 km^2 known as the London Basin and inhabits 9 million people (as estimated for 2018) (Office for National Statistics, 2019). The city was founded in the south-east of the country in approximately 50CE (as part of the Roman Empire) and is focused towards the mouth of the river Thames, which splits the city in half horizontally as it extends from west to east. The Thames has a tidal range of 6.5 metres (amplitudes of 0.5 to 7 metres above mean sea level), which fluctuates every 5 to 9 hours (Meteo365.com Ltd, 2019). The city mostly lies on Tertiary sediments and surrounds the Thames floodplain, which has a gradually sloping topography towards highest points in the North and South of the city. In this area the Köppen climate classification is a temperate maritime climate, where average temperatures range between 7 and 15 °C and precipitation average values hover at about 650mm per year (WeatherBase, n.d.). The city is periodically influenced through the river Thames by tidal and storm events in the North Sea (McRobie, Spencer and Gerritsen, 2005). The infrastructure for the surface transport network in London has radiated outwards over time from the original City of London settlement. When the infrastructure was first laid out, buildings were made of wood and were of low durability. This meant that they were assembled in a haphazard manner at angles from each other and did not necessarily face the same direction along main transport links. Goods and people were transported manually using horse-drawn carriages, with the poorer inhabitants using the roads as communal spaces. Following the industrial revolution, roads were sealed and railway lines across and underneath the city began to be built, however with the exploding population the infrastructure also expanded outwards in an unplanned fashion. It was only in the 20th century that planning and zoning became a key component in the consideration of urban sprawl (Fainstein, 1994).

Bangkok (13.74°N, 100.52°E) is the capital city of Thailand and is located approximately 40km upstream of the Chao Phraya River estuary that feeds into the Gulf of Thailand. Settlement first began in the 15th century CE on two municipalities – Krung Thep and Thon Buri. Both municipalities were merged in 1971 and have developed into a large cosmopolitan city, contrasting against the rest of the country which contains villages and small towns with low populations. The city's metropolitan area is 1,565 km^2 in size, with 10.3million residents (World Population Review, 2019). This makes it comparable to London as a global megacity, and is a hub for tourism, industrial and commercial activity. Since its foundation, the city has

faced a large amount of growth in all directions; urban planning was not an instrument for controlling urban infrastructure until the mid-20th century. Inhabitants spend a large portion of their time around the city's ports which bring goods from neighbouring trade suppliers. Thai locals are highly religious and place large temples and religious shrines in strategic locations around the city. The city's historical centre is located on an artificial island cut into land near the Chao Phraya River bank, where temples such as the Grand Palace, Wat Phra Kaew and Wat Po were built (Encyclopaedia Britannica, n.d.). In a crowded, compact metropolis such as this, residential and market areas are intersected with a series of narrow back alleys and roads. Since the invention of cars and rail transport, development of the city's infrastructure led to the widening of existing roads and demolishing make-shift structures. Bangkok is one of the most congested cities worldwide, which restricts functionality and connectivity even in dry, mild conditions. This is more pronounced in monsoon season where many key arterial and small local roads flood and the underground drainage channels overflow (Boonya-aroonnet *et al.,* 2002). The local climate is a tropical savanna, where rainfall is concentrated into a monsoon season between April and October. The city experiences average temperatures of 28.1 °C and annual precipitation of 1430 mm. The Chao Phraya River has a tidal range of 3.7 metres (amplitudes between 0.1 and 3.8 metres above mean sea level) (WeatherBase, n.d.; Meteo365.com Ltd, 2019).

Mumbai (18.58°N, 72.49°E), known as the commercial capital of India, makes it a megacity comparable to London where it also serves as India's financial powerhouse and most cosmopolitan city in terms of inhabitants and cultures. It is located on the east coast of India in the state of Maharashtra, and is directly exposed to the Arabian Sea. Greater metropolitan Mumbai occupies an area of 4,355 km^2 at an average elevation of 14 metres above sea level, with approximately 20 million inhabitants (United Nations, 2018). This gives it an average population density of 4,600 people per square kilometre, concentrating a large number of people into a small low-lying area. The city, built on a previous archipelago of seven islands (Isle of Bombay, Parel, Mazagaon, Mahim, Colaba, Worli and Little Colaba) was not significantly populated until the early 16th century, when the Mughal Empire offered the islands to the Portuguese. This influence encouraged the development and growth of the city which was then given to the English in the mid-17th century. At this point, due to its strategic location, the population began to grow significantly from 10,000 in 1661 CE to 100,000 in 1780 CE, when the seven islands were merged through the Hornby Vellard causeway (Mumbai.org.uk, n.d.).

These were fully merged in 1845 through land reclamation, when the city's first railway lines were established to connect the city to nearby towns. With the industrial revolution, the city's commercial and strategic importance grew after the construction of the Suez Canal in 1869 (Fletcher, 1958). The close quarters at which people lived and traded encouraged a narrow transport infrastructural network, now developed into a mass transit metro system since 2014 including a suburban rail network transporting up to 8 million passengers per day. Its exploding population in the last 100 years from 1 to 20 million has resulted in a highly congested, polluted

cluster of roads, buildings and railways, and the city places low priority on urban planning practices (Gupta, 2007). As a result, the dense, haphazard network within the city slows down traffic and reduces accessibility to flee vulnerable areas in times of flooding. Mumbai also has a tropical savanna climate like Bangkok; it is however slightly cooler with an average temperature of 27.2°C and has a higher precipitation of 2400mm annually. The rainy season lasts from June to October, where the maximum rainfall generally falls in July and frequently leads to waterlogging of the city's drains and roads (WeatherBase, n.d.; Meteo365.com Ltd, 2019). The city has a tidal range of 4.9 metres (amplitudes of -0.2 to 5.1 metres above mean sea level).

3.2. Data

From relevant and similar studies (Demirel *et al.,* 2015; Hande *et al.*, 2015; Dawson *et al.*, 2016; Malek & Abdalla, 2016; Habel *et al.,* 2017; Xie *et al.*, 2017; Nistora, 2018; Arnesten, 2019), the following data has been used for the study, based on personal ability to access and process organisation specific and open sourced data:

- Urban infrastructure (road networks, railways, building footprints, parks, city boundaries) in vector format from **HERE**.
    - o For the specific purposes of this study, **HERE Navstreets** in ESRI Shapefile format (version Q4-2019) was deemed suitable, rather than through relational database format (RDF).
    - o HERE was chosen as a data source as it offers global coverage of geospatial data maps with frequent (three-monthly) updates. HERE layers are highly compatible with navigation applications and are delivered in GIS-ready data formats.

- Digital elevation model (DEM) data for the United Kingdom, Thailand and India, as explained within Section 1.3 of the Introduction chapter:
    - o **SRTM (Shuttle Radar Topography Mission)**
        - ▪ The data was downloaded for all three study areas in 1 arc-second (~30 metre) spatial resolution and GeoTIFF raster format. It was available following registration at the United States Geological Survey (USGS)'s Earth Explorer portal.
    - o **JAXA (Japanese Aerospace eXploration Agency): ALOS World 3D – 30 m**
        - ▪ Like with SRTM above, the data was downloaded in 1 arc-second (~30 metre) spatial resolution and GeoTIFF raster format for all three study areas. For this, access to the JAXA portal following registration was required.

- o **CoastalDEM**
  - ▪ This dataset was made available by Climate Central in October 2019 following the publication of their machine learning numerical algorithm methods to increase accuracy by repairing artefacts and data gaps in available elevation models. The Interactive map published at http://coastal.climatecentral.org communicate the findings discussed in Kulp and Strauss' scientific report.
  - ▪ This data is available for download at through Climate Central's website, following correspondence expressing my interest with contacts from the Climate Central organisation. Data is only available for free at a 3 arc-second (~90 metre) spatial resolution, however budgetary constraints for this study prevented me from accessing the data at a 1 arc-second (~30 metre) spatial resolution.

- Population numbers for coastal areas:
  - o **WorldPop** gridded raster cell population data (in 3 arc-second/~90 metre spatial resolution), made available on the WorldPop website portal, was downloaded for the three study areas.
    - ▪ Although varying spatial resolutions are available from different sources for each of the study areas (Open Census data for the UK in 1 kilometre resolution, High Resolution High Density Maps for Thailand in 1 arc-second/~30 metre resolution), WorldPop has been used to provide a consistent spatial coverage for comparison across the study areas.
    - ▪ The population data for 2019 was downloaded; chosen as a year to match the vector HERE data above and the latest DEM used in the study (CoastalDEM). This would facilitate contextual temporal comparisons in the discussion stage of the research findings.

3.3. Methodology

The methodology has been applied and described below for a total of nine times: three times for each digital elevation model (DEM) dataset (JAXA, SRTM and CDEM) and three times for each city (Bangkok, London and Mumbai). The steps described may be followed by referring to the simplified methodology flow chart presented in Figure 3.1 below.

3.3.1. Preparing of the HERE vector data

In order to apply GIS interaction tools and methods with the downloaded DEM data, preparation of the HERE vector data containing the cities' urban infrastructure in different layers was required. After downloading and extracting the source HERE Navstreets data in ESRI Shapefile format, the folders containing the coverage area of interest were isolated with the others removed to save on storage space and processing time. The layers containing data for the streets, railways, buildings and parks were spatially projected to an equidistant cylindrical map projection (EPSG:4087 - chosen for its accuracy in calculating real-world lengths and areas) and intersected with the administrative district boundaries layer available in the source folder. This step was necessary to split lines and polygons according to the city districts, from which the name properties were spatially joined to attribute the correct city district name to each feature available in the vector data.

The administrative district boundaries within the greater metropolitan region for one city were then selected and extracted into a new layer, which was ultimately dissolved to provide a single polygon feature for clipping of the data. Clipping the vector data layers was required in order to isolate the vector data of interest and remove the features falling outside of this area. Following this stage, geometric lengths and areas were calculated for the line and polygon features in units of kilometres and kilometres squared respectively.

The oceans and water network (watercourses and hydrological stores) were merged and dissolved to provide a baseline vector layer showing all existing water bodies within the city. These were not clipped to the greater metropolitan region above, instead filling the coverage of the source data folder (which generally extended beyond the metropolitan area). The reason for this was to apply sea-level rise spread accurately to watercourses and stores along the border of the city's metropolitan area.

3.3.2. Preparing the DEM raster data

Prior to intersecting the raster with the vector data, the source DEM data required compatible preparation. Through the source portals, the correct raster data for the three cities was downloaded in 1° (degree) latitude/longitude tiles with the following coverages:

- <u>Bangkok</u>: 13°N to 15°N (latitude), 99°E to 101°E (longitude)
- <u>London</u>: 51°N to 52°N (latitude), 1°W to 1°E (longitude)
- <u>Mumbai</u>: 18°N to 20°N (latitude), 72°E to 74°E (longitude)

These tiles were then merged into one raster dataset for the city being processed, before being re-projected to the EPSG:4087 Equidistant Cylindrical projection to match with the HERE data above. Values within the raster DEM file were converted to integers, which were used as a base data type before reclassifying the source DEM data. Reclassification of the data allowed values between the lowest sea level (estimated at -100m above mean sea level) and 0 through 5m to be extracted individually, resulting in six levels: an area covering the present-day water level, together with five levels containing areas of modelled sea-level rise to 1 through 5 metres respectively. Each of the resulting layers was converted to a vector polygon layer in ESRI Shapefile format, to match the data types and formats between the HERE and DEM datasets.

3.3.3. Simulating landward flow of ocean water

In this step, all the features were selected from the merged baseline water vector data supplied by HERE. From this, only individual data areas (in polygon-type cell blocks) of a -100m to 1m DEM reclassification which touched the boundary of the water vector data were selected. These were saved as a new vector layer, from which a union geoprocessing tool was applied to join this to the HERE water vector data. The result was then dissolved and saved, where one polygon area for the modelled sea-level rise at 1 metre was the output. This was used consequently when extracting the contiguous 2m DEM cell blocks, and repeated one layer at a time until five polygon areas were saved:

- A merged water baseline area with contiguous 1m cells: 1m SLR (high-risk)
- A merged modelled 1m SLR layer with contiguous 2m cells: 2m SLR
- A merged modelled 2m SLR layer with contiguous 3m cells: 3m SLR (medium-risk)
- A merged modelled 3m SLR layer with contiguous 4m cells: 4m SLR
- A merged modelled 4m SLR layer with contiguous 5m cells: 5m SLR (low-risk)

3.3.4. Preparation of the population data

This step was then required in order to use the population data within the GIS analysis by understanding it in relation to the SLR layer extents. A single raster data tile including the population data was downloaded for the country of interest from the WorldPop portal. This was re-projected to the EPSG:4087 equidistant map projection used above and converted to contain integer values. From here, the centroids of each raster cell containing the population value for each 100 x 100m cell were converted to point features in ESRI Shapefile (vector) format. The point features were clipped to the city's metropolitan area as prepared in Step 3.3.1 above, and spatially joined with the city's administrative district areas to apply the district names to the population points. By summing the population values grouped by administrative district area, the total counts of population affected by a specific SLR scenario would then be extracted.

3.3.5. Clipping the urban infrastructure and population data to the SLR areas

Each of the urban infrastructure layers (Streets, Railways, Buildings and Parks) as well as the population data were clipped to each layer extracted from Step 3 above, retaining the original feature types (lines, polygons and points). This resulted in a total of twenty-five clipped vector layers for that particular city, organised as follows (where 'City' and 'DEM' were renamed to correspond to the appropriate city and DEM processed):

- 'Streets_City_DEM_1m' through 'Streets_City_DEM_5m'
- 'Railroads_City_DEM_1m' through 'Railroads_City_DEM_5m'
- 'Buildings_City_DEM_1m' through 'Buildings_City_DEM_5m'
- 'Parks_City_DEM_1m' through 'Parks_City_DEM_5m'
- 'Population_City_DEM_1m' through 'Population_City_DEM_5m'

The results were given new attribute columns, where the clipped line lengths and polygon areas were calculated in kilometres and kilometres squared respectively. At this stage, each layer contained a field with the lengths and areas of the original line and area segments, as well as a field with the clipped lengths and areas of that segment.

3.3.6. Statistical Analysis

The statistics from the outputs of the above steps were extracted to understand the proportions of infrastructure and population data that would be impacted from a permanent sea-level rise as modelled from the original datasets. This was done using ArcMap and Microsoft Excel, where total lengths/areas/population counts and clipped lengths/areas/population counts were summed for each administrative district boundary and compared to the total numbers for the city as a whole. From Microsoft Excel, tables were organised to align with each of the null hypotheses as below:

- o **H$_0$**: There is no significant difference in how much land area is at risk of SLR using the three different SLR models (Japanese Aerospace Exploration Agency, Shuttle Radar Topography Mission, CoastalDEM).
  - ▪ H$_0$ will help to answer Specific Objective 2
- o **H$_1$**: There is no significant difference in how much urban infrastructure is impacted by increasing SLR simulations (for any one SLR model).
  - ▪ This focuses on whether the amount of infrastructure at risk is proportional to the SLR amount. Testing will use total lengths for line layers, total areas for polygon layers, and total counts for the population layer.
  - ▪ H$_1$ will help to answer Specific Objective 3
- o **H$_2$**: There is no significant difference between the amount of a city's land area and each of its urban infrastructural layers flooded by permanent SLR.
  - ▪ This focuses on urban infrastructural layer exposure in each city.
  - ▪ H$_2$ will help to answer Specific Objective 3
- o **H$_3$**: There is no significant difference between the quantity of infrastructure inundated across the three study areas.
  - ▪ This hypothesis tests the three cities' infrastructure planning paradigms with regards to SLR as well as quantifying the infrastructure layers comparatively for the same SLR scenarios.
  - ▪ H$_3$ will help to answer Specific Objective 4
- o **H$_4$**: There is no significant difference between the total population numbers impacted by permanent SLR across the three study areas.
  - ▪ H$_4$ will help to answer Specific Objective 5

3.3.6.1. Kruskal-Wallis statistical testing

The data tables were subsequently loaded into IBM SPSS Statistical Software (version 25) and Kruskal-Wallis H-tests were performed on the data. The variables were set up as follows:

- **Independent variable** (1, with 3 categories/groups):
  - o The administrative boundaries of each city, sampled for a 1 metre, 3 metre and 5 metre sea-level rise.
- **Dependent variables** (18 in total):
  - o Length of roads permanently flooded (by SLR models 1, 2 and 3 respectively)
  - o Length of railway lines permanently flooded (by SLR models 1, 2 and 3 respectively)
  - o Area of buildings permanently flooded (by SLR models 1, 2 and 3 respectively)
  - o Area of parks permanently flooded (by SLR models 1, 2 and 3 respectively)
  - o Counts of populations affected (by SLR models 1, 2 and 3 respectively)

3.3.6.2. Assumptions of the Kruskal-Wallis H test

Initially, the main assumptions of the test (as explained by Lærd Statistics, n.d.) were checked and confirmed using statistical software such as SPSS prior to conducting the Kruskal-Wallis H test. These assumptions apply as follows:

- **Assumption 1**: The dependent variable should contain values of the ordinal or continuous (interval or ratio) type, whereby the dependent variables mentioned above rely on continuous values.
- **Assumption 2**: The independent variable should comprise 2 or more categorical groups (there are three groups that apply to the independent variable above).
- **Assumption 3**: Observations need to be independent, where no relationship exists between groups or between individual observations. Above, each administrative district for the study areas is listed separately.
- **Assumption 4**: The distributions in each group need to have the same shape in order to compare median values; if shapes of distributions vary between the groups, only mean ranks can be compared.

3.3.7. Calculating Risk Indices

The statistics in Microsoft Excel as prepared earlier were then calculated into multi-criteria risk indices to quantify the level of risk involved for each city district and how this compares with other districts and elevation dataset models. The calculations were performed thus:

1. $$R + L + U + P + O = A$$ - Equation 1

2. $$\frac{A}{A_{MAX}} = B$$ - Equation 2

3. Risks (totalling 100% or 1.0) were weighted across the SLR extents as follows:
   - 1m rise = 60% (0.6)
   - 3m rise = 30% (0.3)
   - 5m rise = 10% (0.1)

4. The three measurements for each elevation dataset (9 columns) were merged into one per elevation set (3 in total) using the following weighted attribution:

5. $$(B_{1M} * 0.6) + (B_{3M} * 0.3) + (B_{5M} * 0.1) = C$$ - Equation 3

6. $$\frac{C}{C_{MAX}} = D$$ - Equation 4

- D shows a scale of relative indices with the maximum value set as 1 and minimum value as 0

Where:

- R = (Roads length * Roads proportion)
- L = (Railways length * Railways proportion)
- U = (Building areas * Building proportion)
- P = (Park areas * Park proportion)
- O = (Population affected * Population proportion)
- A_{MAX} = The maximum value of A from Equation 1 for a particular city
- B_{1M} = The 1m value for Step 2
- B_{3M} = The 3m value for Step 2
- B_{5M} = The 5m value for Step 2
- C_{MAX} = The maximum value of C from Equation 3 for a particular city

The three columns from Answer 4 (JAXA, SRTM, CDEM) were then averaged into one Risk Index column populated by value D, and then joined to the city district polygon feature attributes before visualisation using ESRI ArcGIS.
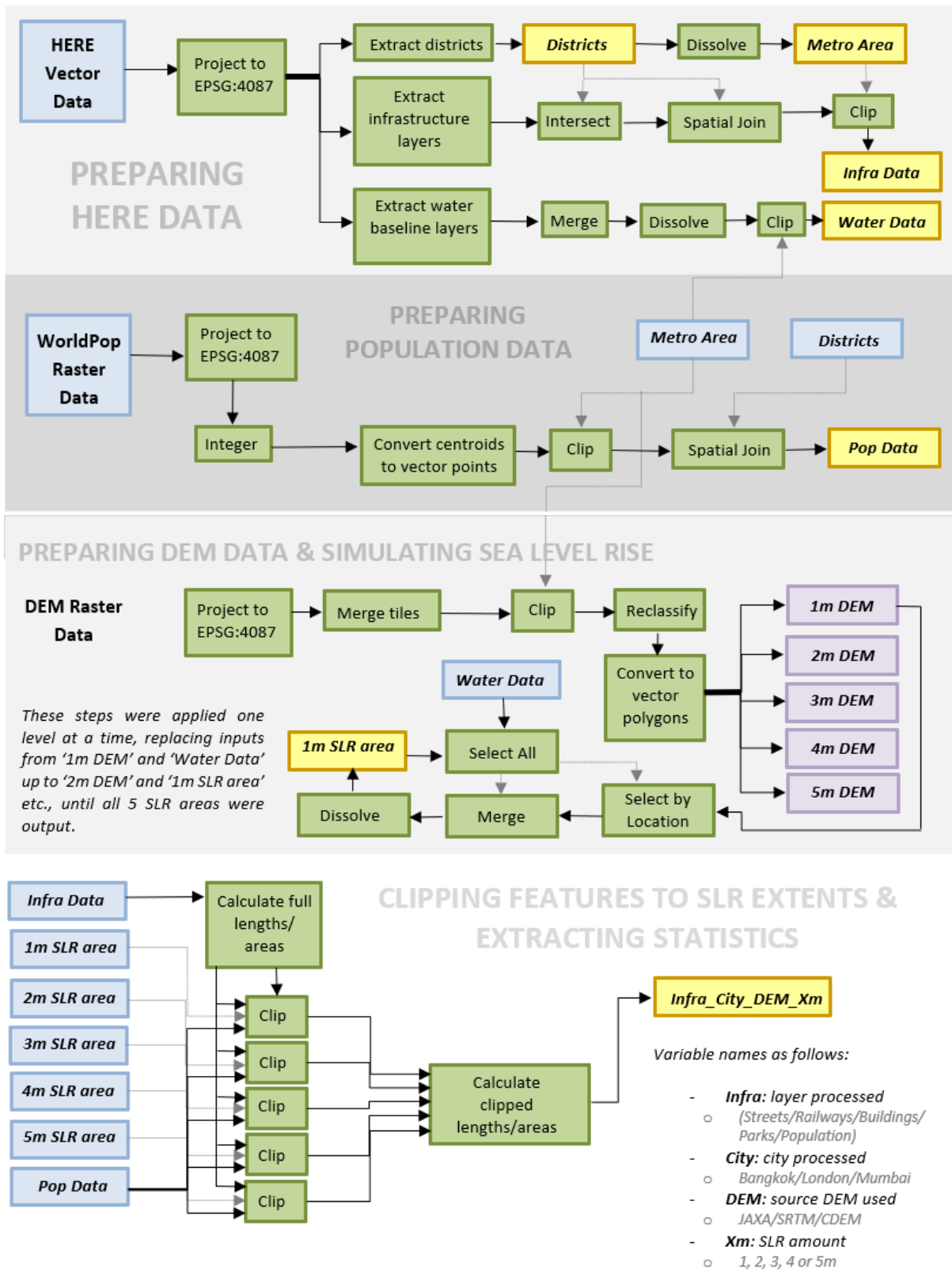
Figure 3.1: Simplified flowchart followed for methodology steps. This flowchart was repeated nine times: three for each study area and three for each DEM input dataset used.

4. Results

As the methodology has taken place for three different elevation datasets but with the same urban infrastructure and population data across three infrastructurally similar cities, this chapter will focus on a comparative approach communicating the findings based on city and sea-level rise (SLR) extent. The focus of this study looks at the difference in results between the previously available JAXA and SRTM elevation datasets, and the newly available CDEM dataset.

The SLR extents have been visualised in the GIS maps as follows:

1-metre sea-level rise = high-risk

3-metre sea-level rise = medium-risk

5-metre sea-level rise = low-risk

The three cities have also been attributed with predefined colours throughout the results for ease of reference when comparing the numbers and maps:

Bangkok

London

Mumbai

4.1. Sea-level rise encroachment extents

The figures for showing visual representations of the SLR inundation extents across the three cities modelled for each elevation dataset are included within this chapter, as well as in more detail in Appendix A.

4.1.1. Objective 1:
How much of each city's land area is at risk from simulated SLR of 1, 3 and 5 metres respectively?
- This objective is answered using simulations in the GIS analysis stage (Methodology Step 3.3.3 above)

Traditionally, the JAXA and SRTM datasets were used as bases to define the extents of permanent SLR across several global cities using a bathtub modelling approach. In this study, these two datasets have been processed in order to compare quantitatively and visually with the findings from the newer CDEM dataset. Table E1 lists the area extents modelled for each city and dataset, while Figures 4.1 through 4.9 below represent this data visually. The resulting numbers and proportions using the SRTM and JAXA elevation datasets were found to be similar due to their technical properties described in Chapter 3, and have therefore been averaged in a set of columns labelled JAXA-SRTM. The results of the original datasets were kept available nevertheless. The JAXA-SRTM columns allow for a clearer comparison between the JAXA-SRTM results and the CDEM results, showing how the traditional datasets vary next to the newer one while keeping this chapter more concise.

The city with the lowest proportions of land found to be at risk from SLR is London, while the proportions of Mumbai and Bangkok at risk depend on the level of risk modelled (Figures 4.1 to 4.9 below). The topography of the three cities as well as their built foundations as defined in the Study Areas chapter partly explain this vulnerability, whereby Bangkok is built on low-lying, gently sloping marshland, London is built around the river Thames where high river bank walls have been constructed to manage flood risk from historic events, and Mumbai's economic hub is built on reclaimed land over several islands. The location of London further inland from the national coastline than Bangkok and Mumbai also helps to explain its lower risk.

In a high-risk scenario, the JAXA-SRTM data found that 1.8 % of London will be inundated from a permanent SLR of 1m above present-day mean sea level, whereas 7.8 % of Mumbai and 5.0 % of Bangkok would be at risk. These numbers contrast with the higher proportions of the CDEM dataset, which attribute proportions of 2.1 %, 9.8 % and 5.8 % to the three cities respectively (Figures 4.1 to 4.9 and Appendix E: Table E1). This puts Mumbai at

greatest risk of inundation according to the models, particularly as the CDEM data considers large proportions of its CBD at sea level unlike the other two datasets.

In a medium-risk scenario of 3m SLR, the JAXA-SRTM averages show that 3.4 %, 14.4 % and 18.7 % of London, Mumbai and Bangkok's city areas would be at risk, where the numbers increase to 5.5 %, 21.4 % and 50.9 % respectively from the modelled CDEM data (Table E1). The differences in figures between the datasets for Mumbai and Bangkok are significant, especially in the latter case where over half of Bangkok's city area is projected to be at risk from such a rise, comparing with just under a fifth from the earlier elevation datasets.

These proportions rise further in a low-risk SLR scenario of 5m, where the JAXA-SRTM averages at 5.5 %, 18.2 % and 58.0 % show much lower proportions of London, Mumbai and Bangkok at risk of submersion than the CDEM values of 13.2 %, 26.5 % and 91.5 %. Under this scenario, over a quarter of the city of Mumbai will be submerged while nearly the full area of Bangkok will be underwater.

4.1.2. Objective 2:
Will SLR simulations using a newer elevation dataset show differences in flooding next to older datasets?

- **H$_0$**: There is no significant difference in how much land area is at risk of SLR using the three different SLR models (Japanese Aerospace Exploration Agency, Shuttle Radar Topography Mission, CoastalDEM)

The differences in land area shown to be at risk of flooding between the traditional elevation datasets (JAXA and SRTM) and the newer CDEM data is significant. The vertical errors found in the SRTM and JAXA data seem to be more noticeable in the cities' business district areas, where clusters of tall buildings are present. This effect is more pronounced in the geographic comparison of flooded areas particularly in Bangkok and Mumbai.

4.1.2.1. Bangkok

The JAXA elevation dataset shows only a coastal area in the centre-south of the city at risk from a 1m SLR, while a 3m SLR spreads on land to the east surrounding the city centre together with a pocket of land in the north west (Figure 4.1). A 5m SLR shows flooding covering most of the city's metropolitan area (59.2 %). In contrast, the SRTM data (Figure 4.2) shows the whole southern part of the metropolitan area (exposed to the coast) at risk from even a 1m SLR, while a 3m SLR spreads to the city's east and north west. On the whole however, slightly less of the city's total area is at risk of flooding in a 5m SLR scenario (56.8 %), even though this

dataset also shows the land at risk to be similar to the JAXA data. The CDEM data (Figure 4.3) shows mostly the same southern belt at risk as the SRTM model, however much of the city is now at risk from a 3m SLR. The areas at 5m risk cover nearly the whole city, including the majority of the city's central business district (91.5 %).

4.1.2.2. London

London is at risk from SLR only on the riverbanks of the River Thames that feeds the city from the North Sea to the east. Minimal differences are visible between all three elevation datasets in a 1m SLR scenario, where the land at risk is concentrated to the east side of the city and varies between 1.7% and 2.1% (Figures 4.4 to 4.6). With a 3m rise, the land flooded from a 1m rise radially spreads about 1-2 kilometres to the north and south, with the JAXA and SRTM datasets showing similar proportions at risk (3.3 % and 3.6 % respectively). In the CDEM elevation dataset, the land at risk from a 3m SLR also spreads north along the river banks of the River Lea and further west to cover the highly economic Canary Wharf area, totalling 5.5 % of the city's area at risk. This area is not at risk of flooding in the traditional datasets until a 5m rise scenario, where 5.3 % to 5.8 % of the city is at risk. The CDEM data in comparison (Figure 4.6) shows that flooding from the river Thames will spread further north and west, to cover 13.2 % of the city metro area.

4.1.2.3. Mumbai

Figures 4.7 to 4.9 show a significant difference in the land at risk of submersion by SLR in all three elevation datasets, particularly with a 1m rise. Here, the city's coastal suburbs to the west are at particularly high risk of flooding in the SRTM data (9.5 %), while less of this land is visible in the CDEM data and the least land in the JAXA data (6 %). The JAXA and SRTM data (Figures 4.7 and 4.8 respectively) show however that two small areas of land in the city's economic centre on the central-west peninsula are at risk of flooding, though since the CDEM dataset (Figure 4.9) treats this reclaimed land as sea-level, the entire CBD of the city is at risk from a 1m rise (9.8 %). JAXA and SRTM show a matching coverage and proportion of land at risk under a 3m rise (13.2 % and 15.5 % respectively), while this affects the whole western coast in the CDEM data (21.4 %). Land at risk of flooding from a 5m rise is incrementally higher than the 3m extents in all three datasets (17.6-26.5 %), potentially due to Mumbai's physical geographic context as a mountainous region particularly in the centre and east of the metropolitan city area.
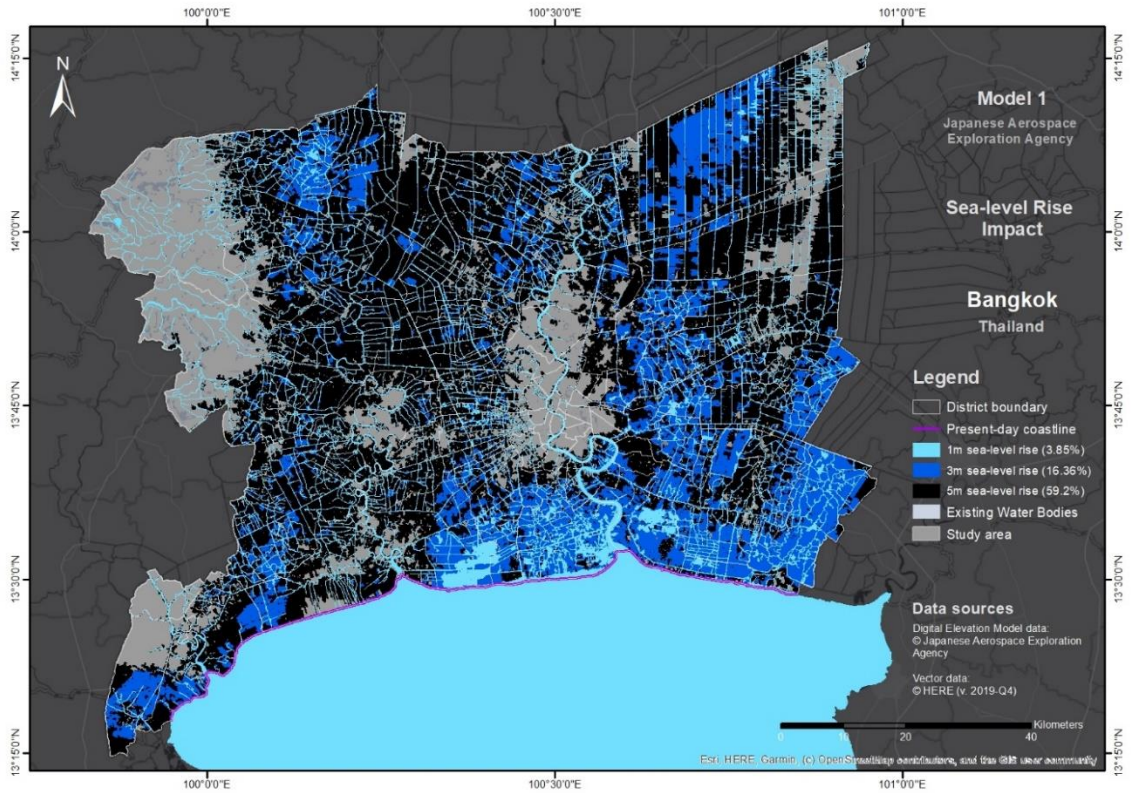
Figure 4.37: Map showing SLR extents for Bangkok modelled using the JAXA elevation dataset
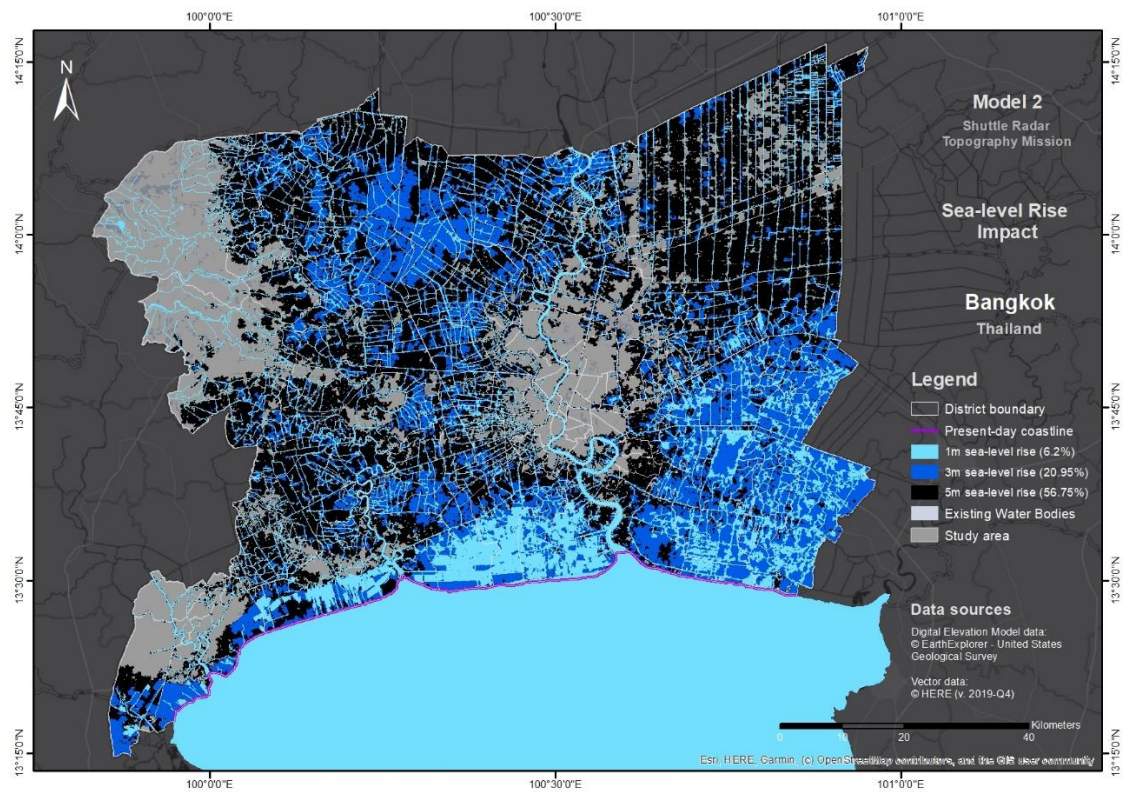
Figure 4.38: Map showing SLR extents for Bangkok modelled using the SRTM elevation dataset

33
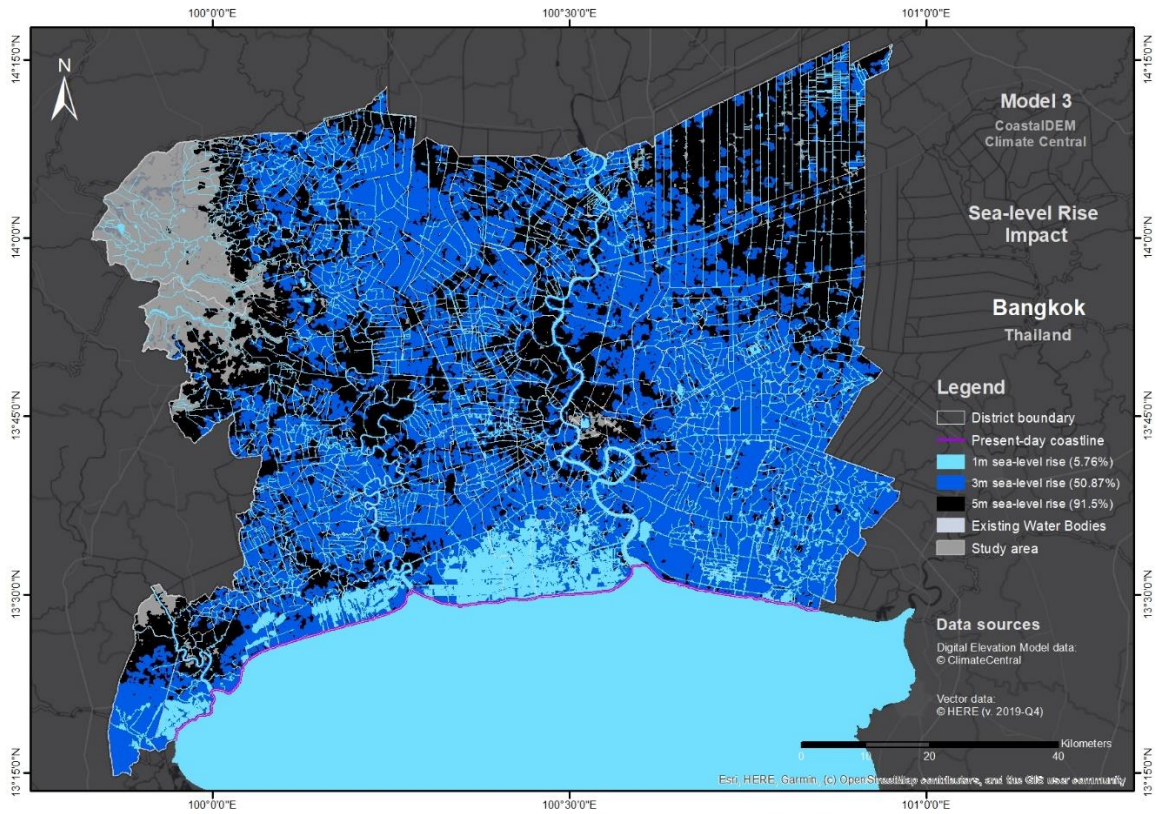
Figure 4.39: Map showing SLR extents for Bangkok modelled using the CDEM elevation dataset
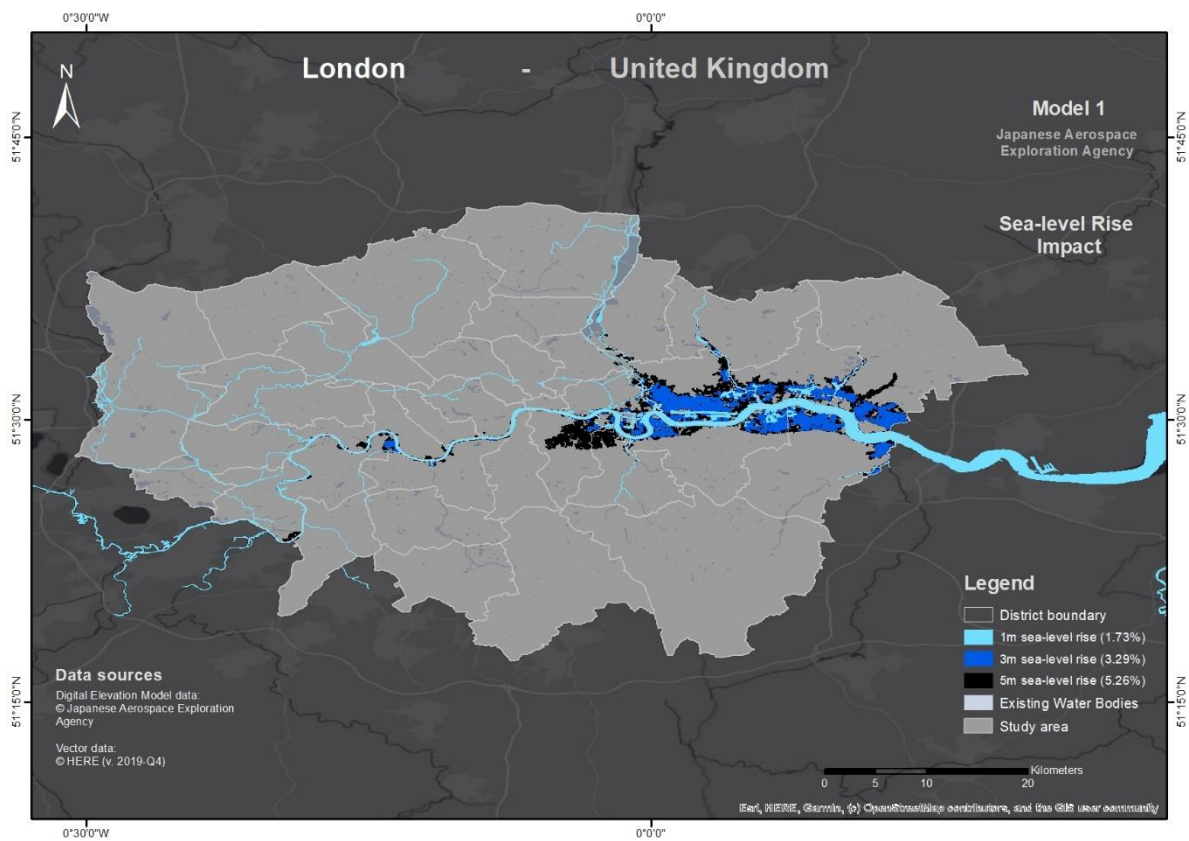
Figure 4.4: Map showing SLR extents for London modelled using the JAXA elevation dataset
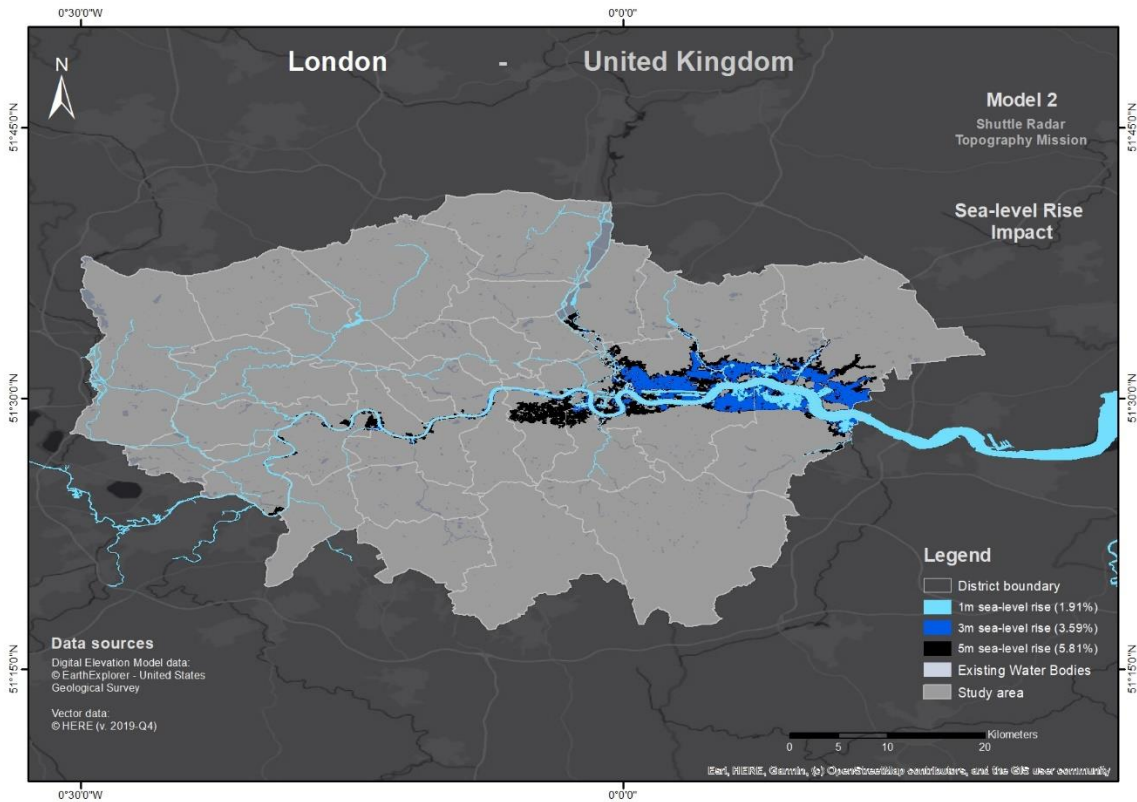
Figure 4.5: Map showing SLR extents for London modelled using the SRTM elevation dataset
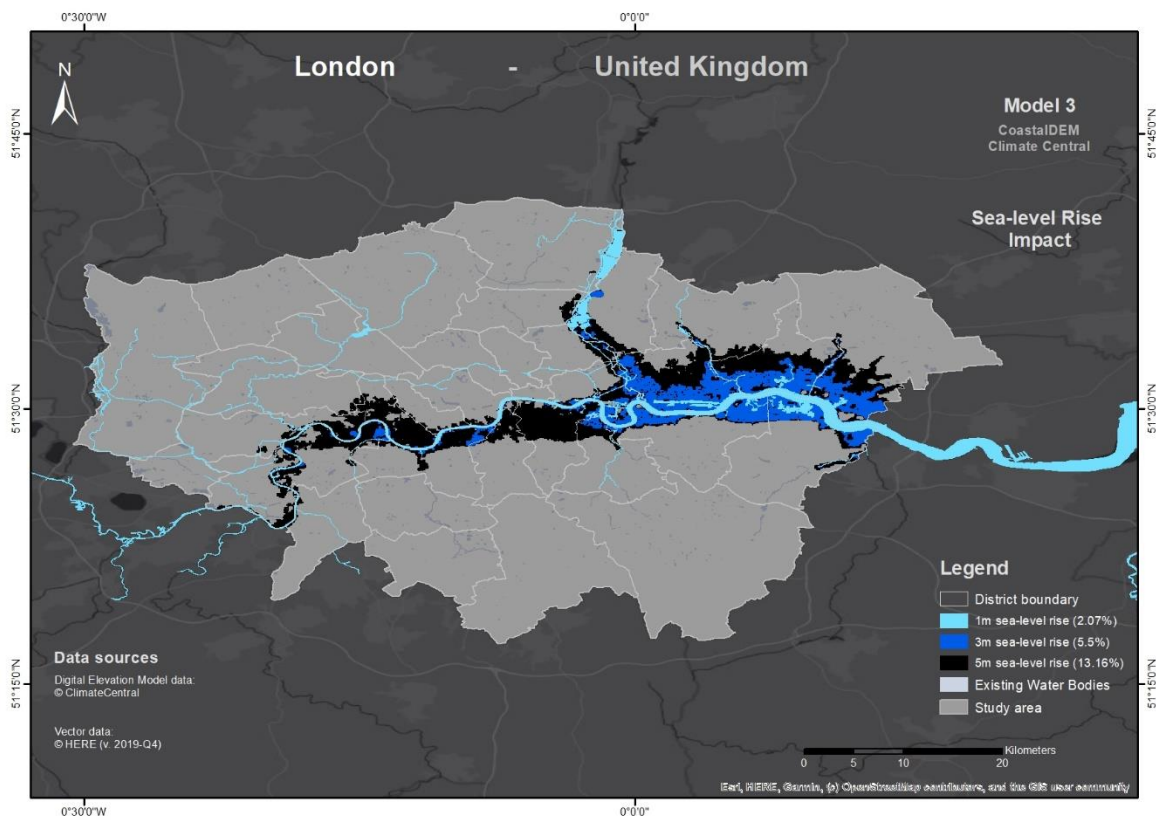
Figure 4.6: Map showing SLR extents for London modelled using the CDEM elevation dataset
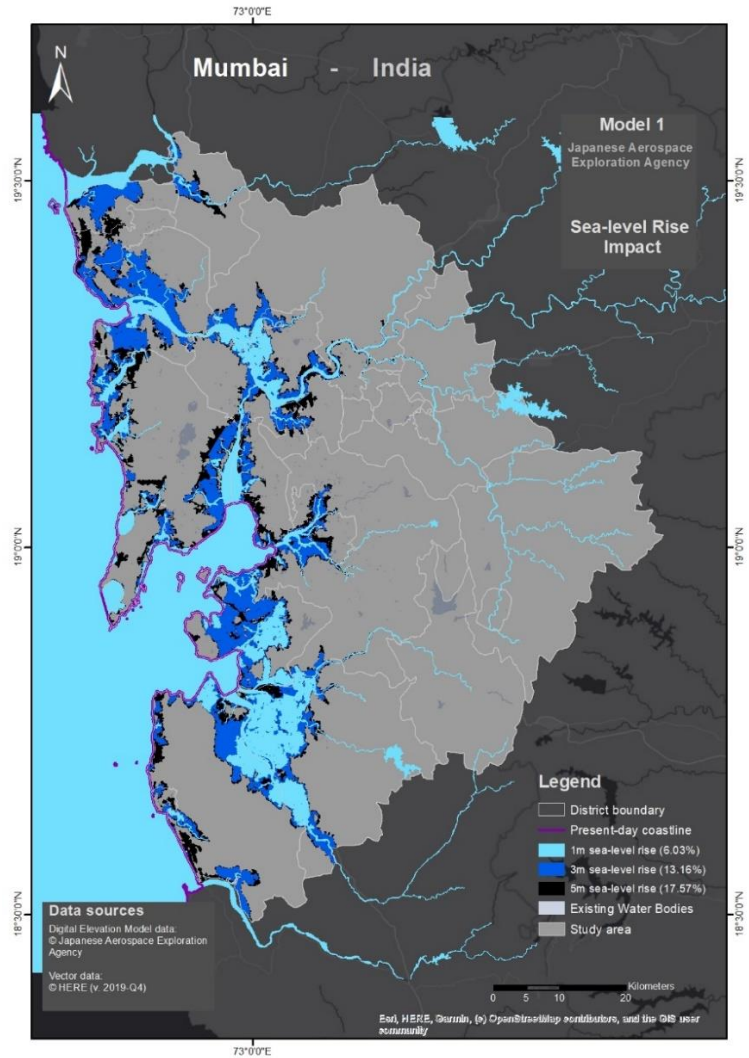
Figure 4.7: Map showing SLR extents for Mumbai modelled using the JAXA elevation dataset
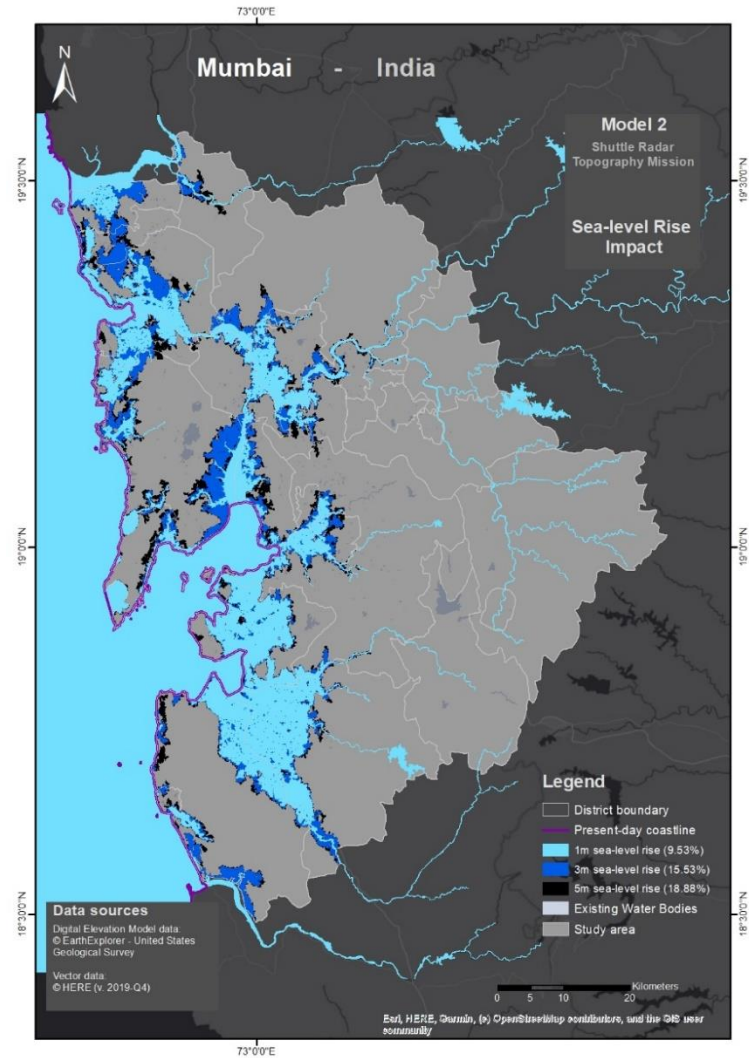
Figure 4.8: Map showing SLR extents for Mumbai modelled using the SRTM elevation dataset
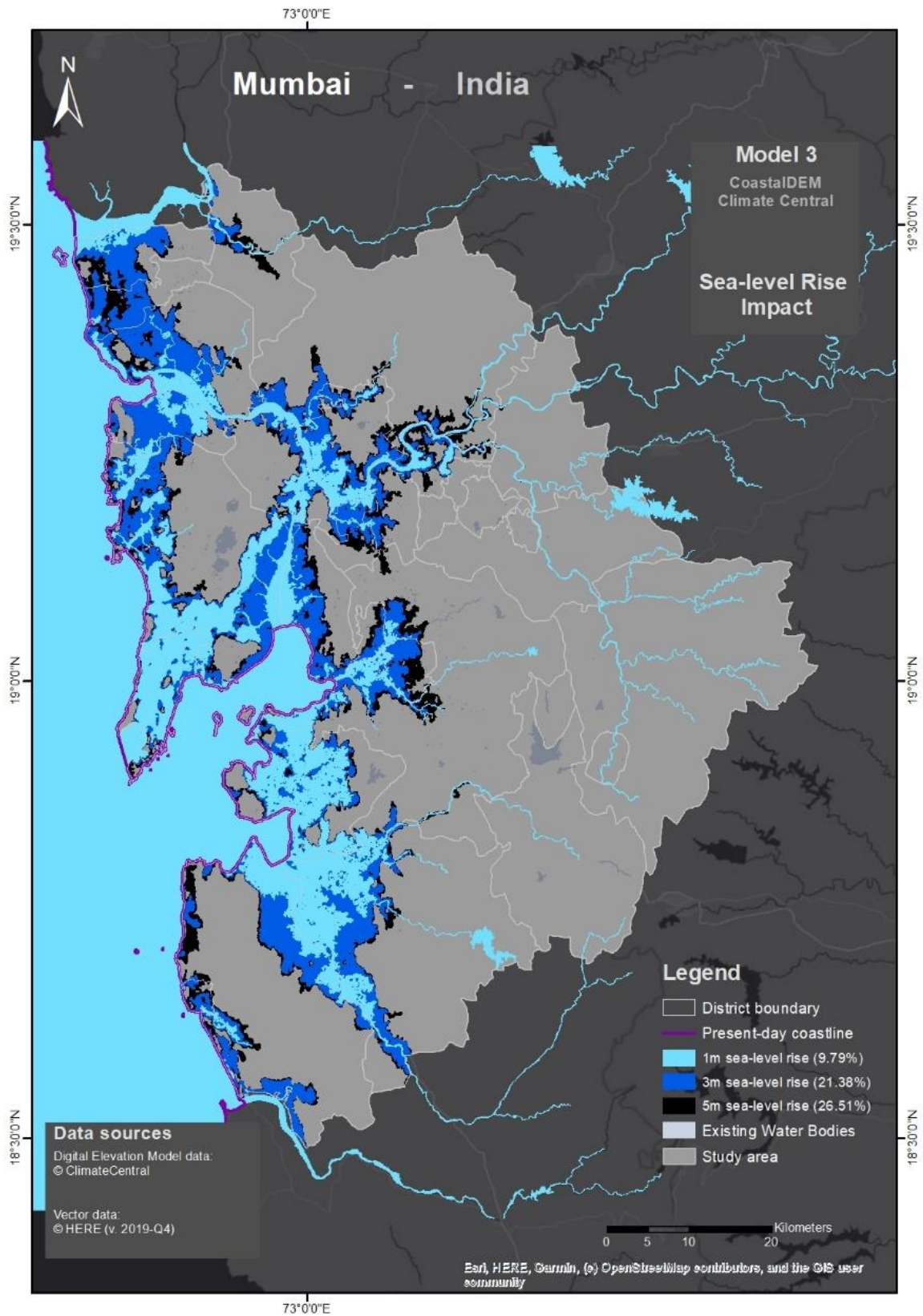
Figure 4.9: Map showing SLR extents for Mumbai modelled using the CDEM elevation dataset

4.1.3. Statistical Analysis

Statistical analysis was performed on the null hypotheses set out in the Methodology, where resulting significance values indicated whether the hypothesis should be accepted/retained, or rejected. The results tables are available in Appendix E (Tables E9 to E15), showing where null hypotheses are rejected (mid-tone orange) or accepted (pale orange).

The results from testing H_0 show that this hypothesis should be rejected for all dependent variables except for roads and population impacted in a 1m SLR scenario (Table E9). This means that for the remaining variables, there is a significant difference between the areas at risk of inundation expected by the three different SLR models used in this study.

4.2. Objective 3:
Within the three cities, where is the urban infrastructure at risk concentrated? Will this affect the cities' future functionality?

- o **H_1**: There is no significant difference in how much urban infrastructure is impacted by increasing SLR simulations (for any one SLR model).
- o **H_2**: There is no significant difference between the amount of a city's land area and each of its urban infrastructural layers flooded by permanent SLR.

Charts showing the same results comparing each urban infrastructure element (roads, railways, buildings and parks) by DEM modelled are visible in the following sections while chart comparisons by study area are provided within Appendix B. Figures 4.11, 4.12, 4.13, 4.16 through to 4.35 below show spatial representations of the infrastructure examined and charts of how the data compares by DEM used (the maps are shown larger in Appendix D). Appendix E contains Tables E2, E3, E4 and E7 where the numerical data is stored. Objective 3 will be answered within the findings below.

4.2.1. Bangkok

4.2.1.1. Roads

As can be seen in Figure 4.10 below and Table E2, the total lengths submerged within Bangkok will be similar in a 1m SLR, or high-risk scenario, as when compared between the different data sets. A total length of 1,095.5 km (1.7 % of the city's total road network of 63,617.6 km) would be submerged on average from the JAXA (722 km or 1.1 %) and SRTM (1469 km or 2.3 %) datasets, whereas the CDEM data results in 1,076.8 km or 1.7 % impacted. Spatially, the roads affected concern the south and east of the city.

A significant difference (Table E11 showing an independent median Kruskal Wallis test for Hypothesis H_2) arises between these datasets in a medium-risk SLR scenario of 3m. The average proportion of the infrastructure submerged (12.5 % or 7,948.2 km) from the JAXA (11.2 % or 7,123.3 km) and SRTM (13.8 % or 8,773.1 km) datasets contrasts with almost half the city's roads (48 % or 30,542.7 km) resulting from the CDEM elevation data.

While approximately this same value (48.5 % or 30,866.8 km) is expected to be submerged in a 5m SLR scenario based off the average of the JAXA (51.5 % or 32,750.9 km) and SRTM (45.6 % or 28,982.6 km) values, the contrast is greater still in the CDEM data, which shows that almost the city's whole road network (92.3 % or 58,719.3 km) would be impacted with this much of a rise (Appendix A: Figures A1, A5 and A9 and Appendix B, Figure B1, B6 and B11). The CDEM data shows that spatially, roads in the city's CBD will be affected; significantly impact city dweller's accessibility to and from the city centre, which will increase congestion since high numbers of people will need to use narrower roads (Figure 4.11 below).
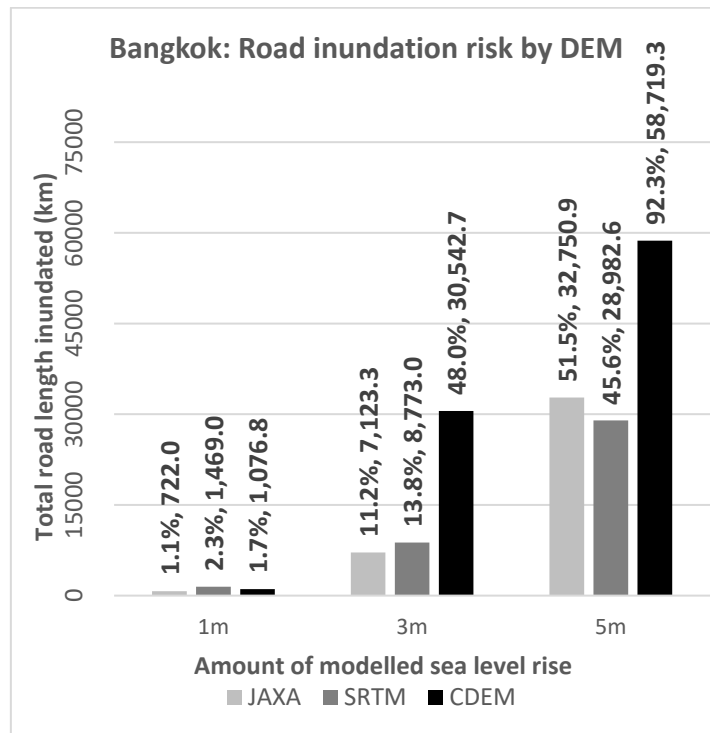
Figure 4.10: Roads at risk of flooding in Bangkok, compared across elevation datasets

4.2.1.2. Railways

Bangkok has a total rail network of 382.8 km, which is the least of the three cities examined (Table E3). It spreads radially from the city's CBD to the four corners of the city's metropolitan area, favouring the southern coastal districts. A 1m SLR scenario is expected to subject 1.3 % or 4.9 km of the rail network to high risk on inundation on average from the JAXA (0.8 % or
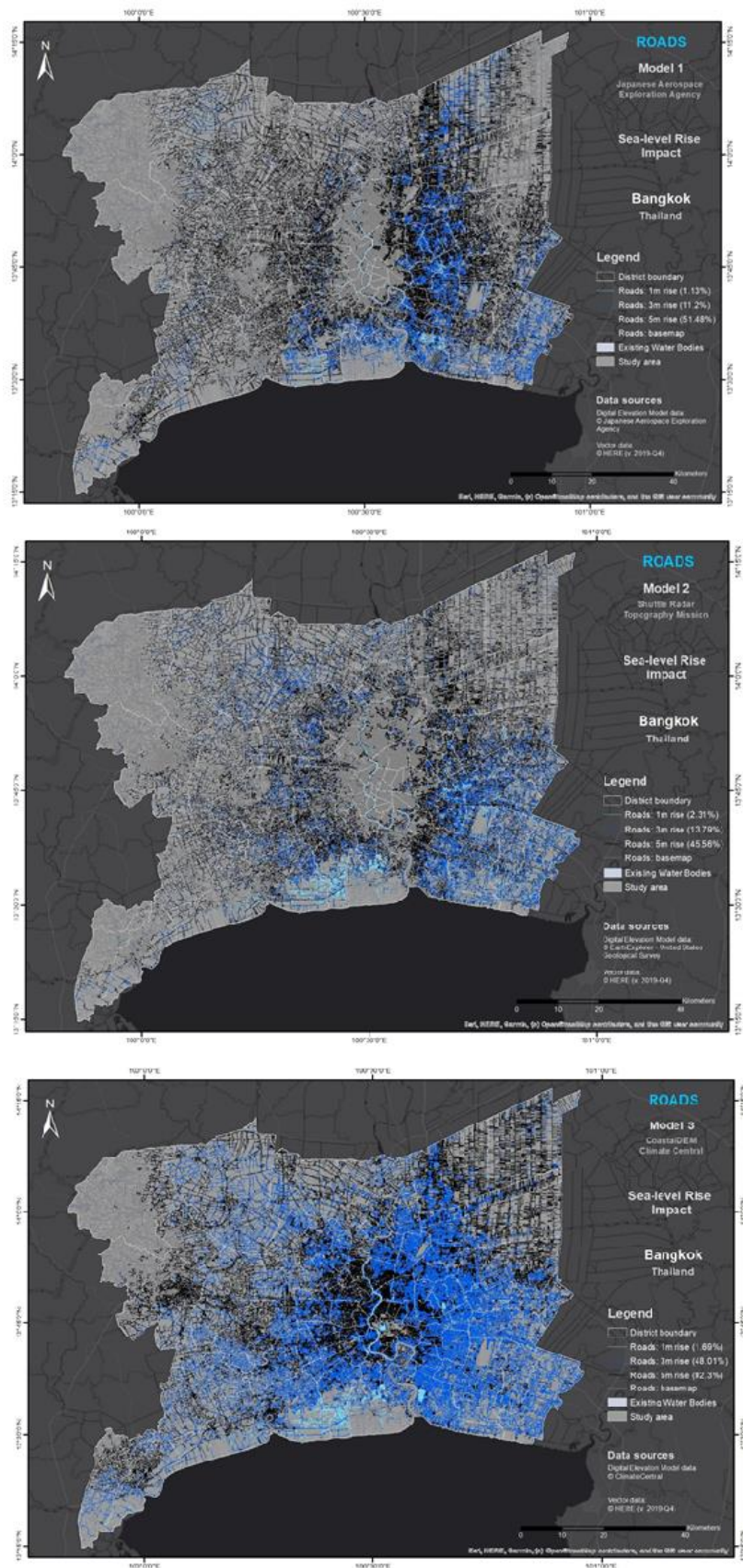
Figure 4.11: A visual representation of Bangkok's road network affected by SLR from the datasets examined (JAXA at the top, SRTM in the middle and CDEM at the bottom) – Figures A1, A5 and A9 (Appendix A) for greater detail

3 km) and SRTM (1.8 % or 6.9 km) elevation datasets. This value increases slightly to 1.5 % or 5.8 km of the rail network when looking at the CDEM data.

A 3m (medium-risk) SLR scenario would submerge on average 8.1 % or 30.8 km of the infrastructure, between the JAXA (4.0 % or 15.3 km) and SRTM (12.1 % or 46.3 km) datasets. The CDEM model however shows almost four times as much railway network (44.1 % or 169 km) at risk of submersion. Spatially, the tracks that will be flooded appear to be mostly outside of Bangkok's central CBD area, however they will be flooded in all directions around the CBD unlike the roads. A 3m rise would flood sections measuring kilometres long in the city's key railway links to the south, east and north, rendering the tracks unusable unless significant flood defence strategies such as levees or raised tracks are implemented.

While just over a third of the city's railways (35.3 % or 135.1 km) is expected to be submerged on average from the JAXA (35.8 % or 137.1 km) and SRTM (34.8 % or 133.2 km) datasets in a lower-risk 5m SLR scenario, this increases to 84.2 % or 322.2 km of the rail network when examined through the CDEM data model (Figure 4.12 below). The spatial distribution of how railways will be inundated may be viewed in Figure 4.13, Figures A2, A6 and A10 (Appendix A) and Figures B2, B7 and B12 (Appendix B). With a 5m rise, the only remaining rail track which wouldn't be flooded is in the elevated north-west part of the city. The rest of it would be permanently submerged.

Figure 4.12: Railways at risk of flooding in Bangkok, compared across elevation datasets

Figure 4.13: A visual representation of Bangkok's railway network affected by SLR from the datasets examined (JAXA at the top, SRTM in the middle and CDEM at the bottom) - Figures A2, A6 and A10 (Appendix A) for greater detail

4.2.1.3. Buildings

From the vector data investigated, the total footprints of buildings collectively cover an area of 228.7 km^2 within Bangkok (Table E7 and Figure 4.17 below). This is the highest value from the three cities studied by up to three-fold.

In a high-risk 1m SLR scenario, between 0.6 % (1.3 km^2) and 0.9 % (2.2 km^2) of buildings are expected to be flooded from the JAXA and SRTM average, and CDEM data respectively. The JAXA (0.1 % or 0.2 km^2) and SRTM (1.0 % or 2.4 km^2) datasets show a high difference, with the latter closer in value to the buildings expected to be impacted under the newer CDEM elevations.

This large difference in values between the JAXA and SRTM models for the 1m SLR scenario reduces in a 3m (medium-risk) scenario, where very similar values of the areas are expected to flood between the former two datasets (5.4 % or 12.3 km^2 for the JAXA dataset, and 6.7 % or 15.4 km^2 for the SRTM dataset), resulting in an average value of 6.1 % or 13.9 km^2. The CDEM data with values of 53.7 % or 122.8 km^2 shows in contrast a nine-fold increase for the infrastructure at risk of submersion.

When examined in a 5m or low-risk SLR scenario, the contrasts are starker. The average of the JAXA (33.4 % or 76.5 km^2) and SRTM (28 % or 64.0 km^2) values at 30.7 % or 70.3 km^2 of the city's building network is less than a third of the city's buildings, while the CDEM data shows almost all Bangkok's buildings (94.6 % or 216.3 km^2 of the building areas) are expected to flood should the Gulf of Thailand rise by 5m (Figure 4.16, Appendix A: Figures A3, A7 and A11, and Appendix B: Figure B3). Unless significant flood defence barriers are put into place at the mouth of the Chao Phraya river, the city's high land-value residential, commercial and industrial properties would be at risk of submersion.

When reviewing the vector data coverage for the buildings available in HERE, it is worth comparing the available data with other infrastructural layers, as can be seen in Figures 4.14 and 4.15 below. Although the road vector data covers the entirety of all three cities, the building vector data only focuses around the central business districts (CBDs) of the three cities. The representation of how much of the city's building footprint would be impacted by sea level rise is therefore dependent on whether the SLR extents in Section 4.1.1 above flood the city's economic hubs. Buildings located in suburban fringes of the cities are not represented in this data layer and therefore not counted.
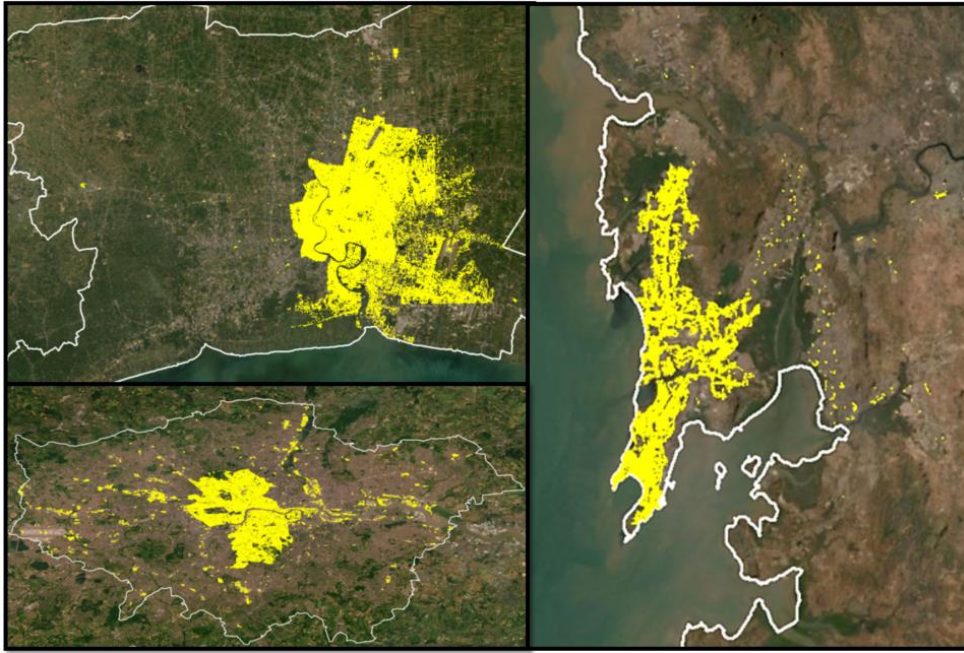
Figure 4.14: Screenshot showing buildings vector data coverage (in yellow) overlaying satellite imagery of Bangkok (top left), Mumbai (right) and London (bottom left) zoomed in to the data extents. Bangkok's coverage is more representative of the city's built-up area than London and Mumbai, where full built-up areas are represented in warm grey tones across the three satellite images. Refer to Figures D1, D2 and D3 (Appendix D) for greater map detail.
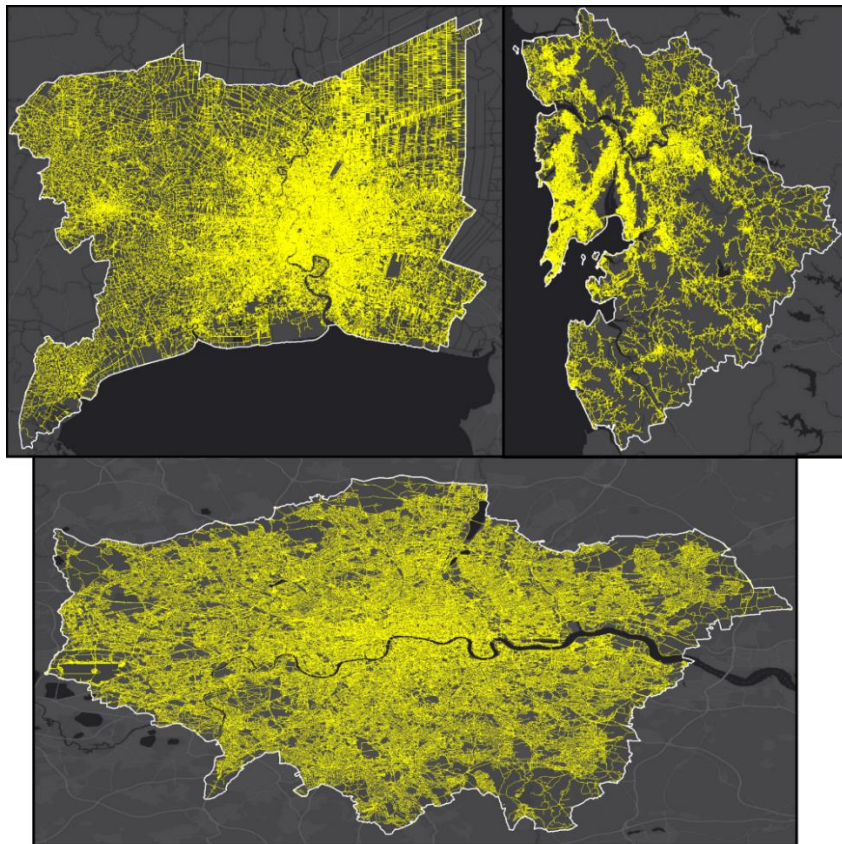
Figure 4.15: Screenshot showing roads vector data coverage (in yellow) in Bangkok (top left), Mumbai (top right) and London (bottom centre). In all three cities, the infrastructure layer coverage is highly representative of real conditions when compared to Figure 4.14 above. Refer to Figures D4, D5 and D6 (Appendix D) for greater map detail.

Figure 4.16: A visual representation of Bangkok's building footprint affected by SLR from the datasets examined (JAXA at the top, SRTM in the middle and CDEM at the bottom) - Figures A3, A7 and A11 (Appendix D) for greater detail

Figure 4.17: Buildings at risk of flooding in Bangkok, compared across elevation datasets

4.2.1.4. Parks

From the findings, it appears that Bangkok has the lowest total amount of parkland (18.4 km^2) by a wide margin (less than 10% of the parkland in London and less than 2 % of Mumbai's parkland), as can be seen in Table E4. The spatial distribution of how parkland in Bangkok will be affected can be seen in Figure 4.18 below and Figures A4, A8 and A12 (Appendix A) and Figures B4, B9 and B14 (Appendix B). Although a 1m (high-risk) SLR scenario shows that 1.2 % or 0.2 km^2 of the city's parks will be submerged on average using the JAXA (1.2 % or 0.2 km^2) and SRTM (1.3 % or 0.2 km^2) data models, this time the CDEM data shows a lower value of 0.8 % or 0.1 km^2 of parks at high risk of submersion.

The trends reverse for a 3m SLR, however. While on average 9 % of the city's parks (1.7 km^2) are expected to be flooded when interpreting the JAXA (10.6 % or 1.9 km^2) and SRTM (7.4 % or 1.4 km^2) data models, while the CDEM data shows almost a third of the full area (30.8 % or 5.7 km^2) will be flooded permanently with the same amount of SLR.

This contrast increases for a 5m (low-risk) SLR scenario. While an average of 35.2 % (6.5 km^2) of Bangkok's parks show risk of flooding from the JAXA (47 % or 8.6 km^2) and SRTM (23.3 % or 4.3 km^2) datasets, the CDEM data highlights nine-tenths (89.6% or 16.45 km^2) of the parks at risk of flooding. The parks that would be flooded are scattered evenly across the city's area (Figure 4.19 below), and the relatively low number of parks present means that only a limited amount of land (up to 16.5km^2) would be flooded even with a 5m SLR scenario.
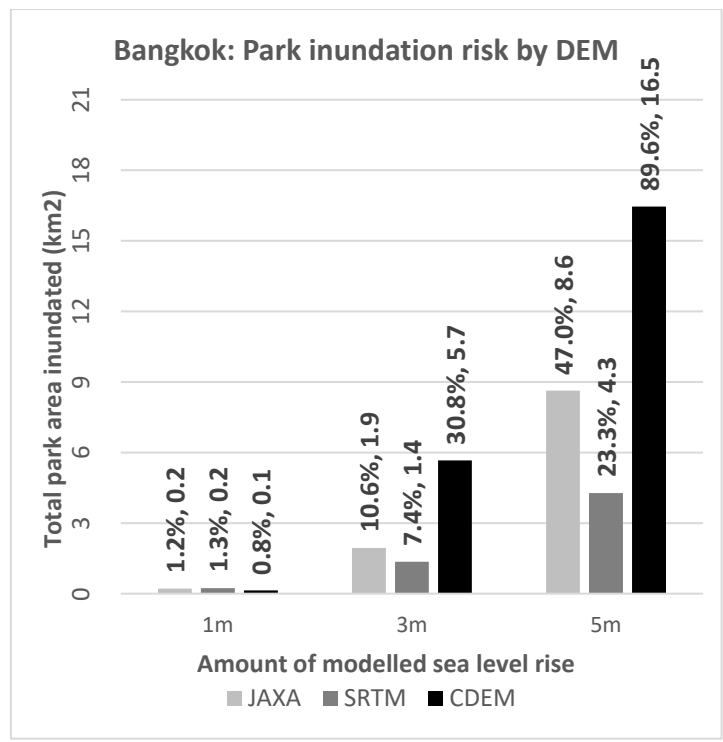
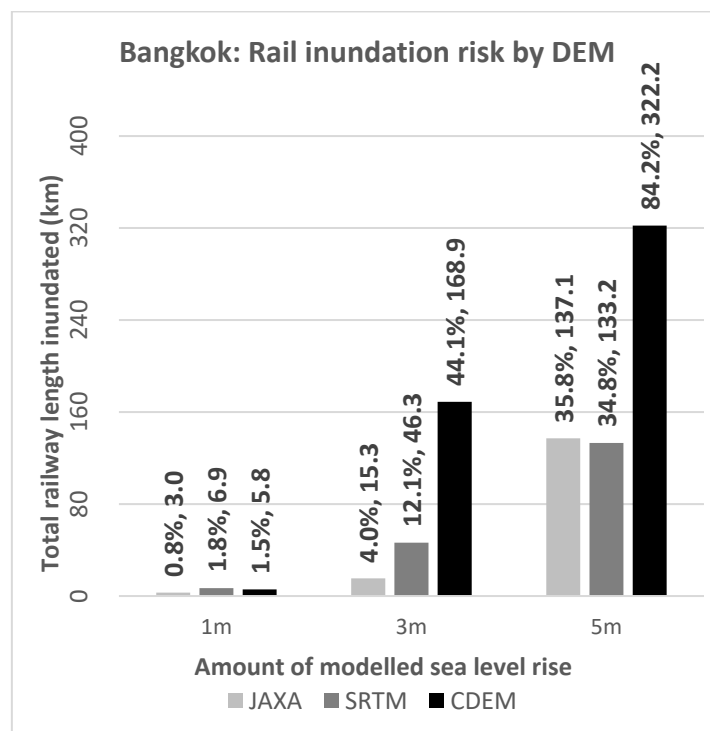*Figure 4.18: Parks at risk of flooding in Bangkok, compared across elevation datasets*

Figure 4.19: A visual representation of Bangkok's parklands affected by SLR from the datasets examined (JAXA at the top, SRTM in the middle and CDEM at the bottom) - Figures A4, A8 and A12 (Appendix A) for greater detail

4.2.2. London

A key difference between the encroaching sea-level rise in London from the other two studied cities is that it's not located on the ocean's coast, but further upstream. This reduces the coast at risk of flooding significantly to the banks of the river Thames, particularly in the east which is closest to the river's mouth. As a result, the city's functionality will be minimally affected according to the JAXA and SRTM datasets (Figures 4.4 and 4.5), with low levels of disruption to the city's roads, railways and key buildings expected.

The infrastructure at risk from the CDEM elevation data however shows that additional flood defence structures possibly towards the river's mouth require investment to reduce the larger-scale disruption along the city's river banks (Figure 4.6). As the sea-level rises beyond 3m, this will flood westward (upstream), reaching and impacting areas of the city including the historic CBD and key road/rail bridges.

4.2.2.1. Roads

The dense and compact structure of London as a city means that despite having the lowest area of the three examined cities at 2,557.5 km^2, it contains a density value of 10 km roads/km^2 (for a total of 25,550.4 km); higher in density than both Bangkok (7.6 km roads/km^2) and Mumbai (4.2 km roads/ km^2) (Figure 4.21). Table E2 and the charts within Appendix B: B3, B8 and B13 show findings for London's road data comparatively, where the lowest proportions of the cities' total road networks are at risk from the three (high, medium and low risk) SLR scenarios in London.

Similar proportions (JAXA: 0.2 % or 61.5 km, SRTM: 0.3 % or 83.8 km, CDEM: 0.3 % or 64.8 km) are at high risk from a 1m SLR scenario, however contrasts start to appear in a 3m SLR (medium-risk) scenario. Here, the average of the JAXA (2 % or 512.2 km) and SRTM (2.3 % or 585.4 km) values at 2.2 % (548.8 km) show half the road network at risk from the CDEM data (4.3 % or 1,121.9 km) (Figure 4.20 below and Appendix A: Figures A13, A17 and A21).

This contrast increases to three-fold between the JAXA-SRTM average proportions (5 % or 1,275.9 km) and the CDEM proportions (15.2 % or 3,884.6 km) at risk from a 5m (low-risk) SLR scenario. The JAXA-SRTM average was calculated from the values for the JAXA (4.7 % or 1,211.7 km) and SRTM (5.3 % or 1,340.1 km) data models.
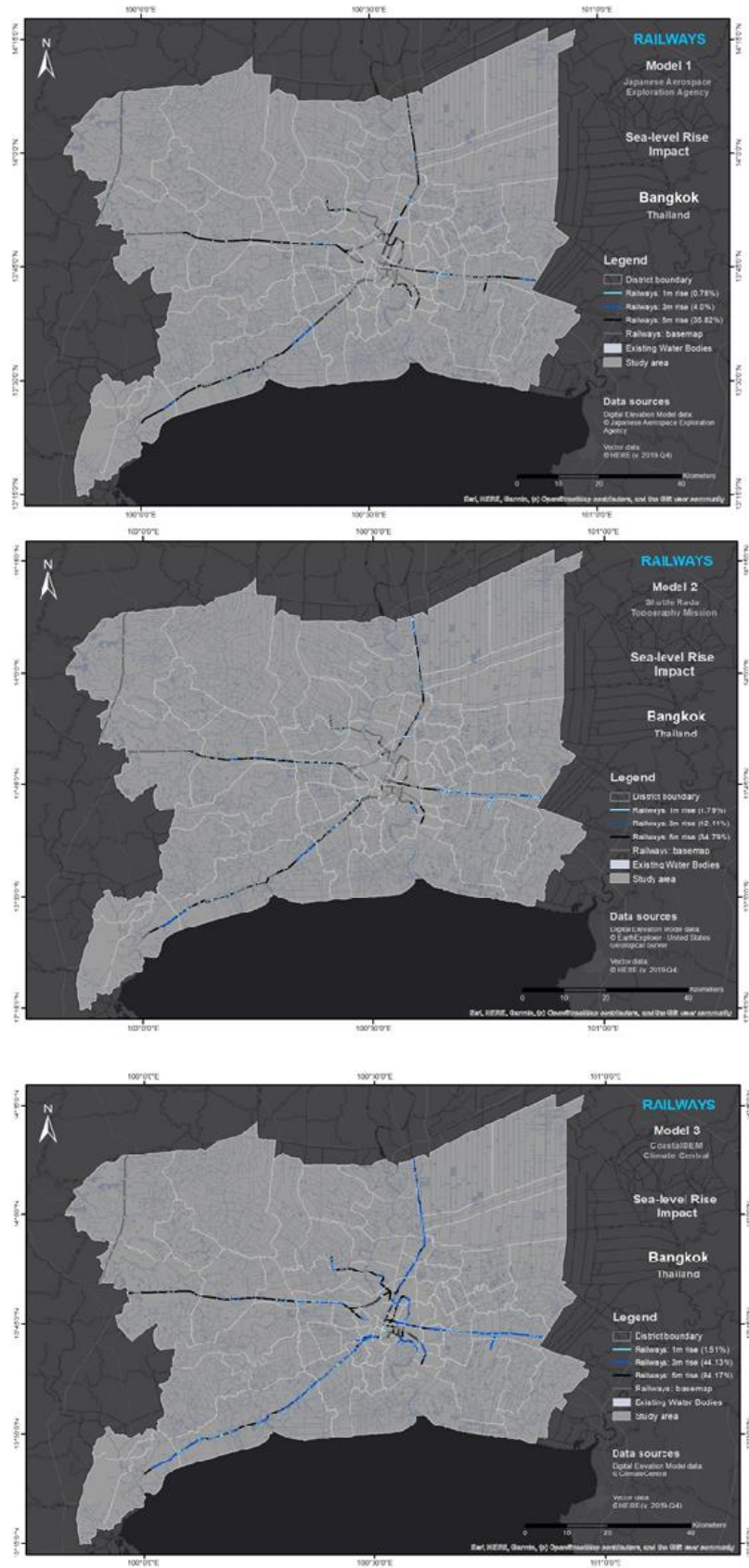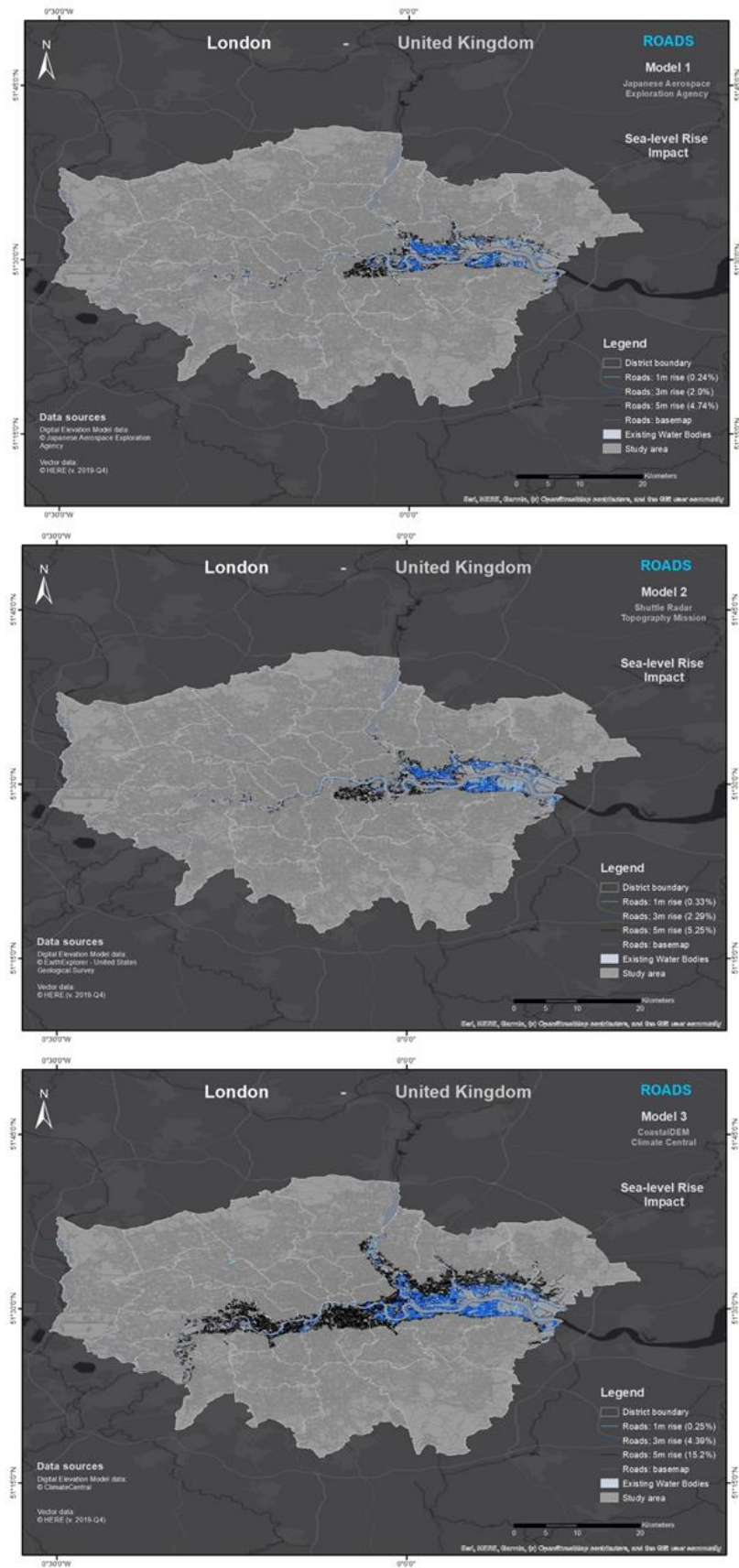
Figure 4.20: A visual representation of London's road network affected by SLR from the datasets examined (JAXA at the top, SRTM in the middle and CDEM at the bottom) - Figures A13, A17 and A21 (Appendix D) for greater detail

50
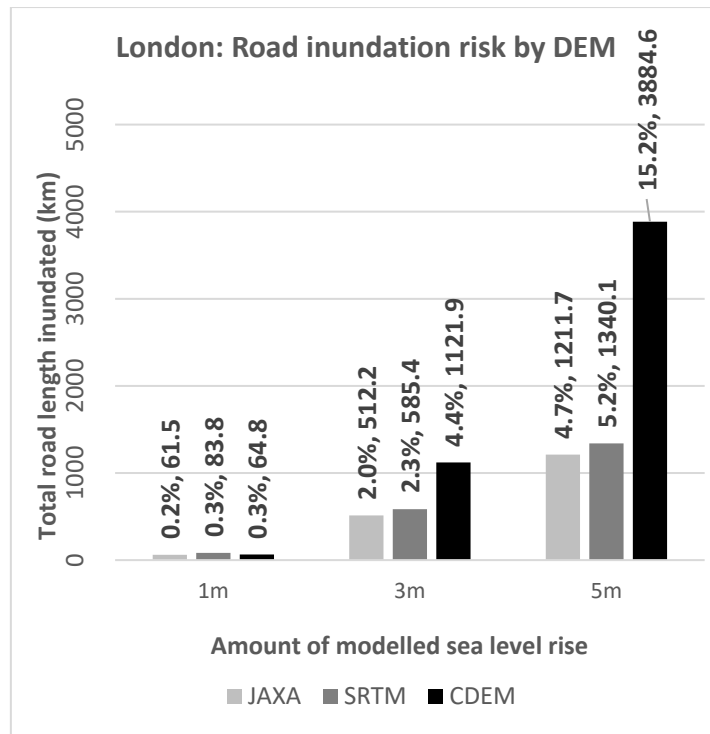
Figure 4.21: Roads at risk of flooding in London, compared across elevation datasets

4.2.2.2. Railways

Comparatively, London has the highest total length of railways (1,826.5 km) from the three studied cities; over double Mumbai's rail network and almost five-fold Bangkok's (Figure 4.23 below and Table E3), with spatial representation displayed in Figures 4.22 below and Figures A14, A18 and A22 (Appendix A)). On average the JAXA (0.5 % or 9.9 km) and SRTM (0.7 % or 11.8 km) models with a value of 0.6% (or length of 10.9 km) show a greater value of the city's rail network at high-risk of flooding (with a 1m SLR) than those extracted from the CDEM data model (0.4% or 8.1 km). It is possible in this particular case that the elevation data for JAXA and SRTM around the railways in London is lower than 1 metre, while the CDEM data (due to its larger spatial resolution) averages raster cells along the railways as being on higher ground.

Similar to the trend seen for roads earlier, the infrastructure at risk reverses in medium- and low- risk scenarios (3m and 5m SLR scenarios respectively). In a medium-risk SLR scenario, the JAXA-SRTM average of 3.1 % or 57 km is just under half that found by the CDEM data (6.2 % or 112.5 km); whereas in a low-risk SLR scenario of 5m, the JAXA-SRTM average (6.1 % or 111.1 km) shows a third of all railways expected to be permanently flooded from the CDEM data (18.5 % or 338.7 km).

Figure 4.22: A visual representation of London's railway network affected by SLR from the datasets examined (JAXA at the top, SRTM in the middle and CDEM at the bottom) - Figures A14, A18 and A22 (Appendix A) for greater detail

52
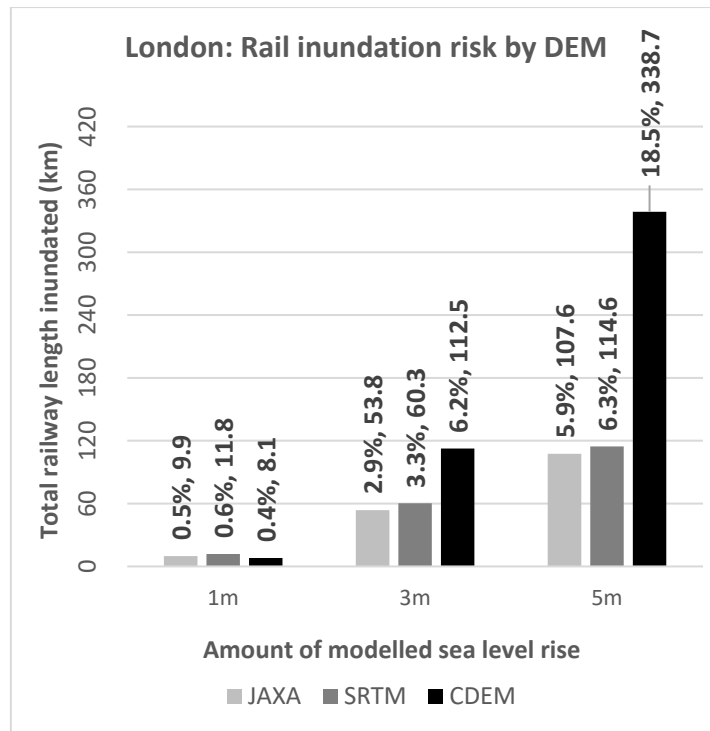
Figure 4.23: Railways at risk of flooding in London, compared across elevation datasets

4.2.2.3. Buildings

From the three cities studied, London has the lowest coverage of digitised available vector data in the form of buildings across the city's metropolitan area (80.7 km^2), as can be seen in the numbers from Figure 4.25 below, as well as spatially in Figure 4.24 below and Figures A15, A19 and A23 (Appendix A). While the JAXA-SRTM average shows 0.1 % (0.1 km^2) of the city's total building footprint at high-risk of permanent flooding from a 1m SLR rise (from 0.1 % or 0.1 km^2 in the JAXA data and 0.2 % or 0.2 km^2 from the SRTM data), the CDEM data shows a lower proportion at such risk, with a value of 0.1 % or 0.1 km^2 of London's building footprint.

In a 3m (medium-risk) SLR scenario, approximately one third of the infrastructure is at risk of permanent flooding from the JAXA-SRTM average (1.6 % or 1.3 km^2) than the CDEM values (6.1 % or 4.9 km^2). The JAXA and SRTM proportions lie at 0.8 % (0.7 km^2) and 2.3 % (1.9 km^2) respectively.

The contrast between datasets rises to four-fold in a 5m SLR scenario. The JAXA-SRTM average here shows a value of 5.9 % or 4.7 km^2 (4.3 % or 3.5 km^2 from the JAXA data model and 7.4 % or 6 km^2 from the SRTM model) at risk, while the proportions of the CDEM findings are almost a fifth of the buildings located in London's economic focus area at 20.4 % (16.5 km^2) of the total footprint.
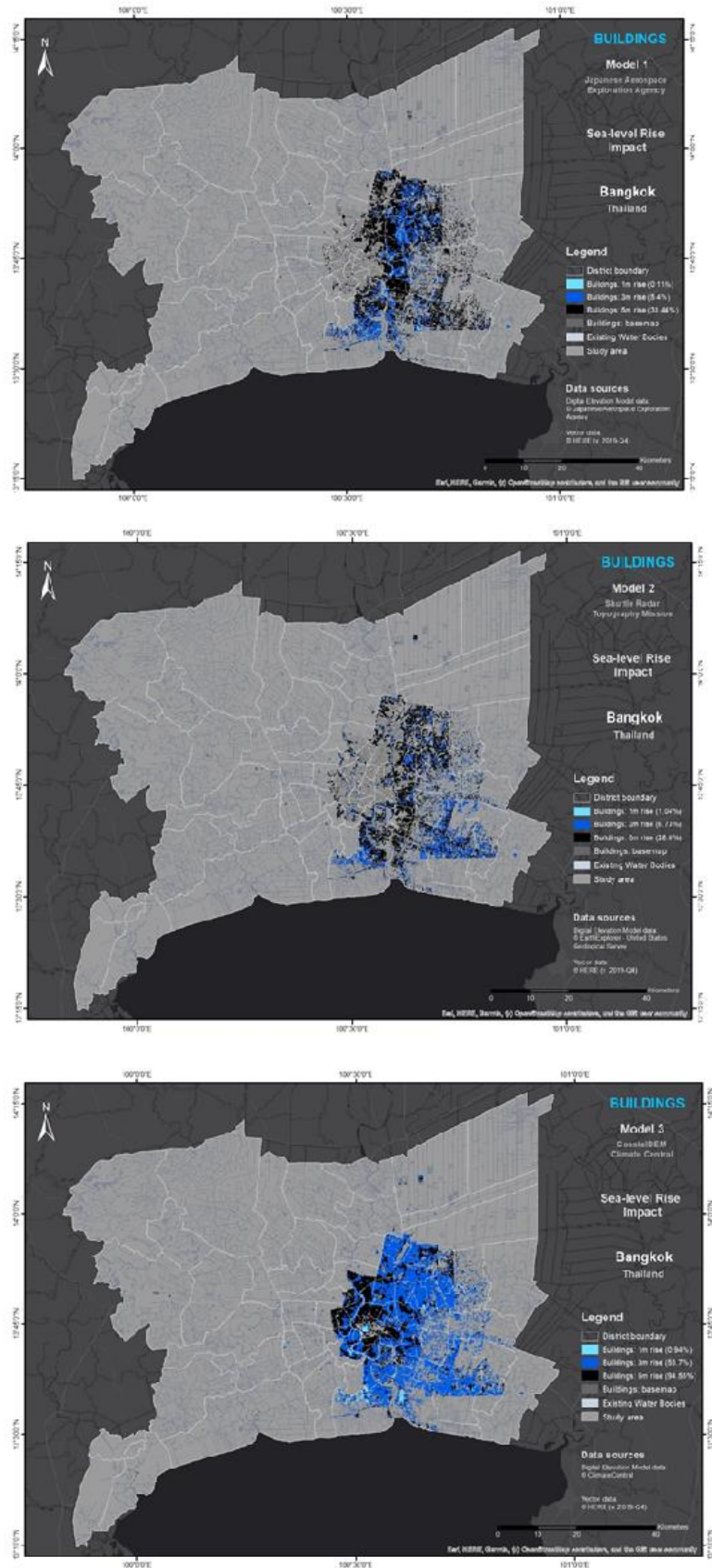
53
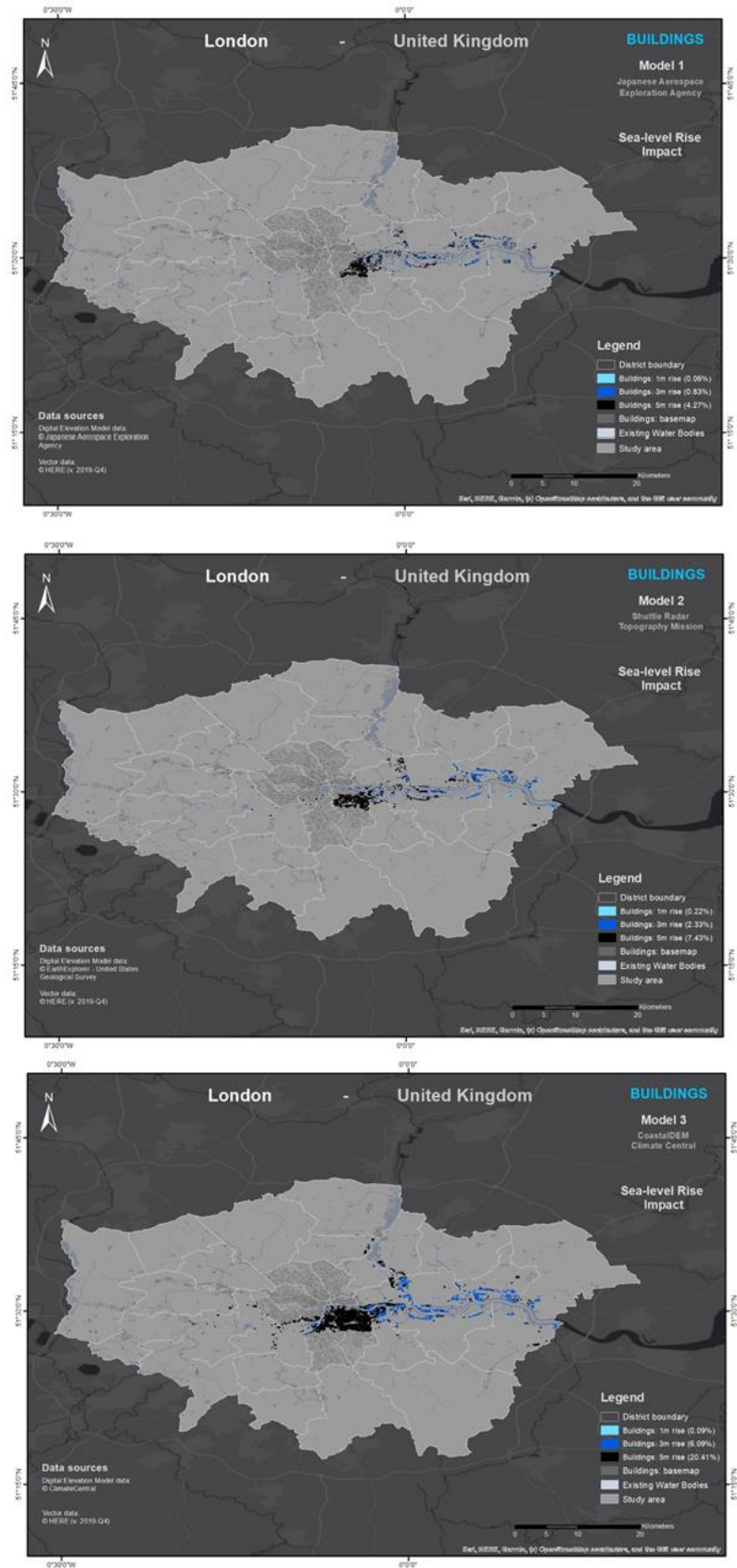
Figure 4.24: *A visual representation of London's building footprint affected by SLR from the datasets examined (JAXA at the top, SRTM in the middle and CDEM at the bottom) - Figures A15, A19 and A23 (Appendix A) for greater detail*
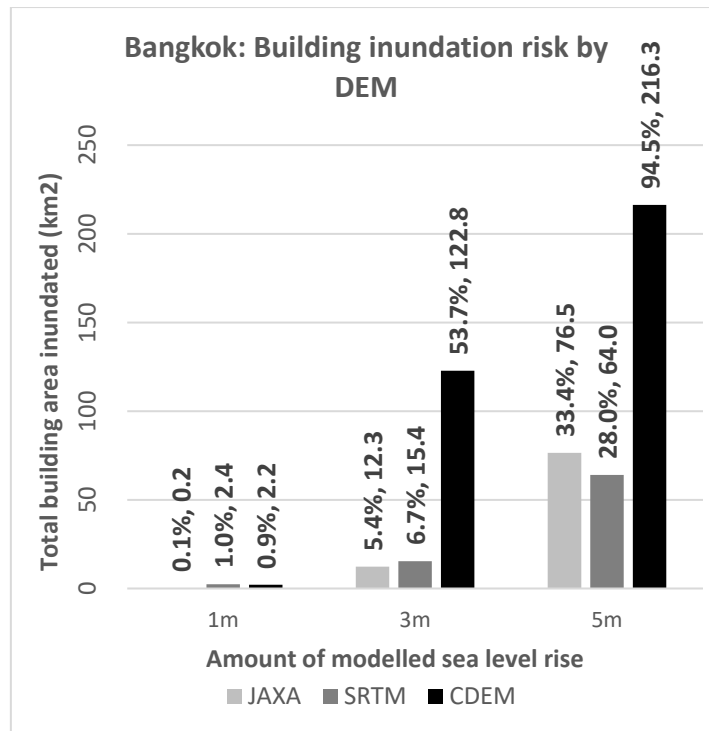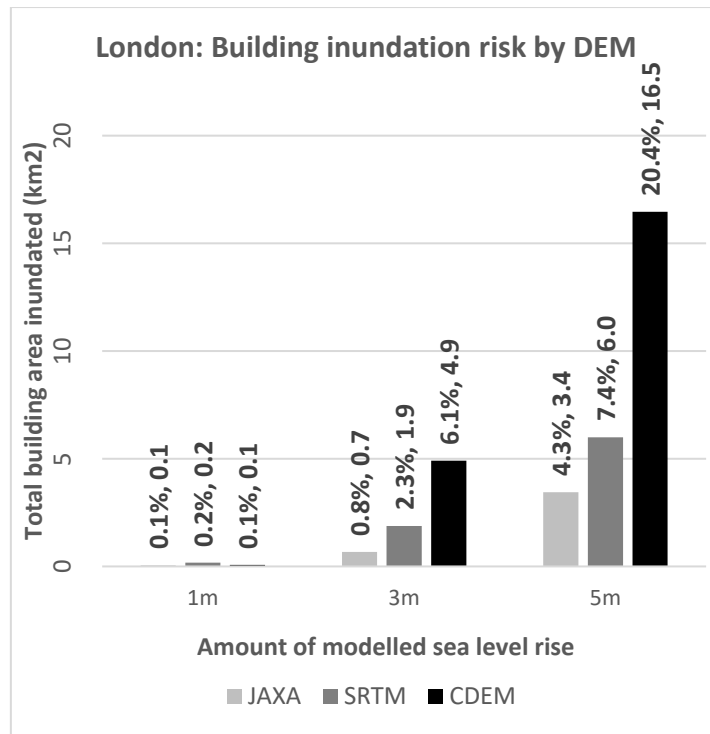
Figure 4.25: Buildings at risk of flooding in London, compared across elevation datasets

4.2.2.3. Parks

Figures 4.26 and 4.27 as well as Table E2 show the values of London's parklands at risk from the three examined SLR scenarios in comparison to the results for Bangkok and Mumbai. With a total digitised parkland area of 251.9 km^2, the spatial distribution means that they are impacted to a low degree in comparison to the other cities. The JAXA and SRTM data models have resulted in very similar findings for all three risk levels, whereas the CDEM data shows more parks will be affected at higher SLR scenarios.

In a 1m (high-risk) scenario, almost equal amounts of parkland are at risk of permanent flooding between the JAXA-SRTM average (0.5 % or 1.2 km^2) and the CDEM data (0.5% or 1.2 km^2). These proportions increase to a greater range for a 3m (medium-risk) SLR scenario. The JAXA-SRTM average here shows that 1.8% (amounting to 4.5 km^2) is at risk of permanent inundation in comparison to the 3.1 % (7.9 km^2) found from assessing the CDEM data.

A 5m SLR (low-risk) scenario shows that the JAXA-SRTM average results in a proportion over a third that found of the CDEM data. For the former, 3.9 % of the city's parks (9.9 km^2) would be at risk, whereas the latter shows that 13.2 % (33.1 km^2) would be flooded by such an increase in the Thames river encroaching on the city's land (Appendix A: Figures A16, A20 and A24 and Appendix B: Figure B4, B9 and B14).
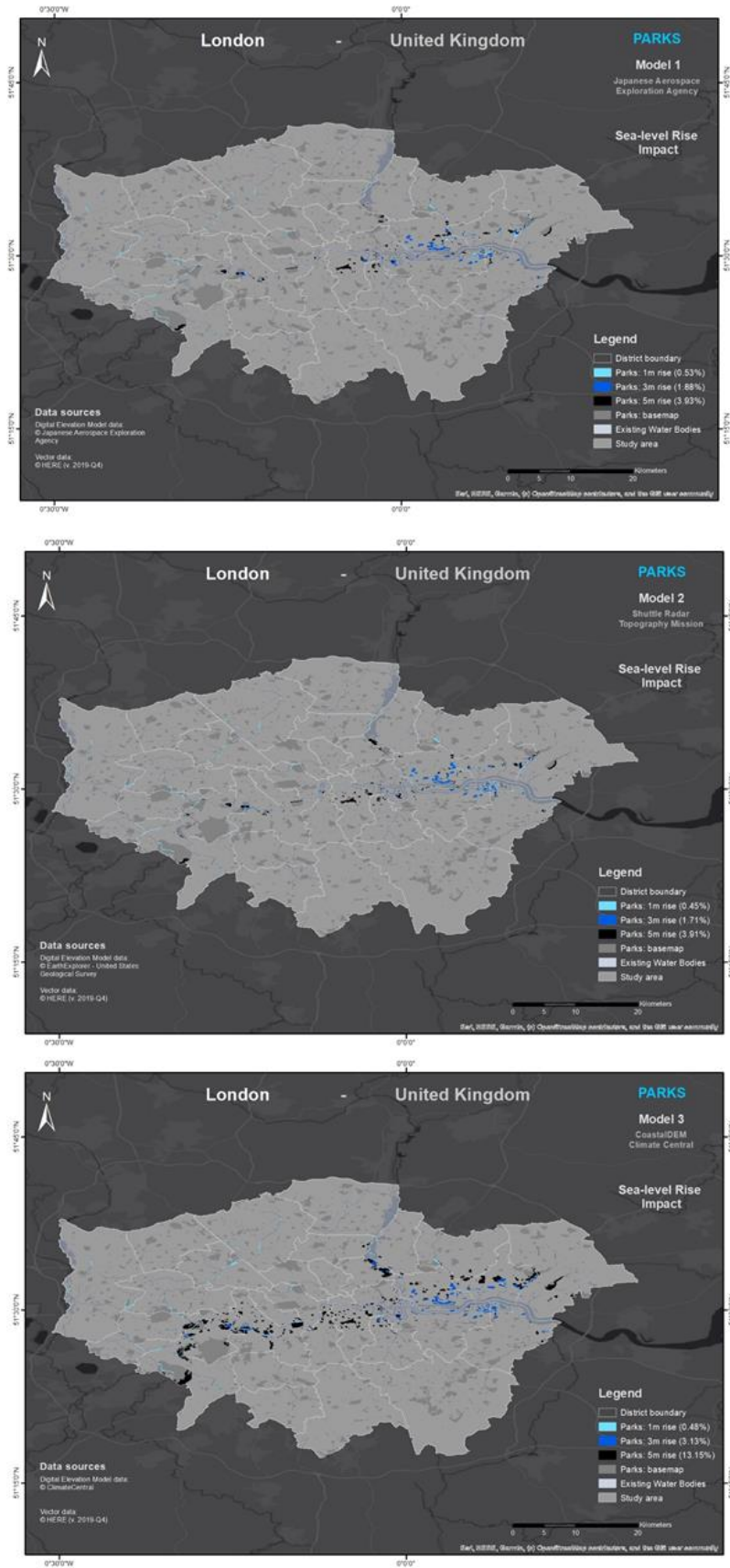
Figure 4.26: A visual representation of London's parklands affected by SLR from the datasets examined (JAXA at the top, SRTM in the middle and CDEM at the bottom) - Figures A16, A20 and A24 (Appendix D) for greater detail
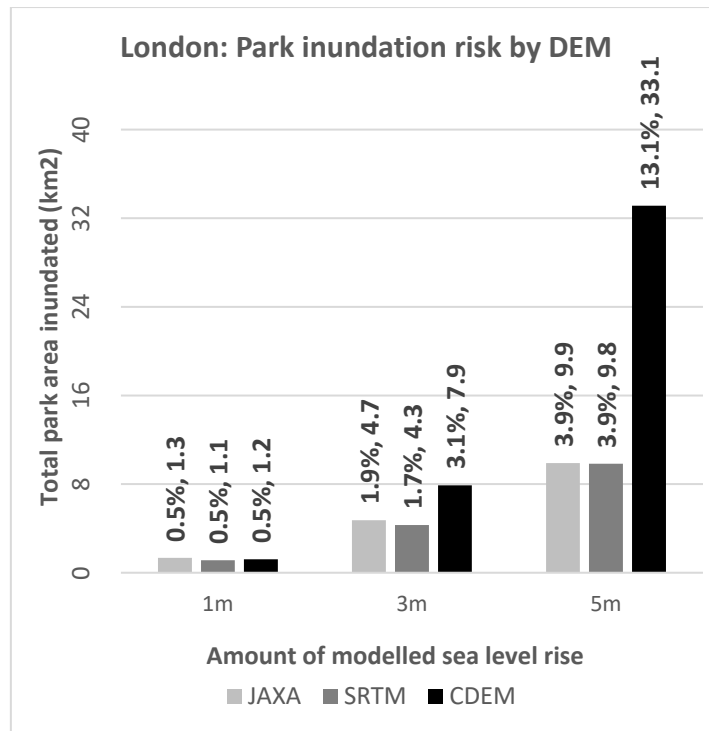
Figure 4.27: Parks at risk of flooding in London, compared across elevation datasets

4.2.3. Mumbai

4.2.3.1. Roads

From the three cities surveyed, Mumbai contains the lowest road network density for the city's metropolitan area (with a density of 4.2km roads/km^2, total road network length of 24,603.7 km and area of 5,851.3 km^2). The differences in elevation data mapping for the city's CBD means that while for the JAXA and SRTM datasets, the city's economic hub is beyond 5 metres above the present-day sea level in elevation, much of the Mumbai peninsula is already submerged under a 1m SLR scenario within the CDEM dataset. This reflects the large contrasts in the proportions of urban infrastructure at risk seen between the JAXA-SRTM average values and the CDEM values.

With a 1m SLR scenario, the JAXA-SRTM average stands at 2.6 % or 635.6 km of the city's road network (Figure 4.28 below and Table E2, with spatial representations in Figure 4.32 below and Appendix A: Figures A25, A29 and A33). This aligns the larger differences seen in the JAXA (1 % or 235.4 km) data and the SRTM (4.2 % or 1,035.8 km) data. Nevertheless, a 1m rise would already inundate 12.6 % or 3,102.8 km of Mumbai's total road network length, showing a five-fold increase than previously expected.

The amount of Mumbai's roads flooded increases steadily with an increase in sea levels. Under a 3m SLR scenario, an average of 8.1 % or 2,000.5 km is expected to be inundated (as calculated from the JAXA [5.9 % or 1,457 km] and SRTM [10.3 % or 2,543.8 km] datasets). However, the CDEM data shows that almost a third (30.0 % or 7,374.3 km) would be permanently flooded by such a rise.

At lower risk in a 5m SLR scenario, the JAXA-SRTM average shows that 15.0 % or 3,700.3 km would be covered in water (from the similar JAXA and SRTM numbers at 12.7 %/3,120.3 km and 17.4 %/4,280.3 km respectively). Just under three times this amount is projected to be flooded using the newer CDEM data, at 42.1 % or 10,345 km of the road network.
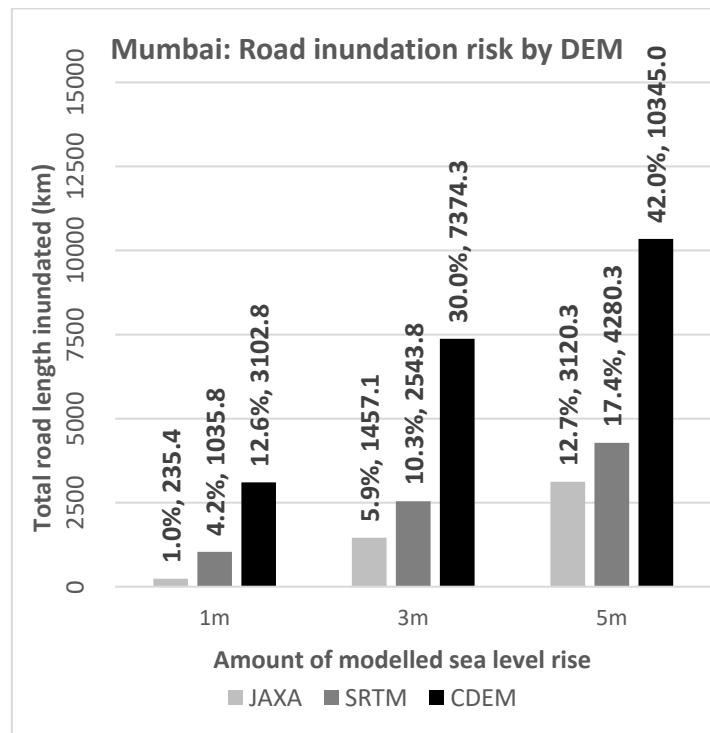
Figure 4.28: Roads at risk of flooding in Mumbai, compared across elevation datasets

4.2.3.2. Railways

Mumbai's railway network of 790.9 km spreading radially from the city's CBD to other districts along the west Maharashtra coast would be significantly impacted from SLR scenarios of all risk types (Figure 4.29 below and spatially in Figure 4.33 below and Appendix A: Figures A26, A30 and A34 as well as Table E3). With a 1m (high-risk) SLR, the JAXA-SRTM average (2 % from JAXA, 5.8 % from SRTM) results in 3.9 % (30.79 km) being impacted, whereas the CDEM data shows a seven-fold increase of 27.4 % (216.8 km) which is at great risk of being permanently flooded in the short term.

This discrepancy between the datasets becomes greater as the sea level is modelled to rise further. A 3m (medium-risk) rise scenario results in a 11.3 % (89.1 km) and 49.7 % (392.9 km) proportional difference between the JAXA-SRTM average and the CDEM data values respectively. This means that according to the CDEM data, already half of the city's existing railway network would be submerged. This increases to a proportion of 63.2 % (500.1 km) under a 5m SLR scenario – much higher than the JAXA-SRTM average of 23.0 % (181.8 km), which is already a large amount in its own right.

The infrastructure at greatest risk from this set is the city's railways, which are focused towards the city's CBD and spread radially to other suburbs inland and along the coast (over a quarter of the city's railways will be impacted from a 5m SLR).
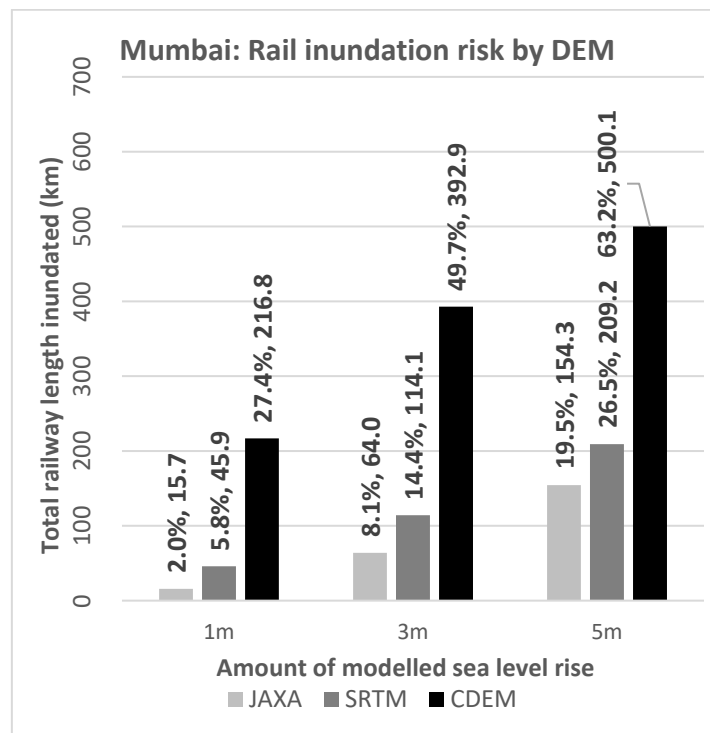
Figure 4.29: Railways at risk of flooding in Mumbai, compared across elevation datasets

4.2.3.3. Buildings

The vector representation of the building footprint within the HERE data corresponds to the coverage in the London set, with a total area of 88.9 km^2 (refer to Table E7). Within Appendix A: Figures A27, A31 and A35 and Appendix B: Figures B3, B8 and B13, it can be seen that expected volumes of buildings affected by the modelled high-, medium- and low-risk SLR scenarios vary significantly between the JAXA-SRTM and CDEM datasets. Although a 1m SLR would correspond with just 0.1 % (0.1 km^2) of the city's buildings being flooded at ground floor level from the JAXA-SRTM average, the findings from the modelled CDEM at 16.3 %

(14.5 km^2) show a larger expanse of built-up land at risk since these buildings are focused in the city's CBD area.

The contrasts between datasets are also apparent for a 3m SLR scenario, whereby the JAXA-SRTM average shows 0.3 % (0.3 km^2) of building areas at risk, while CDEM proportions show that 22.5 % (20 km^2) would be flooded at such a sea-level increase.

At 5m SLR, the city is under less temporally urgent vulnerability, as it would take many decades for such a rise to occur (under current projection probabilities). Nevertheless, the CDEM findings show that over a quarter (26.9 % or 23.9 km^2) of the city's buildings would be at risk from such a rise in sea level, significantly greater than the 1.2 % (1.1 km^2) proportion projected to flood from the JAXA-SRTM data average. A large expanse of buildings in Mumbai's CBD district (14.4 km^2) would have their ground levels and basements flooded, since the CDEM data considers Mumbai's CBD at sea level unlike the other two datasets (Figure 4.34).
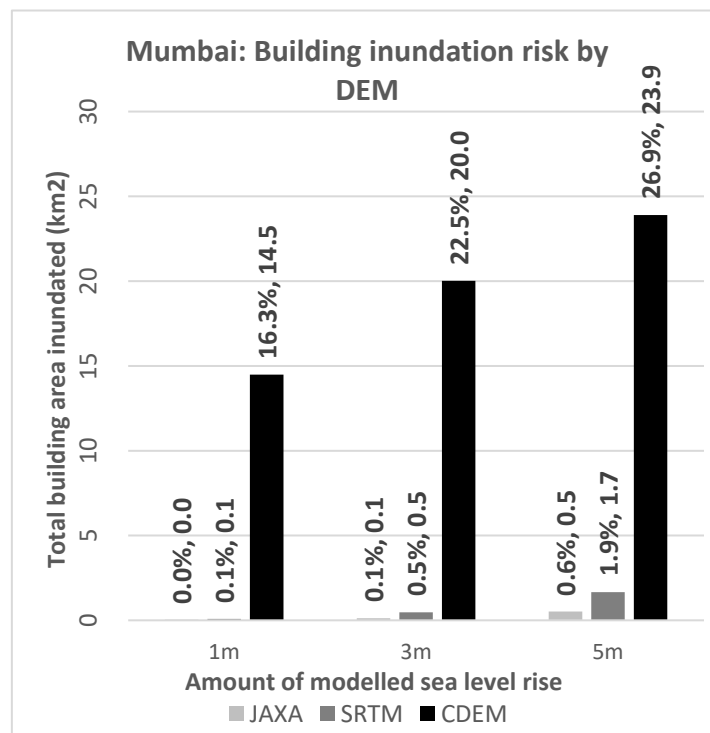
Figure 4.30: Buildings at risk of flooding in Mumbai, compared across elevation datasets

4.2.3.4. Parks

Mumbai has the largest amount of parkland from the three cities surveyed (1,002.1 km^2 in comparison with London's 251.9 km^2 and Bangkok's 18.4 km^2). However, as many of these parks are located at a higher elevation than the western coast, they are less likely to be flooded than other infrastructural elements.

In a 1m (high-risk) SLR scenario, the JAXA-SRTM average of 0.01 % (0.2 km^2) of parkland which would be flooded is less than the findings from the CDEM data at 0.2 % (2.2 km^2). This trend is replicated in a medium-risk (3m SLR) scenario, whereby the JAXA-SRTM average of 0.1 % (1 km^2) shows a lower amount than the 0.6 % (5.8 km^2) parkland inundated from the CDEM data. Similarly, in a 5m (low-risk) SLR scenario, 0.8 % (8.3 km^2) are found to be affected from the CDEM data, in comparison to the 0.3 % (3.0 km^2) JAXA-SRTM proportion average. Having a total proportion of inundation at less than 1 % of the infrastructural area total means that Mumbai's parks would be quantitively the least impacted from the SLR modelling scenarios (Table E4, Figures 4.31 and 4.35 below and Appendix A: Figures A28, A32 and A36).

The parks that will be impacted (Figure 4.35) are limited to fragmented areas around the city's western coastal regions, where the majority of parkland is focused into three parks (Sanjay Gandhi, Tungareshwar and Karnala) in high mountainous regions bordering western city districts.
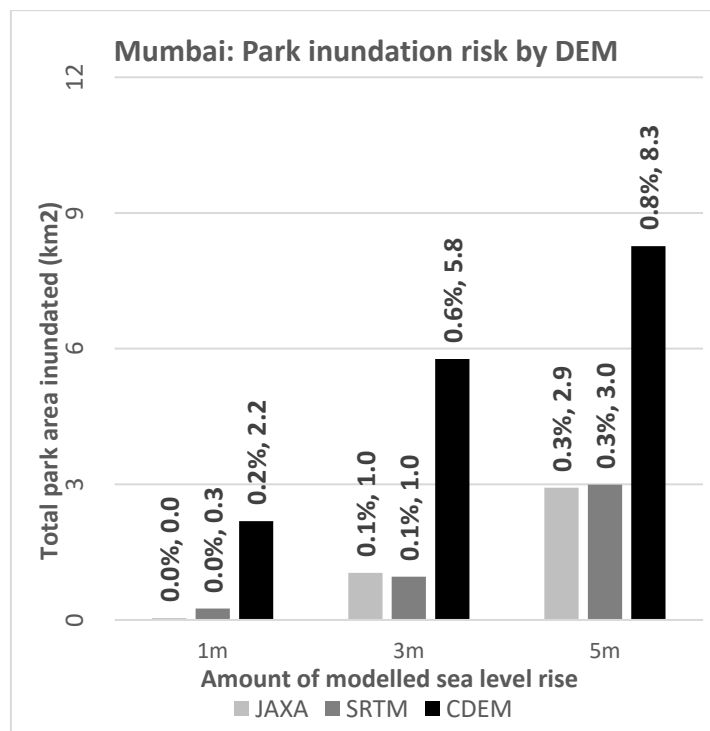
Figure 4.31: Parks at risk of flooding in Mumbai, compared across elevation datasets
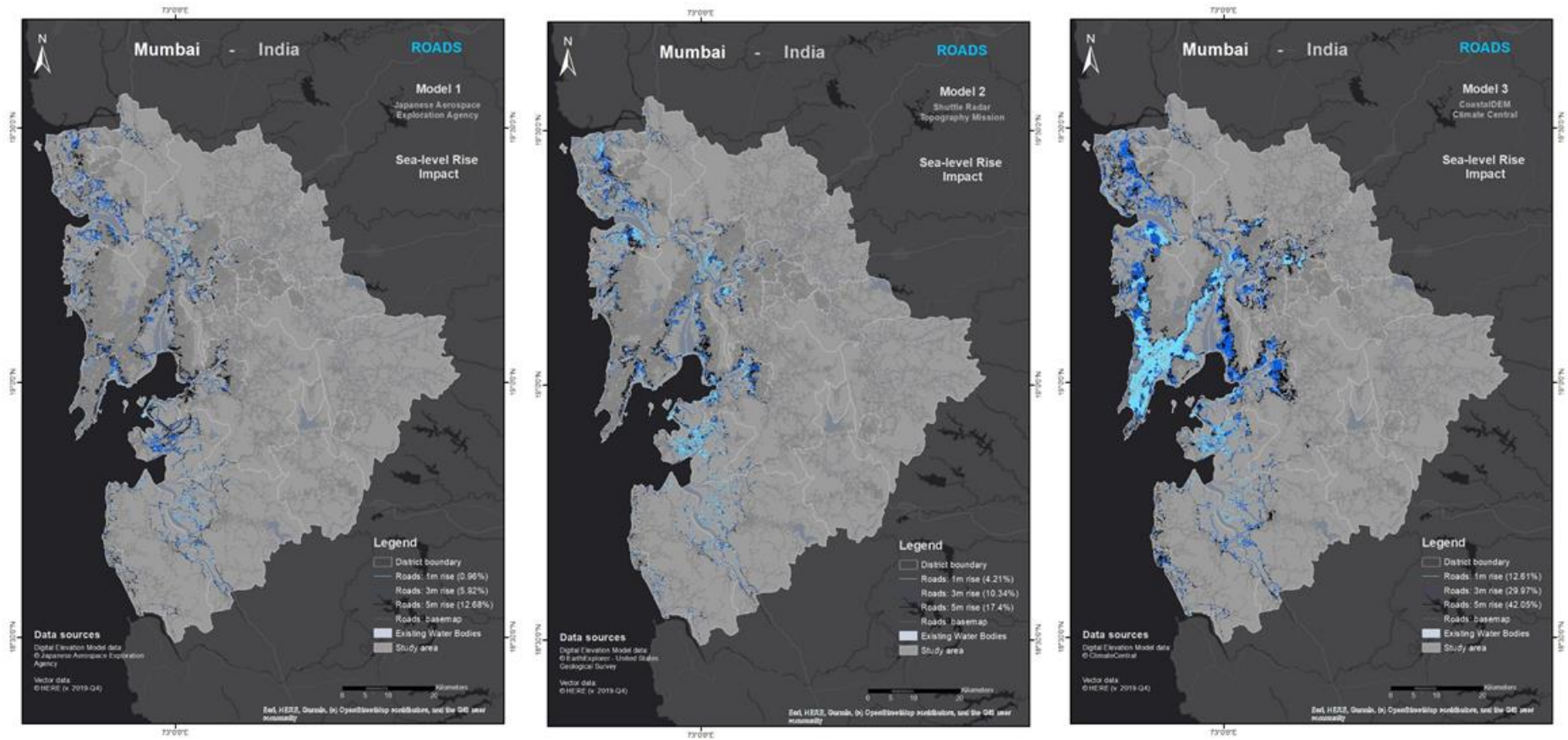
Figure 4.32: A visual representation of Mumbai's road network affected by SLR from the datasets examined (JAXA on the left, SRTM in the middle and CDEM on the right) - Figures A25, A29 and A33 (Appendix A) for greater detail
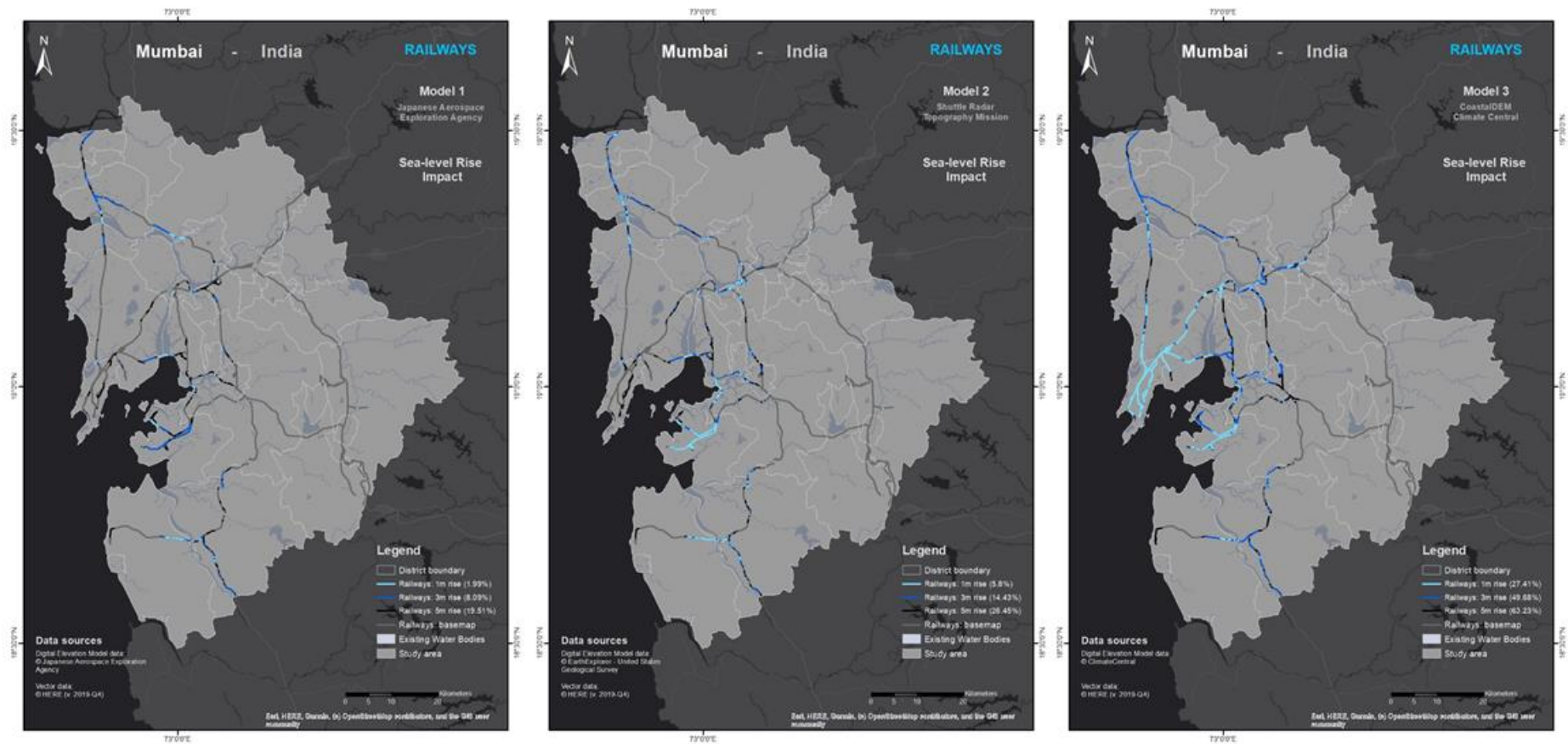
Figure 4.33: A visual representation of Mumbai's railway network affected by SLR from the datasets examined (JAXA on the left, SRTM in the middle and CDEM on the right) - Figures A26, A30 and A34 (Appendix A) for greater detail
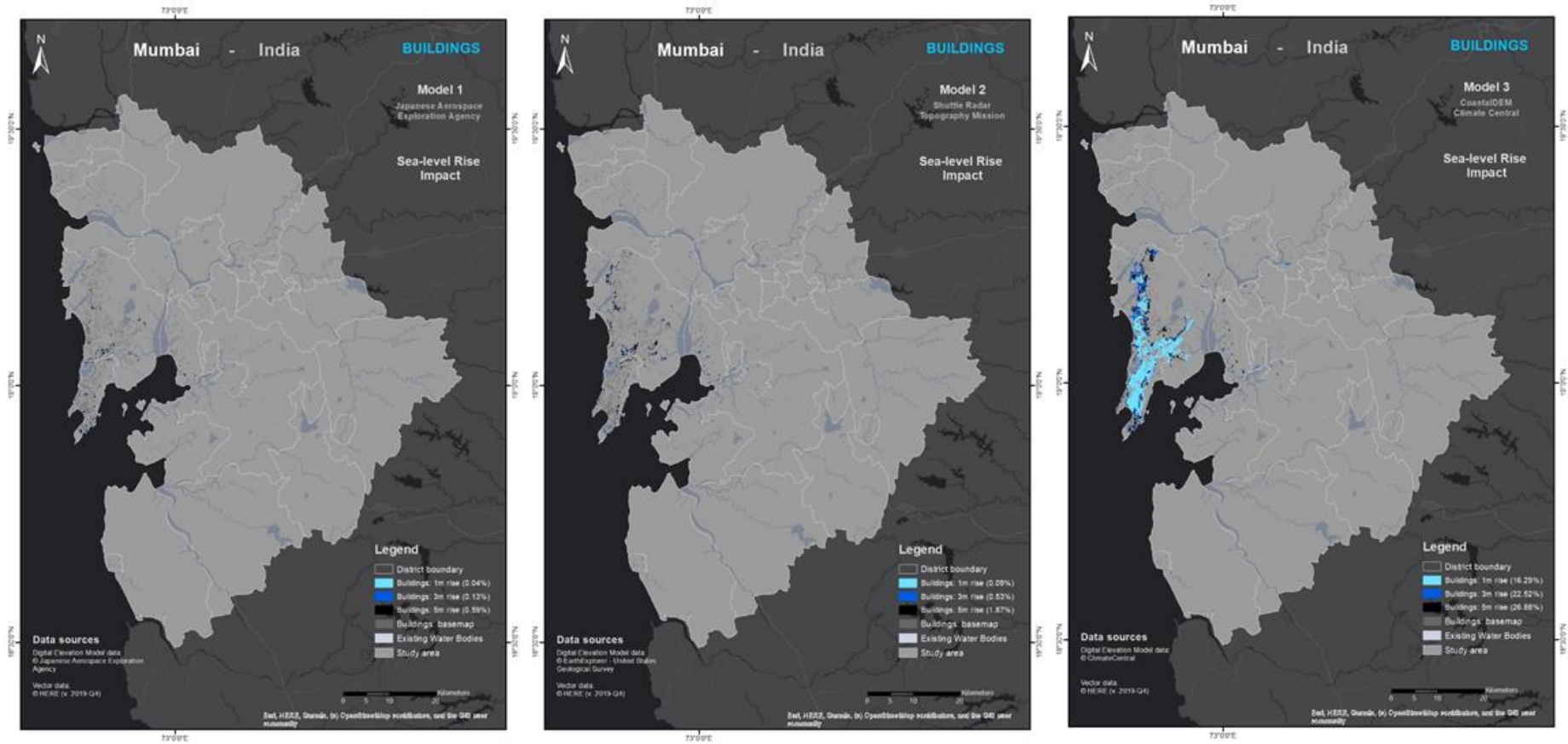
Figure 4.34: *A visual representation of Mumbai's building footprint affected by SLR from the datasets examined (JAXA on the left, SRTM in the middle and CDEM on the right) - Figures A27, A31 and A35 (Appendix A) for greater detail*
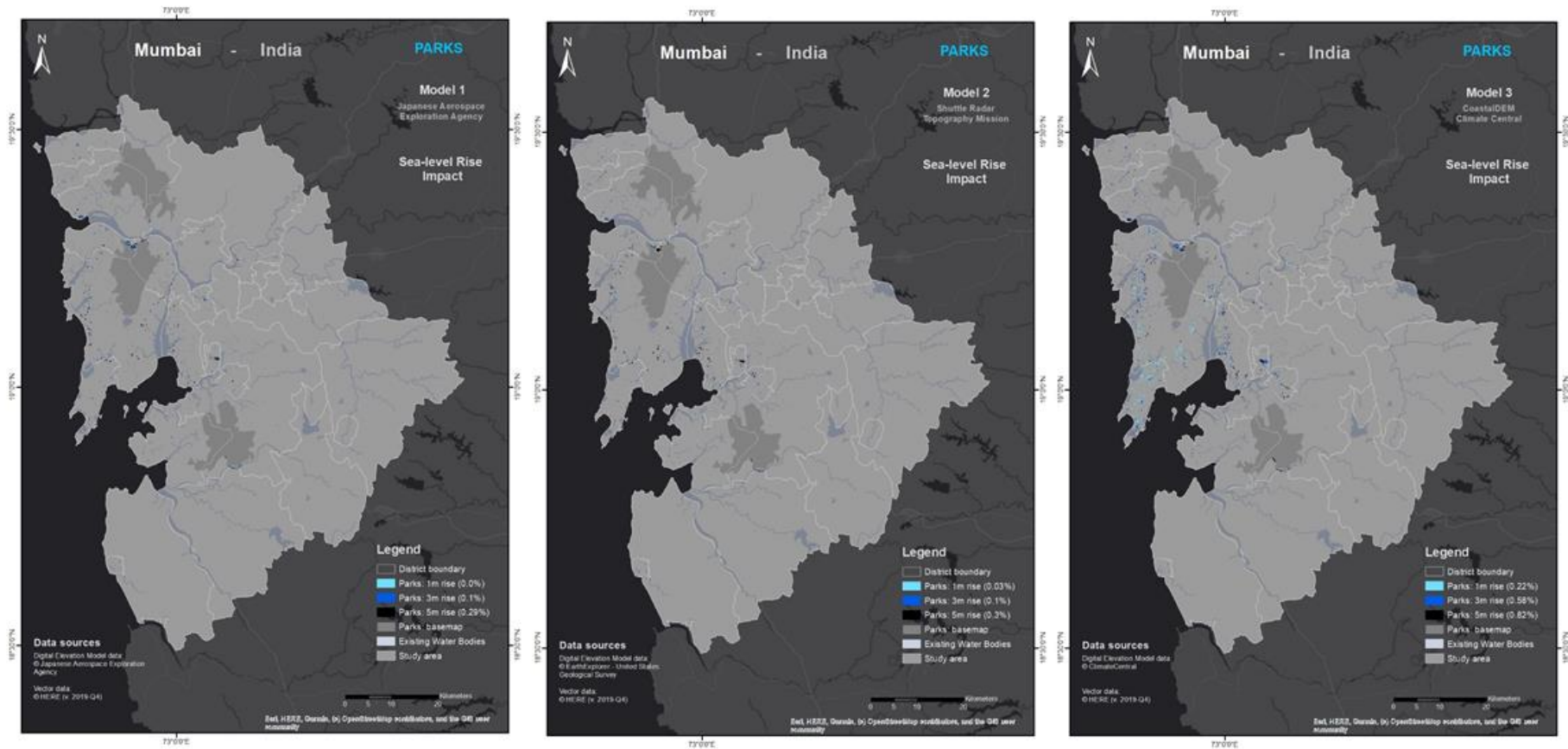
Figure 4.35: A visual representation of Mumbai's parklands affected by SLR from the datasets examined (JAXA on the left, SRTM in the middle and CDEM on the right) - Figures A28, A32 and A36 (Appendix A) for greater detail

4.2.4. Statistical Analysis

Testing of the H_1 dataset has resulted in the acceptance of the null hypothesis for roads, parks and populations impacted across the three cities in a 1m SLR scenario, and parks inundated in a 5m SLR scenario. For these dependent variables, there is no significant difference between the predicted SLR and the rate of infrastructure inundation increase in any specific SLR model. The remaining variables, which constitute the majority, result in a rejection of the null hypothesis, as a significant difference has been found here (Table E10).

Looking at the datasets for H_2, the city districts were isolated into one studied city at a time. Bangkok shows that for most dependent variables in a medium- and low-risk SLR scenario, there is a significant difference between the proportions of infrastructure inundation. The findings agree for Mumbai in a medium- and low-risk SLR scenario, where the null hypothesis is rejected. For London however, only the urban infrastructure elements in a low-risk SLR scenario imply that the null hypothesis should be rejected. Otherwise, it has been found that there is no significant difference between the proportions of flooded urban elements (Tables E11, E12 and E13 in Appendix E).

4.2.4.: Objective 4:
Do the measurements of infrastructural layers at risk match (±20%) across the three cities?

- o **H_3**: There is no significant difference between the quantity of infrastructure inundated across the three study areas.

4.2.4.1. Percentage Values

Table E5 in Appendix E looks at the differences between values in percentage across all three cities and DEM models. From the table (calculated using Tables E2, E3, E4 and E7), it can be noted that very few infrastructure quantities match between cities, where values lie within 20% of each other. Bangkok and London share matching values in a low-risk SLR scenario of 5m for railway lengths between several modelled elevation datasets and with matching values for park areas in the JAXA dataset. Bangkok and Mumbai share matching values of inundated infrastructure in a low-risk SLR scenario for railways, in a medium-risk SLR scenario for park areas (CDEM dataset) and in a high-risk SLR scenario for park areas (SRTM dataset). The only matching values of inundated infrastructure between London and Mumbai lies within railways in a 3m SLR scenario (JAXA dataset).

Within the newer CDEM dataset, the matching values as above are shared between Bangkok and Mumbai in a medium-risk SLR scenario for park areas, and Bangkok and London in a low-risk SLR scenario for railway lengths. An explanation for these values could partially be offset from the coverage amounts for each infrastructure vector layer in each city, as shown in Figure 4.14 for buildings and Figure 4.15 for roads above. These two figures may be viewed with greater detail in Appendix D.

In the case of H_3, the null hypothesis has been accepted outright (Table E14). Here, no significant difference between the quantities of infrastructure inundated for the three cities as whole entities has been found.

4.2.4.2. Vector data coverage matches

Ideally, the HERE vector data coverage is full for the three cities and accurately represented geospatially, however discrepancies in data integrity skew difference results. For example, if London and Bangkok actually had the same summed road network lengths however the availability of the data contains 50 % of London's roads and 90 % of Bangkok's roads, the road lengths inundated by SLR would not be as high an accurate representation of the road network in London as it is for Bangkok, and would imply that there is less of a match between the total road lengths inundated for these two cities using any one particular SLR model. None of the buildings data between the three cities matched (Table E5).

As can be seen in Figure 4.14 above and Table E7, the largest coverage of building vector data has been found to cover Bangkok, where about three times as many buildings are digitally represented (228.7 km^2) than the other two cities (approximately 85 km^2). Figures 4.17, 4.25 and 4.30 as well as Figures B3, B8 and B13 in Appendix B show that significantly more buildings will be flooded in Bangkok than in London and Mumbai, for all three elevation datasets. Although the building vector data coverage is incomplete for London and Mumbai, the study's findings (using all elevation datasets) result in a larger overall area of Mumbai in absolute terms at risk of flooding at the full range of SLR scenarios (particularly medium- and low- risk rises). This is due to where the flooding is expected to impact the city (in the economic centre rather than in coastal fringe suburbs).

Proportionally, this would nevertheless show that Mumbai's buildings would be most at risk in medium- and lower-risk SLR scenarios. For a high-risk (1m) SLR, since more of Mumbai's CBD peninsula is expected to be flooded in the CDEM data than the JAXA and SRTM models, with Figures 4.13, 4.14 and 4.15 above as well as Appendix D: D33 and D34 (with highly representative road and railway networks) showing that key infrastructure would be flooded. Perhaps more complete building data representation would show that in fact the area of buildings directly flooded by SLR would be greater in Bangkok than in Mumbai. This has been recognised as a limitation in the vector data coverage, and thus hinders conclusive results for buildings as an infrastructural layer, in contrast to the findings for the other layers.

4.3. Population counts affected by sea-level rise scenarios

The below charts show the findings of each city's population that is projected to be impacted by the SLR scenarios using the elevation dataset models analysed (numbers in millions of people):
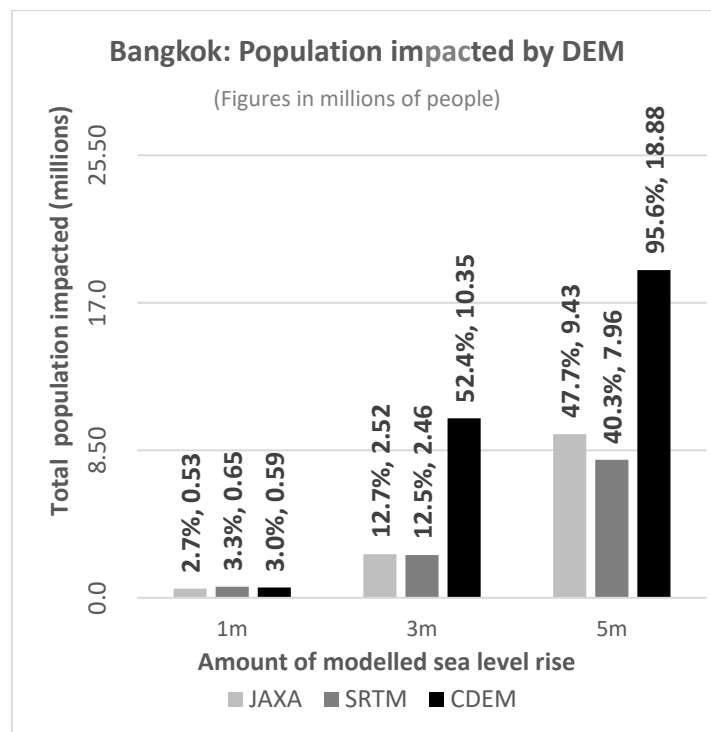
Figure 4.36: Impacted populations by SLR flooding in Bangkok, compared across elevation datasets
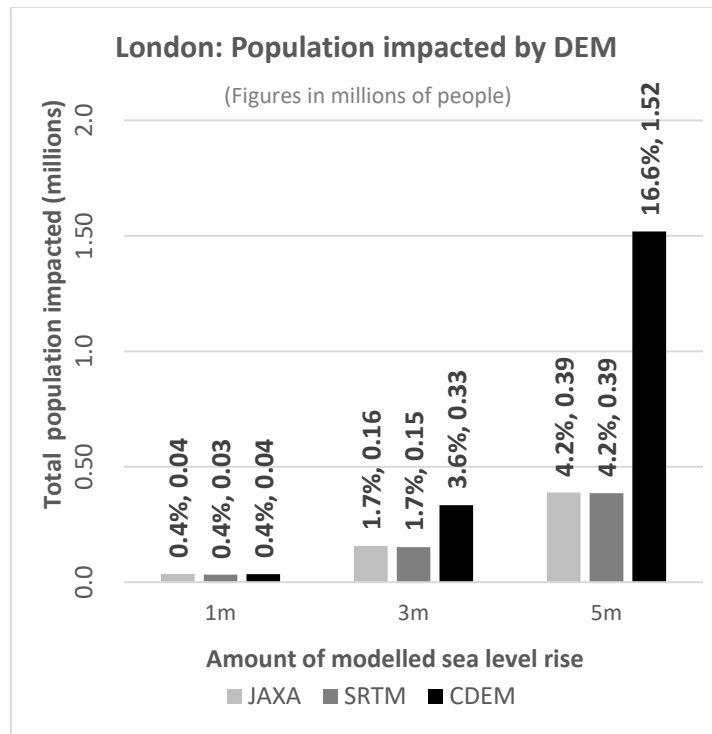
Figure 4.37: Impacted populations by SLR flooding in London, compared across elevation datasets
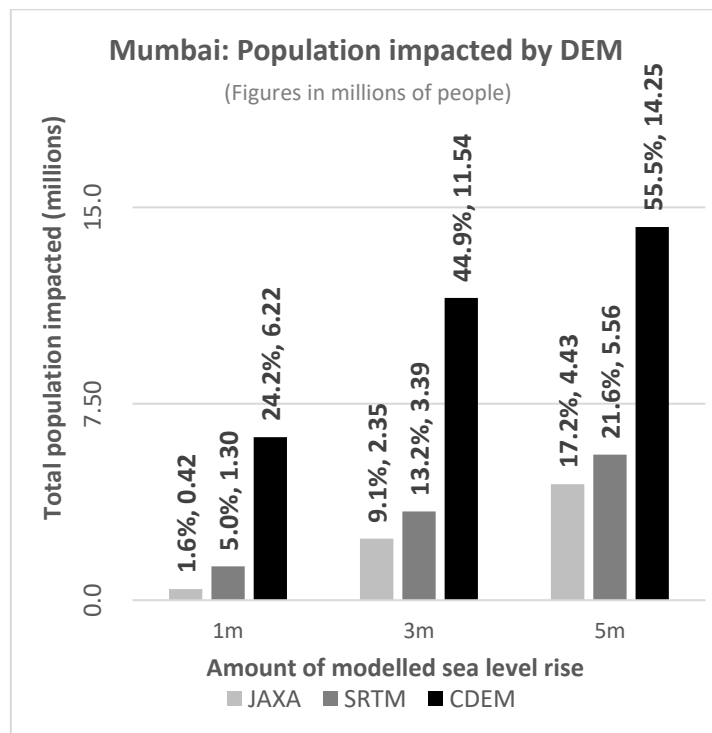
Figure 4.38: Impacted populations by SLR flooding in Mumbai, compared across elevation datasets

4.3.1.: Objective 5:
How many local residents will be impacted by SLR in each city? Do these numbers match (±20%) across the three cities?

     ○ **H₄**: There is no significant difference between the total population numbers impacted by permanent SLR across the three study areas.

Figure 4.36 above and Table E5 show that approximately 3% (0.59 million people) of Bangkok's population of 19.75 million will be impacted by a 1m (high-risk) SLR, while over half of people (52.4 % or 10.35 million) will be impacted by a 3m SLR scenario from the CDEM dataset, and nearly the full population (95.6 % or 18.89 million) would be impacted by a 5m SLR scenario. In London (Figure 4.37), while 0.37-0.38 % of the population (totalling 9.17 million) would be impacted in a 1m SLR scenario, 3.6 % (0.33 million) and 16.57% (1.52 million) would be impacted by a medium- and low-risk SLR scenario respectively using the CDEM dataset. In Mumbai, although the percentages are smaller than in Bangkok, they are closer in number of people affected (Figure 4.38 above). In a 1m SLR scenario (CDEM dataset), 24.2 % (6.2 million) of Mumbai's 25.7 million population will be impacted by the rising water, whereas 44.9 % (11.5 million) would be affected by a 3m rise and 55.5 % (14.25 million) would be affected by a 5m SLR. From Table E6 in Appendix E, the differences between city pairs show similarity in deviation from the average values.

     The only matching values here have been found between Bangkok and Mumbai for a 3m SLR scenario in the JAXA and CDEM datasets, where the former skews the JAXA-SRTM average downward to fit within a matching value. From this table, similar numbers of people will be impacted in Bangkok and Mumbai with a sea-level rise of 3m (2.5 and 2.35 million people respectively for the JAXA dataset and 10.35 and 11.5 million people respectively for the CDEM dataset). Otherwise, significantly varying numbers of people will be affected (for example, a 1m SLR scenario would impact approximately 0.6 million people in Bangkok, 35,000 people in London and 6.2 million people in Mumbai when looking at the CDEM numbers).

     No significant difference between the impacted city inhabitant counts has been found across the three cities (Table E15: null hypothesis H₄). The testing of H₃ and H₄ (resulting in asymptotic significance numbers rather than exact significance numbers) show that dividing the cities into their individual districts (Table E9) results in higher accuracy and confidence for each dependent variable (compare between Tables E9, E14 and E15).

4.4. Comparing risk across the three examined cities (Risk Index findings)

Combining the proportions of the city's urban infrastructure elements and populations into a multi-criteria weighted Risk Index shows how the different city districts are affected with respect to the three input elevation dataset sources (JAXA, SRTM and CDEM). The purpose of this was to examine whether one elevation dataset consistently results in higher risk when divided into districts, and whether the same districts will face consistently greater impacts from a permanent sea-level rise across input elevation dataset models. The results in Appendix C: Tables C1, C2 and C3 show the index values for Bangkok, London and Mumbai respectively.

For all three cities, the risk from all datasets show how infrastructure and population are affected by the modelled SLR extents (Figures 4.39, 4.40 and 4.41 below showing these indices spatially). Within Bangkok, the results (Figure 4.39 and Table C1) show that the south-east of the city would face the greatest impacts, with the 5 districts showing the highest risk indices ranked as follows:

- Bang Phli: 1.0
- Phra Pradaeng: 0.55
- Samut Prakan: 0.516
- Don Mueang: 0.375
- Phra Samut Chedi: 0.371

The greatest collective impacts to London are expected in the east of the city directly bordering the river Thames, as can be seen in Figure 4.40 and Table C2:

- Newham: 1.0
- Barking and Dagenham: 0.813
- Southwark: 0.386
- Greenwich: 0.217
- Wandsworth: 0.190

Whereas the Mumbai city districts at greatest risk concern the central-west coastal region (Figure 4.41 and Table C3) as follows:

- Mumbai: 1.0
- Mira Bhayander: 0.080
- Navi Mumbai: 0.067
- Thane: 0.037
- Uran: 0.032
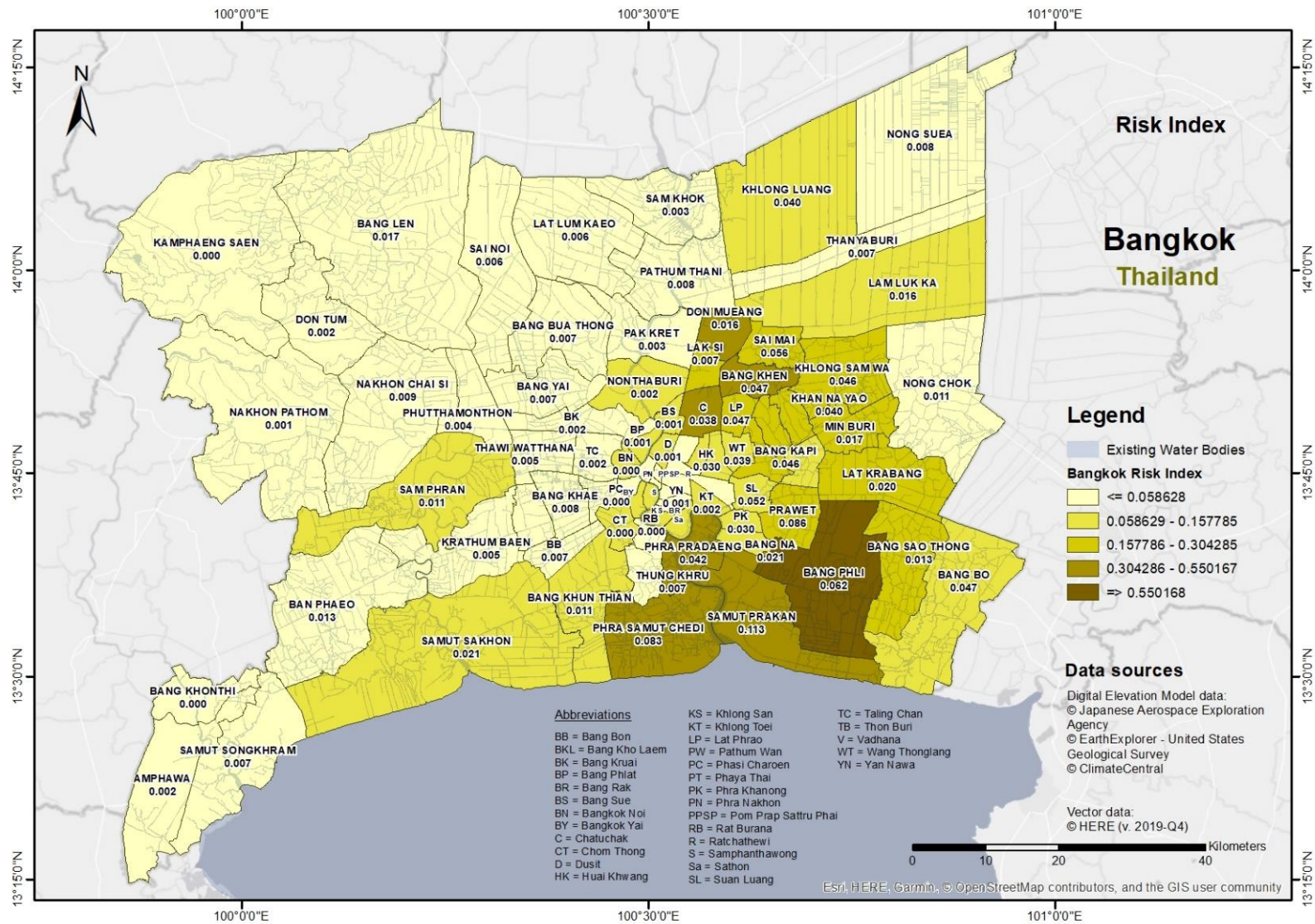
Figure 4.39: A spatial representation of Risk Indices for Bangkok's metropolitan districts, with the south-east coastal area at highest risk from future sea-level rise
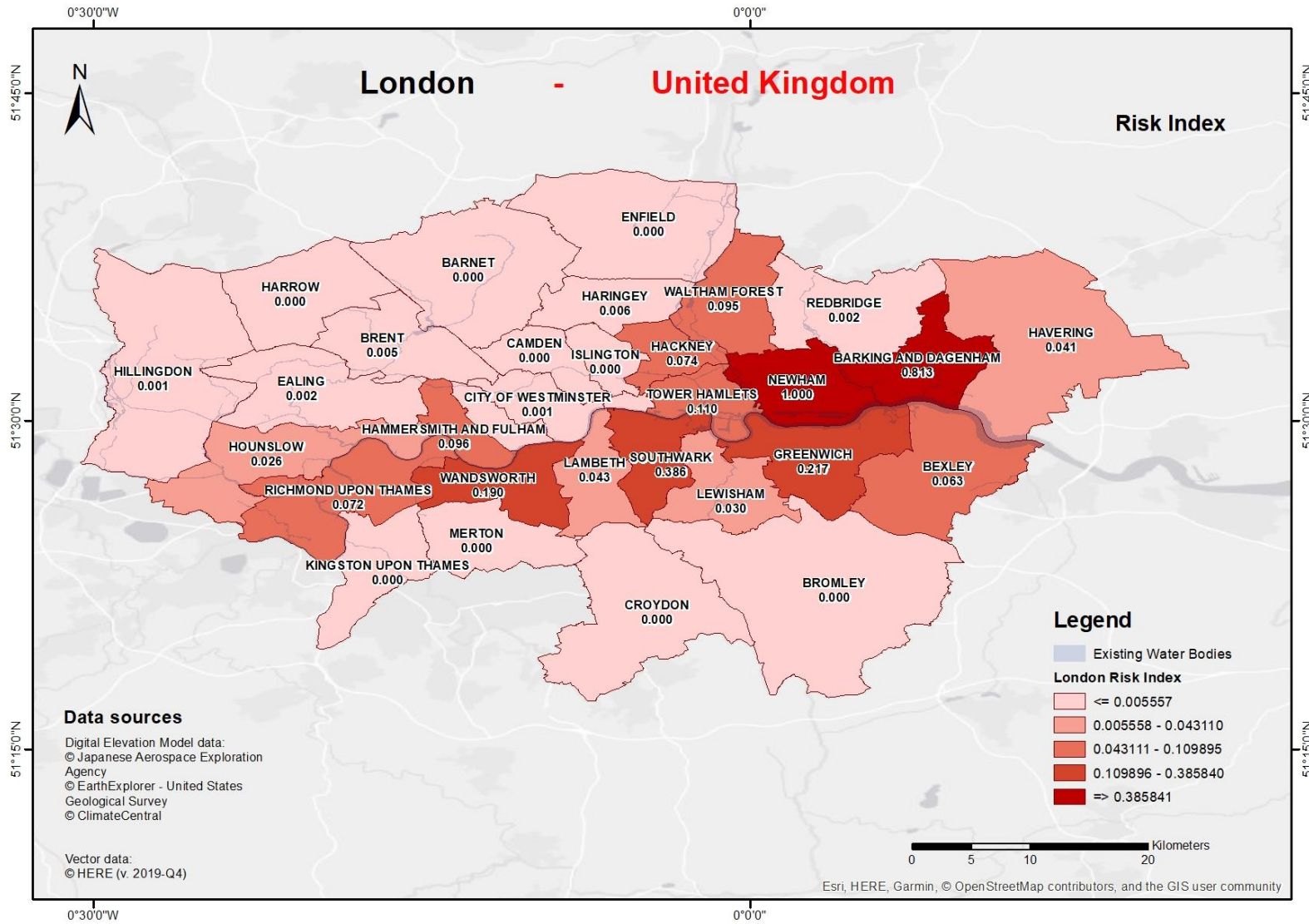
Figure 4.40: *A spatial representation of Risk Indices for the districts of London, where the east of the city is particularly susceptible to impacts from sea-level rise*
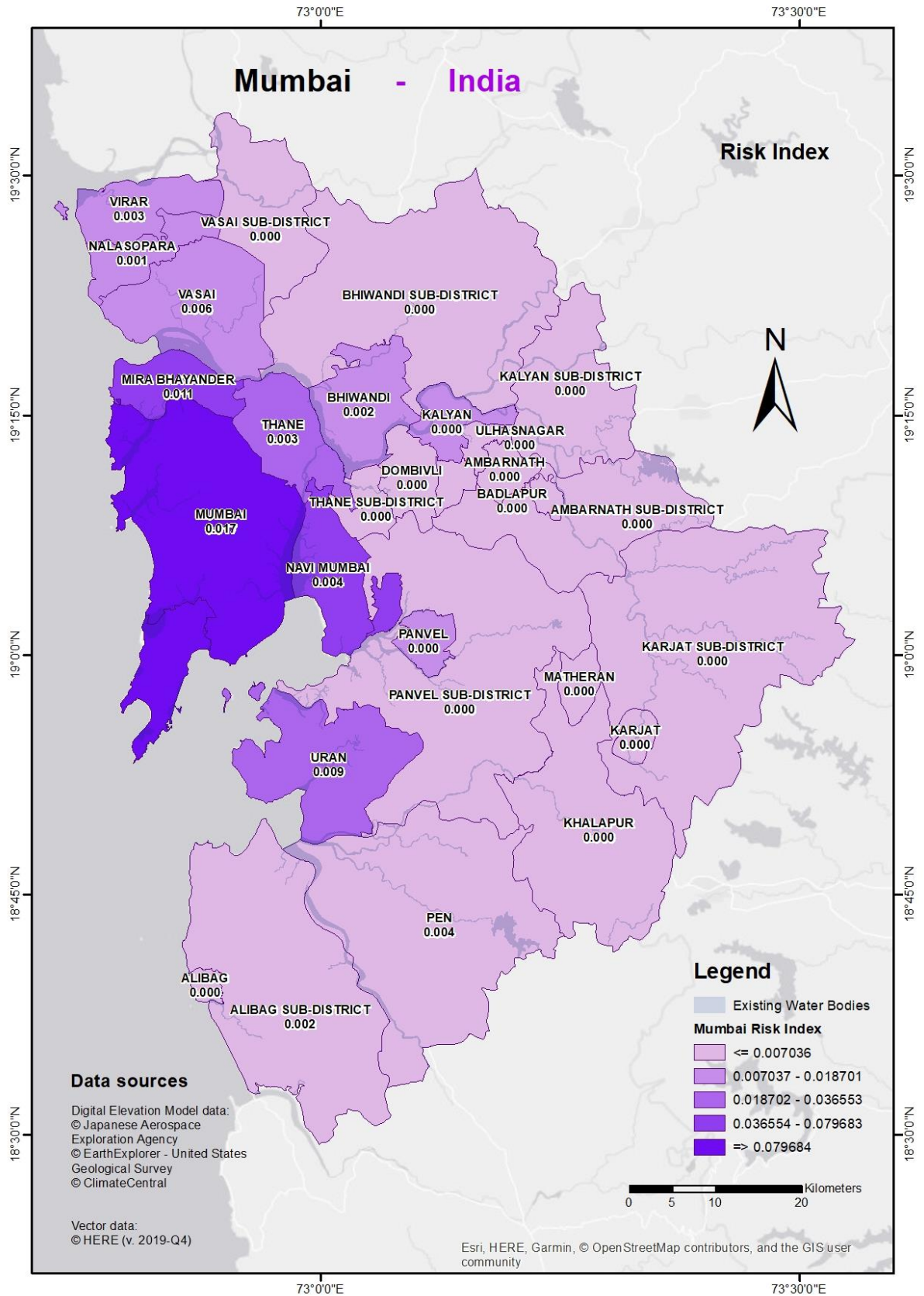
Figure 4.41: *A map showing Risk Indices applied to Mumbai's districts, showing the highest risk of impact from SLR in the coastal west of the city*

-

5. Discussion

5.1. Limitations
5.1.1. Data limitations

Although ideally high-quality source elevation data could be used to assess sea level rise for these three cities with high accuracy, the availability of elevation data varied. The spatial resolution of a source dataset defines its quality, since coarse resolutions could map areas as being vulnerable which may not in fact be at risk, and vice versa. The government of the UK has provided Light Detection and Ranging (LiDAR) quality elevation data at 2-metre, 1-metre and 50-centimetre spatial resolution for the UK, however as of writing the finest open spatial resolution elevation data available for Thailand and India is at approximately 30 metres, or 1 arc-second. The value of a higher quality elevation dataset can be compared with the online interactive map provided by ClimateCentral (2020), where Figure 5.1 below shows an example where raster cells absent from the low-risk 5m SLR scenario in the 3 arc-second data resolution vary from the results in a 1 arc-second resolution set. Budgetary constraints when sourcing the data for this study did not permit the access to 1 arc-second resolution data for the CoastalDEM data, unlike the JAXA and SRTM data.

The inclusion of highly representative vector data for buildings and flood defence structures may strengthen cities' awareness of built-up footprints facing permanent flooding, which may in turn be used to model evacuation maps for short-term flooding scenarios and long-term development planning and ultimately reduce infrastructural losses due to flooding. Economic and socio-demographic data such as monetary values joined to infrastructural data and defined areas of vulnerable populations from potential sources such as demographic segmentation maps and location-tagged economic data (such as residential dwelling vector data with market values attached) may be used to narrow down city areas requiring primary investment.

Further to the limitations above, the infrastructure and populations of the cities within this study have been modelled at present-day configurations and numbers. Cities are rapidly changing settlements, with Bangkok, Mumbai and London having experienced a population increase of over 330%, 310% and 120% respectively in the last 50 years alone (Macrotrends LLC, 2020). This has had knock-on effects to the city's infrastructural elements, which have multiplied significantly in response to the additional demand on the cities' transportation, public structures and core industries (Brueckner, 1997; Bjorvatn, 2000). The increased influence of these cities on global finance, tourism and trade have also raised their status as desirable destinations for economically-driven rural migrants and foreign skilled workers. As a result, the impacts on the three cities as set out by this study assume equal population and infrastructural structure quantities and layouts over the remainder of the 21st century. Applying population and infrastructural change predictions would benefit future studies within these regions, however at the time of study such prediction data remains an uncertainty because of

the difficulty of quantifying future predictions on the several factors mentioned above (Jedwab, Christiaensen and Gindelsky, 2015).
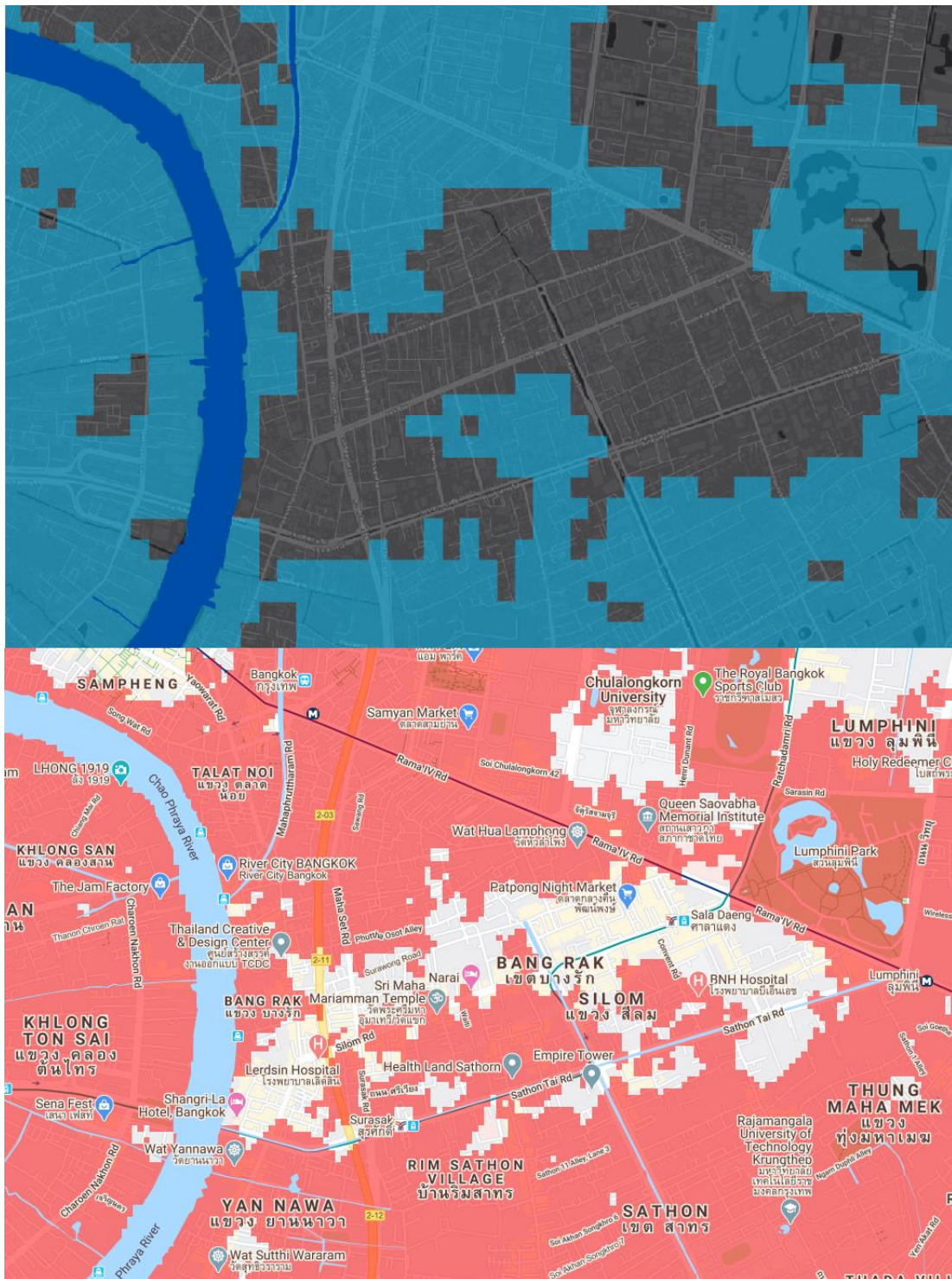
Figure 5.1: *Comparisons between the 90-metre spatial resolution CoastalDEM dataset (above) and the 30-metre resolution data (below) for a 5m SLR scenario. The area focuses on Bang Rak, the CBD of Bangkok city. In the top picture, dark blue shows the existing Chao Phraya river, and light blue shows the flooding extents at medium-risk. In the bottom picture, the Chao Phraya river is light blue and the flooding extents shown in red.*
Source: ClimateCentral, 2020

5.1.2. Geometric limitations

The digital geometric representation of vector data used in the study (sourced by HERE) has also been identified as a limitation. Navigational data at this stage primarily focuses on the accurate and verified data capture of a location's transportation networks such as roads or railways, as well as addresses of commercial enterprises. Data quality checks on the data used for this study (visually merged into Figures 4.16 for buildings and 4.17 for roads, or all figures in Appendix F) show that while road network data is highly representative of real-world conditions, buildings data varies by country and jurisdiction. As a result, the results of this study showing which buildings are at risk may not be as accurate as intended due to missing or unavailable data as of late 2019. The data supplier is however constantly adding and modifying data using multiple ground-truth and remote sensing sources, so future versions of the data are likely to contain additional features across the available layers.

The spatial relationships between the areas of inundation modelled in this study and the vector infrastructural data are dependent on square shapes recalibrated from raster cells to vector polygon areas, rather than smoothened polygon edges which is more realistic when understanding a creeping sea level rise, as it is along present-day coastlines. Although the polygon areas could have been smoothened when preparing the data for intersection and clipping, the raster cells contained the highest accuracy from the source elevation data and thus were retained to their original shape. This limitation could partly be addressed by the amalgamation of LiDAR high-resolution data cells into polygon areas.

The projection used for all the datasets (EPSG:4087 or Equidistant Cylindrical projection) was chosen to calculate accurate lengths and areas for the sea level rise extents and the infrastructure examined. This projection may have distorted measurements depending on their latitude and longitude, where the highest accuracy is closest to the Equator on the Greenwich meridian line (0°N, 0°E) and distortions increase the further away from these standard parallels an object is measured. Bangkok is closest to the Equator at 13.5°N but furthest from the Greenwich meridian line (100°E). Mumbai is further from the Equator at 19°N but closer to the Greenwich meridian line at 73°E, while London is on the Greenwich meridian line but at 51.5°N is the furthest from the Equator. As a result, the projection chosen is a geometric limitation of the true ground-truth accuracy of the measurement of each variable examined in the study, however retaining the same projection throughout would render the proportions of infrastructure and city area impacted close to true values.

5.1.3. Methodology limitations

Predicting sea level rise is a multi-faceted process and not considered to be linear, since data inputs and the local topography of the land studied lead to varying levels of exposure to sea level rise. To model permanent sea level rise spreading from the cities' coasts inland, a linear bathtub-fill modelling approach was used and refined within GIS, similar to the approach undertaken by Nistora (2018) and Arnesten (2019). The study only considers rising water levels from one surrounding water source (the ocean) and not the effects on local sea levels from rises in groundwater or the influence of fluvial inputs from upstream sources, as well as localised tidal changes over time.

Groundwater level considerations depend on the local area's geological structures and their annual precipitation patterns, the latter of which would also impact surface water inputs from tributary sources. Local meteorological patterns due to long-term effects of climate change are predicted to increase local rainfall by over 10% in Mumbai and 5% in Bangkok and London (Christensen *et al.,* 2007), so temporary flooding or drought events may directly influence water levels in localised pockets around the cities. Modelling multiple hydrological inputs may be input into GIS software, however capabilities to process dynamic and localised changes as part of a wider entity (such as a city's metropolitan area) are limited at present. Nevertheless, a benefit of the data preparation and methodology steps applied in this study is that these can be used within a range of GIS software packages. The tools used for this study were based on those available within the ESRI Suite of products, namely ArcMap and the ModelBuilder, Spatial Analyst and Geoprocessing tools within. For geospatial users without access to ESRI, the steps in the ModelBuilder could be applied through Extract, Transform and Load products such as FME and then analysed in QGIS or MapInfo.

Similar to the studies previously set out by Nistora (2018) and Arnesten (2019), this study does not provide a timeline for the projected sea-level rises of 1, 3 and 5 metres above present-day levels. This is because scientific climate change data is constantly changing due to new research and applied methods, as well as uncertainties in the modelling of sea level rise from industrial carbon emissions and the stability of polar ice sheets. With each publication of the IPCC official Assessment Reports, increased data inputs and understanding of the global economy's emissions scenarios results in the alteration of the expected sea level rise throughout the 21st century (Parry *et al.*, 2007; IPCC, 2014). The comparative risk indices calculated for each municipal district and application of risk labels to each SLR scenario enables the reader to understand which municipal areas and urban infrastructure assets require more immediate resilience analysis.

5.2. Outcome of study objectives

The main objective of this study was to identify the amount of spatial urban infrastructural assets exposed to projected sea level rise scenarios of 1, 3 and 5 metres above present-day sea levels, and then compare this data between three globally influential metropolises (London, Bangkok and Mumbai). Together with the urban infrastructural layers such as roads, railways, parks and buildings, the cities' population data was also spatially analysed to quantify the proportion of local residents that would be affected by such a rise in sea levels. By comparing these three cities similar in age, population size and regional economic output, the study aimed to understand whether sea level rise would impact the three cities in the same way or some more substantially than others.

In order to be able to compare the cities like-for-like, elevation data with identical resolutions and properties needed to be sourced, as well as reliable vector data containing urban infrastructural layers. Two elevation datasets traditionally used in sea level rise analyses (JAXA and SRTM) were sourced at 1 arc-second spatial elevation, while a newer elevation dataset designed with algorithms to remove vertical errors of the first two elevation datasets (CDEM) was sourced at 3 arc-second spatial elevation and not 1 arc-second like the first two due to budgetary constraints. The vector data source (HERE) contained navigational data in vector format with multiple context layers, with global coverage and produced to the same standard around the world. This reduced potential discrepancies between locally sampled data, and allowed for the equal comparison of the infrastructural assets across the three cities. Intersecting the elevation data with the urban infrastructural layers through GIS processing and a bathtub-filling modelling approach enabled the cutting out of each layer and calculations as well as spatial representations to be applied. Further to the resulting calculations, risk indices were applied across each administrative district in each city to quantify the level of risk exposure of each district based on the density and quantity of infrastructural assets within to an encroaching sea level. The values were each also subjected to Kruskal-Wallis independent median testing to result in the acceptance or rejection of specified null hypotheses.

Specifically for each study's objective, the following questions were asked with their relevant hypotheses when compiling the study's findings:

1. **How much of each city's land area is at risk from simulated SLR of 1, 3 and 5 metres respectively?**

The study was able to meet this objective, where Table E1 as well as Figures 4.1, 4.2 and 4.3 show that in a 1m sea level rise scenario, Mumbai is proportionally the city at highest risk, with 7.8 % of its area expected to be inundated using the JAXA-SRTM data and 9.8 % using the CDEM data. This is only slightly higher in proportion to Bangkok, while approximately 2 % of London would be impacted by such a rise. For a 3 and 5 metre SLR scenario, Bangkok appears to be the city at highest risk of inundation with 18.7 % and 58.0 % of its area expected to be inundated using the JAXA-SRTM data and 50.9 % and 91.5 % using the CDEM data, for each 3 and 5 metre SLR scenario respectively. Comparatively, a maximum of 26.5 % of Mumbai and 13.2 % of London are projected to be impacted in a 5m SLR scenario using CDEM data.

The variances in proportions and geographical locations for the three cities depends on their individual geomorphological characteristics. Bangkok as an entire city is located on a low-lying, gently sloping floodplain made of soft clay within the catchment of the Chao Phraya River. The land surface here is smooth and this means that slight sea-level rise from the Gulf of Thailand will spread to neighbouring areas. Additionally, the presence of urban infrastructure on the land applies downward pressure in particular to the primary economically developed area, while well pumping drains parts of the floodplain from frequent waterlogging. As a result, together with landward-encroaching sea-level rise, the city is also at a slightly higher risk from land subsidence at a rate of approximately 2-3 cm a year. Assuming that a 1m SLR scenario from the global oceanic water volume takes 50 years to develop in the region, the land subsidence rate means that Bangkok would actually experience this level of sea-level rise in half the time of 25 years.

The economic centre of Mumbai is built on a peninsula of land that connects seven islands on the western coast of India, exposed to the Arabian Sea. The coastal regions of the city contain populated low-lying areas of a swampy nature with a high number of drainage tributaries, whereas further inland the landscape is shaped by denudation of hill ranges that are more sparsely populated. Geographically from Figures 4.1-4.3 and 4.7-4.9, it appears that less of the city's total area is at risk from a 1m SLR than Bangkok is, however larger tracts of land are at risk in densely populated and built-up areas rather than smaller pockets in Bangkok in areas focusing more around rural and industrial development. The rising land surrounding the tributary drainage areas protects inland regions from also being flooded.

London is geomorphologically a balance of the above two cities. Previously low-lying and silty subsiding ground on the river banks of the Thames were reinforced by sea walls in the 19th century, with the aim to protect the inhabited city from tidal river rises. The rivers Thames and Lea are the two main tributaries in the area, where the land elevation rises to an eroded hilly landscape towards the north and south of the city. This concentrates landward-

encroaching SLR from the North Sea to the river banks, flooding land that is predominantly used for industrial and commercial purposes rather than residential.

2. **Will SLR simulations using a newer elevation dataset show differences in flooding next to older datasets?**
   - H_0: There is no significant difference in how much land area is at risk of SLR using the three different SLR models

Significant differences in the land area at risk of SLR flooding were output from the simulations using the CDEM elevation dataset. For all variables except for roads and population in a 1m SLR scenario, H_0 was rejected by the Kruskal-Wallis testing (Table E9). This implies that there is a significant difference between the inundation risk expected across the three datasets and three cities for most variables, as confirmed by Table E1 in Appendix E.

The methods used by ClimateCentral's researchers to cancel out vertical errors in areas containing clusters of tall buildings, and matching this with LiDAR ground truth measurements in different parts of the world, give the researchers a high confidence of the accuracy of their elevation dataset. In all three cities, minimal differences in the land area proportions are present between the JAXA, SRTM and CDEM data in terms of absolute percentages, however significant geographical differences are present when looking at Figures 4.1 to 4.9 in Chapter 4. Whereas the older elevation datasets show the economic hubs of Bangkok and Mumbai on elevated land, where simulated SLR surrounds these areas, the CDEM dataset shows that both cities' economic centres are located on lower lying ground. As a result, the increased risk exacerbates the cities' functionality on a daily basis significantly.

A larger gap in the differences of the findings is present in a 3m SLR scenario using the CDEM data, where land showing exposure to flooding increases by a factor of 1.5 to 2.7 in comparison to the JAXA-SRTM data average. This means that over half of Bangkok will be flooded from the CDEM data rather than just under one fifth. Similarly, over a fifth of Mumbai will be flooded in comparison to its previously estimated one seventh. This is compounded in a 5m SLR scenario, where almost the entirety of Bangkok is at risk of flooding (next to the estimation of just over a half using older data), and over a quarter of Mumbai is at risk rather than just under one fifth.

As mentioned in the data limitations earlier, the spatial resolution of the data used affects its accuracy. A raster dataset with finer cell dimensions for the CDEM data used in the study (3 arc-seconds) would provide an increased level of comparability with the older datasets, which are of 1 arc-second. As Figure 5.1 above shows, the simulation using the CDEM data is coarser than that present from the JAXA and SRTM datasets. This provides an opportunity to simulate SLR in the three cities using finer-resolution CDEM data, which couldn't be sourced for this particular study.

3. **Within the three cities, where is the urban infrastructure at risk concentrated? Will this affect the cities' future functionality?**
    a. **H_1**: There is no significant difference in how much urban infrastructure is impacted by increasing SLR simulations (for any one SLR model)
        i. This focuses on whether the amount of infrastructure at risk is proportional to the SLR amount.
    b. **H_2**: There is no significant difference between the amount of a city's land area and each of its urban infrastructural layers flooded by permanent SLR
        i. This focuses on urban infrastructural layer exposure in each city.

The spatial distribution of the risk modelled across the three cities as well as charts are visible in Figures 4.11 through 4.35 in Chapter 4 above, whereas risk index maps are present in Figures 4.39 to 4.41. In Bangkok, the infrastructure at risk appears to the fringes surrounding the city's economic centre and the south from the JAXA-SRTM datasets, while the CDEM dataset shows the sea level encroaching on much of the city's area including the economic centre in a 3m SLR scenario. In Mumbai, the JAXA and SRTM datasets show flooding on the eastern lower population density fringes of the city (Uran and Mira Bhayander in particular), however the CDEM dataset model shows that most of the city's highly populated economic hub will also be at risk of flooding. Flooding in London is retained to the eastern section of the Thames river, as well as parts of the River Lea northward using the CDEM dataset.

Although all infrastructural layers that are flooded will impact the cities' functionality, they do so differently. Roads that are flooded slightly or incompletely are still passable, unlike rail tracks which are unusable beyond the point of flooding. The permeable ground and vegetation in parks helps to absorb incoming excess water, however these areas are mostly used for social recreation and not vital economic function. Due to limitations in departmental network contacts and the availability of detailed local data such as social and economic values for each city, the implications suggested by this study can only be comparatively from a geographical perspective. Bangkok and Mumbai in particular will however face significant impacts on the cities' ability to function on a day-to-day basis from the CDEM data and to a lesser extent from the JAXA-SRTM data, because their respective business district areas and coastal industries are projected to be inundated even with a 1m rise in sea levels.

Tables E10 to E13 from Appendix E show varying results depending on locality; while H_1 is rejected outright, H_2 is rejected for Bangkok and Mumbai and accepted for London. This means that when looking at the urban infrastructure, when looking at all cities collectively and the two Asian cities at greater risk, there is a significant difference both in how much infrastructure is impacted by SLR, and between the proportion of a city's land area and each of the urban infrastructural layers impacted. Due to the HERE's greater digital vector data representation particularly for buildings in and around the economic city centres, this correlates with the land at risk for these two cities. H_2 is accepted for London because a comparatively small percent of the city and its infrastructure is at risk from the findings in Chapter 4. Although answers have been provided, they are partly inconclusive where buildings are concerned as this representation in the statistical analysis is dependent on the completeness of the source data.

The lack of complete building data for all the study areas has been identified as a limitation and could be addressed in future studies where more comprehensive building data is available.

From a geographic standpoint and assumption that roads and railways are operated in the same way across the three cities, the implications for the accessibility of transportation networks in SLR scenarios are significant for each city. A 1m SLR will impact road networks minimally in all cities using the JAXA and SRTM models, where the flooded streets could be circumvented by local populations on a daily basis (Figures 4.11 to 4.35 in Chapter 4). Using the CDEM model however, access to Mumbai's road network in and around the city's economic hub would be hindered enough to affect the city's functionality on the basis of people commuting, moving goods and being able to drive across the densely populated city centre. The railway network in Mumbai will be the most affected by a 1m SLR, while Bangkok and London will not face disruptive impacts to the railway lines until the 3m SLR scenario, using all datasets. Without detailed knowledge of local transportation networks for the three cities, the specific impacts on the cities' transportation networks cannot be concluded from this study and as such this is a limitation which could be used for future study.

4. **Do the measurements of infrastructural layers at risk match across the three cities?**
   o **H₃**: There is no significant difference between the quantity of infrastructure inundated across the three study areas.

Tables E2 to E4 and E7 in Appendix E as well as the charts in Chapter 4 and Appendix B show the total lengths and areas of each infrastructural layer that would be inundated by each SLR scenario across the three different elevation datasets used. These are compared for matching in Table E5 where values were checked to be within 20 % of each other. Table E14 shows that the Kruskal-Wallis independent testing accepts H₃, so no significant difference has been found from the statistical analysis in the quantity of infrastructure across the three study areas. This is however not the case when one compares the aforementioned tables, charts and figures visually and numerically. It is therefore likely that another method of statistical testing than the Kruskal-Wallis test or a reorganisation of the data before running the tests would be a better way to test these values' significance against each other.

5. **How many local residents will be impacted by SLR in each city? Do these numbers match across the three cities?**
   o **H₄**: There is no significant difference between the total population numbers impacted by permanent SLR across the three study areas.

Section 4.3 in the results including the relevant charts (Figures 4.36 to 4.38 in Chapter 4, Figures B5, B10, B15 in Appendix B) quantify the permanent city residents expected to be impacted daily by the permanent sea level rise scenarios. The JAXA, SRTM and CDEM models all confirm that the most residents will be impacted by a 1m rise in Mumbai (3.3 % for

the JAXA-SRTM average and 24.2 % using the CDEM data), while this changes to Bangkok as the sea level rises to 3 and then 5 metres (12.6 % of Bangkok's population impacted by a 3m SLR using JAXA-SRTM and 52.4 % using CDEM data; 44.0 % impacted by a 5m SLR using JAXA-SRTM and 95.6 % using CDEM data). The results using the CDEM data imply that at the least, 1.5 million people will be impacted in London and at most, 18.89 million or nearly the whole population of Bangkok will be impacted in Bangkok in a 5m SLR scenario. The numbers between the cities do not match for most scenarios and show large differences (Tables E6 and E8), however hypothesis H_4 has been accepted across the three cities, suggesting that there is no significant difference between the total population numbers impacted across the three cities (Table E15). The data for Bangkok and Mumbai likely affected the exact significance number of the p-value in the statistical testing, as these two cities both contain comparable levels of population at risk from SLR, unlike London which has far fewer inhabitants at risk.

6. Is a bathtub-fill modelling approach effective in simulating local SLR?

The methodological approach undertaken in this study serves to simulate landward-encroaching sea-level rise from the oceans present near the chosen cities, increasing the volume of the tributaries in the local catchment area while marking that increased elevation as water instead of land. As an example, raster cells in the elevation dataset having an original value of -1 metre in elevation have been changed to a zero-metre elevation, raising the coastline and tributary edges by 1 metre. The land intersecting this new changed coastline has been marked as inundated by permanent sea level rise. This was then compounded to achieve the simulations for 2 through 5 metres, though only the 3- and 5-metre rise scenarios were used for this study.

Although this is a reliable way of modelling permanent sea-level rise above mean sea level and indicating which tracts of land are vulnerable to flooding, this depends on the accuracy of the original elevation data as mentioned in the similar studies described in the Background section of this report. Objective 2 (and Figures 4.1 through 4.9) in this study show that all three elevation datasets used result in different areas of land at risk for each city in different SLR scenarios. Surface elevation value errors noticed in the SRTM and JAXA datasets have been repaired using neural networks and Gaussian model processes in the CDEM data by ClimateCentral, though the spatial resolution of the data used also affects local accuracy.

Further to this, sea-level rise using this methodological approach only takes two main hydrological features into consideration, that is the oceans present around the cities and the tributaries present in their geographical metropolitan areas at mean sea level. Sea-level rise is influenced by multiple hydrological sources including increasing groundwater volume, rainfall causing flooding over impermeable urban surfaces and increasing water in tributaries from the source, and diurnal tidal ranges. Landward-encroaching sea-level rise therefore gives a highly

accurate simulation of land at risk of flooding in areas where hydrological inputs are limited, such as those with minimal rainfall and no groundwater present underneath the land surface.

In reality, all three cities experience high values of local rainfall and varying tidal ranges while containing subterranean groundwater networks. Pockets of land containing groundwater at a shallow depth may break the ground surface and cause permanent puddles or lakes to form apart from areas along the city's water tributaries. Localised rainfall may exacerbate this effect and form a stream running from this area of water downhill to the nearest tributary. This simulation might therefore be sufficient to alert locals and authorities of the city areas exposed to the SLR scenarios, however it is likely that this study underestimates how the flooding will affect the land within each local metropolitan area.

5.3. Recommendations for future research

Several opportunities have been identified for future research from this study, which may be applicable not only to these three economically active, highly populated cities but also to other coastal regions of environmental and social importance. The key priority would be to engage in data collection and dissemination efforts of high-resolution LiDAR elevation data to fill in the current gap between available data for more and less economically developing countries, and use this to model SLR to a highly accurate level (as was also suggested by Nistora in her 2018 study). The methods used could also be replicated with a larger available budget using 1 arc-second spatial resolution elevation data from ClimateCentral, to quantify impacts to infrastructural elements on the same resolution as the elevation data by the United States Geological Survey (SRTM) and the Japanese Aerospace Exploration Agency (JAXA). Following this, dynamic sea level rise modelling may be performed using locally available groundwater, fluvial morphology, drainage and tidal data from municipal departments, which could be applied within combined hydrological analyses to better understand local patterns of multi-input SLR extents (Bender and Ginis, 2000; Boonya-aroonnet *et al.*, 2002; Gupta, 2007; Saito, 2014; Singh, 2018; Dhiman *et al.*, 2019; Phamornpol, n.d., Phatak, n.d.).

Economic and socio-demographic values of land at risk for each city are opportunities which can be investigated. Whereas physical infrastructure roads, railways, buildings and parks have been examined, they have been treated as having equal economic and socio-demographic value across the three cities in this study. In reality, certain parts of the city (such as the outskirts) might contain infrastructure which is cheaper to replace than in other parts. Comparing the risks on their commercial and industrial centres to suburban areas has been described in this study from a geographic perspective, however specific locations and values of necessary infrastructure to keep the city functioning and economically active (such as trading ports, water sewage treatment plants and power stations) have not been included within the risk

index calculations. This leaves a gap in the findings whereby the risk to individual city districts have been treated on an equal infrastructural basis. Going forward, studies could focus on these aspects of the cities from locally sourced and available relevant data and used to provide clear impacts on sea level rise to these components, as has been studied by Brueckner (1997), Clarke *et al.* (2002), Johnston *et al.* (2014), Demirel *et al.* (2015), Dawson *et al.* (2016), and Azhar *et al.* (2020).

Applications of studies using locally available detailed hydrological and socio-economic information could be used as material for municipal planning agencies, where conclusive results could influence policy-makers and planners when considering whether to invest in existing structures on the present day coastline or re-locate municipal elements of high-value inland. Measures to increase the resilience of existing fixed assets where possible could include a blend of both strategies, such as by construction on floating platforms (Strangfeld and Stopp, 2014).

Finally, the findings of this study are intended to simulate permanent sea-level rise above the average mean sea level of the present day. On a more short-term basis, the three cities all experience tidal ranges (Bangkok of 3.7 metres, London of 6.5 metres and Mumbai of 4.9 metres) and can at times be exposed to storm surges from the surrounding seas and oceans. The effects of high tides and storm surges will impact the cities more extensively than the land areas that the findings show here, particularly where intense rainfall events occur such as the Great Floods of 1928 and 1953 (London), Maharashtra floods of 2005 (Mumbai), 2011 Thailand floods (Bangkok) and 2019 Indian floods (Mumbai).

6. Conclusions

This study simulated landward-encroaching sea-level rise (SLR) on urban infrastructure and population numbers in the metropolitan areas of London (UK), Bangkok (Thailand) and Mumbai (India) using a bathtub-filled modelling approach within GIS software. Risk index maps were created, where statistical analysis tested hypotheses to understand the vulnerability and exposure of these cities to SLR.

By comparing traditionally used elevation data (JAXA and SRTM) to newer elevation data (CDEM) that smoothened out known elevation value errors, different flooding extents were extracted. Whereas the JAXA and SRTM datasets showed that Bangkok is at the greatest risk from flooding due to permanent SLR, with Mumbai as the city at slightly less risk, and London at least risk, the CDEM data showed that Mumbai is at the highest risk in a 1m SLR scenario whereas Bangkok is at highest risk in simulated 3- and 5-m SLR scenarios.

Using the traditional elevation data averages, a 1m SLR scenario would put 1.8 % of London, 5 % of Bangkok and 7.8 % of Mumbai at risk. This increases to 3.4 % of London, 18.7 % of Bangkok and 14.3 % of Mumbai with a 3m rise, and 5.5 % of London, 58% of Bangkok and 18.2% of Mumbai with a 5m rise. In comparison, the CDEM data shows significantly greater areas where 2.1 % of London, 5.8 % of Bangkok and 9.8 % of Mumbai are at risk in a 1m SLR scenario; 5.5 % of London, 50.9 % of Bangkok and 21.4 % of Mumbai are at risk in a 3m SLR scenario, and 13.2 % of London, 91.5 % of Bangkok and 26.5 % of Mumbai are at risk in a 5m SLR scenario. As a result, both the cities of Bangkok and Mumbai face significant impacts to their day-to-day functionalities and ability to host populations long-term.

The measurements of urban infrastructural layers and populations at risk do not match between the three cities and SLR scenarios, both in terms of proportion of infrastructure at risk and geographic concentration of the city areas at greatest risk. The urban infrastructure and populations to the south and south-east of Bangkok are at greatest risk in a 1m SLR scenario, which spreads northwards through the city to affect the whole city and its functionality in a 5m SLR scenario. In Mumbai, the city's western coast including its central business district are at greatest risk in a 1m SLR scenario, with increasing sea levels affecting estuaries and river banks in low-lying drainage catchment areas, still to the west of the city's area. London's urban infrastructure and populations along the banks of the river Thames and Lea are at greatest risk of impact from permanent flooding, in particular to the east of the city (leading to the river's estuary with the North Sea). Geographically, the urban infrastructures and city populations at risk reflect the cities' geomorphological characteristics and channels of hydrological drainage.

In a 1m SLR scenario, 0.4 % (3.0×10^4) of London's population of 9.17 million people will be impacted, increasing to 1.7 % (1.5×10^5) and 4.2 % (3.9×10^5) in a 3m and 5m SLR scenario for the traditional datasets; while these numbers rise to 3.7 % (3.3×10^5) and 16.6 % (1.52×10^6) using the CDEM dataset. In Bangkok's population of 19.75 million, 3 % (5.9×10^5) would be impacted in a 1m SLR scenario, rising to 12.6 % (2.49×10^6) and 44 % (8.60×10^6) using the traditional elevation datasets and 52.4 % (10.35×10^6) and 95.6 % (18.9×10^6) using the newer CDEM dataset in 3- and 5-metre SLR scenarios respectively. In Mumbai, although the traditional elevation datasets show 3.3 % (8.6×10^5) of its population of 25.7 million at risk with a 1m SLR, almost a quarter (24.2 % or 6.22×10^6) would be impacted when simulated using the CDEM dataset. In this dataset, the proportion of population at risk increases to 44.9 % (11.5×10^6) with a 3m rise and 55.5 % (14.3×10^6) with a 5m rise in sea levels.

The study shows consistent analysis methods applied using different elevation datasets and shows a geographic comparison of SLR impacts to the three cities, however limitations in sourcing high-resolution elevation data (such as CDEM or LiDAR) and comprehensive vector coverage of each infrastructural layer ultimately presented margins of error in the results. Furthermore, the effectiveness of the bathtub-fill modelling approach used in the methodology is limited to simple hydrological inputs for sea-level rise (landward-encroaching sea levels from oceans and local tributaries) rather than taking additional local hydrological data into account such as rainfall, groundwater storage and surface water runoff flows. Future research could be undertaken (for these three cities or other highly populated coastal cities) with new elevation data as well as detailed local hydrological and/or socio-economic data inputs to increase the accuracy and effectiveness of SLR simulations.

As new research pertaining to the climate is constantly being released in contemporary society, this methodology can be refined for greater accuracy and to cover different areas. In this way, research efforts may help pin-point localised areas of interest for local policy makers and researchers to investigate or to keep in mind when planning for greater city resilience to expected global sea-level rise over the future decades.

7. References

Abuodha, P.A. and Woodroffe, C.D., 2010. Assessing vulnerability to sea-level rise using a coastal sensitivity index: a case study from southeast Australia. *Journal of coastal conservation*, *14*(3), pp.189-205.

Adam, H.N., Parthasarathy, D. and Narayanan, N.C., 2018. Transforming Urban Governance to Manage Uncertainty and Climate Change in Mumbai, India.

Adler, C.E. and Hirsch Hadorn, G., 2014. The IPCC and treatment of uncertainties: topics and sources of dissensus. *Wiley Interdisciplinary Reviews: Climate Change*, *5*(5), pp.663-676.

Ahsan, R., Kellett, J. and Karuppannan, S., 2016. Climate migration and urban changes in Bangladesh. In *Urban Disasters and Resilience in Asia* (pp. 293-316). Butterworth-Heinemann.

Aleem, K.F. and Aina, Y.A., 2014. Using SRTM and GDEM2 data for assessing vulnerability to coastal flooding due to sea-level rise in Lagos: a comparative study. *FUTY Journal of the Environment*, *8*(1), pp.53-64.

Alganci, U., Besol, B. and Sertel, E., 2018. Accuracy assessment of different digital surface models. *ISPRS International Journal of Geo-Information*, *7*(3), p.114.

Anthes, R.A., Corell, R.W., Holland, G., Hurrell, J.W., MacCracken, M.C. and Trenberth, K.E., 2006. Hurricanes and global warming—Potential linkages and consequences. *Bulletin of the American Meteorological Society*, *87*(5), pp.623-628.

Arnesten, E., 2019. Impacts of future sea-level rise and high water on roads, railways and environmental objects: a GIS analysis of the potential effects of increasing sea levels and highest projected high water in Scania, Sweden. *Master Thesis in Geographical Information Science*.

Azhar, H.N., Fatima, H.H.P. and Tamas, I.N. (2020). Preliminary study of indonesia capital city relocation based on disaster mitigation principle with mental model approach. In *E3S Web of Conferences* (Vol. 148, p. 06002). EDP Sciences.

Babel, M.S., 2009. *Climate change impact and adaptation study for Bangkok Metropolitan Region*. Panya Consultants Company, Limited.

Barnett, T.P., 1984. The estimation of "global" sea level change: a problem of uniqueness. Journal of Geophysical Research: Oceans, 89(C5), pp.7980-7988.

Bender, M.A. and Ginis, I., 2000. Real-case simulations of hurricane–ocean interaction using a high-resolution coupled model: Effects on hurricane intensity. *Monthly Weather Review*, *128*(4), pp.917-946.

Bjorvatn, K., 2000. Urban infrastructure and industrialization. *Journal of urban economics*, *48*(2), pp.205-218.

Blumberg, A.F. and Mellor, G.L., 1987. A description of a three-dimensional coastal ocean circulation model. *Three-dimensional coastal ocean models*, *4*, pp.1-16.

Boonya-aroonnet, S., Weesakul, S. and Mark, O., 2002. Modeling of urban flooding in Bangkok. In Global Solutions for Urban Drainage (pp. 1-14).

Boyd, E. and Ghosh, A., 2015. Climate change adaptation in Mumbai, India. In *The Urban Climate Challenge* (pp. 149-165). Routledge.

Brueckner, J.K., 1997. Infrastructure financing and urban development:: The economics of impact fees. *Journal of Public Economics*, *66*(3), pp.383-407.

Butsch, C., Kraas, F., Namperumal, S. and Peters, G., 2016. Risk governance in the megacity Mumbai/India: A complex adaptive system perspective. *Habitat International*, *54*(2), pp.100-111.

Carter, J.G., 2011. Climate change adaptation in European cities. Current opinion in environmental sustainability, 3(3), pp.193-198.

Christensen, J.H., Hewitson, B., Busuioc, A., Chen, A., Gao, X., Held, I., Jones, R., Kolli, R.K., Kwon, W.T., Laprise, R. and Magana Rueda, V. (2007). Mearns. *L., Menéndez, CG, Räisänen, J., Rinke, A., Sarr, A., and Whetton, P.: Regional Climate Projections, in: Climate Change*.

Church, J.A., Godfrey, J.S., Jackett, D.R. and McDougall, T.J., 1991. A model of sea-level rise caused by ocean thermal expansion. *Journal of Climate*, *4*(4), pp.438-456.

Church, J.A., White, N.J., Coleman, R., Lambeck, K. and Mitrovica, J.X., 2004. Estimates of the regional distribution of sea-level rise over the 1950–2000 period. Journal of climate, 17(13), pp.2609-2625.

Church, J.A., Clark, P.U., Cazenave, A., Gregory, J.M., Jevrejeva, S., Levermann, A., Merrifield, M.A., Milne, G.A., Nerem, R.S., Nunn, P.D. and Payne, A.J., 2013. Sea level change. *Climate change*, *1975*.

Clarke, S., Kersey, J., Trevorrow, E., Wilby, R., Shackley, S., Turnpenny, J., Wright, A., Hunt, A. and Crichton, D., 2002. London's warming: The impacts of climate change on London. *UK Climate Impacts Programme and Greater London Authority, Oxford*.

ClimateCentral (2020). Coastal Risk Screening Tool: Land below 5.0 meters of water [Interactive map]. Available at: https://coastal.climatecentral.org/map/15/100.529/13.7277/?theme =water_level&map_type=water_level_above_mhhw&contiguous=true&elevation_mod el=best_available&water_level=5.0&water_unit=m (Accessed: 12/12/2019)

Committee on Climate Change, 2008. *Building a Low-carbon Economy: The UK's Contribution to Tackling Climate Change*. Stationery Office.

Dasgupta, S., Laplante, B., Meisner, C., Wheeler, D. and Yan, J., 2007. *The impact of sea-level rise on developing countries: a comparative analysis*. The World Bank.

Dawson, D., Shaw, J. and Gehrels, W.R., 2016. Sea-level rise impacts on transport infrastructure: The notorious case of the coastal railway line at Dawlish, England. *Journal of Transport Geography*, *51*, pp.97-109.

Demirel, H., Kompil, M. and Nemry, F., 2015. A framework to analyze the vulnerability of European road networks due to Sea-Level Rise (SLR) and sea storm surges. *Transportation Research Part A: Policy and Practice*, *81*, pp.62-76.

Department for Environment Food and Rural Affairs, 2018. The National Adaptation Programme and the third strategy for climate adaptation reporting. Available online from: https://assets.publishing.service.gov.uk /government/uploads/system/uploads/attachment_data/file/727252/national-adaptation-programme-2018.pdf [Accessed 29/03/2019]. ISBN 978-1-5286-0758-2

Dhiman, R., VishnuRadhan, R., Eldho, T.I. and Inamdar, A. (2019). Flood risk and adaptation in Indian coastal cities: Recent scenarios. *Applied Water Science*, *9*(1), p.5.

Encyclopaedia Britannica, n.d. Bangkok – History [Website] Available online from: https://www. britannica.com/place/Bangkok/History [Accessed 19/11/2019]

Environment Agency (2012). TE2100 strategic environmental assessment (SEA) statement of environmental particulars; 2012. http://www.environment-agency.gov.uk/static/documents /Research/SE_TE2100_environmentalparticulars.pdfGarside, R., Johnston, D., Saunders, W. and Leonard, G., 2009. Planning for tsunami evacuations: the case of the Marine Education Centre, Wellington, New Zealand. *Australian Journal of Emergency Management, The*, *24*(3), p.28.

Fainstein, S.S., 1994. The city builders: property, politics, and planning in London and New York. Oxford: Blackwell.

Fitton, J.M., Hansom, J.D. and Rennie, A.F., 2018. A method for modelling coastal erosion risk: the example of Scotland. *Natural Hazards*, *91*(3), pp.931-961.

Fletcher, M.E., 1958. The Suez Canal and world shipping, 1869-1914. *The Journal of Economic History*, *18*(4), pp.556-573.

Gluckman, R. (2019). Bangkok: The Sinking City Faces Severe Climate Challenges. [Article] Available online at: https://urbanland.uli.org/sustainability/bangkok-the-sinking-city-faces-severe-climate-challenges/ [Accessed 19/11/2019]

Golding, B., Waite, T. and Murray, V., 2019. Lessons from Cases of Coastal Risks Governance in the United Kingdom. *Facing Hydrometeorological Extreme Events: A Governance Issue*, pp.461-481.

Gupta, K., 2007. Urban flood resilience planning and management and lessons for the future: a case study of Mumbai, India. *Urban Water Journal*, *4*(3), pp.183-194.

Hasan, E., Khan, S.I. and Hong, Y., 2015. Investigation of potential sea-level rise impact on the Nile Delta, Egypt using digital elevation models. *Environmental monitoring and assessment*, *187*(10), p.649.

Highways England, 2016. *Climate Adaptation Risk Assessment Progress Update – 2016.* [Report]. Available online at: https://assets.publishing.service.gov.uk/government/uploads/system/ uploads/ attachment_data/file/596812/climate-adrep-highways-england.pdf. Accessed [09/06/2019].

IPCC, 2014: Climate Change 2014: Synthesis Report. Contribution of Working Groups I, II and III to the Fifth Assessment Report of the Intergovernmental Panel on Climate Change [Core Writing Team, R.K. Pachauri and L.A. Meyer (eds.)]. IPCC, Geneva, Switzerland, 151 pp

Jayaram, D. (2019). Why has climate change adaptation become more important than ever in India? [Article] Available online at: https://www.climate-diplomacy.org/news/why-has-climate-change-adaptation-become-more-important-ever-india [Accessed 18/11/2019]

Jedwab, R., Christiaensen, L. and Gindelsky, M., 2015. *Demography, urbanization and development: Rural push, urban pull and… urban push?*. The World Bank.

Johnston, A., Slovinsky, P. and Yates, K.L., 2014. Assessing the vulnerability of coastal infrastructure to sea-level rise using multi-criteria analysis in Scarborough, Maine (USA). *Ocean & coastal management*, *95*, pp.176-188.

Kopp, R.E., DeConto, R.M., Bader, D.A., Hay, C.C., Horton, R.M., Kulp, S., Oppenheimer, M., Pollard, D. and Strauss, B.H., 2017. Evolving understanding of Antarctic ice-sheet physics and ambiguity in probabilistic sea-level projections. *Earth's Future*, *5*(12), pp.1217-1233.

Koppikar, S. (2018). Climate change is here. What's Mumbai doing about it? Hindustan Times [Article] Available online at: https://www.hindustantimes.com/mumbai-news/climate-change-is-here-what-s-mumbai-doing-about-it/story-4X8vDPDOXsdCwFU44e0NZP.html [Accessed 19/11/2019]

Kulp, S. and Strauss, B.H., 2016. Global DEM errors underpredict coastal vulnerability to sea-level rise and flooding. Frontiers in Earth Science, 4, p.36.

Kulp, S.A. and Strauss, B.H., 2019. New elevation data triple estimates of global vulnerability to sea-level rise and coastal flooding. *Nature communications*, *10*(1), pp.1-12.

Lærd Statistics, n.d. Kruskal-Wallis H Test using SPSS Statistics [Web Article]. Available online at: https://statistics.laerd.com/spss-tutorials/kruskal-wallis-h-test-using-spss-statistics.php [Accessed 01/05/2020].

Lucas, K. and Pangbourne, K., 2012. Chapter 11 Transport and Climate Change Policy in the United Kingdom: A Social Justice Perspective. In *Transport and Climate Change* (pp. 287-312). Emerald Group Publishing Limited.

Macrotrends LLC (2020). *Global Metrics: Population*. Available at: https://www.macrotrends.net/ cities (Accessed: 10/06/2020)

Malik, A. and Abdalla, R., 2016. Geospatial modeling of the impact of sea-level rise on coastal communities: application of Richmond, British Columbia, Canada. *Modeling Earth Systems and Environment*, *2*(3), p.146.

McRobie, A., Spencer, T. and Gerritsen, H., 2005. The big flood: North Sea storm surge. *Philosophical Transactions of the Royal Society A: Mathematical, Physical and Engineering Sciences*, *363*(1831), pp.1263-1270.

Meteo365.com Ltd, 2019. *Tide Chart*. [Website] Available online from: https://www.tide-forecast.com. [Accessed 01/10/2019].

Mumbai.org.uk. (n.d.).. Mumbai History [Website], Available online from: https://www.mumbai.org .uk/history.html#:~:targetText=The%20name%20Mumbai%20is%20an,Worli%20and %20Old%20Woman's%20Island. [Accessed 19/11/2019]

Natakun, B., Marome, W., Phanthuwongpakdee, N. and Archer, D., 2019. Climate crisis planning: a toolkit for building local urban resilience.

Network Rail, 27 January 2017. Weather Resilience and Climate Change Adaptation Strategy 2017-2019. [Report]. Available online at: https://safety.networkrail.co.uk/wp-content/uploads/ 2017/02/NR-WRCCA-Strategy-2017-2019.pdf. [Accessed 01/06/2019]

Neumann, B., Vafeidis, A.T., Zimmermann, J. and Nicholls, R.J., 2015. Future coastal population growth and exposure to sea-level rise and coastal flooding-a global assessment. *PloS one*, *10*(3), p.e0118571.

Nguyen, H. and Tran, P., 2016. Urban Disaster Risk Reduction in Vietnam: Gaps, Challenges, and Approaches. In *Urban Disasters and Resilience in Asia* (pp. 123-140). Butterworth-Heinemann

Nicholls, R.J. and Cazenave, A., 2010. Sea-level rise and its impact on coastal zones. *science*, *328*(5985), pp.1517-1520.

Nistora, A., 2018. Inundation scenarios in a changing climate: assessing potential impacts of sea-level rise on the coast of South-East England. *Master Thesis in Geographical Information Science*.

Office for National Statistics, 2019. *Estimates of the population for the UK, England and Wales, Scotland and Northern Ireland* [Website]. Available online from: https://www.ons.gov.uk/peoplepopulationandcommunity/populationandmigration/popu lationestimates/datasets/populationestimatesforukenglandandwalesscotlandandnortherni reland. [Accessed 01/10/2019]

Office of National Resources and Environment Policy and Planning, Government of Thailand (ONEP) (2008), "Thailand's National Strategy on Climate Change," Presentation, Government of Thailand, Bangkok.

Oppenheimer, M., B.C. Glavovic , J. Hinkel, R. van de Wal, A.K. Magnan, A. Abd-Elgawad, R. Cai, M. Cifuentes-Jara, R.M. DeConto, T. Ghosh, J. Hay, F. Isla, B. Marzeion, B. Meyssignac, and Z. Sebesvari, 2019: Sea-level rise and Implications for Low-Lying Islands, Coasts and Communities. In: IPCC Special Report on the Ocean and Cryosphere in a Changing Climate [H.-O. Pörtner, D.C. Roberts, V. Masson-Delmotte, P. Zhai, M. Tignor, E. Poloczanska, K. Mintenbeck, A. Alegría, M. Nicolai, A. Okem, J. Petzold, B. Rama, N.M. Weyer (eds.)]. In press. Available online at: https://www.ipcc.ch/srocc/chapter/chapter-4-sea-level-rise-and-implications-for-low-lying-islands-coasts-and-communities/ [Accessed 25/06/2020]

Parry, M.L., Canziani, O.F., Palutikof, J.P., Van Der Linden, P.J. and Hanson, C.E., 2007. IPCC, 2007: climate change 2007: impacts, adaptation and vulnerability. Contribution of working group II to the fourth assessment report of the intergovernmental panel on climate change. *Cambridge University Press, Cambridge, UK*.

Phamornpol, K. (n.d.). 'Flood Mitigation and Management in Bangkok Metropolitan Area' [Presentation]. Departm*ent of Drainage and Sewerage, Bangkok Metropolitan Administration*. Available at: https://www.unescap.org/sites/default/files/S3b4_Thailand.pdf (Accessed: 15/03/2020)

Phatak, J. (n.d.). 'Management of Urban Floods: Mumbai, India' [Presentation]. *Municipal Corporation of Greater Mumbai (MCGM)*. Available at: https://www.preventionweb.net/files/section/ 230_mumbaifloodShanghai.pdf (Accessed: 15/03/2020)

Rahmstorf, S., 2007. A semi-empirical approach to projecting future sea-level rise. *Science*, *315*(5810), pp.368-370.

Ranger, N., Hallegatte, S., Bhattacharya, S., Bachu, M., Priya, S., Dhore, K., Rafique, F., Mathur, P., Naville, N., Henriet, F. and Herweijer, C., 2011. An assessment of the potential impact of climate change on flood risk in Mumbai. Climatic change, 104(1), pp.139-167.

Rasmussen, D.J., Bittermann, K., Buchanan, M.K., Kulp, S., Strauss, B.H., Kopp, R.E. and Oppenheimer, M., 2018. Extreme sea level implications of 1.5 C, 2.0 C, and 2.5 C temperature stabilization targets in the 21st and 22nd centuries. *Environmental Research Letters*, *13*(3), p.034040.

Saito, N. (2014). Challenges for adapting Bangkok's flood management systems to climate change. *Urban climate*, *9*, pp.89-100.

Saroar, M.M. and Routray, J.K., 2012. Impacts of climatic disasters in coastal Bangladesh: why does private adaptive capacity differ?. *Regional Environmental Change*, *12*(1), pp.169-190.

Singh, D. (2018). Mumbai: The 'Rain Ready' city that floods every year. Category: Mumbai [Article]. Available online at: http://www.acclimatise.uk.com/tag/mumbai/ [Accessed 27/11/2019]

Solecki, W., Leichenko, R. and O'Brien, K., 2011. Climate change adaptation strategies and disaster risk reduction in cities: connections, contentions, and synergies. Current Opinion in Environmental Sustainability, 3(3), pp.135-141.

Solomon, S., Qin, D., Manning, M., Averyt, K. and Marquis, M. eds., 2007. *Climate change 2007-the physical science basis: Working group I contribution to the fourth assessment report of the IPCC* (Vol. 4). Cambridge university press.

Strangfeld, P. and Stopp, H., 2014. Floating houses: An adaptation strategy for flood preparedness in times of global change. WIT Transactions on Ecology and the Environment, 184(10), pp.277-286.

Suzuki, T. and Ishii, M., 2011. Regional distribution of sea level changes resulting from enhanced greenhouse warming in the Model for Interdisciplinary Research on Climate version 3.2. Geophysical Research Letters, 38(2).

Thanvisitthpon, N., Shrestha, S. and Pal, I., 2018. Urban flooding and climate change: a case study of Bangkok, Thailand. *Environment and Urbanization ASIA*, *9*(1), pp.86-100.

Tol, R.S., 2007. The double trade-off between adaptation and mitigation for sea-level rise: an application of FUND. *Mitigation and Adaptation Strategies for Global Change*, *12*(5), pp.741-753.

United Nations, 2018. "The World's Cities in 2018" (PDF). Archived (PDF) from the original on 21 October 2019. Retrieved 18 November 2019.

Wachsmuth, J., Schaeffer, M. and Hare, B., 2018. The EU long-term strategy to reduce GHG emissions in light of the Paris Agreement and the IPCC Special Report on 1, 5° C (No. S22/2018). Working Paper Sustainability and Innovation.

WeatherBase, n.d.. *Weather*. [Website] Available online from: https://www.weatherbase.com. [Accessed 01/10/2019].

Webster, D., McElwee, P. and Worldbank, 2009, June. Urban adaptation to climate change: Bangkok and Ho Chi Minh City as test beds. In *Fifth urban research symposium, cities and climate change: Responding to an urgent agenda* (pp. 28-30).

World Population Review, 2019. Bangkok Population 2019 [Website] Available online from: http://worldpopulationreview.com/world-cities/bangkok-population/ [Accessed 20/11/2019]

Zhang, Y., Ayyub, B.M., Zhang, D., Huang, H. and Saadat, Y., 2019. Impact of Water Level Rise on Urban Infrastructures: Washington, DC, and Shanghai as Case Studies. *Risk Analysis*.

8. Figure References

Figure 1.1

Rahmstorf, S., 2002, "Ocean circulation and climate during the past 120,000 years", *Nature* , v. 419., p. 207-214.
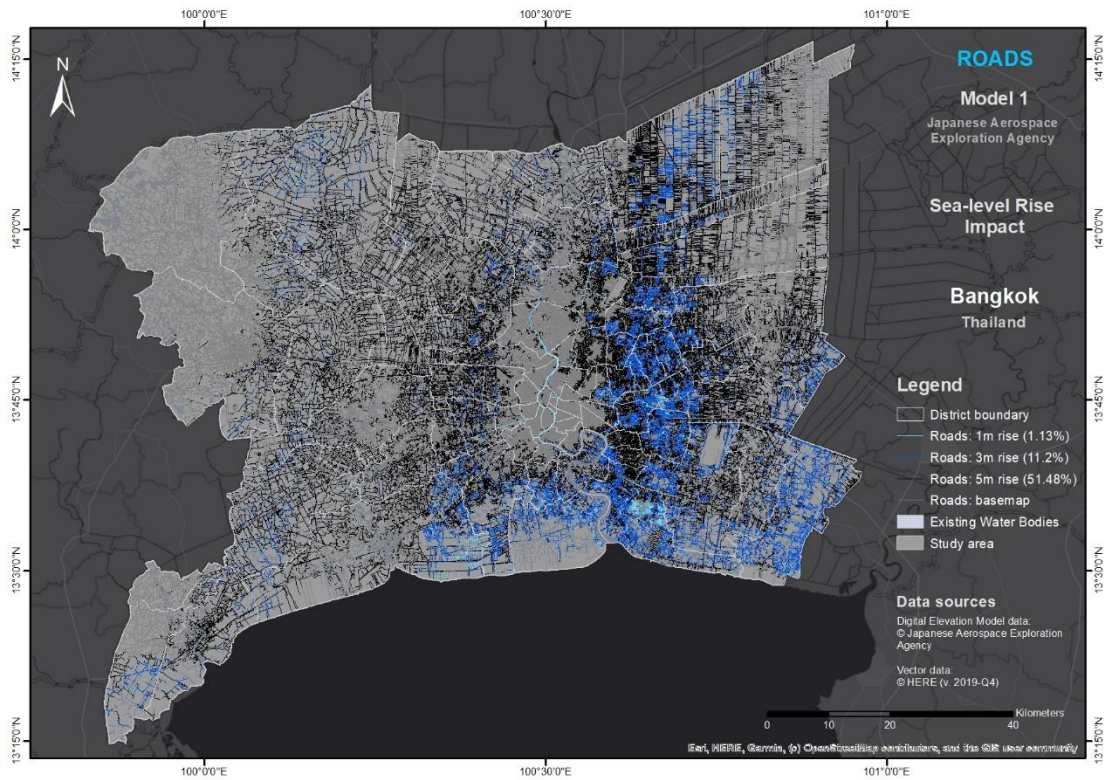
Appendix A

Figure A40: A visual representation of Bangkok's road network affected by SLR (JAXA dataset)

Figure A41: A visual representation of Bangkok's railway network affected by SLR (JAXA dataset)
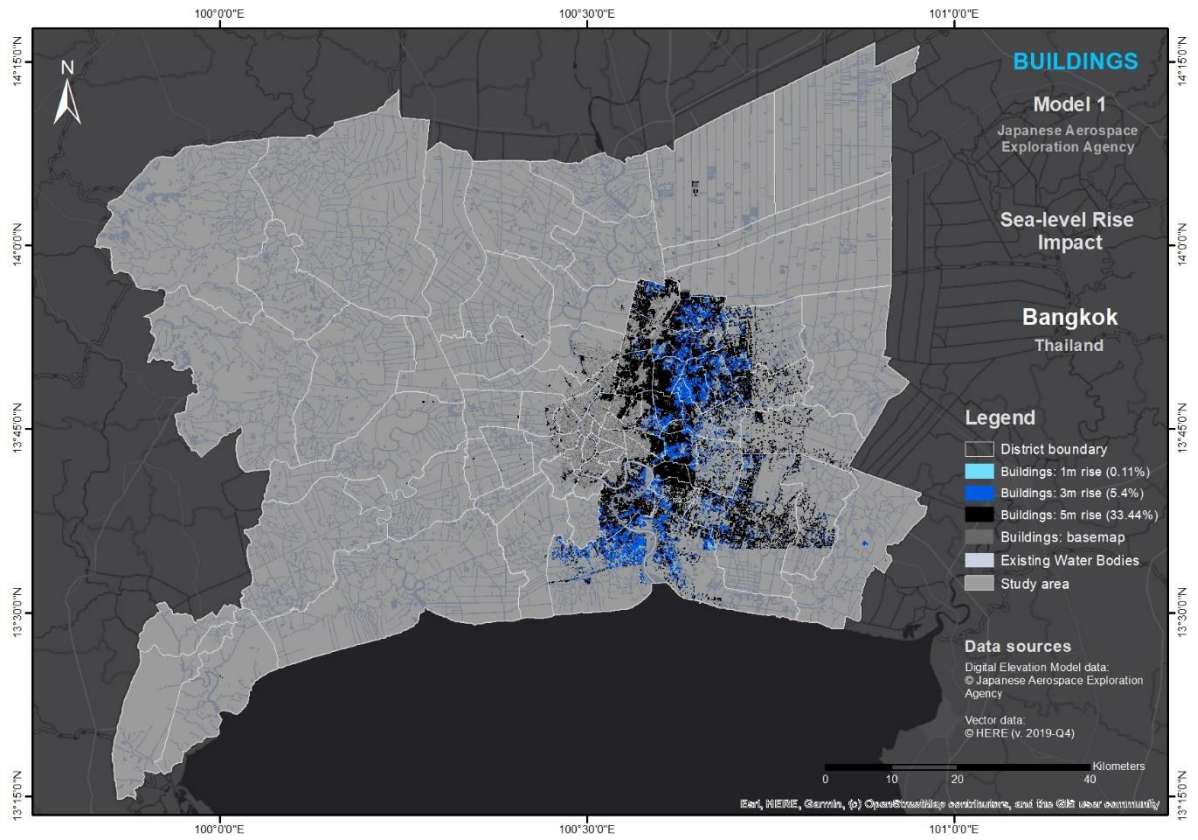
Figure A42: A visual representation of Bangkok's building footprint affected by SLR (JAXA dataset)
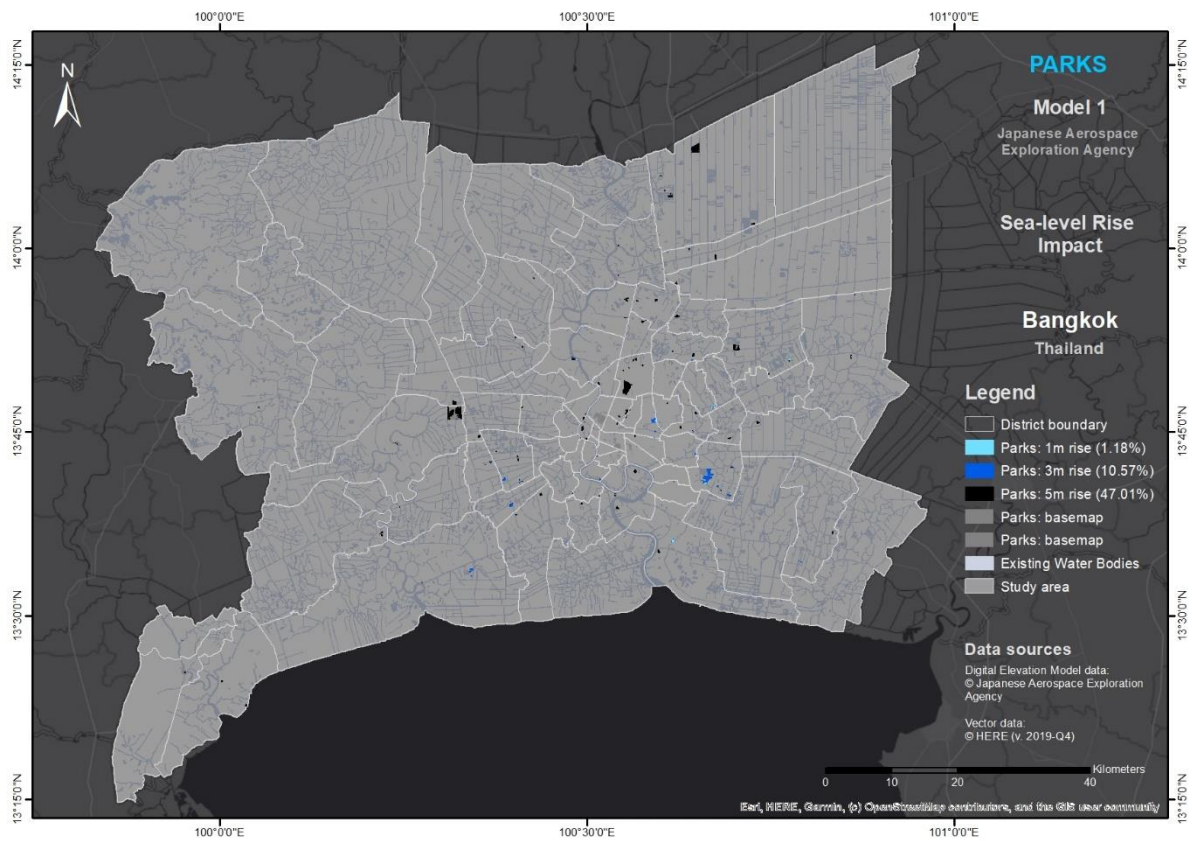

Figure A43: A visual representation of Bangkok's park areas affected by SLR (JAXA dataset)

98

Figure A44: A visual representation of Bangkok's road network affected by SLR (SRTM dataset)

Figure A45: A visual representation of Bangkok's railway network affected by SLR (SRTM dataset)

Figure A46: A visual representation of Bangkok's building footprint affected by SLR (SRTM dataset)

Figure A47: A visual representation of Bangkok's park areas affected by SLR (SRTM dataset)
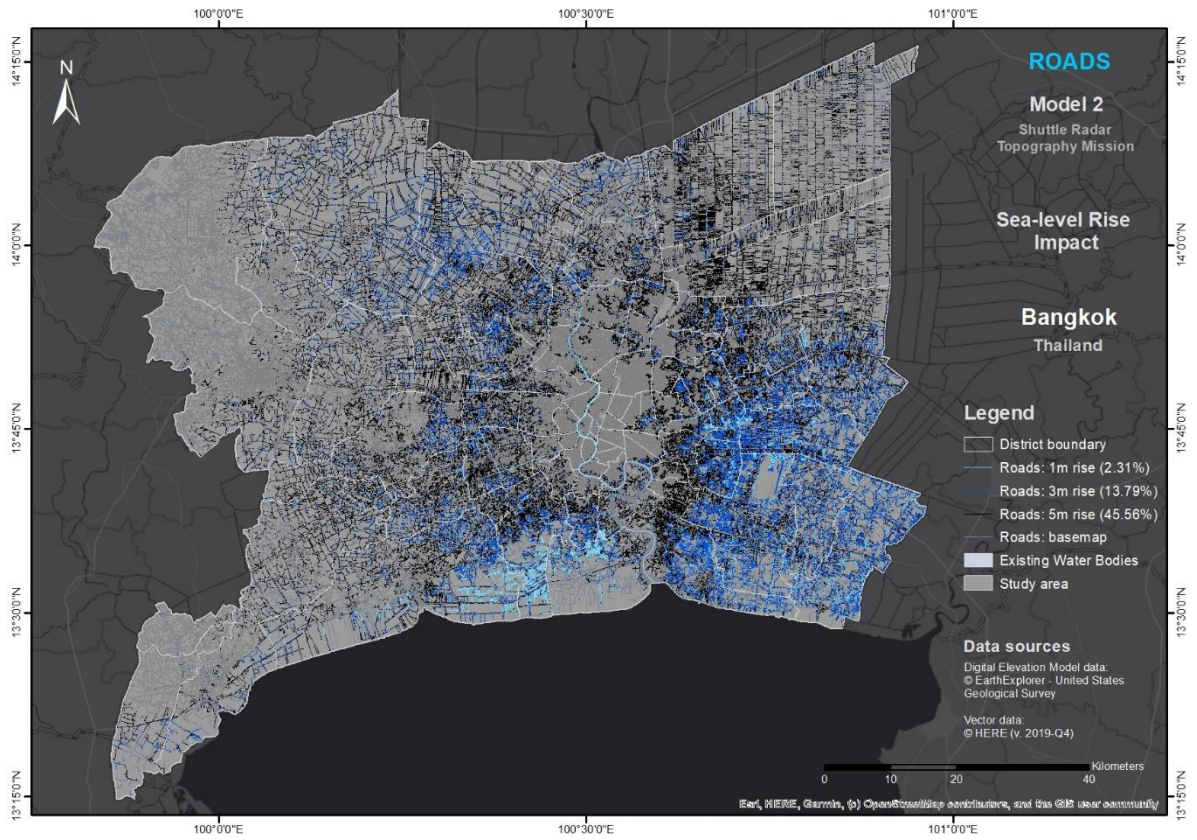
100

Figure A48: A visual representation of Bangkok's road network affected by SLR (CDEM dataset)

Figure A49: A visual representation of Bangkok's railway network affected by SLR (CDEM dataset)
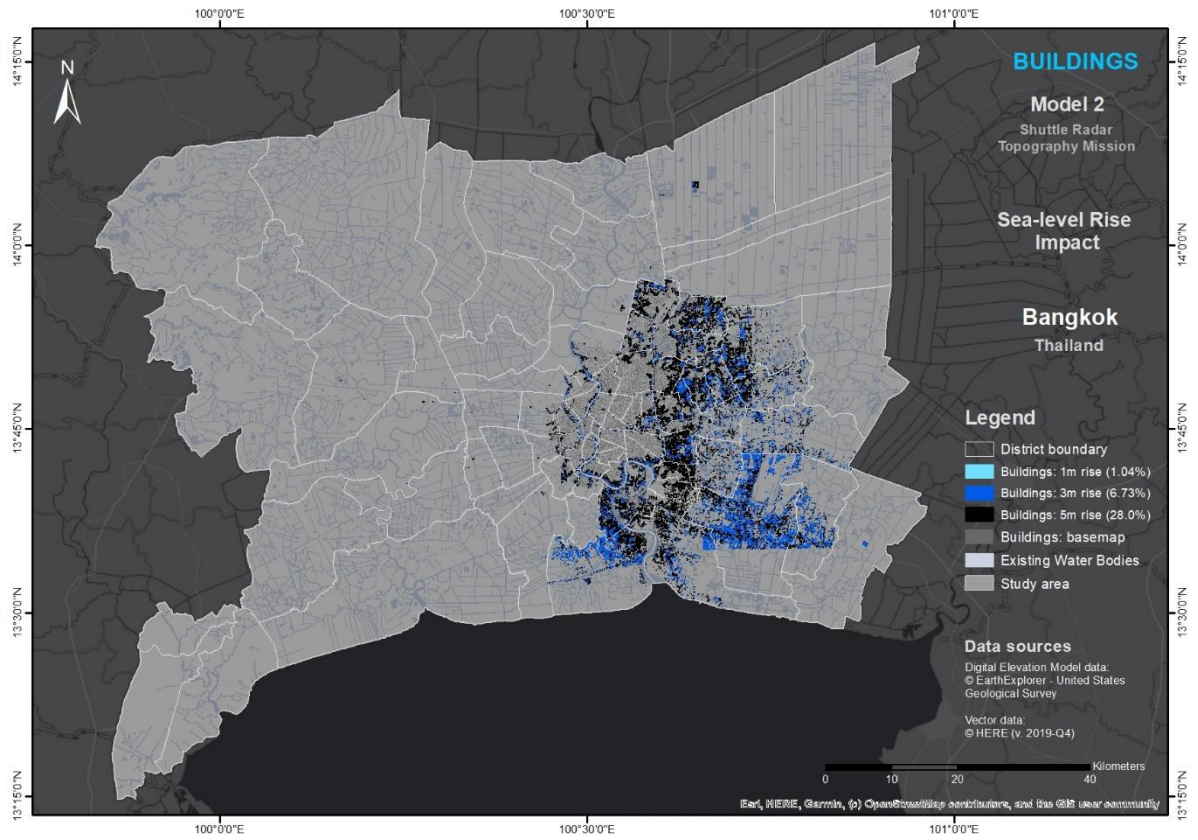
101

Figure A50: A visual representation of Bangkok's building footprint affected by SLR (CDEM dataset)

Figure A51: A visual representation of Bangkok's park areas affected by SLR (CDEM dataset)

Figure A52: A visual representation of London's road network affected by SLR (JAXA dataset)

Figure A53: A visual representation of London's railway network affected by SLR (JAXA dataset)

Figure A54: A visual representation of London's building footprint affected by SLR (JAXA dataset)

Figure A55: A visual representation of London's park areas affected by SLR (JAXA dataset)

Figure A56: A visual representation of London's road network affected by SLR (SRTM dataset)

Figure A57: A visual representation of London's railway network affected by SLR (SRTM dataset)

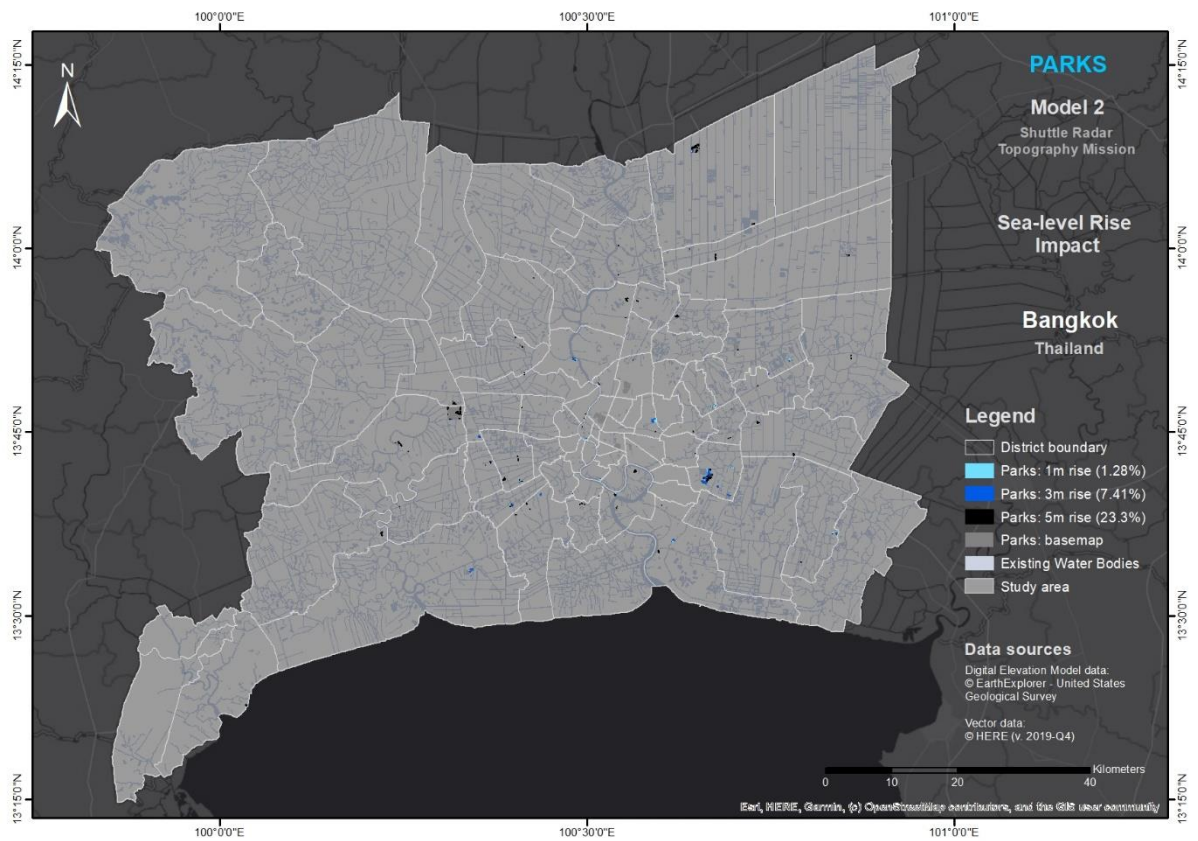*Figure A58: A visual representation of London's building footprint affected by SLR (SRTM dataset)*
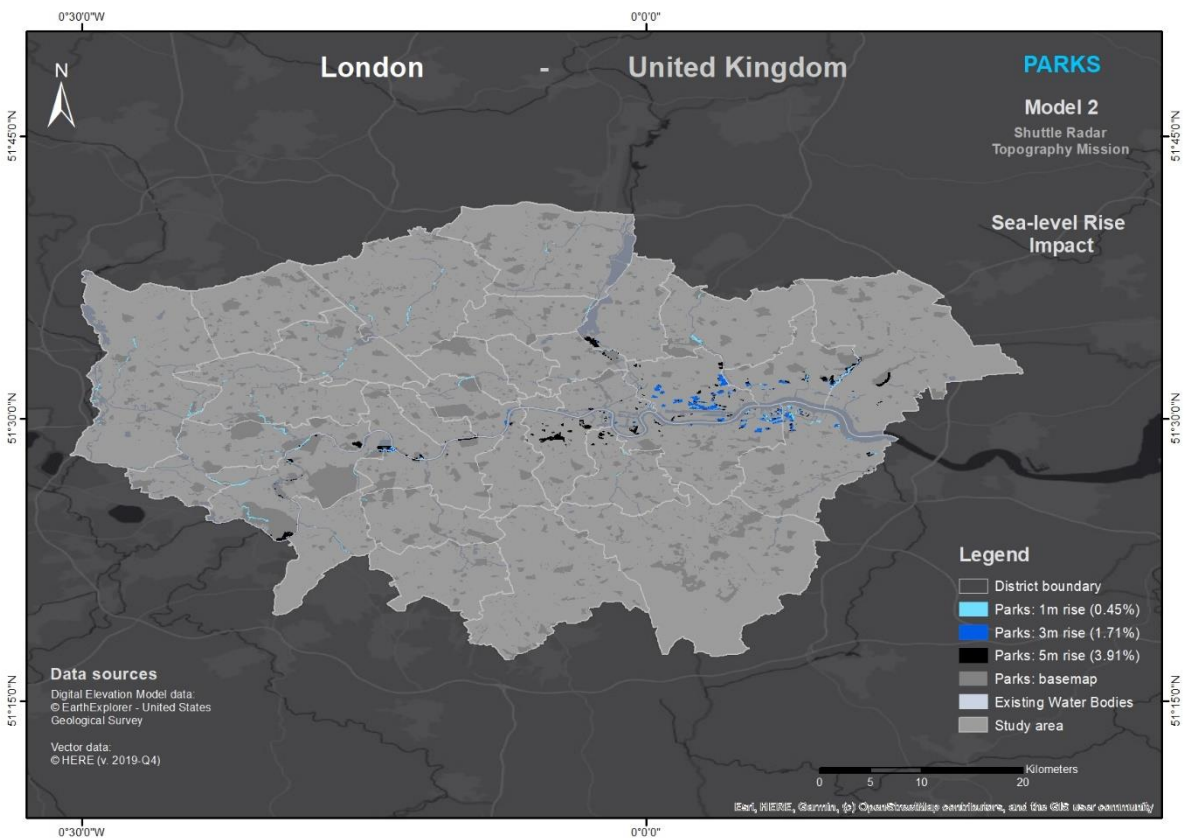
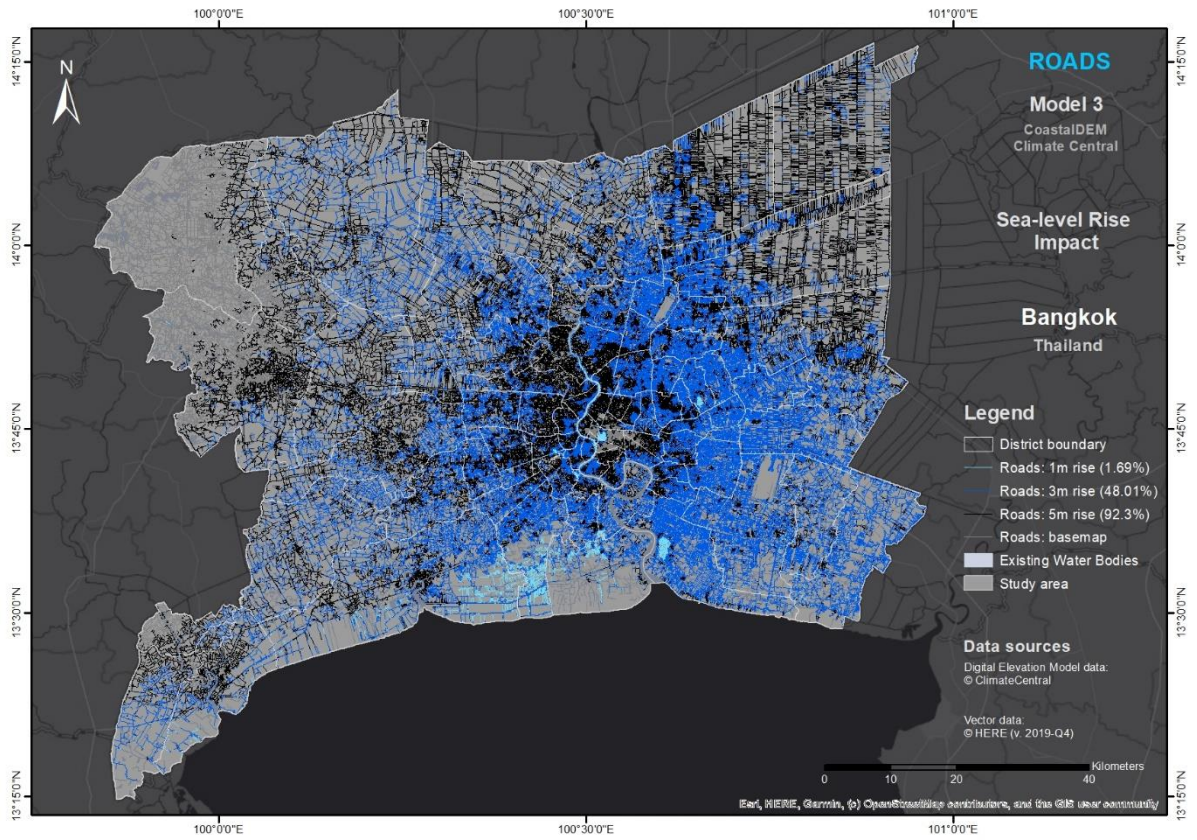*Figure A59: A visual representation of London's park areas affected by SLR (SRTM dataset)*
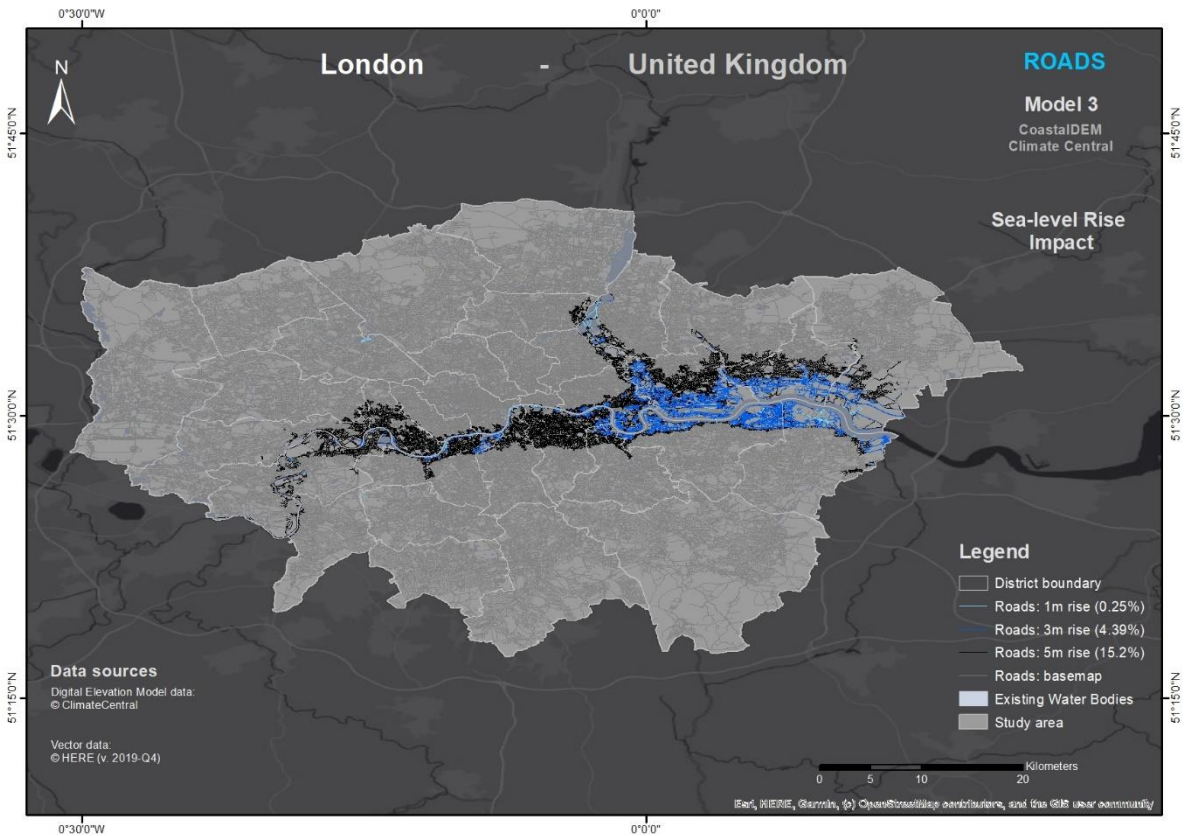
Figure A60: A visual representation of London's road network affected by SLR (CDEM dataset)
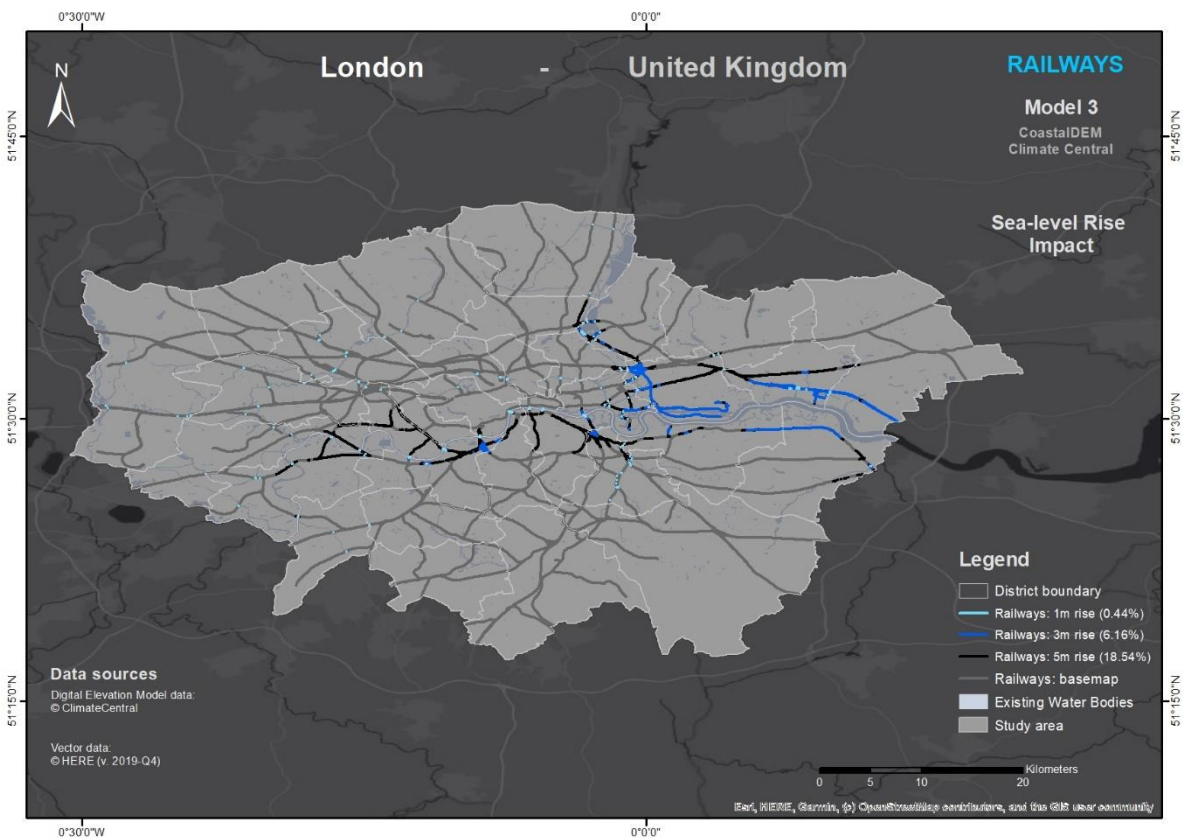
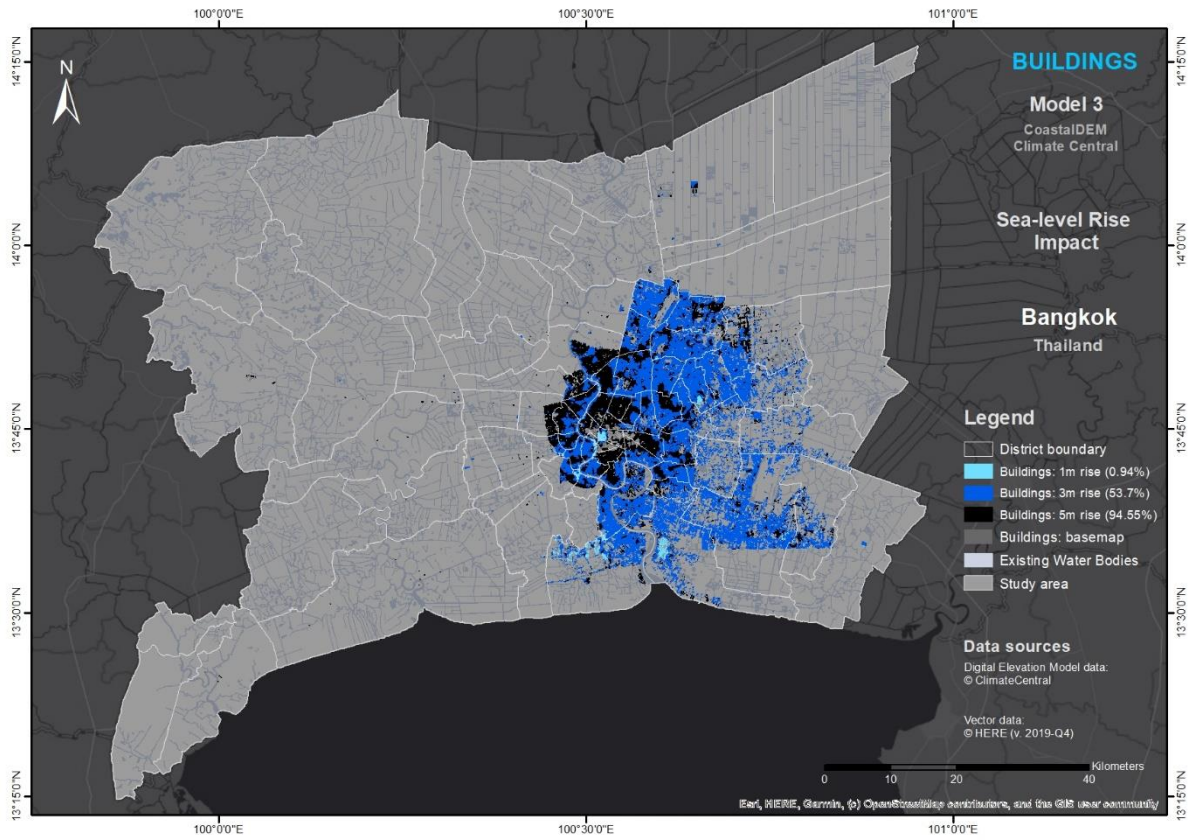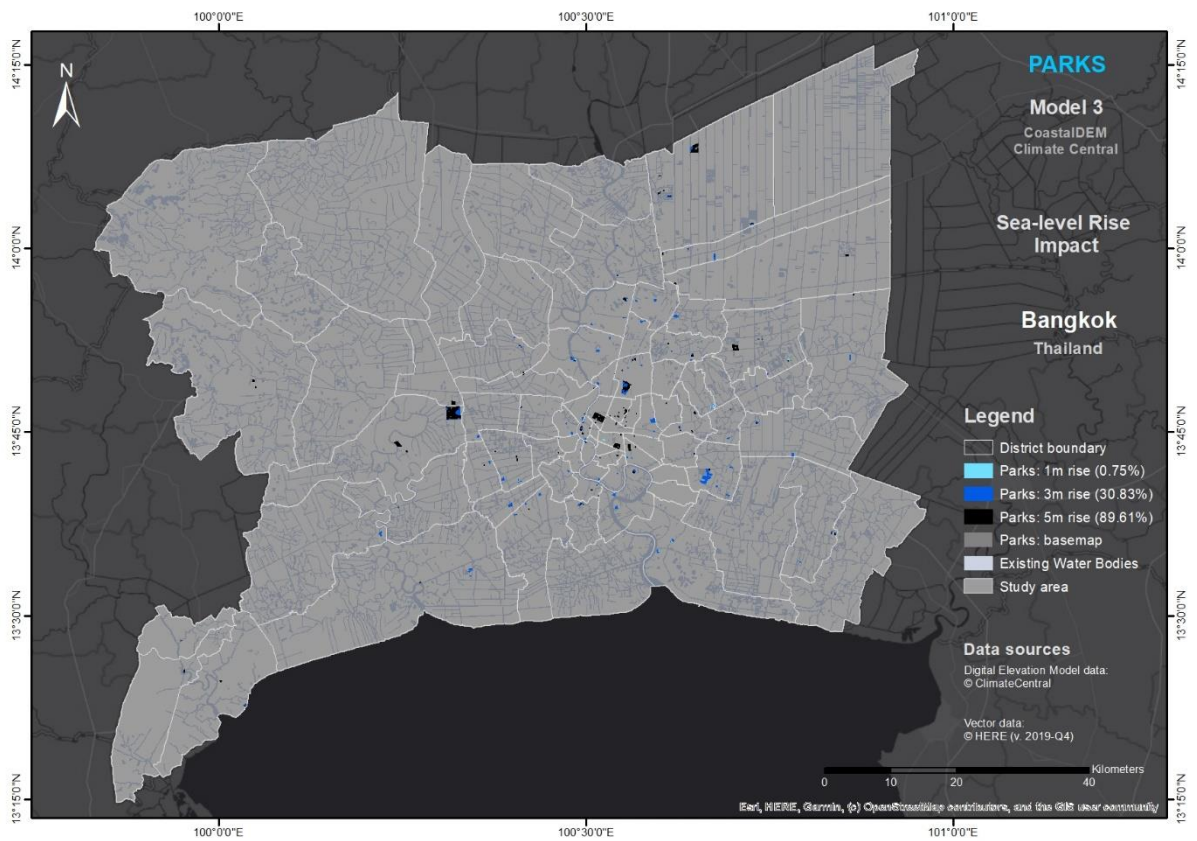*Figure A61: A visual representation of London's railway network affected by SLR (CDEM dataset)*

107
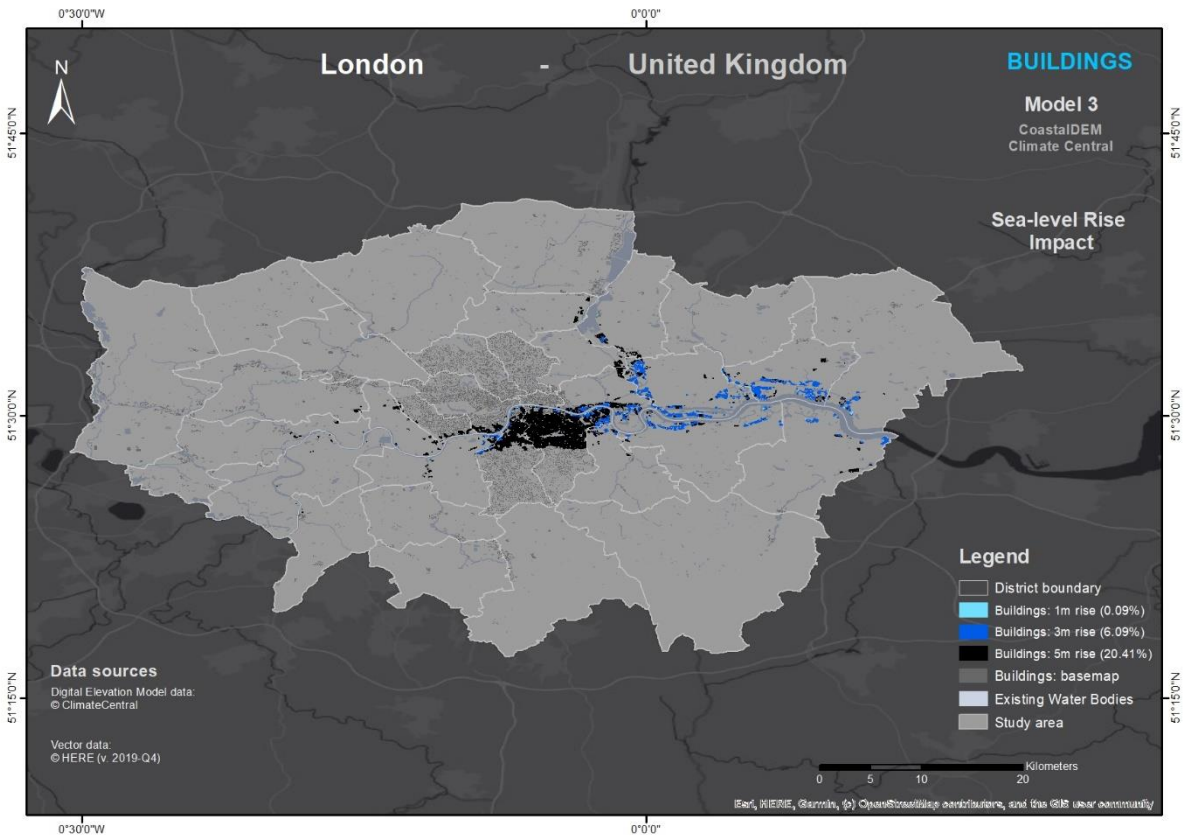
Figure A62: A visual representation of London's building footprint affected by SLR (CDEM dataset)
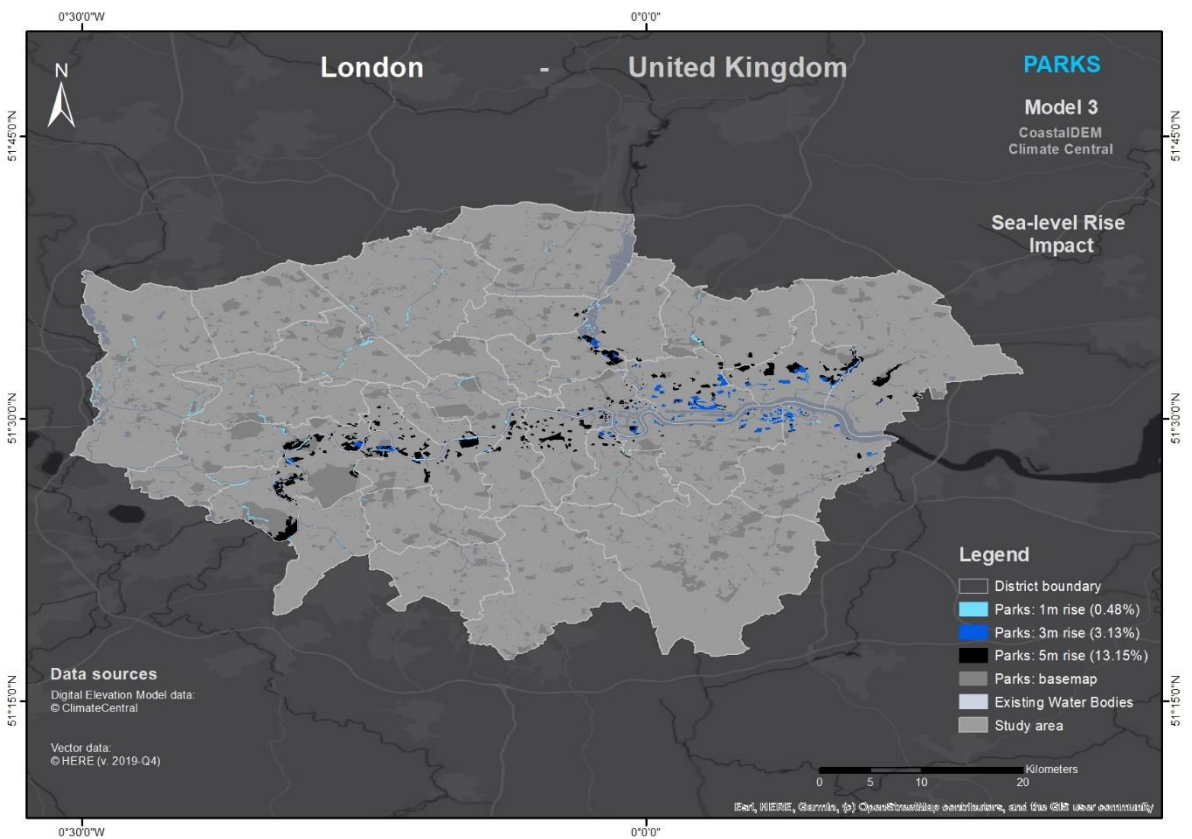
Figure A63: A visual representation of London's park areas affected by SLR (CDEM dataset)

108
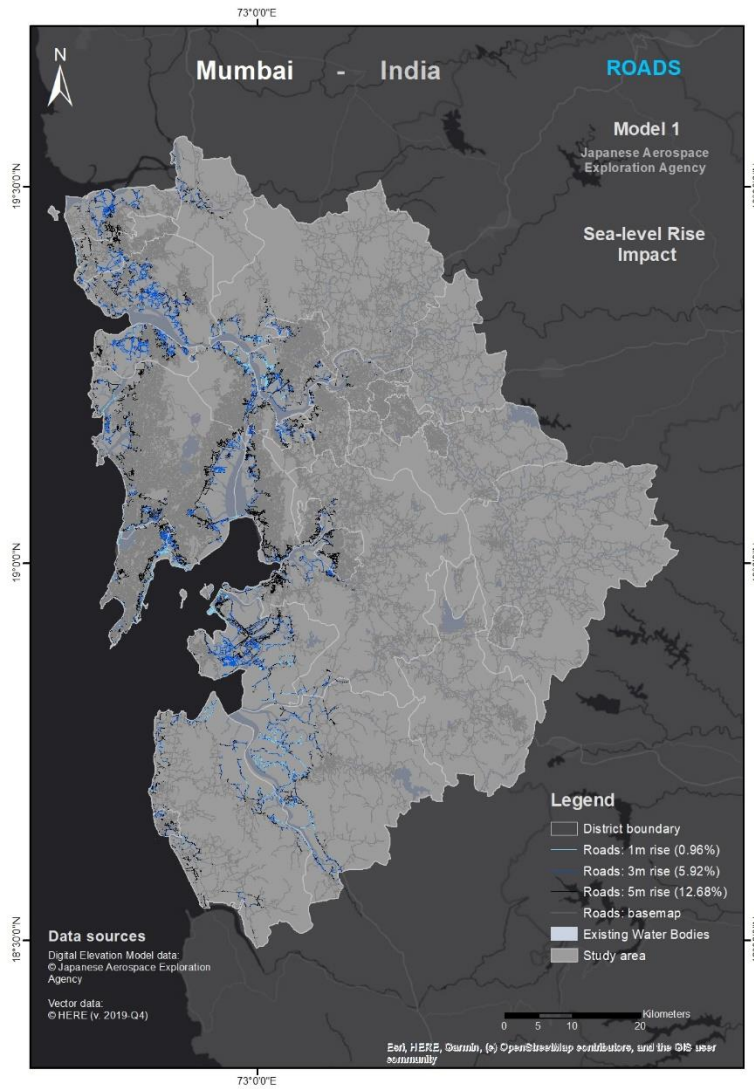
Figure A64: A visual representation of Mumbai's road network affected by SLR (JAXA dataset)
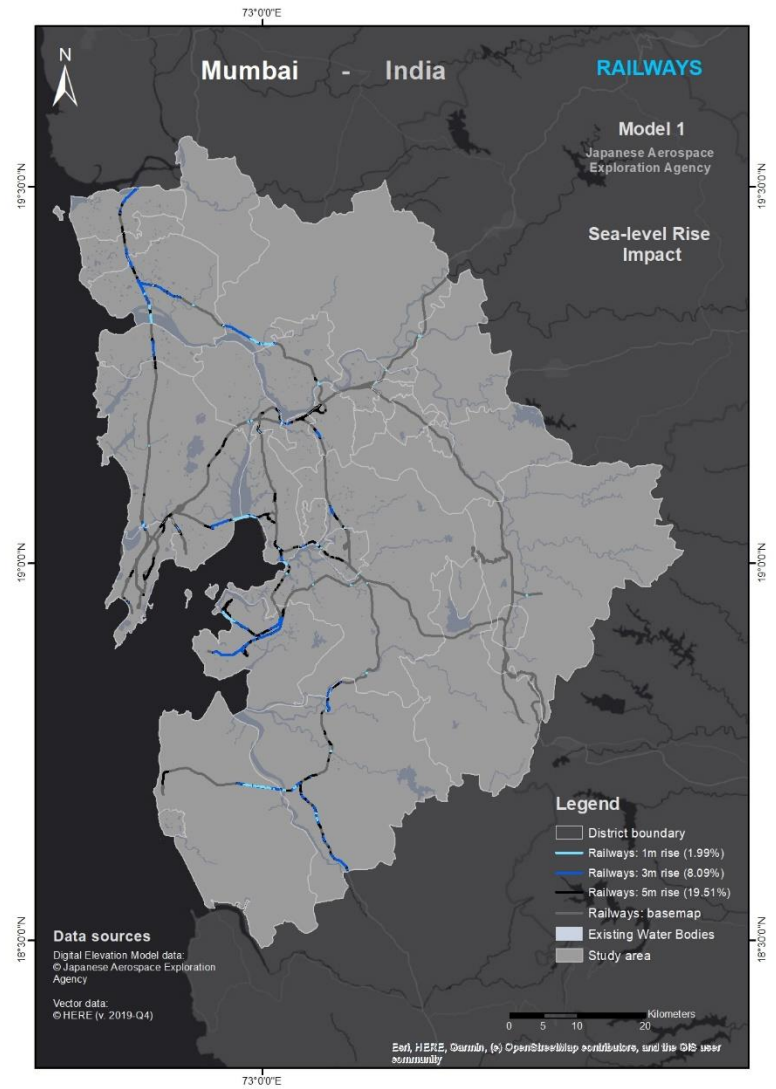
Figure A65: A visual representation of Mumbai's railway network affected by SLR (JAXA dataset)
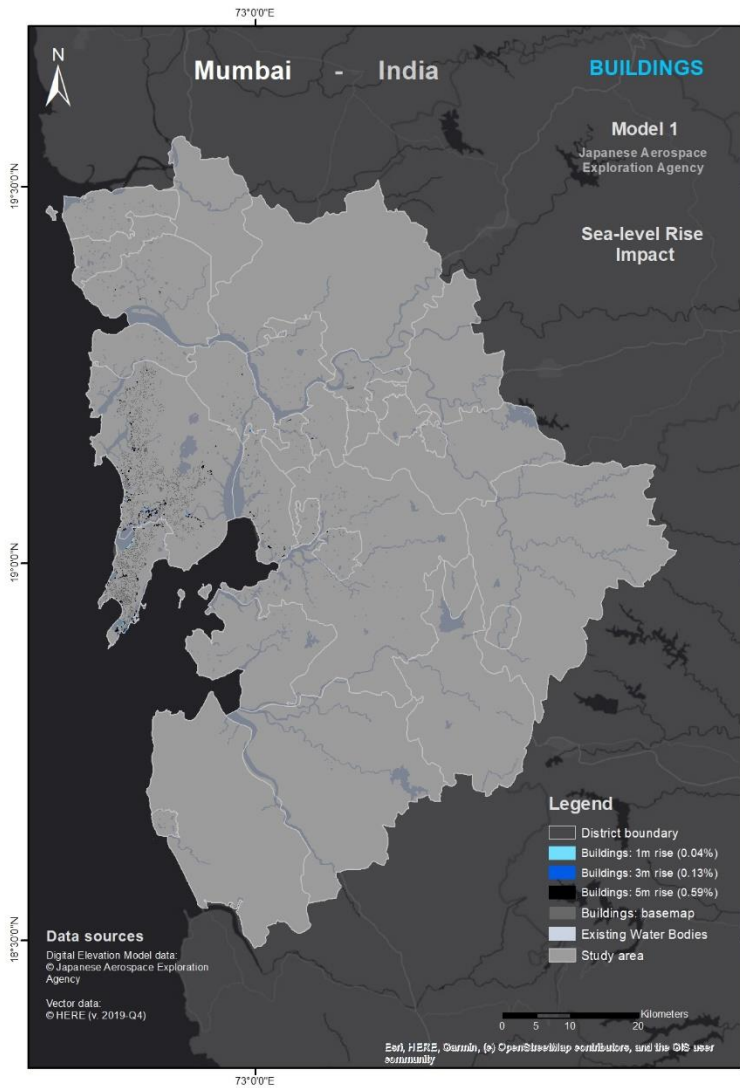
Figure A27: A visual representation of Mumbai's building footprint affected by SLR (JAXA dataset)
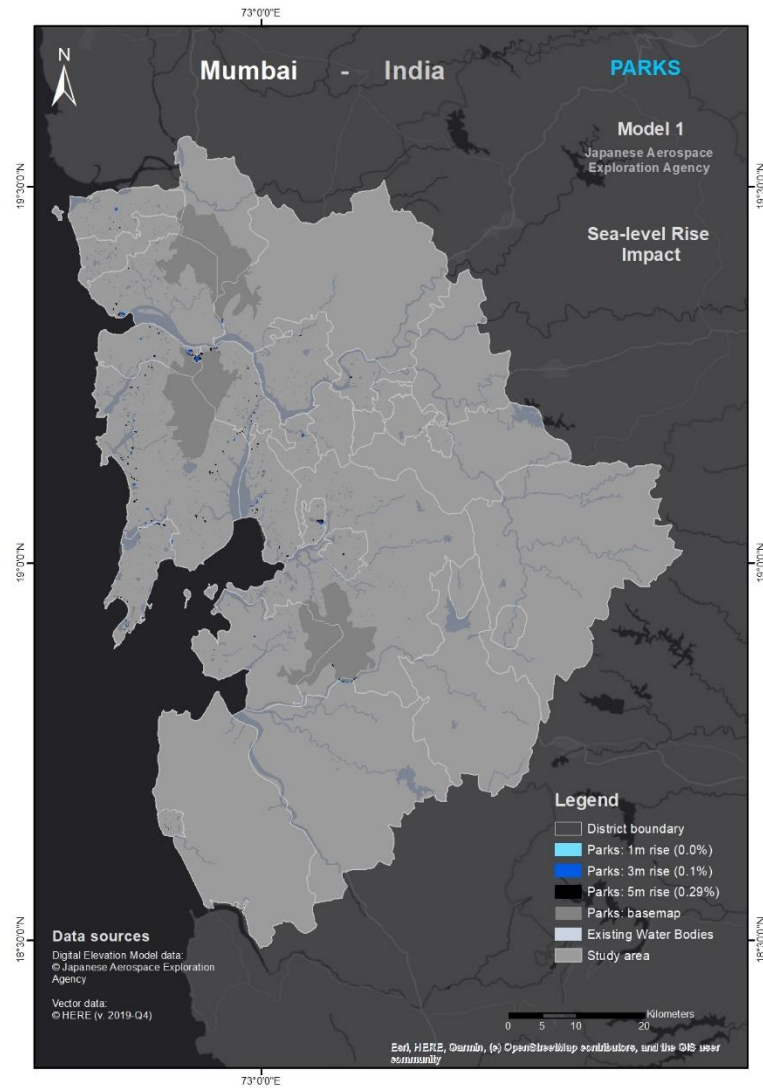
Figure A66: A visual representation of Mumbai's park areas affected by SLR (JAXA dataset)
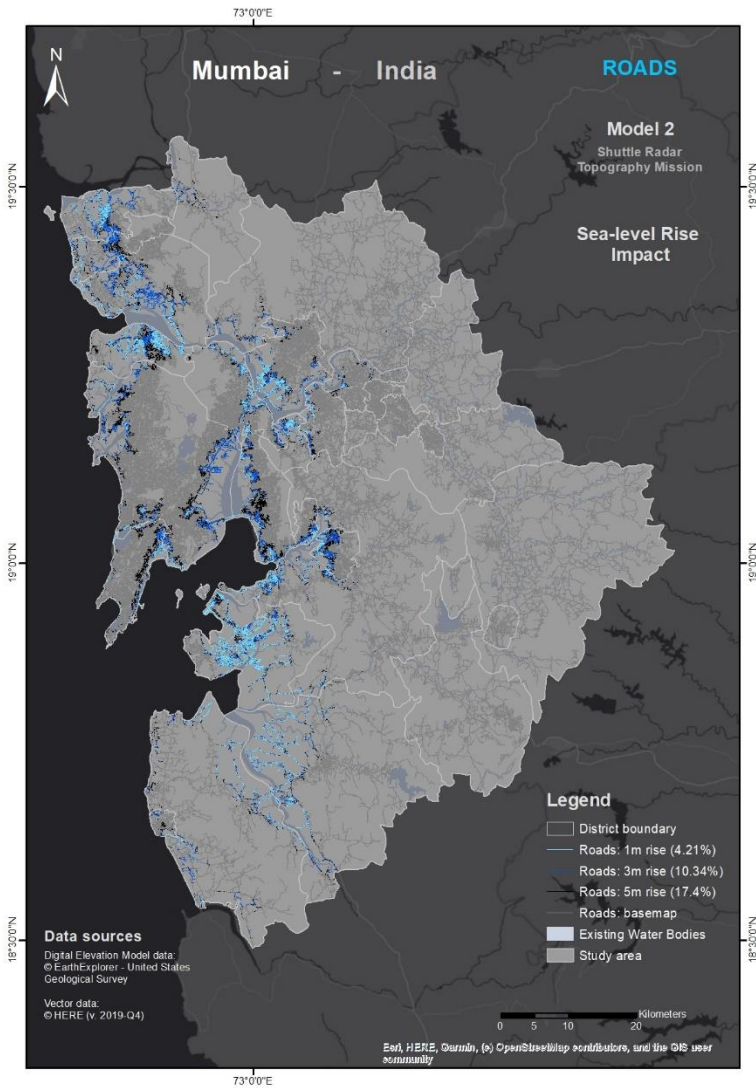
Figure A29: A visual representation of Mumbai's road network affected by SLR (SRTM dataset)
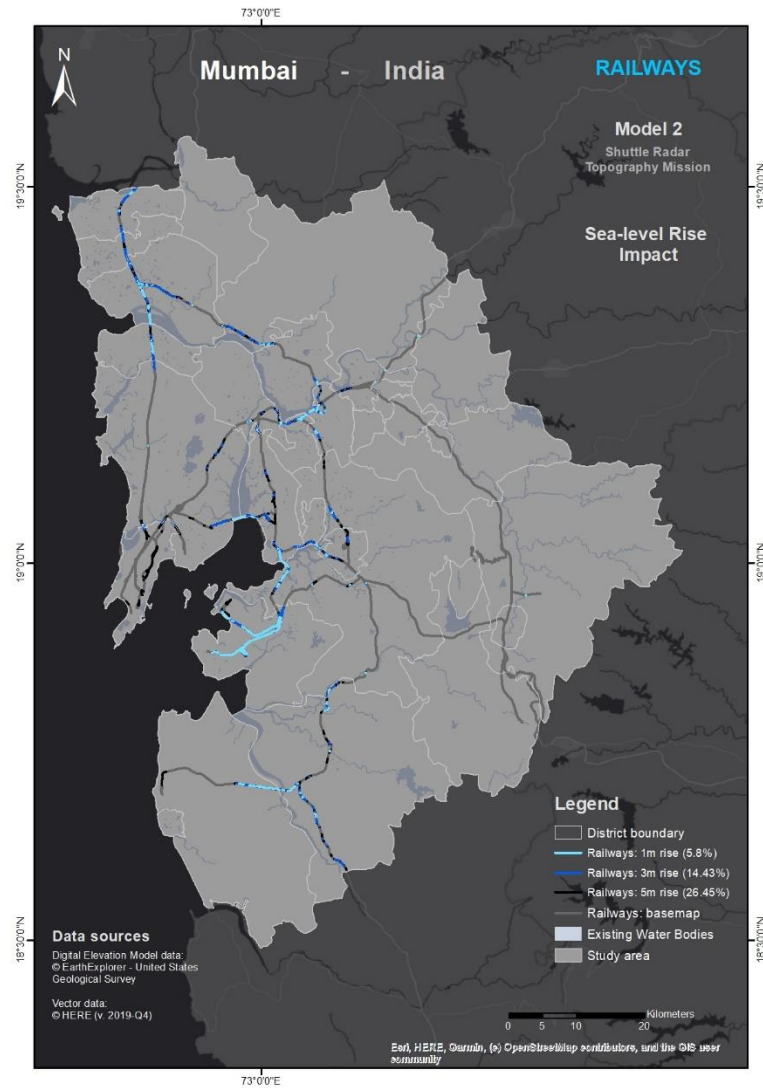
Figure A67: A visual representation of Mumbai's railway network affected by SLR (SRTM dataset)
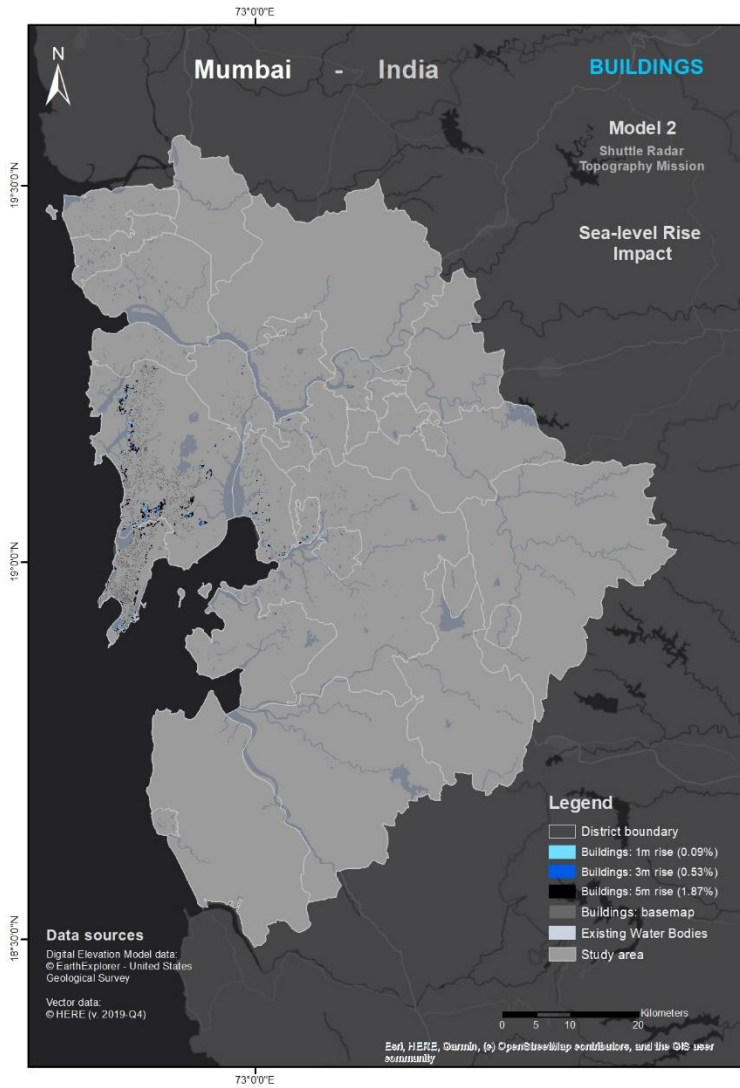
Figure A31: A visual representation of Mumbai's building footprint affected by SLR (SRTM dataset)
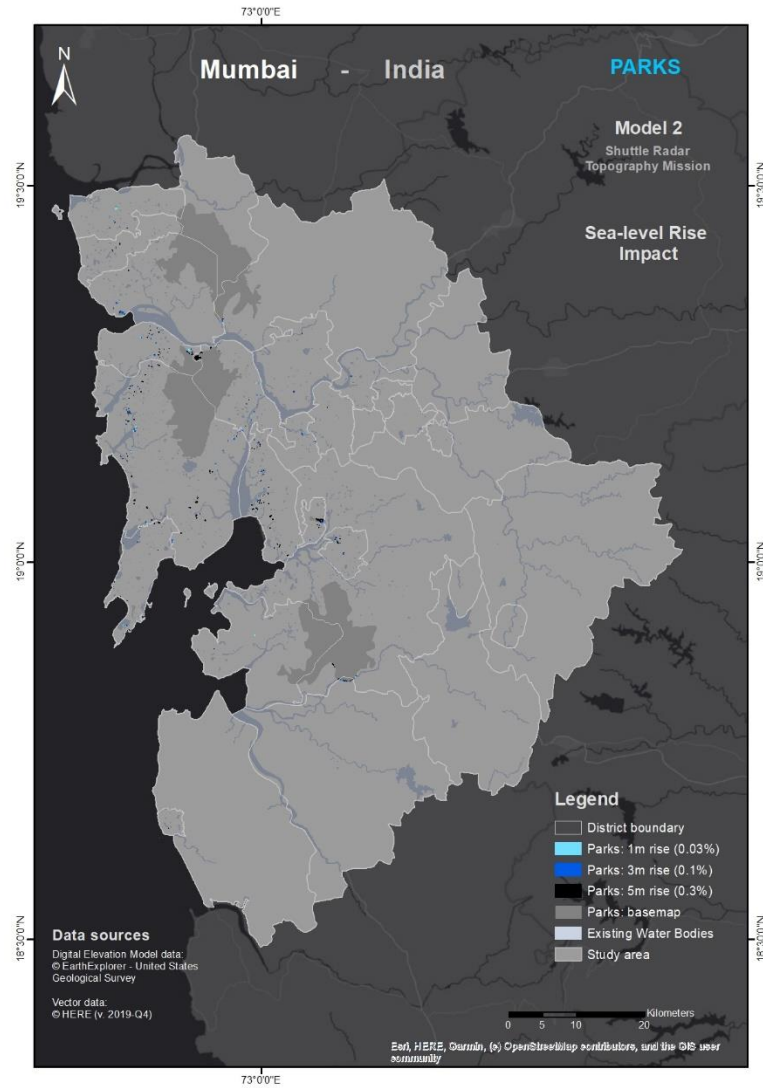
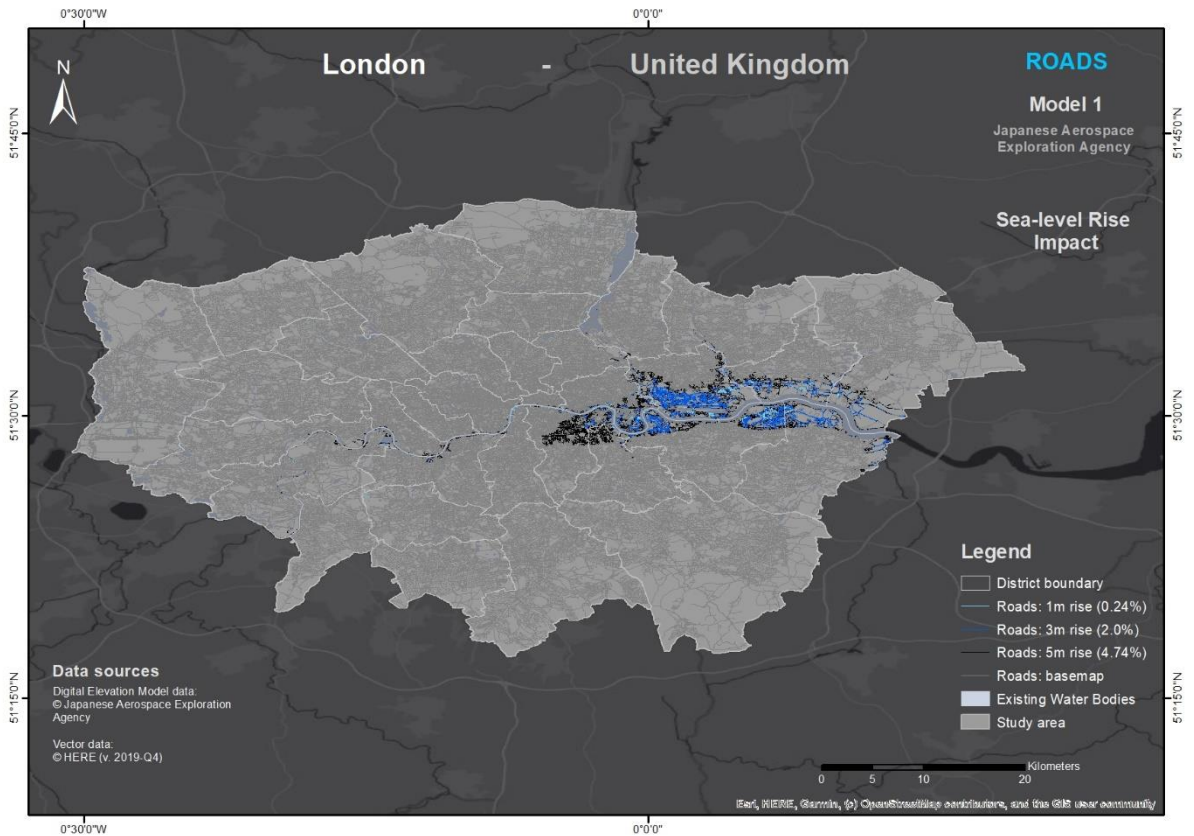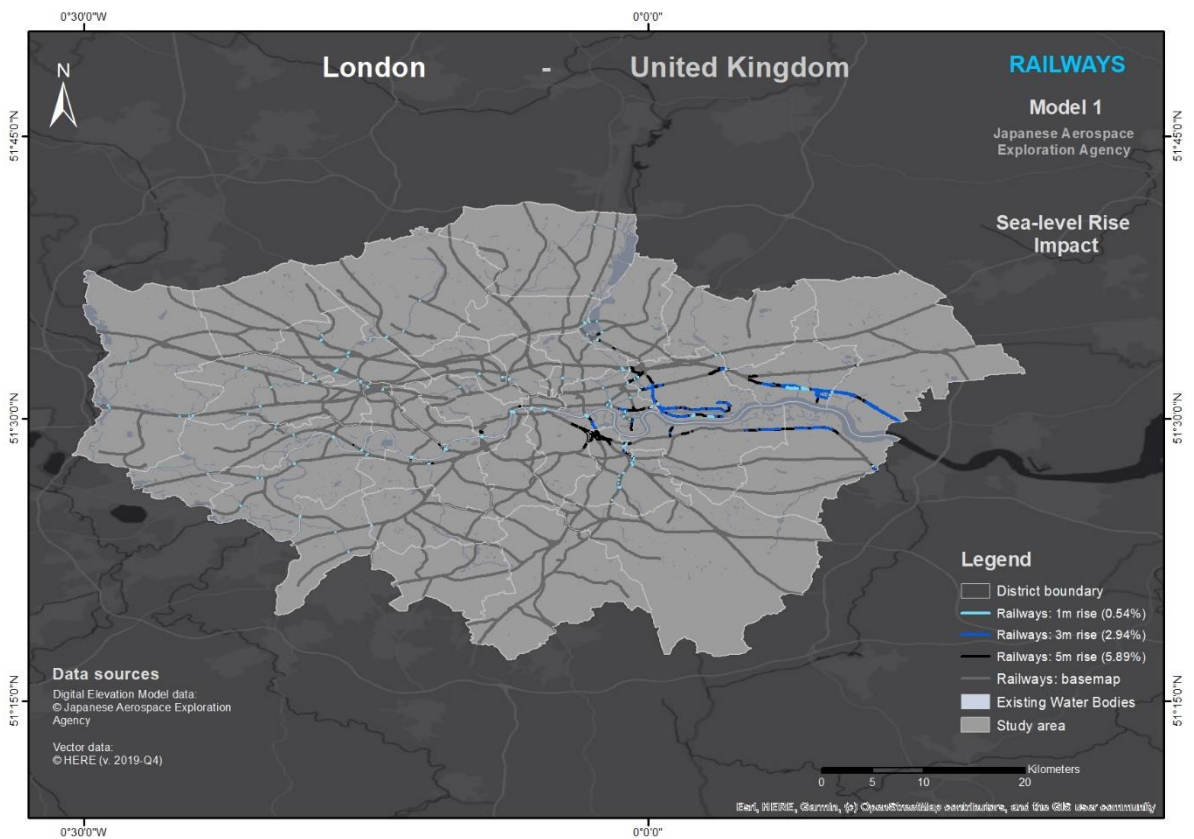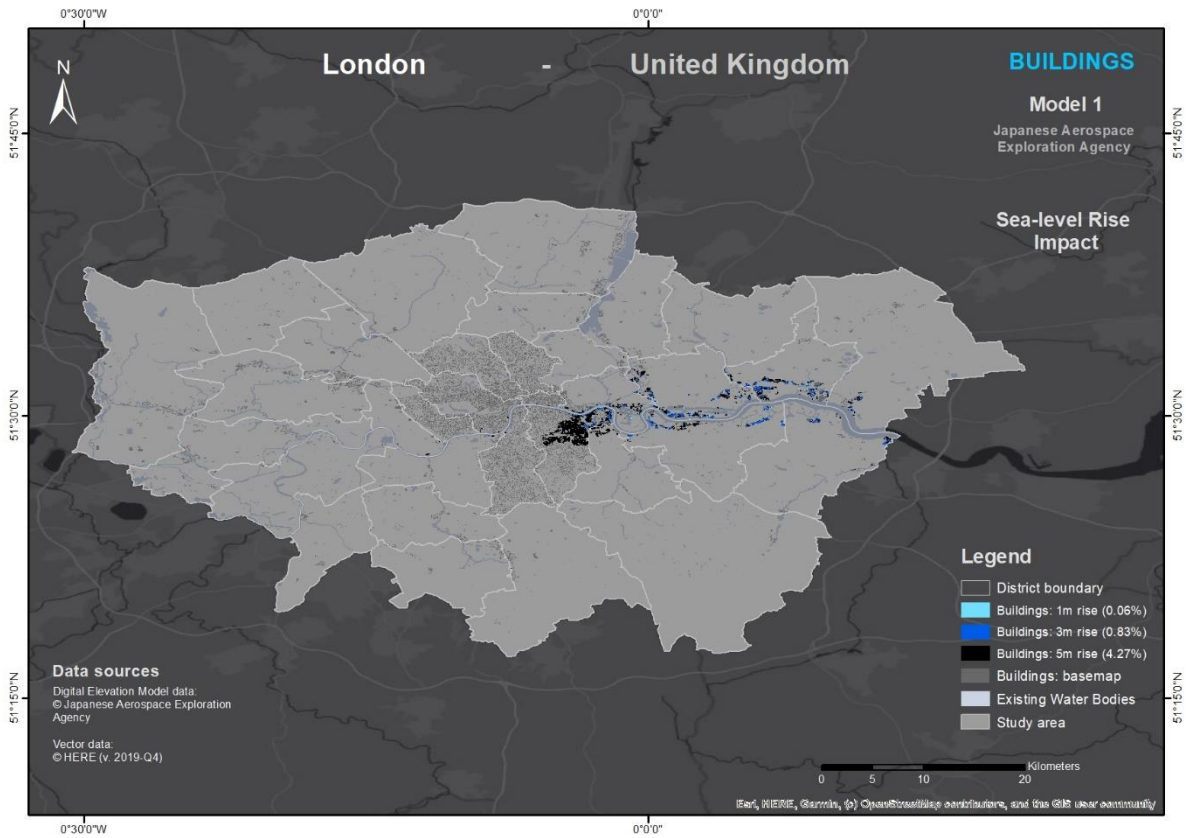*Figure A32: A visual representation of Mumbai's park areas affected by SLR (SRTM dataset)*
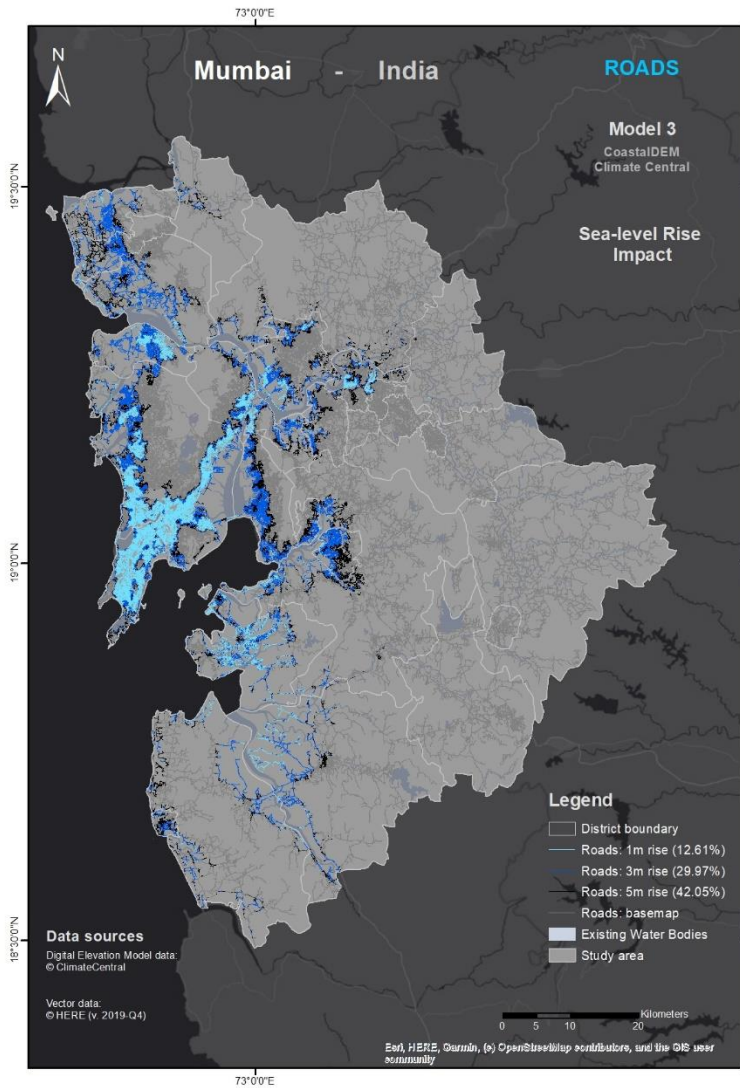
Figure A33: A visual representation of Mumbai's road network affected by SLR (CDEM dataset)
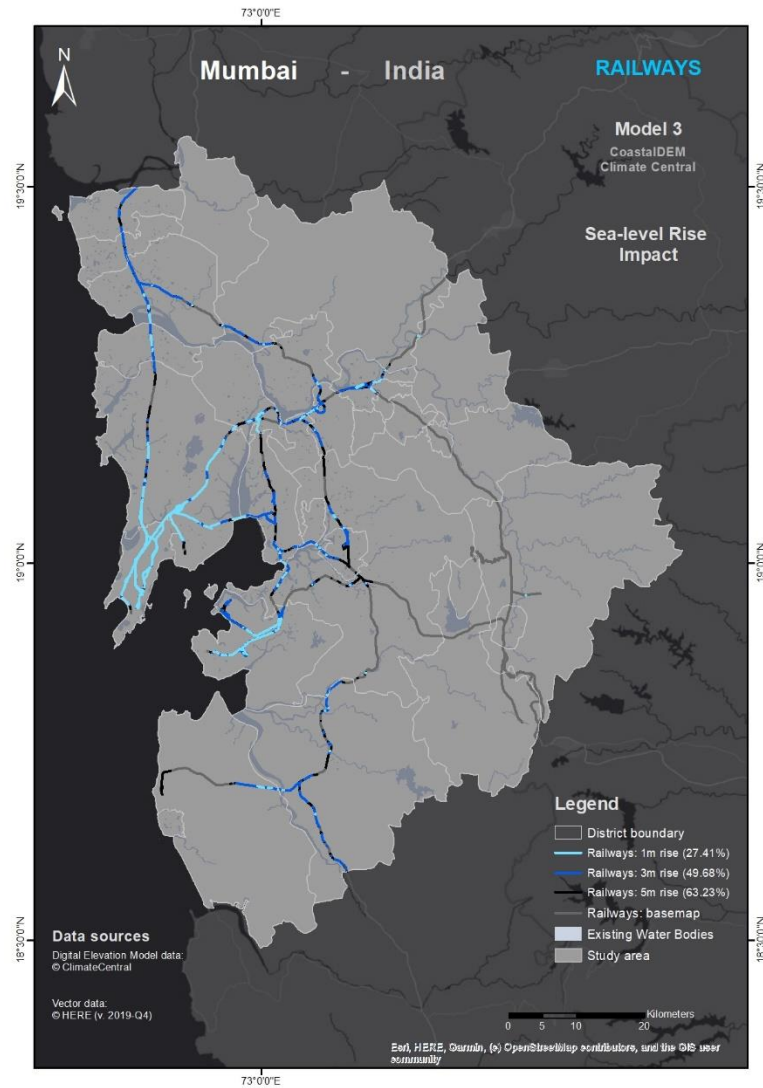
Figure A684: A visual representation of Mumbai's railway network affected by SLR (CDEM dataset)

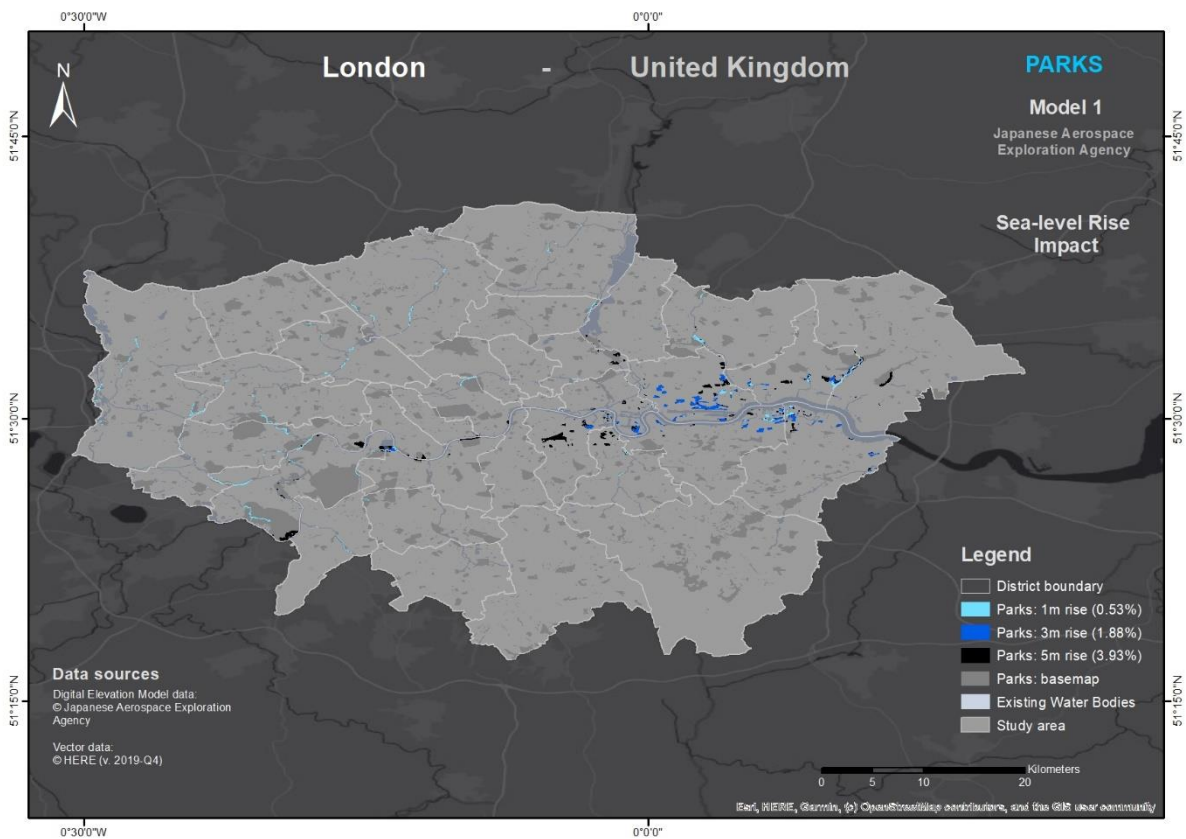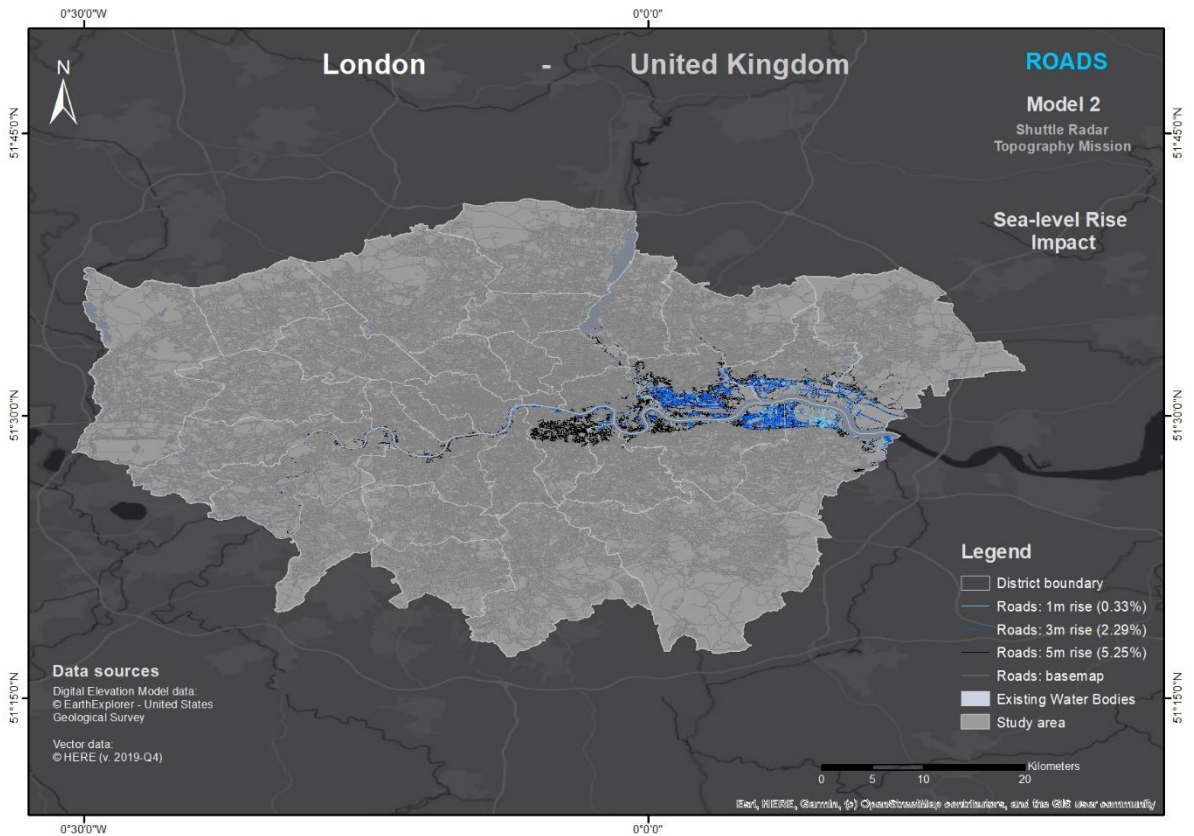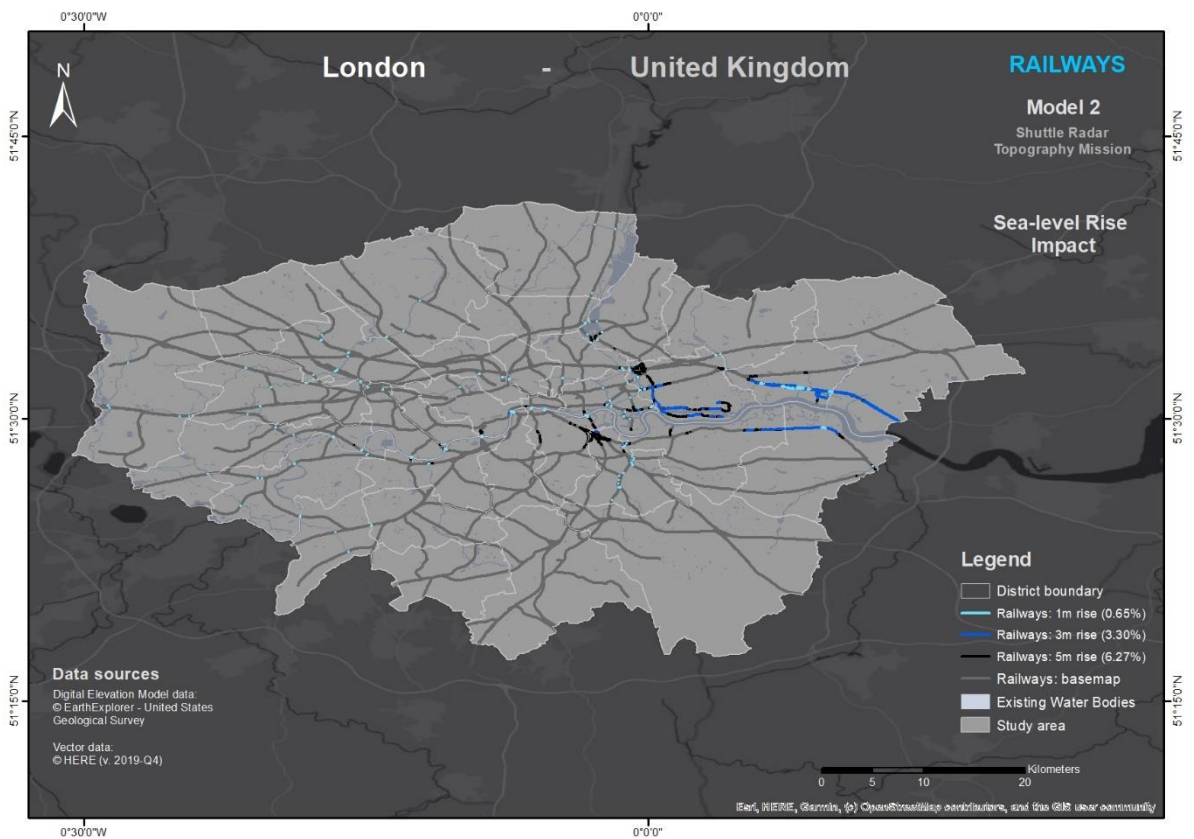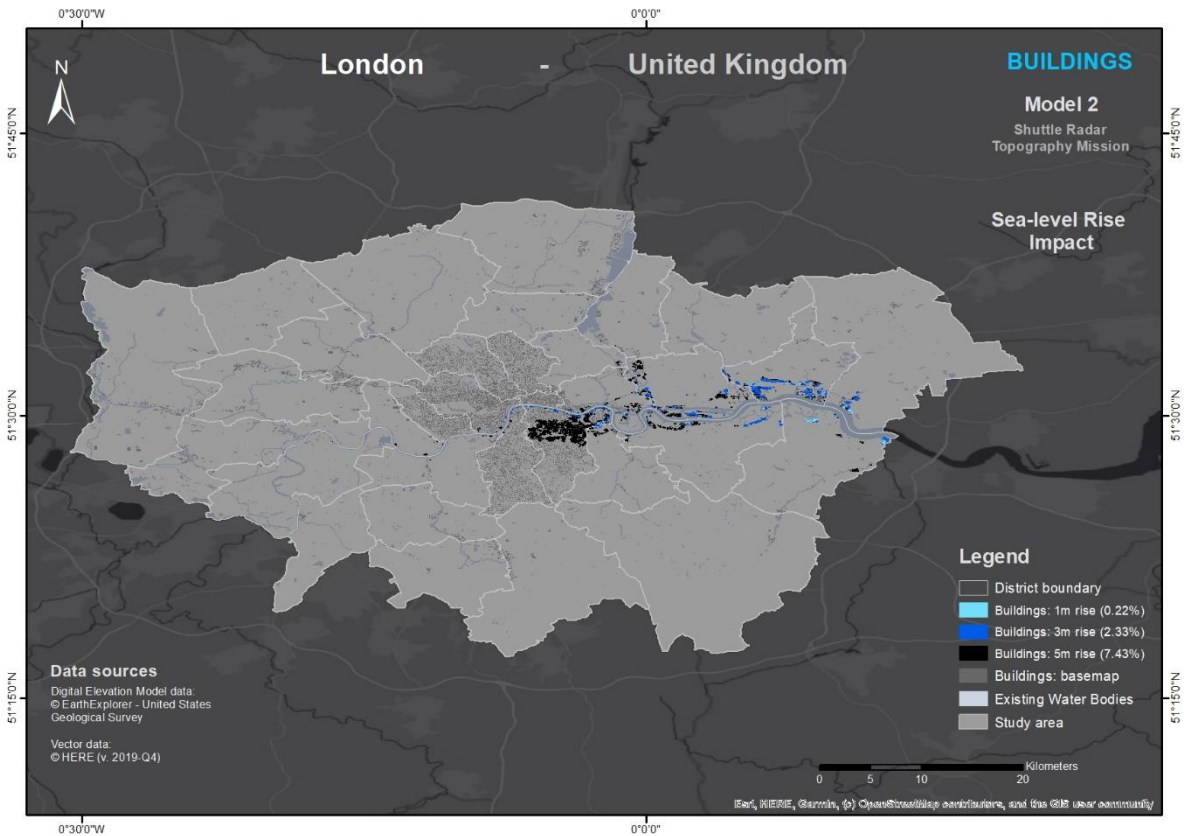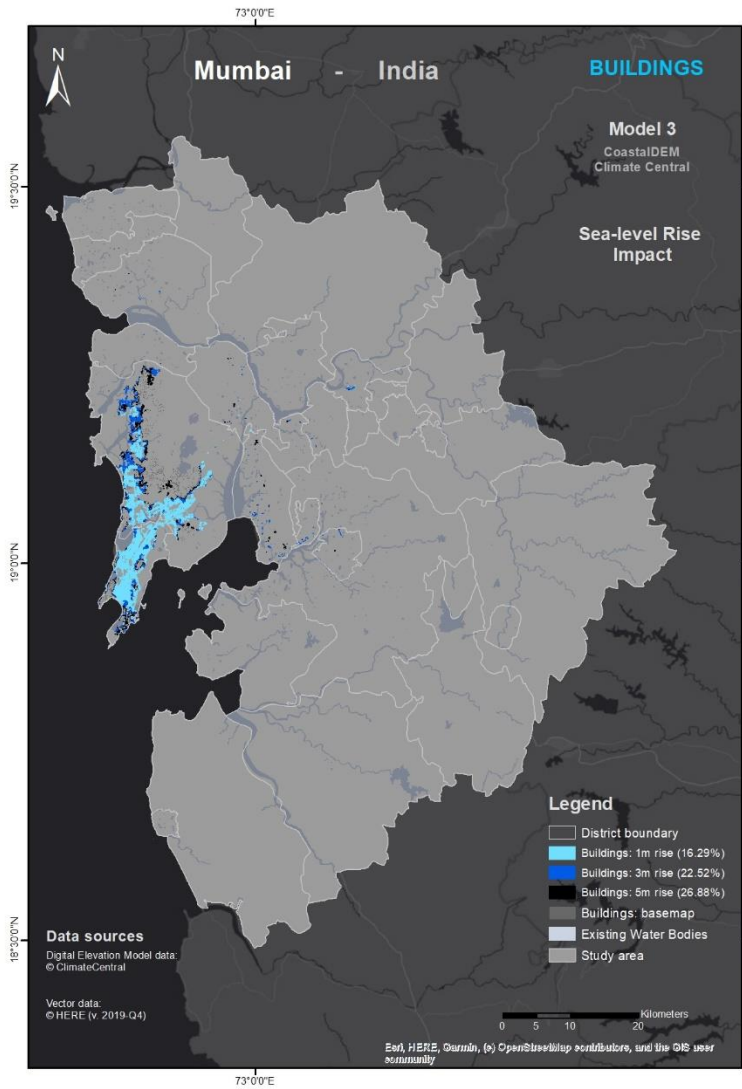*Figure A35: A visual representation of Mumbai's building footprint affected by SLR (CDEM dataset)*
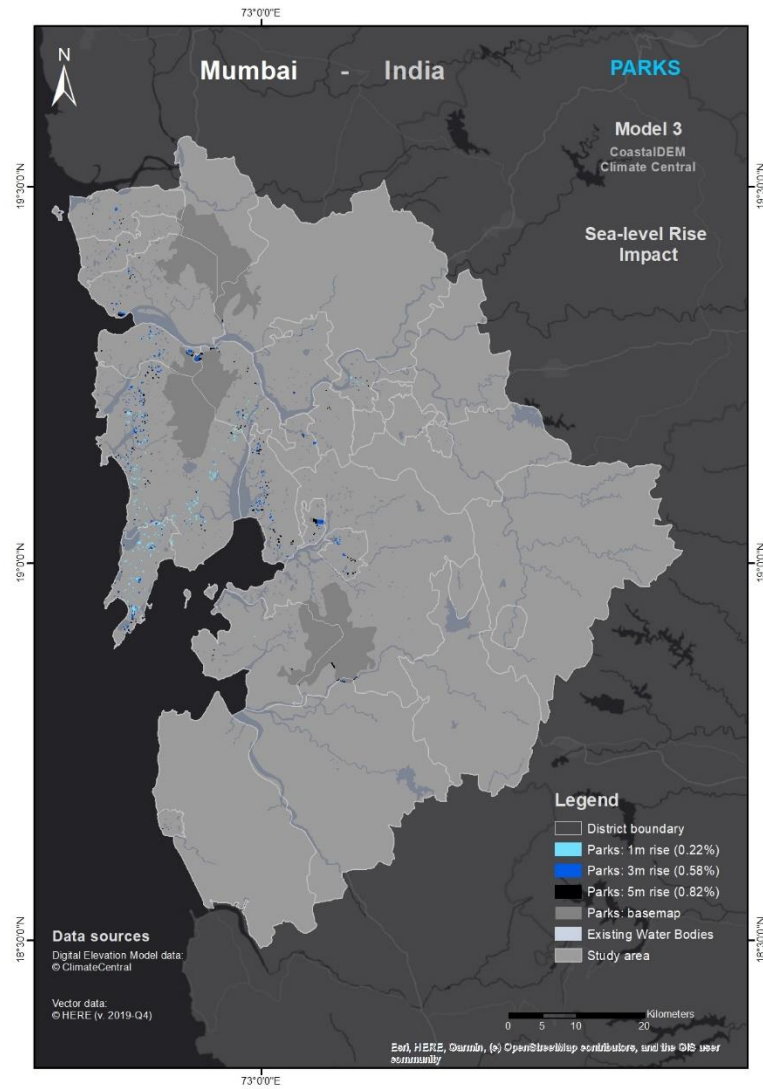
Figure A36: A visual representation of Mumbai's park areas affected by SLR (CDEM dataset

Appendix B

Results broken down by city and infrastructure layer by elevation dataset (comparing cities)
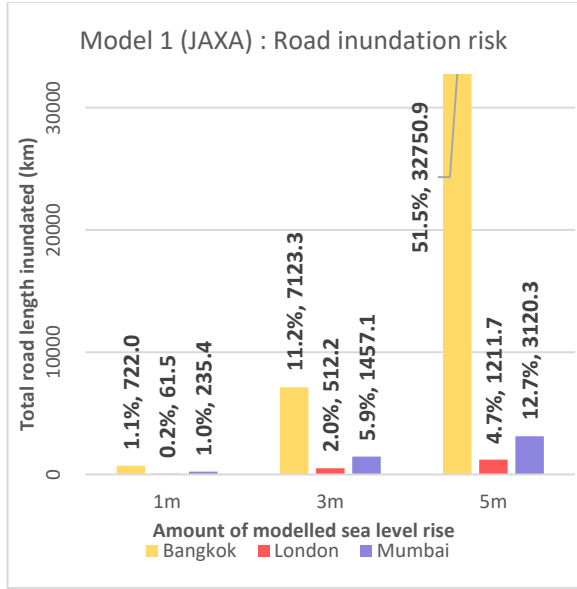
Figure B1: Roads at risk of flooding using the JAXA DEM, compared across cities
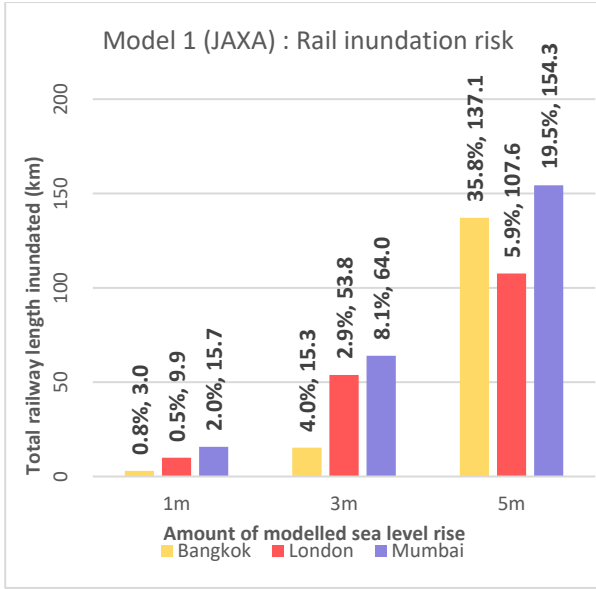
Figure B2: Railways at risk of flooding using the JAXA DEM, compared across cities
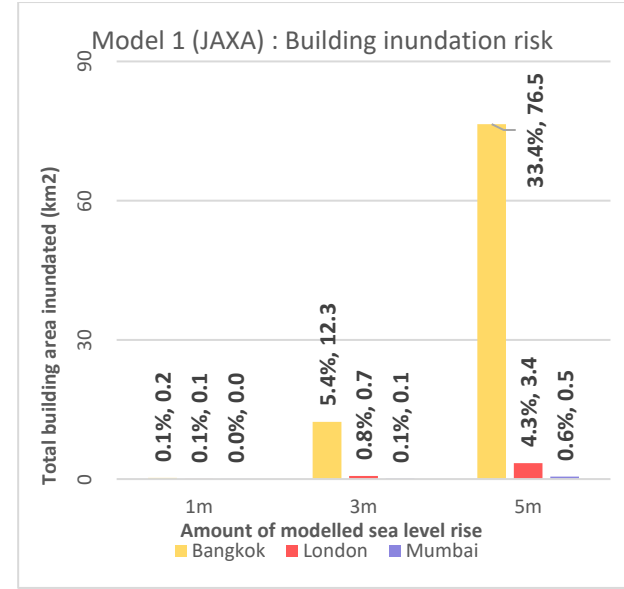
Figure B3: Buildings at risk of flooding using the JAXA DEM, compared across cities
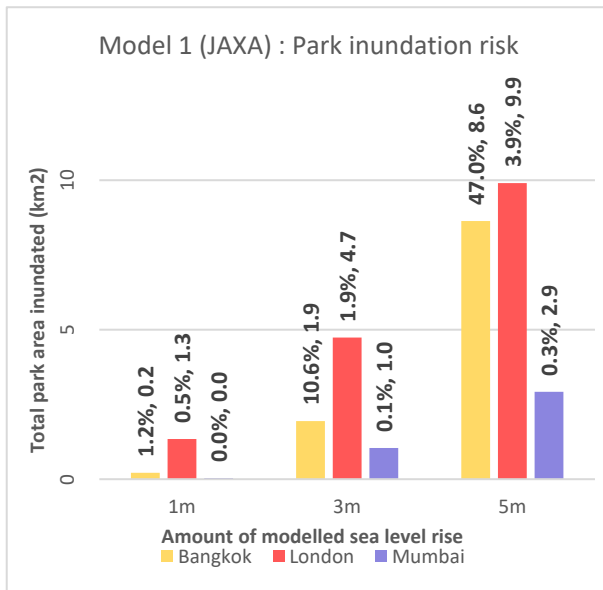
Figure B4: Parks at risk of flooding using the JAXA DEM, compared across cities
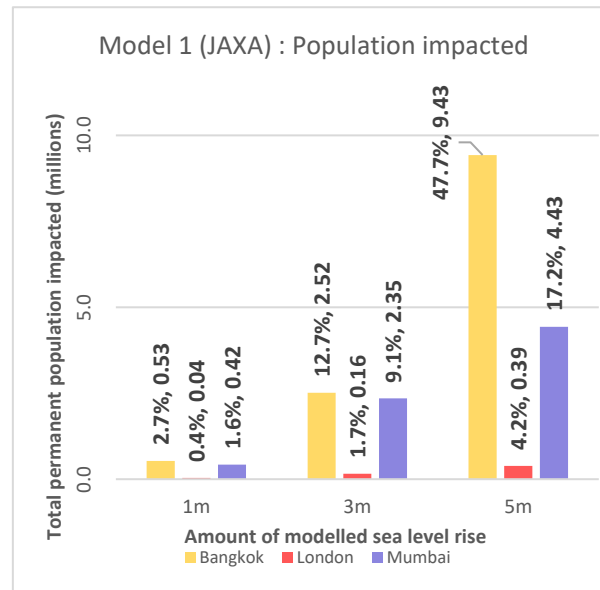
Figure B5: Impacted populations by SLR flooding using the JAXA DEM, compared across cities
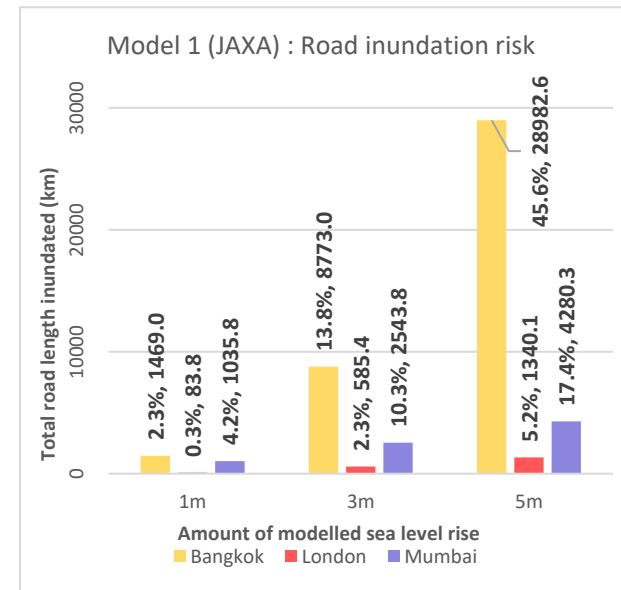
Figure B6: Roads at risk of flooding using the SRTM DEM, compared across cities
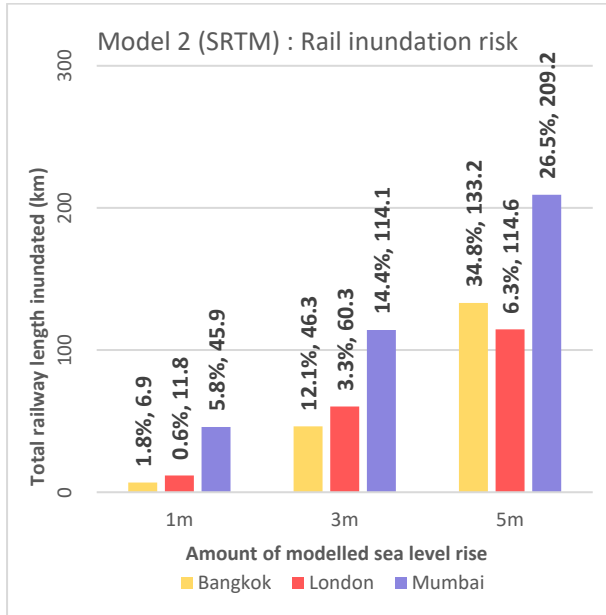
Figure B7: *Railways at risk of flooding using the SRTM DEM, compared across cities*
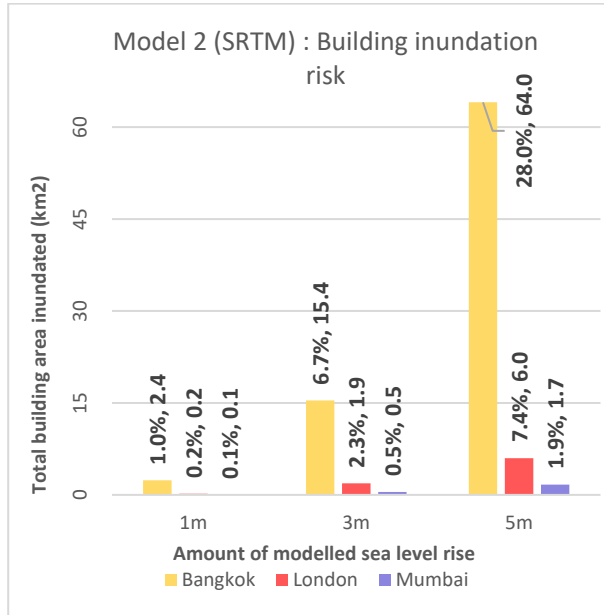
Figure B8: *Buildings at risk of flooding using the SRTM DEM, compared across* cities
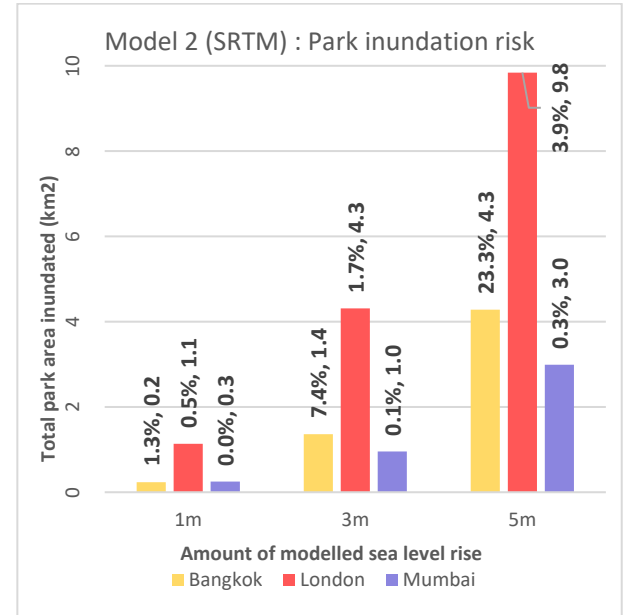
Figure B9: *Parks at risk of flooding using the SRTM DEM, compared across cities*
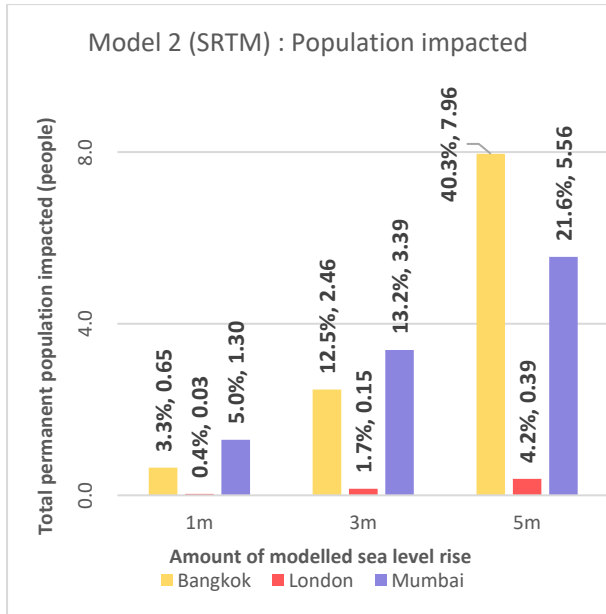
Figure B10: *Impacted populations by SLR flooding using the SRTM DEM, compared across* cities
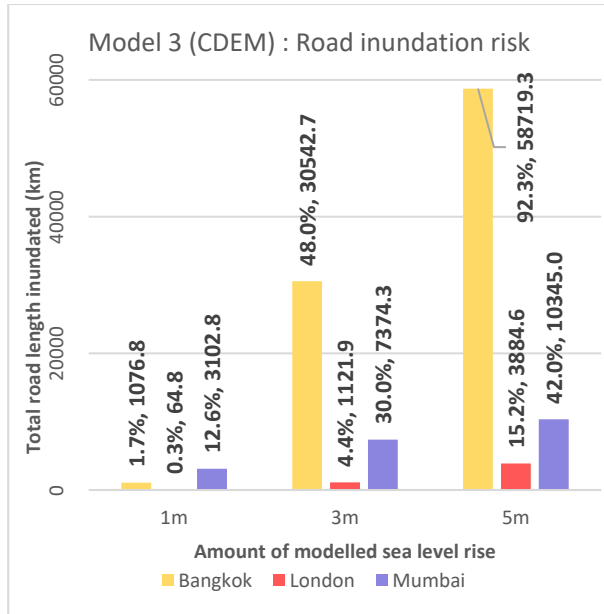
Figure B11: *Roads at risk of flooding using the CDEM DEM, compared across* cities
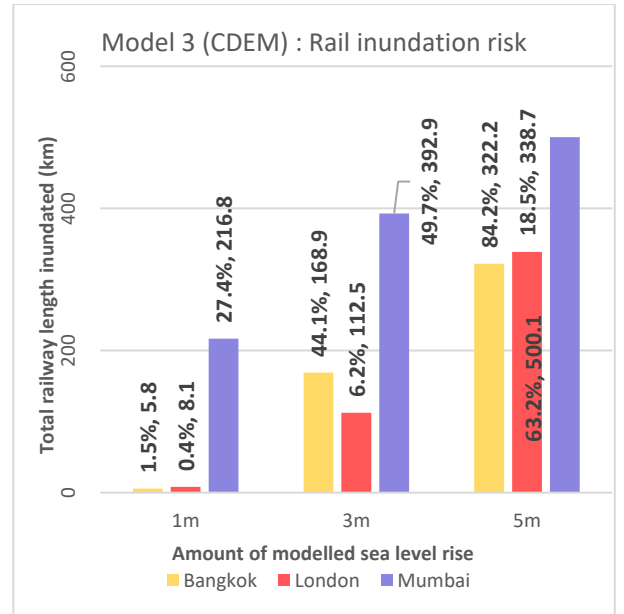
Figure B12: *Railways at risk of flooding using the CDEM DEM, compared across cities*
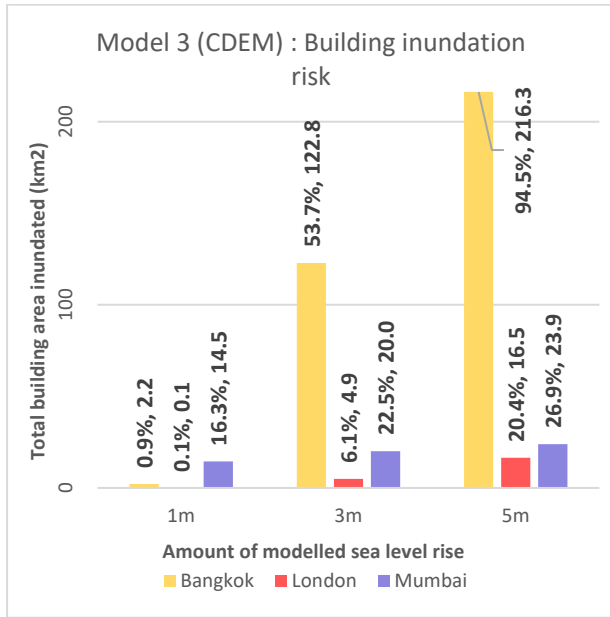
Figure B13: Buildings at risk of flooding using the CDEM DEM, compared across cities
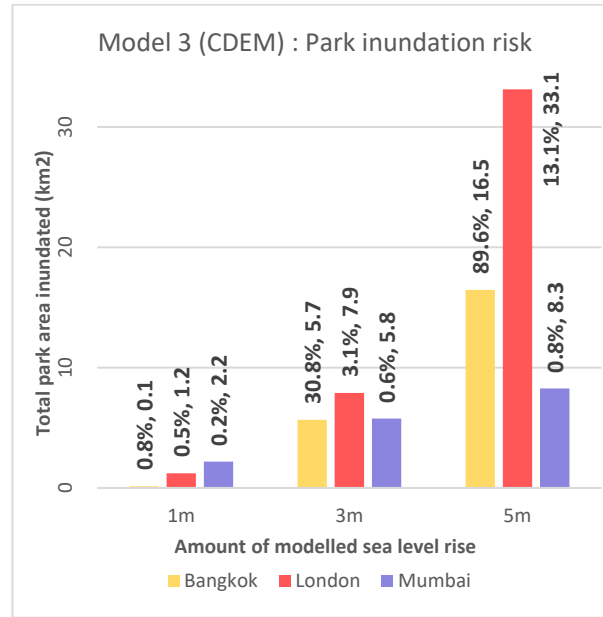
Figure B14: Parks at risk of flooding using the CDEM DEM, compared across cities
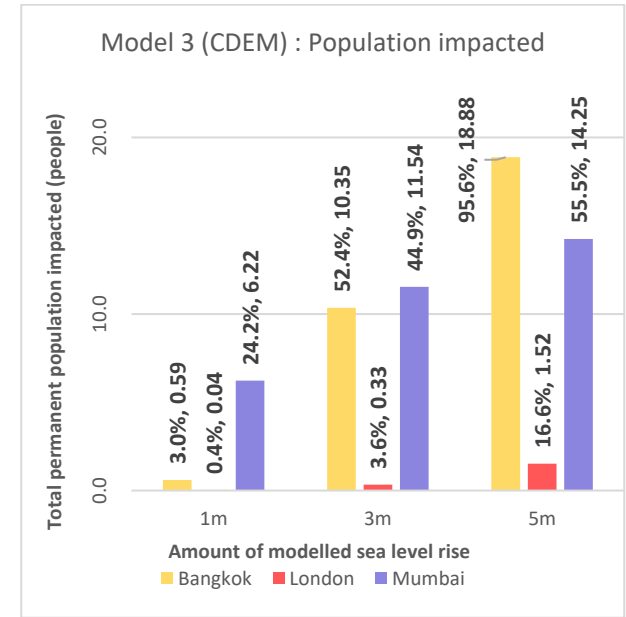
Figure B15: Impacted populations by SLR flooding using the CDEM DEM, compared across cities

Appendix C

Rank	London District Name	JAXA Index	SRTM Index	CDEM Index
1	NEWHAM	0.35	0.40	1.00
2	BARKING AND DAGENHAM	0.07	0.18	0.81
3	SOUTHWARK	0.05	0.06	0.39
4	GREENWICH	0.04	0.06	0.22
5	WANDSWORTH	0	0.01	0.19
6	TOWER HAMLETS	0.01	0.01	0.11
7	HAMMERSMITH AND FULHAM	0	0	0.10
8	WALTHAM FOREST	0	0.01	0.10
9	HACKNEY	0	0	0.07
10	RICHMOND UPON THAMES	0	0	0.07
11	BEXLEY	0.01	0.04	0.06
12	LAMBETH	0	0	0.04
13	HAVERING	0	0.01	0.04
14	LEWISHAM	0	0	0.03
15	HOUNSLOW	0	0	0.03
16	HARINGEY	0	0	0.01
17	BRENT	0	0	0.01
18	KENSINGTON AND CHELSEA	0	0	0
19	EALING	0	0	0
20	REDBRIDGE	0	0	0
21	CITY OF WESTMINSTER	0	0	0
22	HILLINGDON	0	0	0
23	KINGSTON UPON THAMES	0	0	0
24	BARNET	0	0	0
25	CAMDEN	0	0	0
26	CITY OF LONDON	0	0	0
27	MERTON	0	0	0
28	ENFIELD	0	0	0
29	CROYDON	0	0	0
30	BROMLEY	0	0	0
31	ISLINGTON	0	0	0
32	HARROW	0	0	0

Tables C1 (right), *C2* (above left) and *C3* (below left) show the risk index results for Bangkok, London and Mumbai respectively, ranked per district (the district at highest risk has a ranking of 1, with rank inversely proportional to the risk present)

Rank	Mumbai District Name	JAXA Index	SRTM Index	CDEM Index
1	MUMBAI	0.02	0.02	1.00
2	MIRA BHAYANDER	0.01	0.04	0.08
3	NAVI MUMBAI	0	0.01	0.07
4	THANE	0	0.01	0.04
5	URAN	0.01	0.03	0.03
6	VASAI	0.01	0.01	0.02
7	PANVEL	0	0	0.02
8	VIRAR	0	0.01	0.01
9	KALYAN	0	0	0.01
10	BHIWANDI	0	0	0.01
11	NALASOPARA	0	0	0.01
12	DOMBIVLI	0	0	0.01
13	PEN	0	0.01	0.01
14	THANE SUB-DISTRICT	0	0	0
15	ALIBAG SUB-DISTRICT	0	0	0
16	PANVEL SUB-DISTRICT	0	0	0
17	ALIBAG	0	0	0
18	BHIWANDI SUB-DISTRICT	0	0	0
19	ULHASNAGAR	0	0	0
20	VASAI SUB-DISTRICT	0	0	0
21	KALYAN SUB-DISTRICT	0	0	0
22	KARJAT SUB-DISTRICT	0	0	0
23	AMBARNATH SUB-DISTRICT	0	0	0
24	KHALAPUR	0	0	0
25	KARJAT	0	0	0
26	BADLAPUR	0	0	0
27	AMBARNATH	0	0	0
28	MATHERAN	0	0	0

| Rank	Bangkok District Name	JAXA Index	SRTM Index	CDEM Index
1	BANG PHLI	0.06	0.24	1.00
2	PHRA PRADAENG	0.04	0.04	0.55
3	SAMUT PRAKAN	0.11	0.08	0.52
4	DON MUEANG	0.02	0.01	0.37
5	PHRA SAMUT CHEDI	0.08	0.09	0.37
6	CHATUCHAK	0.04	0	0.36
7	BANG KHEN	0.05	0.01	0.35
8	BUENG KUM	0.07	0.02	0.30
9	SAI MAI	0.06	0.02	0.29
10	LAT PHRAO	0.05	0.01	0.27
11	KHAN NA YAO	0.04	0.01	0.27
12	KHLONG SAM WA	0.05	0.04	0.25
13	PRAWET	0.09	0.05	0.23
14	MIN BURI	0.02	0.02	0.23
15	BANG KAPI	0.05	0.01	0.20
16	LAK SI	0.01	0	0.20
17	LAT KRABANG	0.02	0.06	0.19
18	BANG SAO THONG	0.01	0.07	0.17
19	SUAN LUANG	0.05	0.03	0.16
20	WANG THONGLANG	0.04	0.01	0.15
21	NONTHABURI	0	0	0.14
22	HUAI KHWANG	0.03	0.02	0.14
23	PHRA KHANONG	0.03	0.01	0.12
24	SAMUT SAKHON	0.02	0.03	0.11
25	BANG NA	0.02	0.01	0.10
26	SAM PHRAN	0.01	0.01	0.10
27	BANG SUE	0	0	0.10
28	BANG BO	0.05	0.06	0.10
29	KHLONG LUANG	0.04	0.01	0.09
30	SAPHAN SUNG	0.02	0.02	0.08
31	THON BURI	0	0	0.08
32	KHLONG TOEI	0	0	0.08
33	BANGKOK NOI	0	0	0.08
34	BANG KHUN THIAN	0.01	0.02	0.08
35	CHOM THONG	0	0	0.07
36	DIN DAENG	0	0	0.07
37	BANG PHLAT	0	0	0.07
38	YAN NAWA	0	0	0.07
39	KHLONG SAN	0	0	0.07
40	BANG KHO LAEM	0	0	0.07
41	DUSIT	0	0	0.07
42	LAM LUK KA	0.02	0.01	0.06
43	RAT BURANA	0	0	0.06
44	BANG LEN	0.02	0.02	0.06
45	BANG KRUAI	0	0	0.05
46	NONG CHOK	0.01	0.02	0.05
47	PAK KRET	0	0	0.05
48	PATHUM THANI	0.01	0.01	0.05
49	BANG BUA THONG	0.01	0.01	0.05
50	VADHANA	0.01	0	0.05
51	PHAYA THAI	0	0	0.05
52	KRATHUM BAEN	0.01	0.01	0.05
53	THANYABURI	0.01	0	0.04
54	BAN PHAEO	0.01	0.01	0.04
55	BANGKOK YAI	0	0	0.04
56	TALING CHAN	0	0	0.04
57	PHASI CHAROEN	0	0	0.04
58	THUNG KHRU	0.01	0.01	0.04
59	PATHUM WAN	0	0	0.04
60	BANG KHAE	0.01	0	0.03
61	SAI NOI	0.01	0.01	0.03
62	NONG KHAEM	0	0	0.03
63	SATHON	0	0	0.03
64	BANG BON	0.01	0	0.03
65	THAWI WATTHANA	0.01	0.01	0.03
66	BANG YAI	0.01	0	0.03
67	NAKHON CHAI SI	0.01	0	0.03
68	NONG SUEA	0.01	0	0.02
69	LAT LUM KAEO	0.01	0.01	0.02
70	SAMUT SONGKHRAM	0.01	0	0.02
71	RATCHATHEWI	0	0	0.02
72	PHRA NAKHON	0	0	0.02
73	NAKHON PATHOM	0	0	0.02
74	SAM KHOK	0	0	0.02
75	AMPHAWA	0	0	0.01
76	PHUTTHAMONTHON	0	0	0.01
77	DON TUM	0	0	0.01
78	BANG RAK	0	0	0
79	BANG KHONTHI	0	0	0
80	POM PRAP SATTRU PHAI	0	0	0
81	SAMPHANTHAWONG	0	0	0
82	KAMPHAENG SAEN	0	0	0

Appendix D
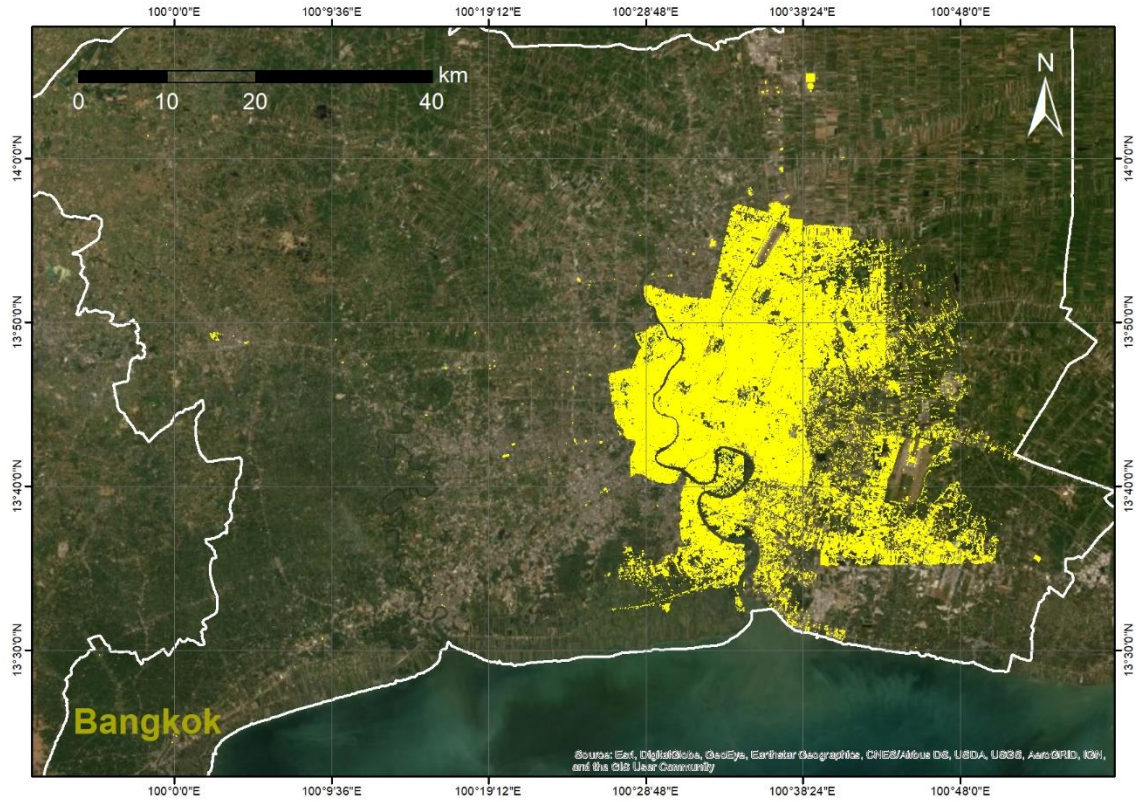
Figure D69: HERE Buildings vector data coverage (in yellow) for version 2019-Q4 overlaying satellite imagery of Bangkok
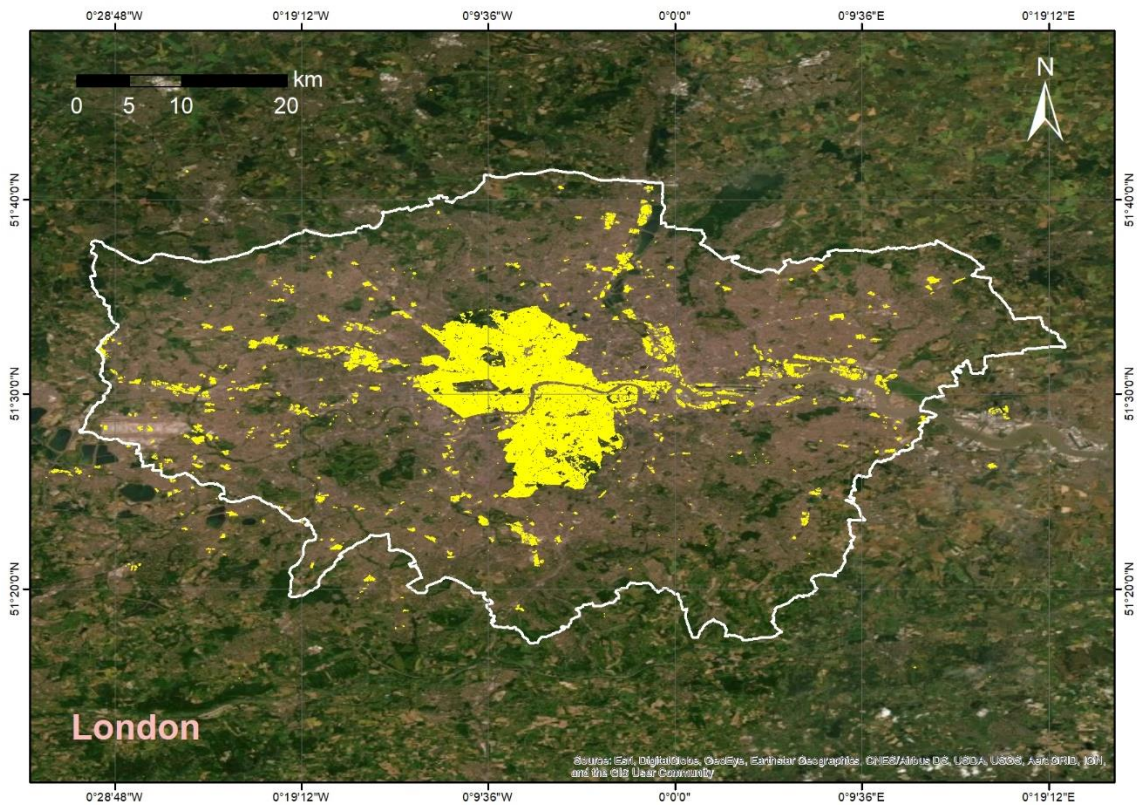
Figure D70: HERE Buildings vector data coverage (in yellow) for version 2019-Q4 overlaying satellite imagery of London
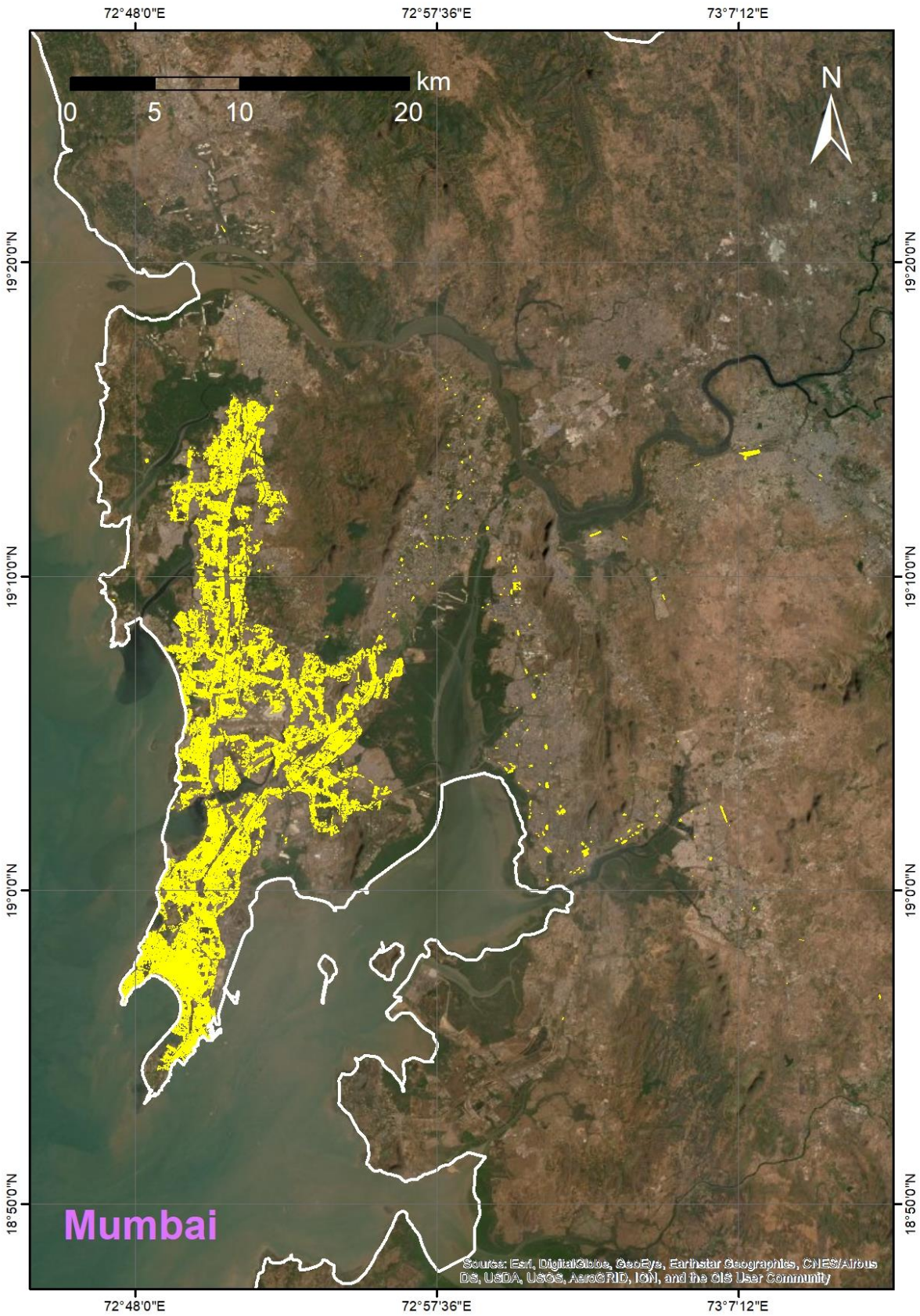
Figure D71: HERE Buildings vector data coverage (in yellow) for version 2019-Q4 overlaying satellite imagery of Mumbai
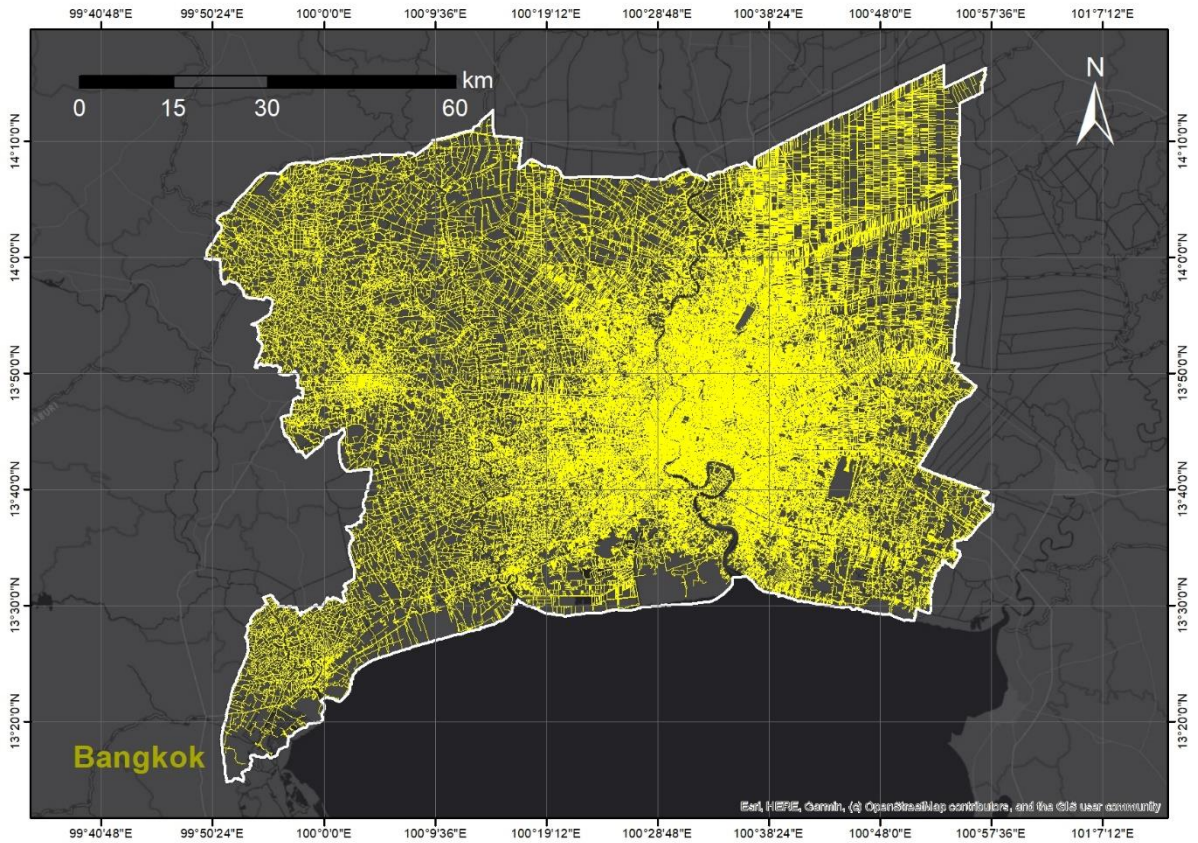
Figure D72: HERE Roads vector data coverage (in yellow) showing the metropolitan city area of Bangkok
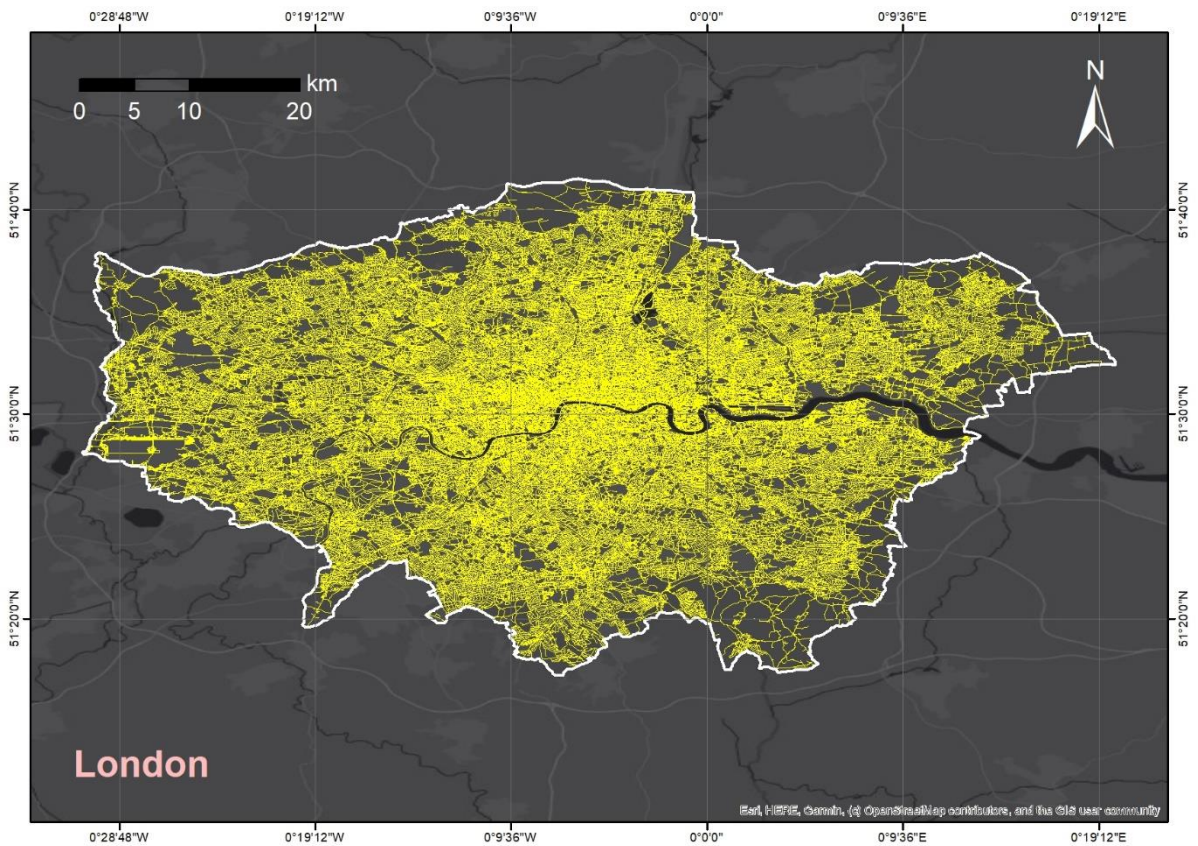
Figure D5: HERE Roads vector data coverage (in yellow) showing the metropolitan city area of London
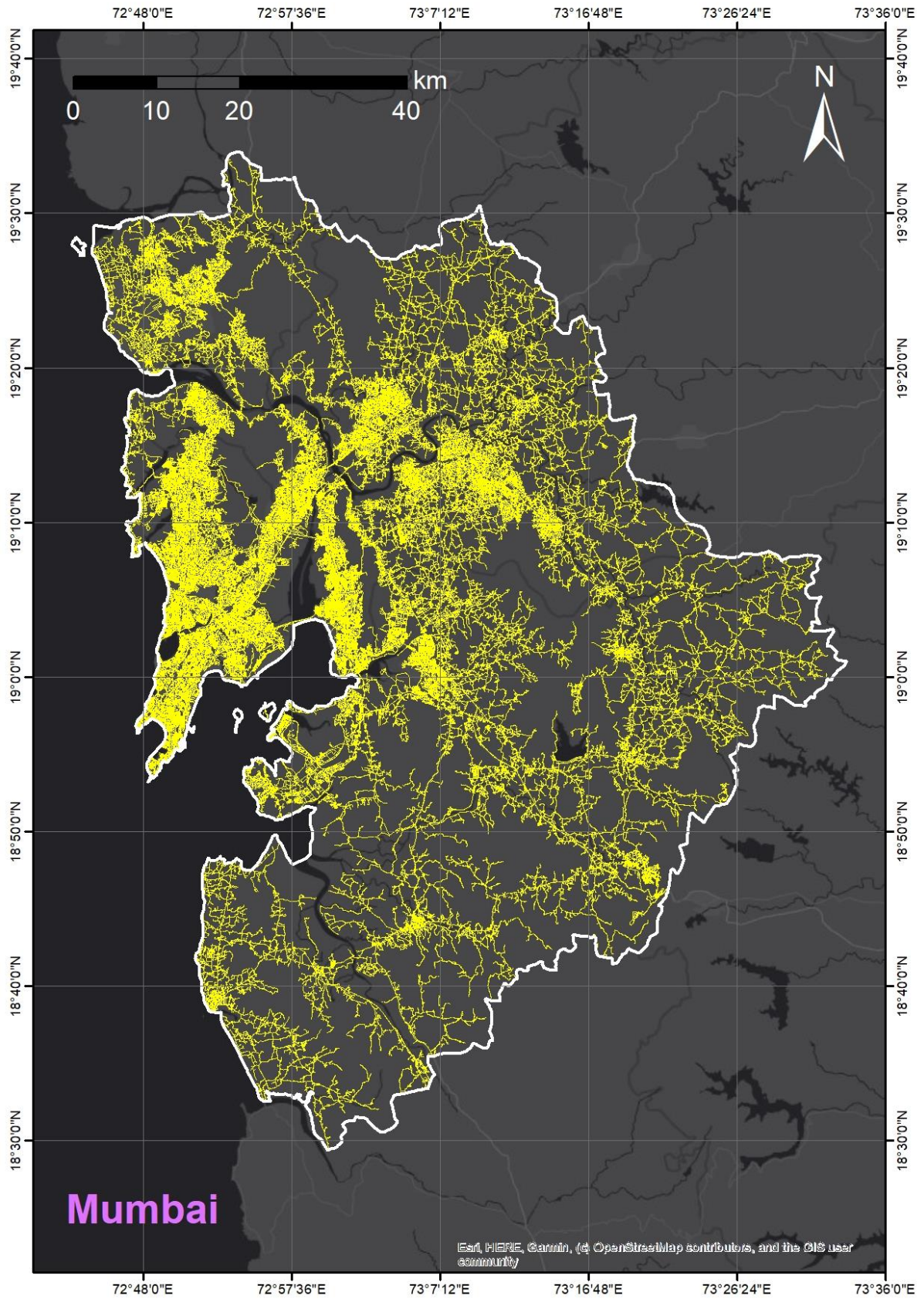
Figure D6: HERE Roads vector data coverage (in yellow) showing the metropolitan city area of Mumbai

Appendix E

Table E2: *Areas and proportions of SLR inundation extents on the three cities examined*

City	Total area (km2)	Inundated area (km2)											
		JAXA 1m	JAXA 3m	JAXA 5m	SRTM 1m	SRTM 3m	SRTM 5m	JAXA-SRTM 1m	JAXA-SRTM 3m	JAXA-SRTM 5m	CDEM 1m	CDEM 3m	CDEM 5m
Bangkok	8338.8	321.3	1364.2	4936.2	516.9	1747.2	4732.2	419.1	1555.7	4834.2	480.3	4242.0	7630.1
London	2557.5	44.3	84.2	134.5	48.8	91.7	148.6	46.5	87.9	141.5	53.0	140.7	336.7
Mumbai	5851.3	352.6	770.0	1027.9	557.9	908.7	1104.6	455.2	839.4	1066.3	573.1	1250.8	1551.4

City	Total share (%)	Share of total (%)											
		JAXA 1m	JAXA 3m	JAXA 5m	SRTM 1m	SRTM 3m	SRTM 5m	JAXA-SRTM 1m	JAXA-SRTM 3m	JAXA-SRTM 5m	CDEM 1m	CDEM 3m	CDEM 5m
Bangkok	100%	3.9%	16.4%	59.2%	6.2%	21.0%	56.7%	5.0%	18.7%	58.0%	5.8%	50.9%	91.5%
London	100%	1.7%	3.3%	5.3%	1.9%	3.6%	5.8%	1.8%	3.4%	5.5%	2.1%	5.5%	13.2%
Mumbai	100%	6.0%	13.2%	17.6%	9.5%	15.5%	18.9%	7.8%	14.3%	18.2%	9.8%	21.4%	26.5%

Table E2: *The results of the city road lengths and proportions of the total impacted by the modelled SLR scenarios*

City	Total length (km)	Inundated total lengths (km)											
		JAXA 1m	JAXA 3m	JAXA 5m	SRTM 1m	SRTM 3m	SRTM 5m	JAXA-SRTM 1m	JAXA-SRTM 3m	JAXA-SRTM 5m	CDEM 1m	CDEM 3m	CDEM 5m
Bangkok	63617.6	722.0	7123.3	32750.9	1469.0	8773.0	28982.6	1095.5	7948.2	30866.8	1076.8	30542.7	58719.3
London	25550.4	61.5	512.2	1211.7	83.8	585.4	1340.1	72.7	548.8	1275.9	64.8	1121.9	3884.6
Mumbai	24603.7	235.4	1457.1	3120.3	1035.8	2543.8	4280.3	635.6	2000.5	3700.3	3102.8	7374.3	10345.0

City	Total share (%)	Share of total (%)											
		JAXA 1m	JAXA 3m	JAXA 5m	SRTM 1m	SRTM 3m	SRTM 5m	JAXA-SRTM 1m	JAXA-SRTM 3m	JAXA-SRTM 5m	CDEM 1m	CDEM 3m	CDEM 5m
Bangkok	100%	1.1%	11.2%	51.5%	2.3%	13.8%	45.6%	1.7%	12.5%	48.5%	1.7%	48.0%	92.3%
London	100%	0.2%	2.0%	4.7%	0.3%	2.3%	5.2%	0.3%	2.1%	5.0%	0.3%	4.4%	15.2%
Mumbai	100%	1.0%	5.9%	12.7%	4.2%	10.3%	17.4%	2.6%	8.1%	15.0%	12.6%	30.0%	42.0%

Table E3: The results of the city railway lengths and proportions of the total impacted by the modelled SLR scenarios

City	Total length (km)	Inundated total lengths (km)											
		JAXA 1m	JAXA 3m	JAXA 5m	SRTM 1m	SRTM 3m	SRTM 5m	JAXA-SRTM 1m	JAXA-SRTM 3m	JAXA-SRTM 5m	CDEM 1m	CDEM 3m	CDEM 5m
Bangkok	382.8	3.0	15.3	137.1	6.9	46.3	133.2	4.9	30.8	135.1	5.8	168.9	322.2
London	1826.5	9.9	53.8	107.6	11.8	60.3	114.6	10.9	57.0	111.1	8.1	112.5	338.7
Mumbai	790.9	15.7	64.0	154.3	45.9	114.1	209.2	30.8	89.1	181.8	216.8	392.9	500.1

City	Total share (%)	Share of total (%)											
		JAXA 1m	JAXA 3m	JAXA 5m	SRTM 1m	SRTM 3m	SRTM 5m	JAXA-SRTM 1m	JAXA-SRTM 3m	JAXA-SRTM 5m	CDEM 1m	CDEM 3m	CDEM 5m
Bangkok	100%	0.8%	4.0%	35.8%	1.8%	12.1%	34.8%	1.3%	8.1%	35.3%	1.5%	44.1%	84.2%
London	100%	0.5%	2.9%	5.9%	0.6%	3.3%	6.3%	0.6%	3.1%	6.1%	0.4%	6.2%	18.5%
Mumbai	100%	2.0%	8.1%	19.5%	5.8%	14.4%	26.5%	3.9%	11.3%	23.0%	27.4%	49.7%	63.2%

Table E4: The results of the city park areas and proportions of the total impacted by the modelled SLR scenarios

City	Total area (km2)	Inundated area (km2)											
		JAXA 1m	JAXA 3m	JAXA 5m	SRTM 1m	SRTM 3m	SRTM 5m	JAXA-SRTM 1m	JAXA-SRTM 3m	JAXA-SRTM 5m	CDEM 1m	CDEM 3m	CDEM 5m
Bangkok	18.4	0.2	1.9	8.6	0.2	1.4	4.3	0.2	1.7	6.5	0.1	5.7	16.5
London	251.9	1.3	4.7	9.9	1.1	4.3	9.8	1.2	4.5	9.9	1.2	7.9	33.1
Mumbai	1002.1	0.0	1.0	2.9	0.3	1.0	3.0	0.1	1.0	3.0	2.2	5.8	8.3

City	Total share (%)	Share of total (%)											
		JAXA 1m	JAXA 3m	JAXA 5m	SRTM 1m	SRTM 3m	SRTM 5m	JAXA-SRTM 1m	JAXA-SRTM 3m	JAXA-SRTM 5m	CDEM 1m	CDEM 3m	CDEM 5m
Bangkok	100%	1.2%	10.6%	47.0%	1.3%	7.4%	23.3%	1.2%	9.0%	35.2%	0.8%	30.8%	89.6%
London	100%	0.5%	1.9%	3.9%	0.5%	1.7%	3.9%	0.5%	1.8%	3.9%	0.5%	3.1%	13.1%
Mumbai	100%	0.0%	0.1%	0.3%	0.0%	0.1%	0.3%	0.0%	0.1%	0.3%	0.2%	0.6%	0.8%

127

Table E5: Table showing percentage differences between values across two cities comparatively, with matching values (±20%) highlighted in yellow

ROADS	JAXA 1m	JAXA 3m	JAXA 5m	SRTM 1m	SRTM 3m	SRTM 5m	JAXA-SRTM 1m	JAXA-SRTM 3m	JAXA-SRTM 5m	CDEM 1m	CDEM 3m	CDEM 5m
Bangkok:London	168.6%	173.2%	185.7%	178.4%	175.0%	182.3%	175.1%	174.2%	184.1%	177.3%	185.8%	175.2%
Bangkok:Mumbai	101.6%	132.1%	165.2%	34.6%	110.1%	148.5%	53.1%	119.6%	157.2%	-96.9%	122.2%	140.1%
London:Mumbai	117.1%	96.0%	88.1%	170.0%	125.2%	104.6%	159.0%	113.9%	97.4%	191.8%	147.2%	90.8%

RAILWAYS	JAXA 1m	JAXA 3m	JAXA 5m	SRTM 1m	SRTM 3m	SRTM 5m	JAXA-SRTM 1m	JAXA-SRTM 3m	JAXA-SRTM 5m	CDEM 1m	CDEM 3m	CDEM 5m
Bangkok:London	107.6%	111.3%	-24.1%	52.7%	26.1%	-15.0%	75.2%	59.6%	-19.6%	33.7%	-40.1%	5.0%
Bangkok:Mumbai	136.1%	122.8%	11.8%	147.9%	84.5%	44.4%	144.8%	97.1%	29.4%	189.6%	79.7%	43.3%
London:Mumbai	45.0%	17.3%	35.7%	118.2%	61.8%	58.5%	95.7%	43.9%	48.3%	185.6%	111.0%	38.5%

BUILDINGS	JAXA 1m	JAXA 3m	JAXA 5m	SRTM 1m	SRTM 3m	SRTM 5m	JAXA-SRTM 1m	JAXA-SRTM 3m	JAXA-SRTM 5m	CDEM 1m	CDEM 3m	CDEM 5m
Bangkok:London	129.2%	179.3%	182.8%	172.6%	156.5%	165.8%	168.1%	166.3%	174.8%	186.8%	184.6%	171.7%
Bangkok:Mumbai	149.4%	196.2%	197.3%	186.8%	188.1%	189.9%	183.0%	191.7%	193.9%	-148.2%	143.9%	160.2%
London:Mumbai	39.0%	139.7%	147.5%	72.8%	119.7%	113.1%	64.3%	124.8%	124.8%	-198.0%	-121.2%	-36.8%

PARKS	JAXA 1m	JAXA 3m	JAXA 5m	SRTM 1m	SRTM 3m	SRTM 5m	JAXA-SRTM 1m	JAXA-SRTM 3m	JAXA-SRTM 5m	CDEM 1m	CDEM 3m	CDEM 5m
Bangkok:London	144.6%	83.7%	13.7%	131.1%	104.0%	78.8%	138.3%	93.1%	41.8%	158.9%	32.9%	67.2%
Bangkok:Mumbai	137.9%	60.3%	98.8%	-6.3%	34.8%	35.5%	43.4%	49.1%	74.3%	-176.1%	-1.9%	66.3%
London:Mumbai	188.5%	127.9%	108.8%	127.5%	127.3%	106.8%	158.0%	127.6%	107.8%	-57.3%	31.1%	120.1%

Table E6: Differences calculated between population values affected by SLR scenarios across all elevation datasets. Matching values (within ±20% of each other) are highlighted in yellow.

POPULATION	JAXA 1m	JAXA 3m	JAXA 5m	SRTM 1m	SRTM 3m	SRTM 5m	JAXA-SRTM 1m	JAXA-SRTM 3m	JAXA-SRTM 5m	CDEM 1m	CDEM 3m	CDEM 5m
Bangkok:London	174.5%	176.6%	184.2%	180.9%	176.7%	181.5%	178.0%	176.6%	183.0%	177.8%	187.5%	170.2%
Bangkok:Mumbai	22.8%	6.8%	72.1%	-67.0%	-31.5%	35.6%	-37.5%	-14.1%	54.1%	-165.1%	-10.9%	27.9%
London:Mumbai	168.5%	175.0%	167.8%	190.3%	182.8%	174.0%	184.7%	179.6%	171.2%	197.8%	188.8%	161.5%

Table E7: The results of the city building areas and proportions of the total impacted by the modelled SLR scenarios

City	Total area (km2)	Inundated area (km2)											
		JAXA 1m	JAXA 3m	JAXA 5m	SRTM 1m	SRTM 3m	SRTM 5m	JAXA-SRTM 1m	JAXA-SRTM 3m	JAXA-SRTM 5m	CDEM 1m	CDEM 3m	CDEM 5m
Bangkok	228.7	0.2	12.3	76.5	2.4	15.4	64.0	1.3	13.9	70.3	2.2	122.8	216.3
London	80.7	0.1	0.7	3.4	0.2	1.9	6.0	0.1	1.3	4.7	0.1	4.9	16.5
Mumbai	88.9	0.0	0.1	0.5	0.1	0.5	1.7	0.1	0.3	1.1	14.5	20.0	23.9

City	Total share (%)	Share of total (%)											
		JAXA 1m	JAXA 3m	JAXA 5m	SRTM 1m	SRTM 3m	SRTM 5m	JAXA-SRTM 1m	JAXA-SRTM 3m	JAXA-SRTM 5m	CDEM 1m	CDEM 3m	CDEM 5m
Bangkok	100%	0.1%	5.4%	33.4%	1.0%	6.7%	28.0%	0.6%	6.1%	30.7%	0.9%	53.7%	94.5%
London	100%	0.1%	0.8%	4.3%	0.2%	2.3%	7.4%	0.1%	1.6%	5.9%	0.1%	6.1%	20.4%
Mumbai	100%	0.0%	0.1%	0.6%	0.1%	0.5%	1.9%	0.1%	0.3%	1.2%	16.3%	22.5%	26.9%

Table E8: Populations of each city projected to be impacted by the SLR scenarios as modelled in this study

City	Model	Total population (millions)	Counts (millions) (1m SLR)	Counts (millions) (3m SLR)	Counts (millions) (5m SLR)	Proportion 1m (%)	Proportion 3m (%)	Proportion 5m (%)
Bangkok	JAXA	19.75	0.53	2.52	9.43	2.7%	12.7%	47.7%
London	JAXA	9.17	0.04	0.16	0.39	0.4%	1.7%	4.2%
Mumbai	JAXA	25.70	0.42	2.35	4.43	1.6%	9.1%	17.2%
Bangkok	SRTM	19.75	0.65	2.46	7.96	3.3%	12.5%	40.3%
London	SRTM	9.17	0.03	0.15	0.39	0.4%	1.7%	4.2%
Mumbai	SRTM	25.70	1.30	3.39	5.56	5.0%	13.2%	21.6%
Bangkok	JAXA-SRTM	19.75	0.59	2.49	8.69	3.0%	12.6%	44.0%
London	JAXA-SRTM	9.17	0.03	0.15	0.39	0.4%	1.7%	4.2%
Mumbai	JAXA-SRTM	25.70	0.86	2.87	4.99	3.3%	11.2%	19.4%
Bangkok	CDEM	19.75	0.59	10.35	18.88	3.0%	52.4%	95.6%
London	CDEM	9.17	0.04	0.33	1.52	0.4%	3.6%	16.6%
Mumbai	CDEM	25.70	6.22	11.54	14.25	24.2%	44.9%	55.5%

Statistical Analysis Tables

Table E9: Kruskal-Wallis Independent test results for the H_0 dataset, showing that H_0 should be rejected (this test checked the quantities of urban infrastructure inundated across the three elevation datasets used for modelling)

Dependent variable	Minimum	Mean	Maximum	Asymptotic significance	Decision
Roads (1m SLR)	28.98	19532.04	2229154.94	.063	Accept H0
Roads (3m SLR)	28.98	146781.87	3300467.01	.000	Reject H0
Roads (5m SLR)	28.98	351909.53	3916761.15	.000	Reject H0
Railways (1m SLR)	3.01	8546.50	273062.23	.001	Reject H0
Railways (3m SLR)	3.01	27488.95	1630213.82	.000	Reject H0
Railways (5m SLR)	11.38	61871.29	2553612.06	.000	Reject H0
Buildings (1m SLR)	.49	102440.71	14426874.53	.000	Reject H0
Buildings (3m SLR)	.50	652315.09	19305440.24	.000	Reject H0
Buildings (5m SLR)	.21	1258135.21	22755727.21	.000	Reject H0
Parks (1m SLR)	12.59	34326.09	1983010.61	.000	Reject H0
Parks (3m SLR)	9.78	132372.55	3357190.55	.000	Reject H0
Parks (5m SLR)	.37	312640.33	5691281.21	.000	Reject H0
Population (1m SLR)	0.00	24419	4979335	.285	Accept H0
Population (3m SLR)	0.00	81694	7658847	.000	Reject H0
Population (5m SLR)	0.00	152803	8971024	.000	Reject H0

Table E10: Kruskal-Wallis Independent test results for H_1 dataset (testing the rate of infrastructure inundation increase with rising sea levels), showing a preference to reject H_1

Dependent variable	Minimum	Median	Mean	Maximum	Asymptotic significance	Decision
Roads (1m SLR)	4.95	3895.30	19386.61	2229154.94	.273	Accept H1
Roads (3m SLR)	0.00	23206.15	91621.28	2047121.68	.000	Reject H1
Roads (5m SLR)	0.00	71916.14	164646.45	4747742.11	.000	Reject H1
Railways (1m SLR)	11.11	217.77	1652.07	170024.05	.005	Reject H1
Railways (3m SLR)	0.00	1161.35	3619.25	39774.99	.000	Reject H1
Railways (5m SLR)	0.00	2243.08	4400.00	30832.53	.010	Reject H1
Buildings (1m SLR)	0.49	11611.12	135976.74	14426874.53	.000	Reject H1
Buildings (3m SLR)	0.50	71564.57	648672.89	15499083.56	.000	Reject H1
Buildings (5m SLR)	0.00	138913.49	800841.21	7292620.54	.011	Reject H1
Parks (1m SLR)	4.95	16507.29	47628.19	1983010.61	.498	Accept H1
Parks (3m SLR)	0.00	15954.52	123753.98	2047121.68	.000	Reject H1
Parks (5m SLR)	0.00	33171.58	209730.70	4747742.11	.471	Accept H1
Population (1m SLR)	0	3494	24419	4979335	.320	Accept H1
Population (3m SLR)	1	19165	67143	2679512	.000	Reject H1
Population (5m SLR)	1	51547	79443	1323926	.003	Reject H1

Table E11: Kruskal-Wallis Independent Median test results for H_2 (Bangkok), showing a preference to reject H_2

Dependent variable	Minimum	Median	Mean	Maximum	Exact significance	Decision
Roads (1m SLR)	.0003	.0086	.0216	.2496	.090	Accept H2
Roads (3m SLR)	.0005	.1235	.2240	.9032	.000	Reject H2
Roads (5m SLR)	.0009	.6009	.5749	1.0000	.000	Reject H2
Railways (1m SLR)	.0008	.0082	.0192	.4229	.453	Accept H2
Railways (3m SLR)	.0014	.0766	.2200	.9943	.000	Reject H2
Railways (5m SLR)	.0026	.5395	.5391	1.0000	.000	Reject H2
Buildings (1m SLR)	.0000	.0012	.0105	.1670	.001	Reject H2
Buildings (3m SLR)	.0000	.0650	.2061	.9838	.000	Reject H2
Buildings (5m SLR)	.0001	.4350	.4777	.9939	.000	Reject H2
Parks (1m SLR)	.0004	.0159	.0750	.3898	1.000	Accept H2
Parks (3m SLR)	.0000	.3198	.3745	.9939	.000	Reject H2
Parks (5m SLR)	.0000	.7103	.6378	.9939	.000	Reject H2

Table E12: Kruskal-Wallis Independent Median test results for H_2 (London), showing a preference to accept H_2

Dependent variable	Minimum	Median	Mean	Maximum	Asymptotic significance	Decision
Roads (1m SLR)	.0001	.0013	.0032	.0321	.725	Accept H2
Roads (3m SLR)	.0001	.0026	.0313	.3666	.182	Accept H2
Roads (5m SLR)	.0001	.0129	.0988	.8098	.002	Reject H2
Railways (1m SLR)	.0003	.0022	.0095	.0849	.948	Accept H2
Railways (3m SLR)	.0003	.0037	.0495	.4705	.964	Accept H2
Railways (5m SLR)	.0003	.0243	.1208	.9383	.019	Reject H2
Buildings (1m SLR)	.0000	.0038	.0102	.0902	.401	Accept H2
Buildings (3m SLR)	.0000	.0296	.1215	.6574	.476	Accept H2
Buildings (5m SLR)	.0000	.1429	.2222	.9588	.030	Reject H2
Parks (1m SLR)	.0000	.0043	.0075	.0543	.957	Accept H2
Parks (3m SLR)	.0000	.0066	.0374	.4939	.454	Accept H2
Parks (5m SLR)	.0005	.0293	.1078	.8214	.009	Reject H2

Table E13: Kruskal-Wallis Independent Median test results for H_2 (Mumbai), showing similar preferences to accept/reject H_2

Dependent variable	Minimum	Median	Mean	Maximum	Exact significance	Decision
Roads (1m SLR)	.0003	.0087	.0399	.3742	0.007	Reject H2
Roads (3m SLR)	.0003	.0715	.1395	.7543	0.047	Reject H2
Roads (5m SLR)	.0003	.1641	.2284	.8453	0.047	Reject H2
Railways (1m SLR)	.0012	.0479	.0949	.8301	0.661	Accept H2
Railways (3m SLR)	.0009	.2309	.3001	.9672	0.000	Reject H2
Railways (5m SLR)	.0016	.4551	.4807	1.0000	0.032	Reject H2
Buildings (1m SLR)	.0000	.0157	.0292	.1667	0.266	Accept H2
Buildings (3m SLR)	.0011	.0938	.1787	.5489	0.001	Reject H2
Buildings (5m SLR)	.0047	.2630	.2705	.9944	0.041	Reject H2
Parks (1m SLR)	.0000	.0002	.0131	.2052	0.255	Accept H2
Parks (3m SLR)	.0001	.0081	.0733	.7911	0.109	Accept H2
Parks (5m SLR)	.0003	.0130	.1219	.9661	0.712	Accept H2

Table E14: Kruskal-Wallis Independent test results for H_3 (quantities of inundated infrastructural elements), leading to the acceptance of H_3

Dependent variable	Minimum	Median	Mean	Maximum	Exact significance	Decision
Roads (1m SLR)	61503.68	721972.09	872431.01	3102790.05	0.511	Accept H3
Roads (3m SLR)	512223.08	2543822.46	6670420.30	30542712.22	0.543	Accept H3
Roads (5m SLR)	1211664.18	4280266.34	16070535.18	58719333.66	0.629	Accept H3
Railways (1m SLR)	2986.39	9940.81	35983.99	216818.58	0.879	Accept H3
Railways (3m SLR)	15316.65	64003.31	114245.09	392917.35	0.100	Accept H3
Railways (5m SLR)	107581.47	154325.89	224111.94	500120.33	0.071	Accept H3
Buildings (1m SLR)	34949.74	174394.79	2185899.12	14485690.20	0.339	Accept H3
Buildings (3m SLR)	119448.34	4912479.46	19849498.46	122822186.00	0.196	Accept H3
Buildings (5m SLR)	520086.48	16466137.42	45420576.03	216267503.80	0.511	Accept H3
Parks (1m SLR)	39749.01	251062.92	750693.61	2184105.80	0.721	Accept H3
Parks (3m SLR)	956842.41	4309433.38	3741660.59	7892302.18	0.050	Accept H3
Parks (5m SLR)	2924546.14	8634234.68	10713012.26	33122783.74	0.339	Accept H3

Table E15: Kruskal-Wallis Independent test results for the cities' populations with different SLR scenarios, resulting in the acceptance of H_4

Dependent variable	Minimum	Mean	Maximum	Asymptotic significance	Decision
Population (1m SLR)	32365	1090700.97	6224010	0.733	Accept H4
Population (3m SLR)	152187	3694364.74	11542436	0.430	Accept H4
Population (5m SLR)	385482	6978007.00	18882213	0.430	Accept H4

Department of Physical Geography and Ecosystem Science

Master Thesis in Geographical Information Science

1. *Anthony Lawther:* The application of GIS-based binary logistic regression for slope failure susceptibility mapping in the Western Grampian Mountains, Scotland (2008).
2. *Rickard Hansen:* Daily mobility in Grenoble Metropolitan Region, France. Applied GIS methods in time geographical research (2008).
3. *Emil Bayramov:* Environmental monitoring of bio-restoration activities using GIS and Remote Sensing (2009).
4. *Rafael Villarreal Pacheco:* Applications of Geographic Information Systems as an analytical and visualization tool for mass real estate valuation: a case study of Fontibon District, Bogota, Columbia (2009).
5. *Siri Oestreich Waage:* a case study of route solving for oversized transport: The use of GIS functionalities in transport of transformers, as part of maintaining a reliable power infrastructure (2010).
6. *Edgar Pimiento:* Shallow landslide susceptibility – Modelling and validation (2010).
7. *Martina Schäfer:* Near real-time mapping of floodwater mosquito breeding sites using aerial photographs (2010).
8. *August Pieter van Waarden-Nagel:* Land use evaluation to assess the outcome of the programme of rehabilitation measures for the river Rhine in the Netherlands (2010).
9. *Samira Muhammad:* Development and implementation of air quality data mart for Ontario, Canada: A case study of air quality in Ontario using OLAP tool. (2010).
10. *Fredros Oketch Okumu*: Using remotely sensed data to explore spatial and temporal relationships between photosynthetic productivity of vegetation and malaria transmission intensities in selected parts of Africa (2011).
11. *Svajunas Plunge:* Advanced decision support methods for solving diffuse water pollution problems (2011).
12. *Jonathan Higgins:* Monitoring urban growth in greater Lagos: A case study using GIS to monitor the urban growth of Lagos 1990 - 2008 and produce future growth prospects for the city (2011).
13. *Mårten Karlberg:* Mobile Map Client API: Design and Implementation for Android (2011).
14. *Jeanette McBride:* Mapping Chicago area urban tree canopy using color infrared imagery (2011).
15. *Andrew Farina:* Exploring the relationship between land surface temperature and vegetation abundance for urban heat island mitigation in Seville, Spain (2011).
16. *David Kanyari*: Nairobi City Journey Planner: An online and a Mobile Application (2011).
17. *Laura V. Drews:* Multi-criteria GIS analysis for siting of small wind power plants - A case study from Berlin (2012).
18. *Qaisar Nadeem:* Best living neighborhood in the city - A GIS based multi criteria evaluation of ArRiyadh City (2012).

19. *Ahmed Mohamed El Saeid Mustafa:* Development of a photo voltaic building rooftop integration analysis tool for GIS for Dokki District, Cairo, Egypt (2012).
20. *Daniel Patrick Taylor*: Eastern Oyster Aquaculture: Estuarine Remediation via Site Suitability and Spatially Explicit Carrying Capacity Modeling in Virginia's Chesapeake Bay (2013).
21. *Angeleta Oveta Wilson:* A Participatory GIS approach to *unearthing* Manchester's Cultural Heritage '*gold mine*' (2013).
22. *Ola Svensson:* Visibility and Tholos Tombs in the Messenian Landscape: A Comparative Case Study of the Pylian Hinterlands and the Soulima Valley (2013).
23. *Monika Ogden:* Land use impact on water quality in two river systems in South Africa (2013).
24. *Stefan Rova:* A GIS based approach assessing phosphorus load impact on Lake Flaten in Salem, Sweden (2013).
25. *Yann Buhot:* Analysis of the history of landscape changes over a period of 200 years. How can we predict past landscape pattern scenario and the impact on habitat diversity? (2013).
26. *Christina Fotiou:* Evaluating habitat suitability and spectral heterogeneity models to predict weed species presence (2014).
27. *Inese Linuza:* Accuracy Assessment in Glacier Change Analysis (2014).
28. *Agnieszka Griffin:* Domestic energy consumption and social living standards: a GIS analysis within the Greater London Authority area (2014).
29. *Brynja Guðmundsdóttir:* Detection of potential arable land with remote sensing and GIS - A Case Study for Kjósarhreppur (2014).
30. *Oleksandr Nekrasov:* Processing of MODIS Vegetation Indices for analysis of agricultural droughts in the southern Ukraine between the years 2000-2012 (2014).
31. *Sarah Tressel:* Recommendations for a polar Earth science portal in the context of Arctic Spatial Data Infrastructure (2014).
32. *Caroline Gevaert:* Combining Hyperspectral UAV and Multispectral Formosat-2 Imagery for Precision Agriculture Applications (2014).
33. *Salem Jamal-Uddeen:* Using GeoTools to implement the multi-criteria evaluation analysis - weighted linear combination model (2014).
34. *Samanah Seyedi-Shandiz:* Schematic representation of geographical railway network at the Swedish Transport Administration (2014).
35. *Kazi Masel Ullah:* Urban Land-use planning using Geographical Information System and analytical hierarchy process: case study Dhaka City (2014).
36. *Alexia Chang-Wailing Spitteler:* Development of a web application based on MCDA and GIS for the decision support of river and floodplain rehabilitation projects (2014).
37. *Alessandro De Martino:* Geographic accessibility analysis and evaluation of potential changes to the public transportation system in the City of Milan (2014).
38. *Alireza Mollasalehi:* GIS Based Modelling for Fuel Reduction Using Controlled Burn in Australia. Case Study: Logan City, QLD (2015).
39. *Negin A. Sanati:* Chronic Kidney Disease Mortality in Costa Rica; Geographical Distribution, Spatial Analysis and Non-traditional Risk Factors (2015).

64. *Jonas Sjögren:* Consequences of a flood in Kristianstad, Sweden: A GIS-based analysis of impacts on important societal functions (2017).
65. *Nadine Raska:* 3D geologic subsurface modelling within the Mackenzie Plain, Northwest Territories, Canada (2017).
66. *Panagiotis Symeonidis*: Study of spatial and temporal variation of atmospheric optical parameters and their relation with PM 2.5 concentration over Europe using GIS technologies (2017).
67. *Michaela Bobeck:* A GIS-based Multi-Criteria Decision Analysis of Wind Farm Site Suitability in New South Wales, Australia, from a Sustainable Development Perspective (2017).
68. *Raghdaa Eissa*: Developing a GIS Model for the Assessment of Outdoor Recreational Facilities in New Cities Case Study: Tenth of Ramadan City, Egypt (2017).
69. *Zahra Khais Shahid*: Biofuel plantations and isoprene emissions in Svea and Götaland (2017).
70. *Mirza Amir Liaquat Baig*: Using geographical information systems in epidemiology: Mapping and analyzing occurrence of diarrhea in urban - residential area of Islamabad, Pakistan (2017).
71. *Joakim Jörwall*: Quantitative model of Present and Future well-being in the EU-28: A spatial Multi-Criteria Evaluation of socioeconomic and climatic comfort factors (2017).
72. *Elin Haettner*: Energy Poverty in the Dublin Region: Modelling Geographies of Risk (2017).
73. *Harry Eriksson*: Geochemistry of stream plants and its statistical relations to soil- and bedrock geology, slope directions and till geochemistry. A GIS-analysis of small catchments in northern Sweden (2017).
74. *Daniel Gardevärn:* PPGIS and Public meetings – An evaluation of public participation methods for urban planning (2017).
75. *Kim Friberg:* Sensitivity Analysis and Calibration of Multi Energy Balance Land Surface Model Parameters (2017).
76. *Viktor Svanerud:* Taking the bus to the park? A study of accessibility to green areas in Gothenburg through different modes of transport (2017).
77. *Lisa-Gaye Greene*: Deadly Designs: The Impact of Road Design on Road Crash Patterns along Jamaica's North Coast Highway (2017).
78. *Katarina Jemec Parker*: Spatial and temporal analysis of fecal indicator bacteria concentrations in beach water in San Diego, California (2017).
79. *Angela Kabiru*: An Exploratory Study of Middle Stone Age and Later Stone Age Site Locations in Kenya's Central Rift Valley Using Landscape Analysis: A GIS Approach (2017).
80. *Kristean Björkmann*: Subjective Well-Being and Environment: A GIS-Based Analysis (2018).
81. *Williams Erhunmonmen Ojo*: Measuring spatial accessibility to healthcare for people living with HIV-AIDS in southern Nigeria (2018).
82. *Daniel Assefa*: Developing Data Extraction and Dynamic Data Visualization (Styling) Modules for Web GIS Risk Assessment System (WGRAS). (2018).
83. *Adela Nistora*: Inundation scenarios in a changing climate: assessing potential impacts of sea-level rise on the coast of South-East England (2018).
84. *Marc Seliger*: Thirsty landscapes - Investigating growing irrigation water consumption and potential conservation measures within Utah's largest master-planned community: Daybreak (2018).

85. *Luka Jovičić*: Spatial Data Harmonisation in Regional Context in Accordance with INSPIRE Implementing Rules (2018).
86. *Christina Kourdounouli*: Analysis of Urban Ecosystem Condition Indicators for the Large Urban Zones and City Cores in EU (2018).
87. *Jeremy Azzopardi*: Effect of distance measures and feature representations on distance-based accessibility measures (2018).
88. *Patrick Kabatha*: An open source web GIS tool for analysis and visualization of elephant GPS telemetry data, alongside environmental and anthropogenic variables (2018).
89. *Richard Alphonce Giliba*: Effects of Climate Change on Potential Geographical Distribution of Prunus africana (African cherry) in the Eastern Arc Mountain Forests of Tanzania (2018).
90. *Eiður Kristinn Eiðsson*: Transformation and linking of authoritative multi-scale geodata for the Semantic Web: A case study of Swedish national building data sets (2018).
91. *Niamh Harty*: HOP!: a PGIS and citizen science approach to monitoring the condition of upland paths (2018).
92. *José Estuardo Jara Alvear*: Solar photovoltaic potential to complement hydropower in Ecuador: A GIS-based framework of analysis (2018).
93. *Brendan O'Neill*: Multicriteria Site Suitability for Algal Biofuel Production Facilities (2018).
94. *Roman Spataru*: Spatial-temporal GIS analysis in public health – a case study of polio disease (2018).
95. *Alicja Miodońska*: Assessing evolution of ice caps in Suðurland, Iceland, in years 1986 - 2014, using multispectral satellite imagery (2019).
96. *Dennis Lindell Schettini*: A Spatial Analysis of Homicide Crime's Distribution and Association with Deprivation in Stockholm Between 2010-2017 (2019).
97. *Damiano Vesentini*: The Po Delta Biosphere Reserve: Management challenges and priorities deriving from anthropogenic pressure and sea level rise (2019).
98. *Emilie Arnesten*: Impacts of future sea level rise and high water on roads, railways and environmental objects: a GIS analysis of the potential effects of increasing sea levels and highest projected high water in Scania, Sweden (2019).
99. *Syed Muhammad Amir Raza*: Comparison of geospatial support in RDF stores: Evaluation for ICOS Carbon Portal metadata (2019).
100. *Hemin Tofiq*: Investigating the accuracy of Digital Elevation Models from UAV images in areas with low contrast: A sandy beach as a case study (2019).
101. *Evangelos Vafeiadis*: Exploring the distribution of accessibility by public transport using spatial analysis. A case study for retail concentrations and public hospitals in Athens (2019).
102. *Milan Sekulic*: Multi-Criteria GIS modelling for optimal alignment of roadway by-passes in the Tlokweng Planning Area, Botswana (2019).
103. *Ingrid Piirisaar*: A multi-criteria GIS analysis for siting of utility-scale photovoltaic solar plants in county Kilkenny, Ireland (2019).
104. *Nigel Fox*: Plant phenology and climate change: possible effect on the onset of various wild plant species' first flowering day in the UK (2019).
105. *Gunnar Hesch*: Linking conflict events and cropland development in Afghanistan, 2001 to 2011, using MODIS land cover data and Uppsala Conflict Data Programme (2019).
106. *Elijah Njoku*: Analysis of spatial-temporal pattern of Land Surface Temperature (LST) due to NDVI and elevation in Ilorin, Nigeria (2019).

107. *Katalin Bunyevácz*: Development of a GIS methodology to evaluate informal urban green areas for inclusion in a community governance program (2019).
108. *Paul dos Santos*: Automating synthetic trip data generation for an agent-based simulation of urban mobility (2019).
109. *Robert O' Dwyer*: Land cover changes in Southern Sweden from the mid-Holocene to present day: Insights for ecosystem service assessments (2019).
110. *Daniel Klingmyr*: Global scale patterns and trends in tropospheric NO2 concentrations (2019).
111. *Marwa Farouk Elkabbany*: Sea Level Rise Vulnerability Assessment for Abu Dhabi, United Arab Emirates (2019).
112. *Jip Jan van Zoonen*: Aspects of Error Quantification and Evaluation in Digital Elevation Models for Glacier Surfaces (2020).
113. *Georgios Efthymiou*: The use of bicycles in a mid-sized city – benefits and obstacles identified using a questionnaire and GIS (2020).
114. *Haruna Olayiwola Jimoh*: Assessment of Urban Sprawl in MOWE/IBAFO Axis of Ogun State using GIS Capabilities (2020).
115. *Nikolaos Barmpas Zachariadis*: Development of an iOS, Augmented Reality for disaster management (2020).
116. *Ida Storm*: ICOS Atmospheric Stations: Spatial Characterization of CO2 Footprint Areas and Evaluating the Uncertainties of Modelled CO2 Concentrations (2020).
117. *Alon Zuta*: Evaluation of water stress mapping methods in vineyards using airborne thermal imaging (2020).
118. *Marcus Eriksson*: Evaluating structural landscape development in the municipality Upplands-Bro, using landscape metrics indices (2020).
119. *Ane Rahbek Vierø*: Connectivity for Cyclists? A Network Analysis of Copenhagen's Bike Lanes (2020).
120. *Cecilia Baggini*: Changes in habitat suitability for three declining Anatidae species in saltmarshes on the Mersey estuary, North-West England (2020).
121. *Bakrad Balabanian*: Transportation and Its Effect on Student Performance (2020).
122. *Ali Al Farid*: Knowledge and Data Driven Approaches for Hydrocarbon Microseepage Characterizations: An Application of Satellite Remote Sensing (2020).
123. *Bartlomiej Kolodziejczyk*: Distribution Modelling of Gene Drive-Modified Mosquitoes and Their Effects on Wild Populations (2020).
124. *Alexis Cazorla*: Decreasing organic nitrogen concentrations in European water bodies - links to organic carbon trends and land cover (2020).
125. *Kharid Mwakoba*: Remote sensing analysis of land cover/use conditions of community-based wildlife conservation areas in Tanzania (2021).
126. *Chinatsu Endo*: Remote Sensing Based Pre-Season Yellow Rust Early Warning in Oromia, Ethiopia (2021).
127. *Berit Mohr*: Using remote sensing and land abandonment as a proxy for long-term human out-migration. A Case Study: Al-Hassakeh Governorate, Syria (2021).
128. *Kanchana Nirmali Bandaranayake*: Considering future precipitation in delineation locations for water storage systems - Case study Sri Lanka (2021).

129. *Emma Bylund*: Dynamics of net primary production and food availability in the aftermath of the 2004 and 2007 desert locust outbreaks in Niger and Yemen (2021).

130. *Shawn Pace*: Urban infrastructure inundation risk from permanent sea-level rise scenarios in London (UK), Bangkok (Thailand) and Mumbai (India): A comparative analysis (2021).